

Copyright
by
Faustino Monroy Santiago
2012

The Dissertation Committee for Faustino Monroy Santiago Certifies that this is the approved version of the following dissertation:

Interrelationships Between Carbonate Diagenesis and Fracture Development: Example From Monterrey Salient, Mexico and Implications for Hydrocarbon Reservoir Characterization

Committee:

Randall A. Marrett, Supervisor

Stephen E. Laubach

William L. Fisher

Julia Gale

Charles Kerans

**Interrelationships Between Carbonate Diagenesis and Fracture
Development: Example From Monterrey Salient, Mexico and
Implications for Hydrocarbon Reservoir Characterization**

by

Faustino Monroy Santiago, B.S.; M.Sc.

Dissertation

Presented to the Faculty of the Graduate School of
The University of Texas at Austin
in Partial Fulfillment
of the Requirements
for the Degree of

Doctor of Philosophy

The University of Texas at Austin

May 2012

Dedication

This Dissertation is dedicated to my sons Heomar and Hiram.

To the memory of my friend Bob Goldhammer.

Acknowledgements

My sincere appreciation is extended to my supervisor throughout much of this effort, Randall Marrett, for his guidance and assistance throughout this research. He has encouraged and supported me through the last four years, and has been an excellent mentor and friend. I appreciate Stephen E. Laubach stepping in to supervise the last stages of this study during Dr. Marrett's absence. I would like to thank my committee members, William Fisher, Stephen E. Laubach, Charles Kerans, and Julia Gale for their support and helping during my program, and Dr. Peter Flemings for stepping in at the last moment. Each of them has shared and offered their experiences and expertise.

I would also want to thank Robert Folk, Early McBride, Kitty Milliken, and Robert Reed for providing assistance with the petrographic and diagenetic analyses. To Libby Stern and Larry Mack, my thanks for helping run stable isotope samples through the mass-spectrometer, and immeasurable thanks for taking the time to show me the stable isotope techniques. To Leonel Gómez and Orlando Ortega for providing many helpful suggestions and observations during the development of my research. To Clotilde Prieto for helping me and supporting me in different ways at the last moment.

Thanks are owed to Pemex Exploración-Producción for the economic support during my Ph.D. program. Also I'm in debit with the follow people from Pemex: Antonio Escalera, Adán Oviedo, Fernando López, Miguel A. Gómez, Rodolfo Juarez, Alberto Aquino, Cesar Cabrera, David Zamora, and Jaime Barceló+, each of them helped me and supported me in different ways during my program.

Interrelationships Between Carbonate Diagenesis and Fracture Development: Example From Monterrey Salient, Mexico and Implications for Hydrocarbon Reservoir Characterization

Faustino Monroy Santiago Ph. D.

The University of Texas at Austin, 2012

Supervisor: Randall A. Marrett

Many low matrix-porosity hydrocarbon reservoirs are productive because permeability is controlled by natural fractures. The understanding of basic fracture properties is critical in reducing geological risk and therefore reducing well costs and increasing well recovery. Unfortunately, neither geophysics nor borehole methods are, so far, accurate in the acquisition of key fracture attributes, such as density, porosity, spacing and conductivity. This study proposes a new protocol to predict key fracture characteristics of subsurface carbonate rocks and describes how using a relatively low-cost but rock-based method it is possible to obtain accurate geological information from rock samples to predict fracture attributes in nearby but unsampled areas. This methodology is based on the integration of observations of diagenetic fabrics and fracture analyses of carbonate rocks, using outcrops from the Lower Cretaceous Cupido Formation in the Monterrey Salient of the Sierra Madre Oriental, northeastern Mexico. Field observations and petrographic studies of crosscutting relations and fracture-fill mineralogy and texture distinguish six principal coupled fracturing-cementation events. Two fracture events named F1 and F2 are characterized by synkinematic calcite cement

that predates D2 regional dolomitization. A third fracture event (F3) is characterized by synkinematic dolomite fill, contemporaneous with D2 dolomitization of host strata. The fourth event (F4) is characterized by synkinematic D3 baroque dolomite; this event postdates D2. The fifth fracture event (F5) is characterized by C3 synkinematic calcite, and postdates D3 dolomite. Finally, flexural slip faulting (F6) is characterized by C3t calcite, and postdates D3 dolomite. Carbon and oxygen stable isotopes were used to validate the paragenetic sequences proposed for the Cupido Formation rocks. The dolomite isotopic signatures are consistent with increasing precipitation temperatures for the various fracture cements, as is expected if fractures grew during progressive burial conditions. Three main groups of calcite cement can be differentiated isotopically. Late calcite cement may have precipitated from cool waters under shallow burial conditions, possibly during exhumation of the SMO. The development of the Structural Diagenetic Petrographic Study protocol, and its integration with geological, geophysical and engineering data, can be applied to oil fields in fractured carbonates such as those located in Mexico, to validate its applicability.

Table of Contents

List of Tables	xiv
List of Figures	xvii
Chapter 1 Introduction	1
Background	1
Fracture Data Sources	4
Purpose	7
Hypotheses	7
Objectives	8
Significance of the Study	9
Chapter 2 Geology of Monterrey Salient, Sierra Madre Oriental, Mexico	11
Introduction to Monterrey Salient.....	11
Background: Previous work.....	12
Study area: Monterrey Salient	12
Geologic Setting	15
Regional Stratigraphy	18
Local Stratigraphy.....	22
Stratigraphic columns	22
Chapter 3 Lithofacies and Sedimentary Environments	40
Introduction: Rock types.....	40
Methodology	41
Facies Distribution and Environment Deposition.....	41
Lithofacies Description.....	45
Argillaceous pelagic, lime mudstone.....	45
Intraclastic-bioclastic wackestone-packstone	48
Rudist and coral-dominated packstone, grainstone and boundstone with stromatoporoids.....	51

Crossbedded skeletal-peloidal, packstones-grainstones with ooids and oncolites.....	54
Mudstones-packstones with cryptalgal laminites and evaporites	56
Peloid-foram, wackestone-packstones with pelecypods and green algae	60
Evaporite Solution Breccias.....	63
Possible Origin and Timing of Evaporite Solution Breccias	70
Chapter 4: Diagenesis and Implications for Porosity Evolution of Lower Cretaceous Cupido Formation, Monterrey Salient, Sierra Madre Oriental, Mexico.	72
Summary	72
Diagenesis and Fracture Timing	74
Previous Work on Cupido Formation Diagenesis	77
Study Area: Location of Sections Analyzed	79
Structural-Diagenetic Methodology.....	82
Structural-Diagenetic Petrographic Study (SDPS).....	82
Petrographic Analysis	82
Paragenetic Sequence	86
Description of Diagenetic Processes	92
Calcite Cement.....	92
C1 and C2 calcite cement	92
C3 calcite cement	96
C3t twinned calcite	97
C4 calcite cement ("modern calcite")	97
Dolomite Cement.....	98
Fine grained and laminated dolomite (D1)	98
Replacement dolomite (D2)	102
Baroque dolomite (D3)	105
Ferroan dolomite.....	106
Other Diagenetic Processes.....	108

Microbial micritization	108
Compaction and pressure solution	109
Burial stylolites	110
Tectonic stylolites	113
Recrystallization.....	115
Dedolomitization.....	115
Quartz cement	117
Dissolution	121
Origin and Distribution of Dolomites	123
D1 Dolomite.....	124
D2 Dolomite.....	125
D3 Dolomite.....	129
Origin and Evolution of Porosity System	130
Chapter 5: Fracture Analysis of Lower Cretaceous Cupido Formation	
Monterrey Salient, Sierra Madre Oriental, Mexico.	132
Summary	132
Fracture Terminology	135
Fracture Classification	135
Fracture Set	138
Fracture and Diagenetic Event.....	139
Fracture Cement.....	140
Bridges and Pillars	141
Crack-seal Texture	142
Emergent Threshold.....	143
Characterization and Predicting Fractures	145
Previous Fracture Work in NE Mexico	147
Fracture Study Area	150
Chapter Organization	151
Fracture Methodology.....	151
Fracture Size Data.....	152

Field Identification of Fracture Sets	153
Burial and Tectonic Stylolites.....	154
Fracture Sets W, X, Y, and Z	157
Fracture Events	161
F1-F2 Fracture Event	161
F3 Fracture Event.....	164
F4 Fracture Event.....	168
F5 Fracture Event.....	174
F6 Fracture Event.....	178
Travertine-filled Fractures and Joints	183
Diagenetic Processes and Evidence to Determined Relative Timing	184
Paragenetic Sequence by localities	192
Cañón Santa Rosa-Iturbide	192
Cañón de los Chorros	193
Cañón Boquilla Corral de Palmas	195
Cañón la Escalera.....	197
Regional Paragenetic Sequence	200
Fracture-Cementation Coupled Events	204
Outcrop Scale Fracture Correlation to Microscopic Scale	206
Implication of the Cement Patterns.....	208
Discussion: Structure and Diagenesis	210
Discussion: Fracture History.....	212
 Chapter 6 Stable Isotope Analyses of Fracture Cements in the Cupido Formation, Monterrey Salient, Sierra Madre Oriental, Mexico	 215
Summary	215
Introduction.....	217
Study Area	218
Previous Geochemical Work	220
Methodology	221
Geochemical Sampling and Analytical Methodology	224

Estimation of Marine Carbonate Composition	226
Data Analysis	226
Paleo-temperature Calculation	227
Results of Stable Isotopic Analyses	228
Dolomite Cement Analysis	228
Host Rocks	231
Fracture Dolomite Cements	233
Fault Breccias	235
Collapse (Solution) Breccias	235
Dolomite Isotopic Characterization	237
Calcite Cement Analysis	242
Host Rock Cement	245
Rudists	246
Fracture Calcite Cements	246
Flexural Slip Faults	249
Fault Breccias	250
Calcite in Evaporite Collapse Breccias	251
Anhydrite Nodules	252
Travertine	253
Calcite Isotopic Characterization	254
Meteoric Water Analysis	257
Stable Isotope Analyses and Fracture Development	258
Paragenetic Sequence and Fracture Timing Interpretations	262
Fracture Origins based on Isotopic Results	265
Discussion	269
Conclusions	272

Appendices.....	275
Appendix 2.1- Type sections of the Cupido and Tamaulipas Inferior Formations at four localities included in this study from the Monterrey Salient, Sierra Madre Oriental, Mexico...	275
Appendix 3.1 – List of sedimentologic and structural characteristics of carbonate beds included in this study	276
Appendix 3.2 –List of thin sections prepared and used in this study by locality.....	279
Appendix 4.1 – Petrographic summary sheets.....	282
Appendix 4.2 – Percentage of dolomite.....	321
Appendix 4.3 – Dolomite crystals size measurements	323
Appendix 5.1 – Field fracture data	326
Appendix 5.2 – List of oriented samples and fracture sets orientation. Cupido Formation.....	328
References	330
Vitae	345

List of Tables

Table 4.1:	Sample of petrographic summary sheet of a thin section description	85
Table 4.2:	Diagenetic processes and evidence used to determine relative timing	87
Table 5.1:	Diagenetic processes and evidence used to determine relative timing including fracturing	185
Table 5.2a:	Diagenetic and fracturing processes at Cañón Santa Rosa-Iturbide locality	193
Table 5.2b:	Diagenetic and fracturing processes at Cañón de los Chorros.....	195
Table 5.2c:	Diagenetic and fracturing processes at Cañón Boquilla Corral de Palmas locality	197
Table 5.2d:	Diagenetic and fracturing processes identified at La Escalera	199
Table 5.3:	Regional diagenetic and fracturing processes identified in the Monterrey Salient, based on the four localities	202
Table 5.4:	Generalized paragenetic sequence, relative duration of diagenetic events and inferred diagenetic stages	203
Table 5.5:	Correlation between fracture events determined from the structural- diagenetic petrographic study and fracture sets measured in the field in four localities of the Monterrey Salient ..	207
Table 6.1:	List of samples, localities and composition for carbon and oxygen isotopic analyses	222

Table 6.2:	List of samples by localities, including dolomite isotopic composition and sample origin, used in this study from Cupido and Tamaulipas Inferior Formations, SMO.....	230
Table 6.3:	Carbon and oxygen isotopic composition of host rocks from dolostones and dolomitized limestones of Cupido Formation, SMO.....	232
Table 6.4:	Carbon and oxygen isotopic composition of fracture cements from dolostones and dolomitized limestones of Cupido Formation, SMO	234
Table 6.5:	Carbon and oxygen isotopic composition of baroque dolomite from fault breccias of Cupido Formation, SMO.....	235
Table 6.6:	Carbon and oxygen isotopic composition of baroque dolomite cement from collapse breccias of Cupido Formation, SMO.....	236
Table 6.7:	List of samples by localities, including calcite isotopic composition, and sample origin used in this study from Cupido and Tamaulipas Inferior Formations, SMO.....	243
Table 6.8:	Carbon and oxygen isotopic composition of host rocks (matrix cements) from limestones of Cupido Formation, SMO.....	245
Table 6.9:	Carbon and oxygen isotopic composition of host rocks from rudists in limestones of Cupido Formation, SMO	246
Table 6.10:	Carbon and oxygen isotopic composition of fracture cements from dolostones and limestones of Cupido Formation, SMO	248
Table 6.11:	Carbon and oxygen isotopic composition of calcite cements from samples of flexural-slip fault planes (F6 fractures).....	249

Table 6.12: Carbon and oxygen isotopic composition of calcite cements from fault breccia planes of Cupido Formation, SMO	250
Table 6.13: Carbon and oxygen isotopic composition of calcite cements of collapse breccias from Cupido Formation, SMO	251
Table 6.14: Carbon and oxygen isotopic composition of calcite cements from anhydrite nodule samples	252
Table 6.15: Carbon and oxygen isotopic composition of calcite cements of travertine samples from Los Chorros and Potrero García localities	253
Table 6.16: Oxygen isotopic composition of meteoric water from spring at the Los Chorros locality, SMO	257
Table 6.17: Generalized paragenetic sequence, relative duration of diagenetic events and inferred diagenetic stages.....	264
Table 6.18: Fracture events identified in the Monterrey Salient, SMO and their main characteristics	268

List of Figures

Figure 2.1: Location map of study area, Monterrey Salient, Mexico.....	13
Figure 2.2: Landsat TM satellite image of part of the SMO, showing the Monterrey Salient	14
Figure 2.3: Geologic map of the Monterrey Salient.....	17
Figure 2.4: Chronostratigraphic chart for northeastern Mexico and Texas Gulf Coast showing second-order supersequences as interpreted by Goldhammer et al. (1991).....	19
Figure 2.5: Schematic dip-oriented regional stratigraphic cross-section trending north-northwest to south-southeast.....	21
Figure 2.6a: Thematic mapper satellite image of the Santa Rosa area, showing the measured stratigraphic column location	23
Figure 2.6b: Thematic mapper satellite image of the Cañón de los Chorros showing the measured stratigraphic column location	24
Figure 2.6c: Thematic mapper satellite image of the Cañón Huasteca area showing the measured stratigraphic column location.....	26
Figure 3.1: Idealized vertical section of platform-basin facies model of Cupido Formation	43
Figure 3.2: Barremian to Lower Aptian paleogeographic map showing the Cupido platform developed around the Coahuila High, a positive element at that time	44
Figure 3.3a: Outcrop photograph showing thin- to thick-bedded, basinal lime mudstones of Tamaulipas Inferior Formation. Cañón Santa Rosa locality	46

Figure 3.3b: Detail of Fig. 3.3a showing cherty basinal lime mudstone	47
Figure 3.3c: Photomicrograph illustrating cross section of a calpionellid and organic matter	48
Figure 3.4a: Photomicrograph illustrating fore-reef intraclastic-bioclastic packstone facies	49
Figure 3.4b: Outcrop photograph of syn-sedimentary breccia composed of subangular clasts that vary in size from 0.5 mm to 2 cm	50
Figure 3.4c: Syn-sedimentary breccia composed of clasts of wackestone (Wck) of ooids and intraclasts (Intc) in fine grained dolomite matrix.....	51
Figure 3.5a: Abundant rudists in organic reef facies	52
Figure 3.5b: Reef facies showing caprinid-type rudists	53
Figure 3.5c: Partially dolomitized reef facies showing fragments of mollusk in a peloidal-packstone-grainstone matrix	54
Figure 3.6a: Back-margin sand shoals facies showing cross-bedding	55
Figure 3.6b: Sand shoal facies with bioclasts, ooids and peloids.....	56
Figure 3.7a: Cross-sectional view of burrows in shallow water marine carbonates	57
Figure 3.7b: Detail of Figure 3.7a showing both bedding-perpendicular (Bv) and bedding-parallel (Bh) burrows in a dolostone bed.....	58
Figure 3.7c: Medium-bedded dark gray mudstones-packstones intercalated with light gray algal mats of peritidal platform interior facies	59
Figure 3.7d: Convoluted algal laminations of peritidal platform interior facies..	60
Figure 3.8a: Back-margin lagoon facies of miliolid lime packstone with aggregate grains, gastropods, and green algae fragments.....	61

Figure 3.8b: Pellet packstone showing Favreina sp. Cupido Formation, Cañón de los Chorros locality.....	62
Figure 3.9a: Monomict, clast-supported evaporite collapse breccia (CB) showing upper irregular contact.....	65
Figure 3.9b: Detail of Figure 3.9a showing monomict evaporite solution breccia containing angular dolostone (D) clasts cemented with calcite (C).....	66
Figure 3.10 Monomict, clast-supported breccia showing rectangular shape blocks of dolostones.....	67
Figure 3.11a Polymict, clast-supported solution collapse breccia showing angular clasts and sharp lower contact, characteristic of these breccias	68
Figure 3.11b Detail of Figure 3.11a showing a polymict, clast-supported evaporite solution breccia.	69
Figure 4.1a: Location map of study localities, Monterrey Salient.	80
Figure 4.1b: Barremian to Lower Aptian paleogeographic map showing the Cupido platform developed around the Coahuila High, a subaerial element at that time.	81
Figure 4.2a: Grainstone showing two generations of calcite cement	94
Figure 4.2b: Solution breccia showing non-isopachous equant calcite spar (C2), first generation cement around dolostone clasts, and later poikilotopic twinned calcite spar (C3t) occluded the porosity.	95
Figure 4.2c: Veins in a dolostone.....	96
Figure 4.3a: Photomicrograph of D1 dolomite.	99

Figure 4.3b: Plane-light photomicrograph of laminated dolostone (D1) and algal mats (Am) with calcitized evaporite nodules (V).	100
Figure 4.3c: Photomicrograph of evaporite solution breccia showing a calcite-filled vein (F) and a microcrystalline dolostone clast (D1) in a pellet wackestone-packstone matrix (W-Pm).....	101
Figure 4.4a: Packstone of ooids partially replaced by idiotopic mosaic of sub-euhedral D2 dolomite rhombs.....	103
Figure 4.4b: Thin (<8 cm) to thick (1.8 m) bedded dolostones.....	104
Figure 4.5a: Calcite-filled vein (F) in a dolostone	106
Figure 4.5b: Photomicrograph of euhedral possible Fe-dolomite crystal (FeD) in a basinal mudstone	107
Figure 4.6: Grainstone of bioclasts and ooids showing crushed micrite (M) rims around former fossils and ooids.....	109
Figure 4.7a: Bio- and intraclastic wackestone showing effects of chemical compaction (Cp) at sutured and concavo-convex grain contacts...	111
Figure 4.7b: Bedding-parallel stylolites at bed boundaries	112
Figure 4.7c: Dolomitized sedimentary breccia showing burial stylolites indicated by white arrows cross-cutting some fractures (F), implying that bedding-parallel stylolites postdate these fractures.....	113
Figure 4.7d: High-angle (Sty t) and bedding-parallel (Sty p) stylolites in a dolostone bed	114
Figure 4.8: Recrystallized limestone, Cañón Las Palmas	116
Figure 4.9 Corroded dolomite crystals	117

Figure 4.10a	Detail of bedding-perpendicular stylolite (Sty) with quartz (Qz) cement along its path that cuts a macro-fracture, containing D3 baroque dolomite and C3 calcite crystals, indicating that both stylolites and quartz postdate fracturing	118
Figure 4.10b	Authigenic quartz (Qz) in fracture showing primary fluid and solid inclusions of probable dolomite (Dol), implying simultaneous precipitation	119
Figure 4.10c	Authigenic quartz crystals (Qz).	120
Figure 4.10d	Quartz crystals in macrofracture	121
Figure 4.11	Potrero García caves.	122
Figure 4.12a	Sketch for the three main dolomite types identified in the Cupido Formation	123
Figure 4.12b	Selected thin sections for sketch of Figure 4.12a	124
Figure 4.13	Map showing regional distribution of D2 dolomite in the Monterrey Salient (this study)	128
Figure 5.1a	Fracture classification based on the relative displacement of the material on opposite sides of the fracture	137
Figure 5.1b	Outcrop photograph showing three main fracture sets or families	138
Figure 5.1c	Detail of fracture in a limestone from an oil reservoir.....	140
Figure 5.1d	Detail of fracture in a limestone from an oil reservoir.....	142
Figure 5.1e	Detail of sealed fracture calcite cement in a limestone, with a crack seal texture.....	143
Figure 5.2	Landsat TM satellite image of part of the SMO, showing the Monterrey Salient. Circles mark outcrop and sample localities	150

Figure 5.3: High-angle (Sty t), bedding-parallel (Sty p) stylolites, and fractures (F3) in a dolostone bed	156
Figure 5.4: Equal area, lower hemisphere stereographic projection of fracture orientation at four localities studied. (a) Cañón de La Escalera; (b) Cañón Boquilla Corral de Palmas; (c) Cañón de Los Chorros (d) Santa Rosa-Iturbide	160
Figure. 5.5a: Monomict, clast-supported breccia, showing rectangular shaped blocks, clast-supported breccia	162
Figure 5.5b: Solution breccia constituted of dolostones clasts and showing two fractures.....	163
Figure 5.5c: Dolomitized pellet packstone showing F2 calcite fractures partially replaced by fine grained D2 dolomite matrix	164
Figure 5.6.a: Dolostone beds showing F3 fractures cross cutting several carbonate beds (dolostone)	166
Figure 5.6b: F3 fracture with dolomite and calcite fill.....	167
Figure 5.7.a: Dolostone bed showing bedding perpendicular F4 fractures	169
Figure 5.7b: Wide vein in a dolostone.....	170
Figure 5.7c F4 fracture showing baroque dolomite (D3) bridges.....	171
Figure 5.7d: Detail of F4 fracture petrographic characteristics.....	172
Figure 5.7e: SEM-CL image showing F4 fractures with synkinematic D3 dolomite (light grey) and postkinematic C3 calcite (dark grey) cements mage showing F4 fractures	173
Figure 5.8a: En echelon F5 fractures in a dolostone bed	175

Figure 5.8b: F4 macrofracture filled with D3 baroque dolomite and C3 calcite	176
Figure 5.8c: Detail of Fig. 5.8b showing broken D3 baroque dolomite crystals	177
Figure 5.8d: View of the base of a carbonate mudstone bed showing relationship between F5 fracture (vein) and tectonic stylolites in Tamaulipas Inferior Formation	178
Figure 5.9a: Chevron fold showing flexural slip planes (Flx) containing twinned C3t calcite cement	180
Figure 5.9b: Outcrop of bedding-parallel fault (F6 fractures).....	181
Figure 5.9c: Detail of Fig. 5.9b showing a thick fibrous calcite sheet.	182
Figure 5.9d: Fibrous calcite from sample of Fig. 5.9c showing twins with sharp edges in large crystals	183
Figure 5.10: Fracture events and their corresponding cementations in the Cupido Formation	205
Figure 6.1: Location map of study localities, Monterrey Salient	219
Figure 6.2: Clean-room laboratory equipped with standard light parallel microscope and bench-top drill press with a dental drill bit for micro-sampling	225
Figure 6.3: Oxygen and carbon isotope plot for dolomite from the Cupido Formation.....	239

Figure 6.4	Same oxygen and carbon isotope data shown in Fig. 6.3 for dolomite from the Cupido Formation is plotted here and compared to the $\delta^{18}\text{O}$ range of “least altered” (i.e., isotopically heaviest) Cretaceous marine invertebrates and marine carbonate cements from Allan and Wiggins (1993).....	241
Figure 6.5	Cross-plot of oxygen and carbon isotopic composition of calcite cements from the Cupido and Tamaulipas Inferior Formations ...	256

Chapter 1. Introduction

BACKGROUND

From an economic point of view, water, oil, and gas are the most important fluids in the crust, and fractures are essential conduits for the flow of fluids in the Earth's upper crust (National Research Council, 1996). Within fracture networks, fluids flow through individual fractures that vary in size from the largest faults down to microfractures (Barton et al., 1988; Marrett et al., 1999; Olson et al., 2009). Consequently, a broad range of fracture sizes can play an important role in fluid flow. Many fracture systems in the deeper parts of sedimentary basins also contain, and locally are sealed by, natural mineral cements (Nelson, 1985; Laubach, 2003) although this aspect of fracture arrays has been mostly overlooked (for example, Hancock, 1985; Pollard and Aydin, 1988) until recently.

The preservation of open fractures depends on fracture size, fracture diagenesis, and in situ loading conditions. Accurate prediction of which beds in a sedimentary sequence are most likely to have open fractures and the most fracture-enhanced fluid flow has extremely important economic implications in oil reservoir characterization. The fluid-flow paths through fractures are difficult to predict because fractures typically vary significantly in size (Ortega et al., 2006), are heterogeneously developed in different sedimentary layers (Laubach et al., 2009) and may vary laterally over very short distances (Pollard and Aydin, 1988). Because of this heterogeneity, local data are required in order to characterize fracture attributes that control the flow of fluids in a specific area. Fracture data come from two main sources: subsurface boreholes and surface outcrops. Subsurface fracture data come mainly from oil and gas reservoirs while outcrop fracture data come from field observations from areas that may or may not be good analogs (guides) to structures in reservoir settings. Fracture orientation, spatial distribution, size (opening

displacement, aperture, length, height), opening displacement distribution, degree of mineral fill, and connectivity are the most important attributes for understanding the flow of fluids through fractures in a reservoir. Where fractures form and evolve in a chemically reactive environment such as the deeper parts of sedimentary basins (temperatures greater than about 50°C) or in highly reactive material such as carbonate rocks, both the fractures and their host rocks are susceptible to chemical changes. Recent documentation that some fractures grow slowly over tens of millions of years (Becker et al., 2010) underlines the likelihood that meaningful chemical and mechanical interactions are widespread. This area of concurrent structural and diagenetic processes is a little-explored aspect of structural geology and sedimentary petrology (Laubach et al., 2010). The most straightforward approach to investigate these issues would be thorough description of fracture systems and host rocks for arrays existing in the subsurface, but such an approach is infeasible owing to practical limits on subsurface sample volumes (National Research Council, 1996). It is possible to recognize and characterize fracture attributes directly from outcrops, but in the subsurface there are several problems that limit fracture observation. Therefore, as a primary approach this study is focused on outcrop fracture analyses, to develop a protocol that complement oil reservoir characterization studies.

The fundamental question this study addresses is whether rock mass diagenetic features, including cements, stylolites, and penetrative arrays of macroscopic and microfractures, are part of a continuum of deformation and chemical change such that analysis of the more readily sampled rock mass part of the deformed material can be used to make reliable estimates about attributes of other, unsampled parts of the array (for example, large fractures).

Carbonate rock outcrops of the Lower Cretaceous Cupido Formation, Sierra Madre Oriental (SMO) northeastern Mexico were selected as the main area of research for this study because this area is characterized by multiple fractures sets and abundant cement-filled opening-mode fractures (namely, veins). Easy access to the area and very good exposure of rocks were two more reasons to select this place to carry out fracture research. Determining the relationship between fracturing and diagenesis of these rocks was one of the main objectives of this study.

Data collected in this study include one of the first complete descriptions of fractures of the Cretaceous Cupido Formation dolostones and limestones and complete descriptions of the diagenesis of these rocks. The paragenetic sequence of cements and field observations of fractures (veins) were used to identify six main fracture events that were formed at different times and in different geological settings during the burial history of these rocks. Analysis of fracture-filling cements in particular demonstrated that different fracture events can be distinguished geochemically and integrated with the host-rock diagenetic history. Base on these relationships as a starting point, a protocol to characterize fracture events using core-scale samples and to predict attributes of macroscopic reservoir fractures away from the well bore can be developed.

FRACTURE DATA SOURCES

Fracture studies use data collected from subsurface and outcrops. However, fracture data collected from the subsurface are prone to several problems that limit fracture observation. Subsurface geological data come from two main sources: geophysical techniques (mainly seismic reflection) and borehole techniques. Even three-dimensional (3D) seismic data have critically limited resolution. At depths of 3 km the seismic resolution is typically 30 m (Yielding et al., 1996) yet few fractures have apertures larger than 1 cm. Therefore, with current methods fractures are unlikely to be resolved on surface-based seismic reflection data. Other techniques for seismic detection of fractures are still experimental (some are discussed in Marrett et al., 2007). Cores, image logs, dipole sonic logs, and production tests are the main borehole techniques used to collect fracture data in the subsurface (Nelson, 1985; Cosgrove and Engelder, 2004; Lonergan et al., 2007; Gale, 2008; Hennings, P. ed., AAPG Bulletin theme issue, November, 2009). However, these techniques also suffer from some significant problems. For steeply dipping fractures and vertical wellbores, none of the borehole techniques can detect fractures a significant distance beyond the borehole wall (typically about 1 meter for dipole sonic logs; Prioul and Jocker, 2009). Therefore, fracture data acquired with borehole techniques sample very small volumes in comparison with length scales of common fracture heterogeneity and provide virtually no opportunity to observe some critical fracture attributes (e.g., aperture distribution, spacing, length, and connectivity). In most cases boreholes encounter few macrofractures (i.e., fractures visible without optical magnification and measurable with hand tools; Stearns and Friedman, 1972) because a) both the boreholes and fractures commonly are nearly vertical, and b) macrofracture spacing commonly is much greater than borehole diameter, resulting in

grave under-sampling of subsurface fractures. Moreover, fractures can be modified in the subsurface by many processes related to burial, uplift, exhumation, and erosion that take place during geological history after fractures form (for example, fracture diagenesis; Laubach, 2003). In spite of this, we usually have to work with such incomplete data in the oil industry.

Data from outcrops avoids this sampling problem, since typically much larger areas can be examined, and outcrop datasets can encompass a broad range of fracture sizes. Fracture data collection is most limited by the amount of time required. Nonetheless, fracture properties observed in outcrops can be modified by many overprinting processes such as diagenesis, as is the case in the subsurface, as well as fracture growth due to unloading and exposure (Engelder, 1985; English, in press). Because cements can record temperature information and relative timing patterns through overlapping and crosscutting relations, diagenetic studies can help in part to resolve overprinted processes related to burial, uplift, exhumation, and erosion.

Although open macrofractures are rightly viewed as being the primary control on fluid flow through fractured rock because they are open and persistent (Philip et al., 2005), study of microfractures (those fractures visible only under magnification; Laubach, 1997) avoids the subsurface fracture-sampling problem because microfractures are commonly much more abundant than macrofractures (for example, Marrett et al., 1999). In fact, in many siliciclastic petroleum reservoirs microfractures are common enough that they can be sampled effectively even in volumes of rock as small as a thin section (Laubach, 1989; Laubach et al., 1995; Hooker et al., 2009). Previous outcrop studies (Laubach, 1988a; Ortega and Marrett, 1997; Marrett et al., 1999) have shown that some microfracture attributes can be extrapolated to reservoir scale. Data from these and

other studies support the notions that fractures follow systematic patterns of size distribution, in many cases power-law aperture-size scaling, and that extrapolation of scaling relationships determined at one scale range provide accurate predictions of fracture sizes at other ranges of scale (Yielding et al., 1996; Needham et al., 1996; Marrett et al., 1999; Ortega et al., 2006; Laubach and Ward, 2006; Hooker et al., 2009). This implies that microfractures and macrofractures represent different size fractions of the same populations, so that microfractures can provide useful quantitative information about critical attributes of macrofractures and their impact on fluid flow in a reservoir.

Fractures are pores that form at some point after consolidation (usually) and thus they are like secondary pores and can record aspects of a rock's diagenetic history. However, since fractures have a wide range of sizes, size can matter in what information can be recorded in fractures. In other words, fractures of different sizes may record different aspects of the diagenetic story (Laubach, 2003). An observation in siliciclastic rocks is that in many places there is a characteristic opening-displacement size below which microfractures are sealed with cement broadly contemporaneous with fracture growth, but above which large fractures may be open or contain cements deposited at much later times (for example, after fractures cease growing), (Laubach, 2003; Gale et al., 2010). The cause of this pattern is, primarily, the temperature- and crystal-morphology-controlled rates of quartz cement accumulation (Laubach et al., 2004; Lander et al., 2008; Olson et al., 2009). Although some modeling of dolomite cement precipitation processes in dolostone fractures suggests that a similar processes should be expected in dolostones (Gale et al., 2010), little systematic research has been done on documenting such processes in carbonate rocks or on developing an understanding of how fracturing and diagenesis are interrelated in carbonate rocks.

Therefore outcrop-based study of the main processes that govern fracturing in carbonate rocks and study of interrelationships between fracturing and diagenesis using both macro- and microfracture data can be used to understand fundamental controls on fracture occurrence and pore space preservation and help guide the study of fractures in the subsurface, where data are scarce.

PURPOSE

The aim of my study is to understand fracture development in the context of carbonate diagenetic processes. A specific aim is to develop a protocol to identify the main open fracture sets in subsurface carbonate rocks and to interpret their origins based on understanding relationships between fracturing and diagenetic processes. This study uses veins (opening-mode fractures and small faults having local opening displacement filled with mineral cement) as the main source of fracture data. The role of syn- and post-fracturing in the preservation of fracture porosity is incorporated into this protocol.

HYPOTHESES

The hypotheses proposed and tested by this research are as follows:

- There are intrinsic relationships between fracturing and diagenesis. In particular, mineral fill (cement) precipitated during and post-fracturing provides key elements to understand the diagenetic history of these fractures and constrains the origin, timing and conditions under which fracturing occurred.

- With an understanding of cement-fracture relationships, we can apply this knowledge to the subsurface. Similar relationships in the subsurface are expected where the geological processes that govern fracturing are similar. If this is true, then we can use limited diagenesis and microfracture observations to determine the main fracture sets that act as fluid conduits in the subsurface.

OBJECTIVES

Data from carbonate rock outcrops of the Lower Cretaceous Cupido Formation in the SMO of northeastern Mexico are the basis of this study. These outcrops are characterized by multiple fracture sets and abundant cement-filled opening-mode fractures. As demonstrated in this study, many aspects of these fractures resemble those found in core from oil and gas reservoir rocks. Numerous attempts have been made to interpret the origin and distribution of fractures in the SMO (e.g., Camerlo, 1998; Rico, 1999; Fischer and Jackson, 1999; Lu, 2000; Marrett and Laubach, 2001; Ortega, 2002; Ortega et al., 2006; Laubach and Ward, 2006; Guzzy-Arredondo et al., 2007; Gomez, 2007; Fischer et al., 2009; Ortega et al., 2010). Both syn-folding and pre-folding times of fracture formation have been postulated, but none of these interpretations have taken fracture diagenesis into account.

A primary objective of this study is to use outcrops to develop a subsurface protocol for understanding and predicting fracture characteristics in carbonate strata. Such a protocol must be based on the combined study of the main diagenetic processes along with fractures in carbonate rocks, in order to constrain the genesis and evolution of the rock-fracture system. The methodology to be used focuses on determinations of

fracture timing relative to other diagenetic processes, fracturing environment (e.g., syn-depositional, burial, tectonic, or exhumational) and interrelations between fracturing and cementation stages.

This methodology is based on the integration of independent diagenetic and fracture analyses of outcrop rocks. Three types of analyses were conducted in this investigation: First, field observations were used to differentiate facies, main fracture sets and tectonic features. The main fracture sets were determined by measuring the orientations of veins and observing cross-cutting relations. Second, petrographic analyses were used to identify the main diagenetic processes, and to determine the relative timing of diagenetic and fracture events. Cements in fractures and in host rock were classified as pre-, syn- or postkinematic depending on whether they precipitated before, during, or after fractures of a particular set opened (Laubach, 1988; 2003). Finally, stable isotope analyses (specifically $\delta^{13}\text{C}$ and $\delta^{18}\text{O}$) of samples from both host rocks and fractures were used to constrain the possible origin and conditions of precipitation of fracture-filling cements. Understanding of the main diagenetic processes along with fracturing in carbonate rocks constrains the genesis and evolution of the combined rock-fracture system.

SIGNIFICANCE OF THE STUDY

This study characterized the fracturing and diagenesis of Lower Cretaceous Cupido Formation rocks. Fractures in this study are opening-mode fractures (or extension fractures) having small to moderate height-to-aperture ratios. These fractures are now filled with cement, and so could be termed veins, but cement textures show that in the past they possessed significant open pore space, probably for extended periods of time, as

will be discussed. Based on field observations, six main fracture events were identified in this carbonate sequence. Petrographic and geochemical analyses corroborated that fractures resulting from these six fracture events have different characteristics and origins. Fracture cement characteristics are clearly different in each fracture set. Different mineral cements in the fractures provide a basis to interpret the timing and origin of the fracturing events.

The main fracture-filling mineral phases identified in the Cupido Formation carbonates are dolomite and calcite. Based on the geochemical results and the occurrence of isolated cement deposits in the form of dolomite pillars and bridges in some fractures, some with crack-seal texture, I infer that dolomite may have precipitated progressively in fractures as they opened. Calcite, in many fractures, filled remnant fracture porosity that persisted after fracture growth. Therefore, for several of the fracture sets dolomite was precipitated as synkinematic cement whereas calcite as postkinematic cement. Synkinematic cementation is genetically related to fracturing but postkinematic cementation commonly governs the current-day porosity of fractures. A finding of this study is that these two diagenetic processes fundamentally controlled the evolution of fracture porosity in these rocks. These results are likely generally applicable to dolostones in other regions.

The diagenetic history (paragenetic sequence) documented in this study supports the field interpretation of at least six major fracture events in the Monterrey Salient. The results of this research provide direct evidence for intrinsic relationships between fracturing and diagenetic events: both diagenesis and fracturing modify mechanical properties of a rock mass. Diagenesis can affect fracturing and the fracturing can enhance diagenetic processes, for example, by providing conduits for introducing reactive fluids.

Chapter 2. Geology of Monterrey Salient, Sierra Madre Oriental, Mexico.

INTRODUCTION TO MONTERREY SALIENT

The regional geology of the Monterrey Salient, in the SMO of northeastern Mexico, has been studied for more than eight decades; however, detailed studies of fractures in this marvelous area have only been carried out recently. As a small contribution to the geology of this area, this dissertation describes three stratigraphic sections (columns) measured in the Monterrey Salient. The columns represent more than 900 m of carbonate section in which bed thickness, lithology, sedimentary facies, and structural features were recorded. The columns were measured to document the stratigraphic position of sedimentary beds used in the study of fracture-diagenesis, the main topic of the following chapters of this dissertation. The columns and their descriptions can be used in geological studies related with other attributes of fractures, such as spacing, length or connectivity.

Moreover the area has good exposures due to the semiarid climate, good access, and also several deeply incised canyons cut through large tectonic folds. This physiography also makes the site ideal to study stratigraphy and the relationships between lithofacies, diagenesis and fractures.

BACKGROUND: PREVIOUS WORK

The geology of the SMO was first studied during the 1920s, when several workers (e.g., Bose, 1923) made preliminary reconnaissance surveys. Regional structural interpretations were made during the 1950s and 1960s (e.g., De Cerna, 1955, 1956; Wall et al., 1961). During the 1970s and 1980s more detailed structural and stratigraphic studies were done (e.g., Wilson and Piali, 1977; Padilla y Sanchez, 1985; Campa, 1985). Sequence stratigraphic and structural analyses were the types of studies conducted during the 1990s (e.g., Wilson, 1990; Eguiluz de Antuñano, 1991; Goldhammer et al., 1991; Marrett and Aranda García, 1999). Most of these studies have focused on the Monterrey Salient as an area to explore the stratigraphy and structure of this fold belt because the Cretaceous rocks exposed are arguably excellent examples of rocks found at depth in the nearby Gulf of Mexico Basin (Goldhammer et al., 1991), and structures are good examples of salt-detached fold belts and oroclines (Marrett and Aranda García, 1999).

STUDY AREA: MONTERREY SALIENT

The field area for this study is located in the Monterrey Salient of the SMO (Fig. 2.1). The SMO is the contiguous southern portion of the Laramide-aged North American Cordillera thrust belt (Campa, 1985). The SMO forms a regional salient (Fig. 2.2) about 600 km wide between Torreón and Valles named the SMO Salient (Marrett and Aranda-García, 2001). Structures trend approximately to the west on the northern side of this salient and along the eastern side approximately to the north (Marrett and Aranda-García, 2001). The Monterrey Salient is an approximately 100 km-wide curved fold belt developed in the northeastern-most deformation front of the SMO (Eguiluz de Antuñano,

1991). The approximately 9,000 km² area is dominated by ~ 5-10 km wavelength detachment folds (Padilla y Sánchez, 1985).



Fig. 2.1. Location map of study area, Monterrey Salient, Mexico. The map shows the main physiographic features of Mexico and study area used in this dissertation. Square encompasses the Monterrey Salient, SMO.

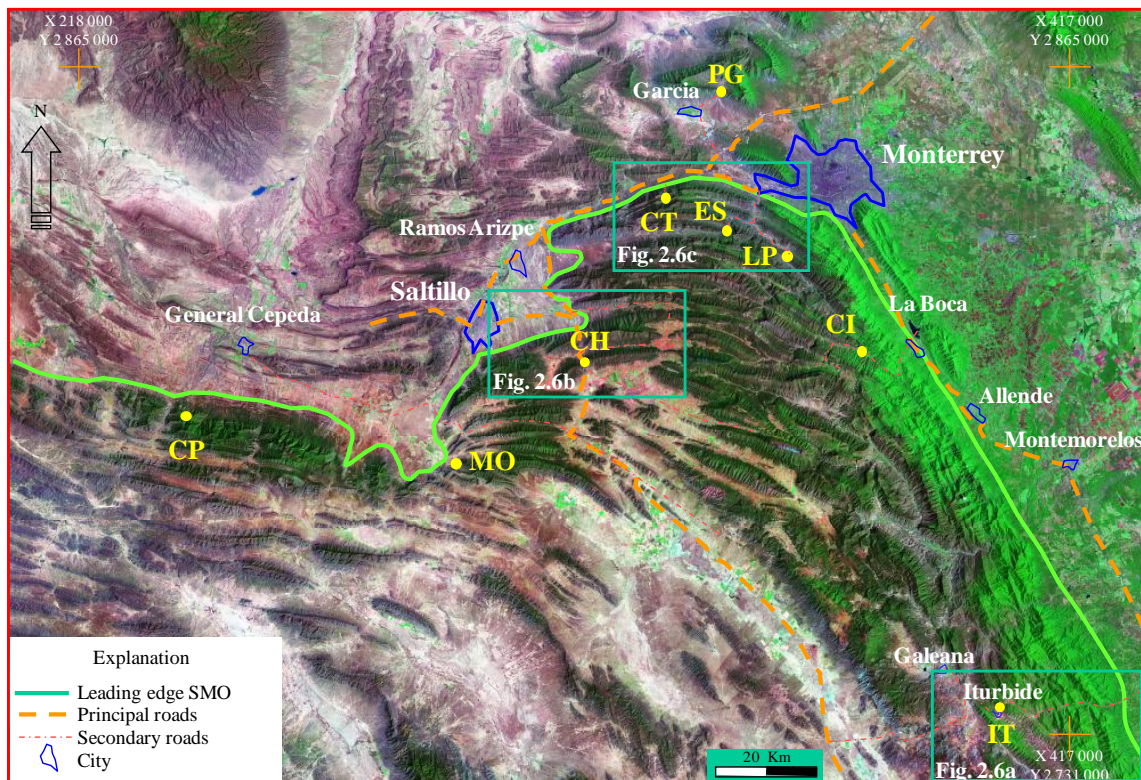


Fig. 2.2. Landsat TM satellite image of part of the SMO, showing the Monterrey Salient. Circles mark outcrop and sample localities: PG, Potrero García; CT, Cañón de las Cortinas; CH, Cañón de los Chorros; ES, Cañón la Escalera; LP, Cañón Boquilla Corral de Palmas; IT, Cañón Santa Rosa-Iturbide; MO, Molano Fault; CP, Cañón Prieto; CI, Cienegas. X and Y are coordinates in the Universal Transverse Mercator (UTM) Projection indicated by small crosses. Main cities and towns are labeled. Continuous line approximates the thin-skinned deformation front, as delimited by lateral continuous exposure of Jurassic-Cretaceous carbonate strata. Dashed lines show main roads. X and Y are coordinates in the Universal Transverse Mercator (UTM) Projection indicated by small crosses. Foreland is to the north and northeast. Rectangles are locations of more detailed satellite images of figures 2.6a, 2.6b and 2.6c.

Outcrops and samples from four canyons are the main basis of this research: Cañón de los Chorros, Cañón la Escalera, Cañón Boquilla Corral de Palmas and Cañón Santa Rosa (Fig. 2.2). Samples from four additional localities within the SMO were also included: Cañón de las Cortinas, Cañón Prieto, Molano Fault, and Cienegas. Finally, samples from Potrero García (Fig. 2.2) outside of the SMO also were included in order to compare rocks in the fold belt with a less deformed area.

Most of the outcrops and samples studied represent carbonate strata of the Cretaceous Cupido Formation; however, a few outcrops and samples from Taraises and Tamaulipas Inferior Formations are included in this study as well to represent both platformal and basinal facies.

GEOLOGIC SETTING

The SMO is a Laramide-age, thin-skinned fold and thrust belt that deformed basinal and platformal sequences composed mainly of carbonate strata of Mesozoic and early Tertiary age (Padilla y Sánchez, 1982, 1985; Suter, 1984; Campa, 1985; Aranda-García, 1991). The carbonate rock sequence is composed of several second-order depositional supersequences (Goldhammer, 1999), which were deposited during and following the opening of the Gulf of Mexico (Wilson, 1990).

The folds of the SMO Salient contracted the Upper Jurassic to Paleogene stratigraphic section above Upper Jurassic evaporites overlying siliciclastic rift-related strata and crystalline basement. The crystalline basement beneath the SMO was only locally involved in Laramide-age deformation (Marrett and Aranda-García, 1999), and where exposed consists of a variety of sedimentary rocks, schists, gneisses, and intrusive rocks of Triassic, Paleozoic, and Precambrian ages (Wilson, 1990). The Upper Jurassic

decollement strata typically occupy the cores of large-amplitude anticlines and contain evaporite (anhydrite) deposits that occur through much of the SMO Salient (Marrett and Aranda-García, 1999). The evaporites constitute a regional decollement that underlies detachment folds (Jamison, 1987) in the Upper Jurassic through Upper Cretaceous strata (Marrett and Aranda-García, 1999; Eguiluz de Antuñano, et al., 2000).

A more than eighty-kilometer long fold train of 4-8 kilometer wavelength folds dominates the structural style within the Monterrey Salient (de Cerna, 1956; Padilla y Sánchez, 1982). The structural geometry exposed in the Salient is characterized by large-amplitude folds that typically have tight to isoclinal, upright geometries. Major thrust faults are mostly absent within the Salient (de Cerna, 1956; Padilla y Sánchez, 1982, Marrett and Aranda-García, 1999); shortening was accommodated primarily through folding. The boundary of the Monterrey Salient locally has a different structural style: Southwest of the Monterrey Salient is an area dominated by series of stacked ramp anticlines (de Cerna, 1956; Quintero-Legorreta and Aranda-García, 1985; Padilla y Sánchez, 1982, Marrett and Aranda-García, 1999). The Laramide tectonic front along the eastern side of the Monterrey Salient is dominated by a large frontal thrust (Fig. 2.3). The northern deformation front is dominated by a series of unfaulted kilometer-scale anticlines.

The age of local deformation within the study area is not well constrained, however, the youngest strata affected by contractional deformation in the SMO are Eocene (e.g., Padilla y Sánchez, 1985; Vega-Vera and others, 1989; Gray and Johnson, 1995) suggesting that deformation in the SMO ceased during the Eocene. Lack of angular unconformity in the Paleocene and older strata indicated local deformation began after this period.

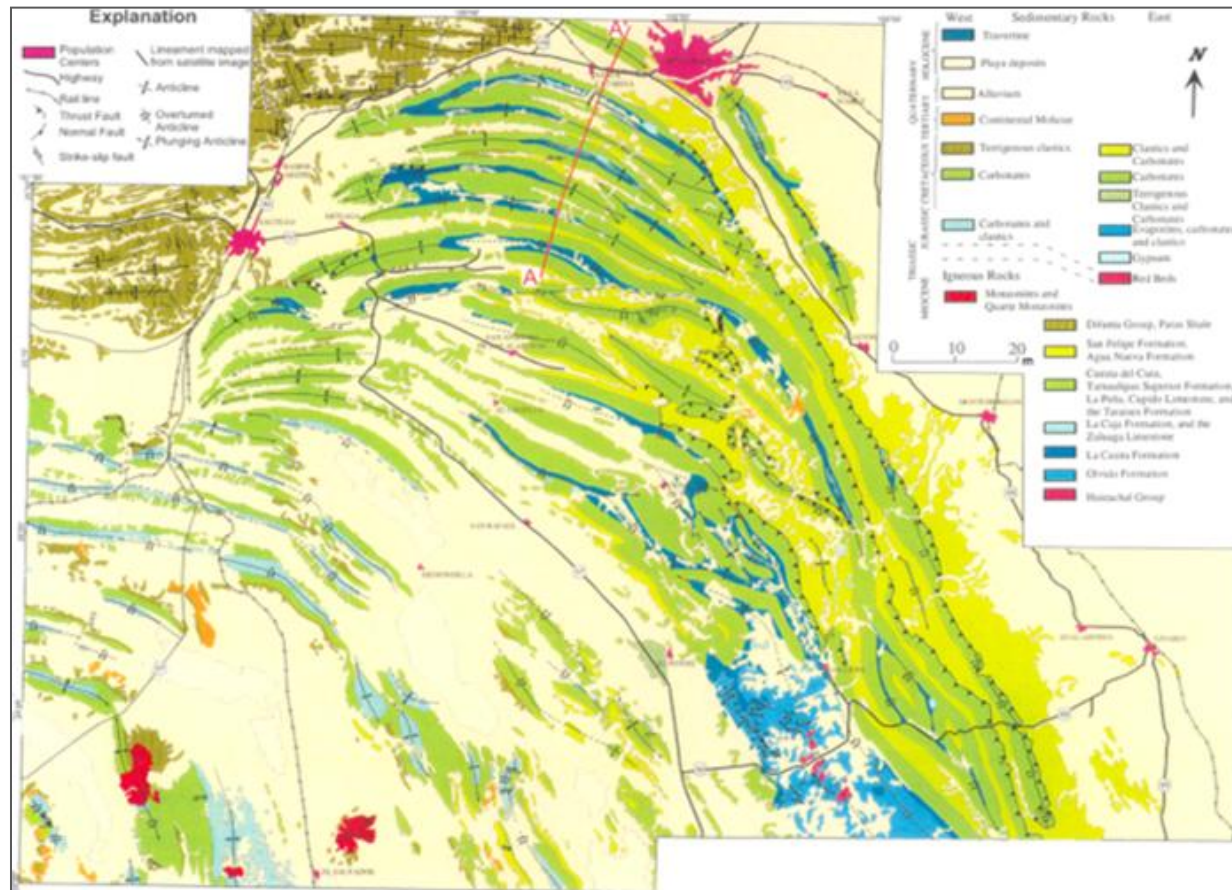


Fig. 2.3. Geologic map of the Monterrey Salient (modified from Padilla y Sanchez, 1985; Marrett and Eguluz de Antuñano, 2001).

Regional Stratigraphy

The stratigraphy of northeastern Mexico has been studied for more than 65 years and is well documented (Imlay, 1936; Humphrey, 1949; Conklin and Moore, 1977; Smith, 1981; Campa, 1985; Padilla y Sánchez, 1985; Quintero-Legorreta and Aranda García, 1985; Wilson, 1989; Eguluz de Antuñano, 1990; Goldhammer and Lehmann, 1991; Goldhammer et al., 1991, Goldhammer, 1999; Lehmann et al., 1999, and Giles and Lawton, 1999). Below is a brief review of the part of the stratigraphy important to this study.

The Middle Jurassic to Lower Cretaceous stratigraphy of northeastern Mexico (Fig. 2.4) can be subdivided into four major, second-order depositional supersequences (~15 m.y. duration), defined as large regionally correlative, retrogradational to aggradational-progradational accommodation packages (Goldhammer et al., 1991). These supersequences are: supersequence 1 from Upper Bathonian to Lower Kimmeridgian (158.5-144 Ma); supersequence 2 from Lower Kimmeridgian to Berriasian (144-128.5 Ma); supersequence 3 from Valanginian to Lower Aptian (128.5-112 Ma); and supersequence 4 from Lower Aptian to Albian (112-98 Ma) (Goldhammer, 1999). Second-order sequence boundary ages are approximations.

These supersequences are: supersequence 1 from Upper Bathonian to Lower Kimmeridgian (158.5-144 Ma); supersequence 2 from Lower Kimmeridgian to Berriasian (144-128.5 Ma); supersequence 3 from Valanginian to Lower Aptian (128.5-112 Ma); and supersequence 4 from Lower Aptian to Albian (112-98 Ma) (Goldhammer, 1999). Second-order sequence boundary ages are approximations.

TEXAS

N.E. MEXICO

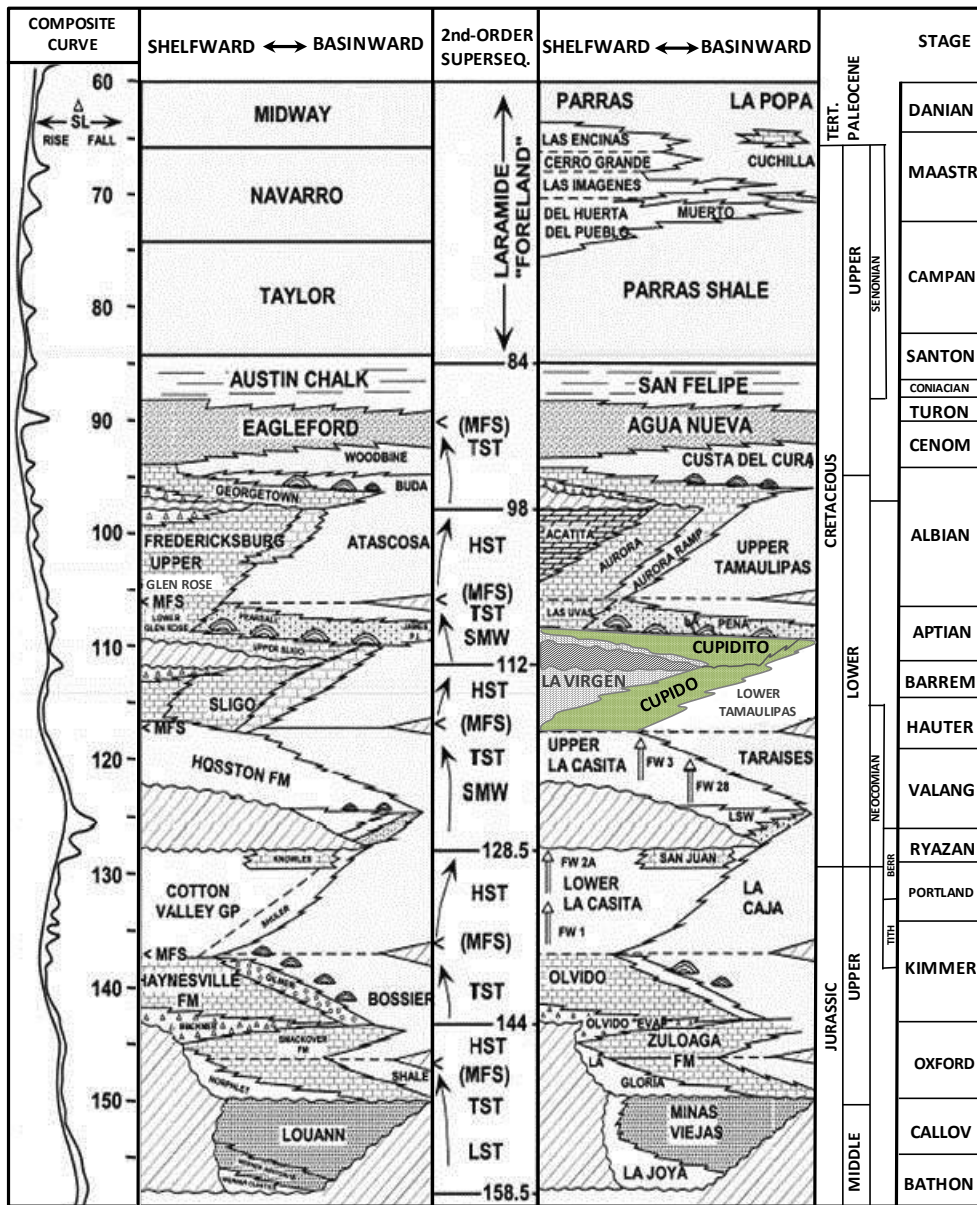


Fig. 2.4. Chronostratigraphic chart for northeastern Mexico and Texas Gulf Coast showing second-order supersequences as interpreted by Goldhammer et al. (1991).

A schematic, dip-oriented regional stratigraphic cross section, taken from Goldhammer (1991), shows the formational stratigraphy and lithologies of the major second-order supersequences for northeastern Mexico (Fig. 2.5). Major second-order supersequences are defined as large-scale basin-fill cycles marked by regionally correlative facies patterns of retrogradation and progradation (Goldhammer, 1999). Outcrops of the SMO in the study area are dominated by carbonate strata of the Cupido Formation, which is Hauterivian to early Aptian in age (McFarlan and Stone, 1977; Conklin and Moore, 1977; Wilson and Pialli, 1977; Goldhammer et al., 1991) and is equivalent to the Sligo Formation of the northern Gulf of Mexico (Fig. 2.4). The Cupido Formation and its basinal equivalent, the Tamaulipas Inferior Formation, overlie the La Casita and Taraises formations (McFarlan and Stone, 1977; Conklin and Moore, 1977; Wilson and Selvius, 1984).

The top of the Cupido Formation is marked by the onlapping La Peña Formation (3-9 m thick) that consists of deep-water shales and argillaceous carbonates (Figs. 2.4 and 2.5). In general, the Cupido Formation (700-1200 m thick) consists of several third order depositional sequences which in turn are made up of higher frequency fourth-order depositional sequences, on the order of 20-65 m thick (Goldhammer and Lehmann, 1991). Fourth order sequences in turn are made up of upward shallowing meter-scale, fifth-order cycles. The uppermost part of the Cupido Formation is known informally as the Cupidito member. This unit was introduced by Wilson and Pialli (1977) to designate the Upper Cupido transgressive interval below the La Peña Fm. Cupidito thickness varies laterally from ~100 m near the Cupido margin (e.g., Potrero García and Potrero Chico) to only a few meters in updip platform interior positions (e.g., Huasteca and Los Chorros) (Goldhammer, 1999).

The lower boundary of Cupidito is marked in many areas by a prominent 2 m thick bed of calcitized evaporite solution breccia within peritidal facies (Goldhammer and Kaufman, 1995). In summary the Cupido Formation consists of a thick platformal succession composed of hundreds of meter-scale upward-shallowing carbonate cycles (Goldhammer and Lehmann, 1991). Complete discussions of the SMO stratigraphy, facies, depositional environments, average thicknesses, and petrography are provided by references cited above.

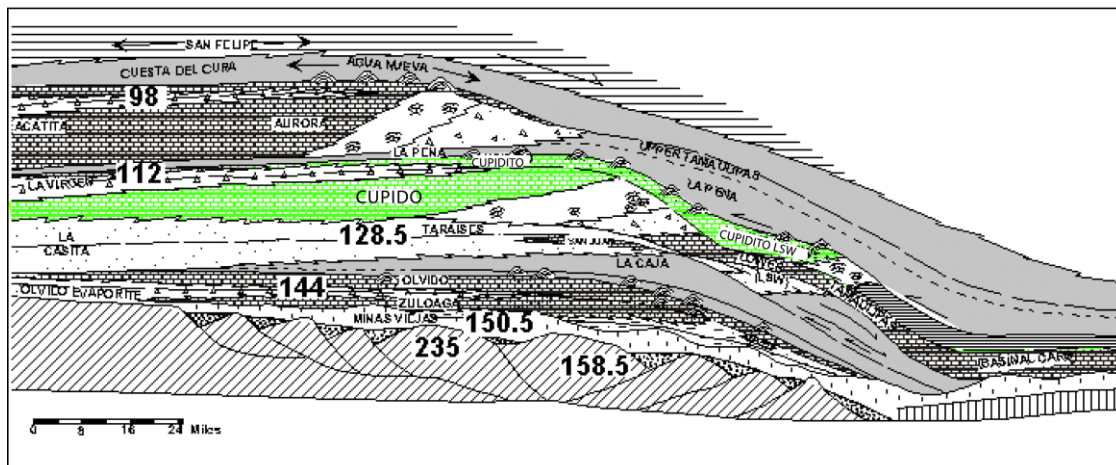


Fig. 2.5. Schematic dip-oriented regional stratigraphic cross-section trending north-northwest to south-southeast. Major second-order supersequence boundaries are shown (approximate ages in Ma). Major second-order supersequences are defined as large-scale basin fill cycles marked by regionally correlative facies patterns of retrogradation and progradation. After Goldhammer et al. (1991).

Local Stratigraphy

Stratigraphic columns

More than 900 m of stratigraphic column were measured in the field as part of my study to provide a stratigraphic context for layers studied in detail. Stratigraphic columns were measured, using a tape and compass, in the following localities: Cañón de los Chorros, Cañón la Escalera, and Cañón Santa Rosa (Fig. 2.2). Additionally, a stratigraphic column of Cañón Boquilla Corral de Palmas from Ortega (2002) is used in my study as context for the diagenetic and structural data I collected. Bed thicknesses, lithology, sedimentary facies, and structural features were described in the field. Sampled bed numbers are indicated in the stratigraphic columns. The following section describes the stratigraphic columns. The ranges for bed thickness (bt) used in this study are based on the classification of Campbell (1967): thin-bedded ($bt < 0.1$ m), medium-bedded ($0.1 \text{ m} < bt < 0.3$ m), and thick-bedded ($bt > 0.3$ m).

Plate I (Appendix 2.1) shows the stratigraphic column of the uppermost part of the La Casita Formation (106 m thick), the Taraises Formation (~20 m thick), and the Lower part of the Tamaulipas Inferior Formation (206 m thick). This column was measured at Cañón Santa Rosa from the forelimb of Iturbide anticline (Fig. 2.6a). The lowest 106 m of this section belongs to La Casita Formation and consists of cyclic alternations of thin-bedded brown shales and fine-grained sandstones overlain by medium-bedded mudstones. The Taraises Formation is represented by ~ 20 m of thin-bedded brown shales intercalated with medium-bedded dark brown shaly carbonate mudstones. The upper 206 m of the section belongs to the Tamaulipas Inferior Formation (basinal equivalent to the Cupido Formation) and is composed of thin- to thick-bedded

brown argillaceous carbonate mudstones intercalated with thin- to thick-bedded cherty carbonate mudstones (more abundant at the top of the section) and a few thin- to medium-bedded black shales.

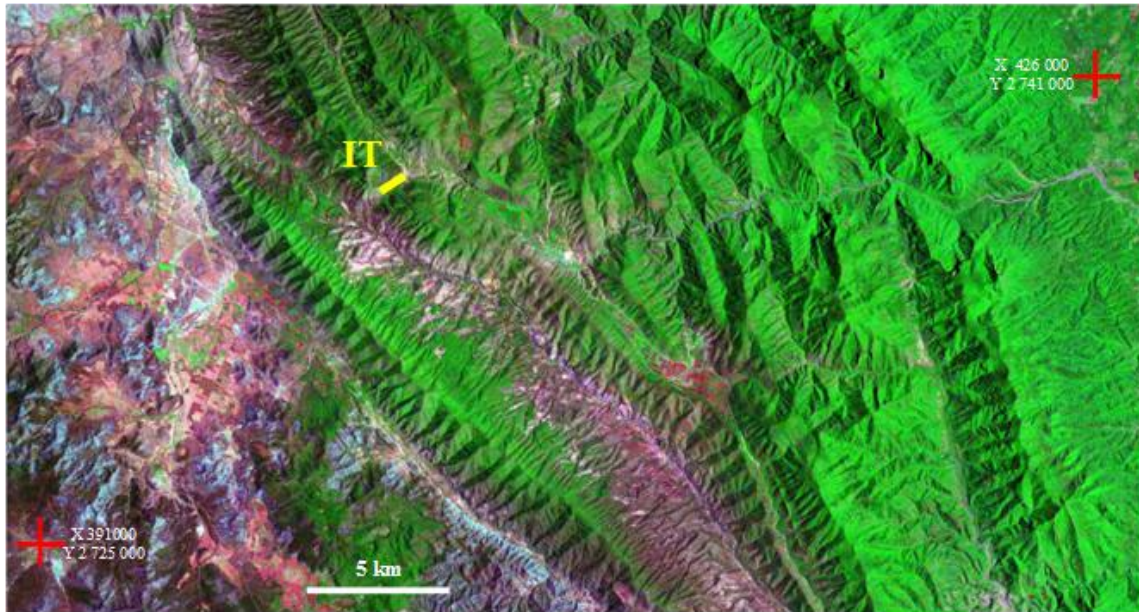


Fig. 2.6a. Thematic mapper satellite image of the Santa Rosa area, showing the measured stratigraphic column location. Short line marks measured stratigraphic column at Cañón Santa Rosa-Iturbide (IT). X and Y are coordinates in the Universal Transverse Mercator (UTM) Projection indicated by small crosses.

Plate II (Appendix 2.1) is a stratigraphic column from the backlimb of El Chorro anticline at Cañon de los Chorros (Fig. 2.6b). The column is about 374 meters thick and represents the upper part of the Cupido Formation, the Cupidito member, and the La Peña Formation (~10 m thick). The Cupido Formation is composed of cyclic alternations of thin- to thick-bedded dark gray limestones (packstone-grainstones), thick-bedded dark

gray limestones (grainstones), thin to medium-bedded gray rudist banks, thin-bedded light gray cryptalgal laminites, medium- to thick-bedded dark gray sedimentary breccias, thin- to thick-bedded gray dolostones, and medium- to thick dark gray dolo-limestones. The Cupidito member is composed of medium-bedded gray burrowed limestones (wackestones), and medium- to thick-bedded gray limestones (packstones). Finally, La Peña Formation comprises ~ 5 m of dark gray to brown shales interbedded with thick-bedded dark gray calcareous shales.

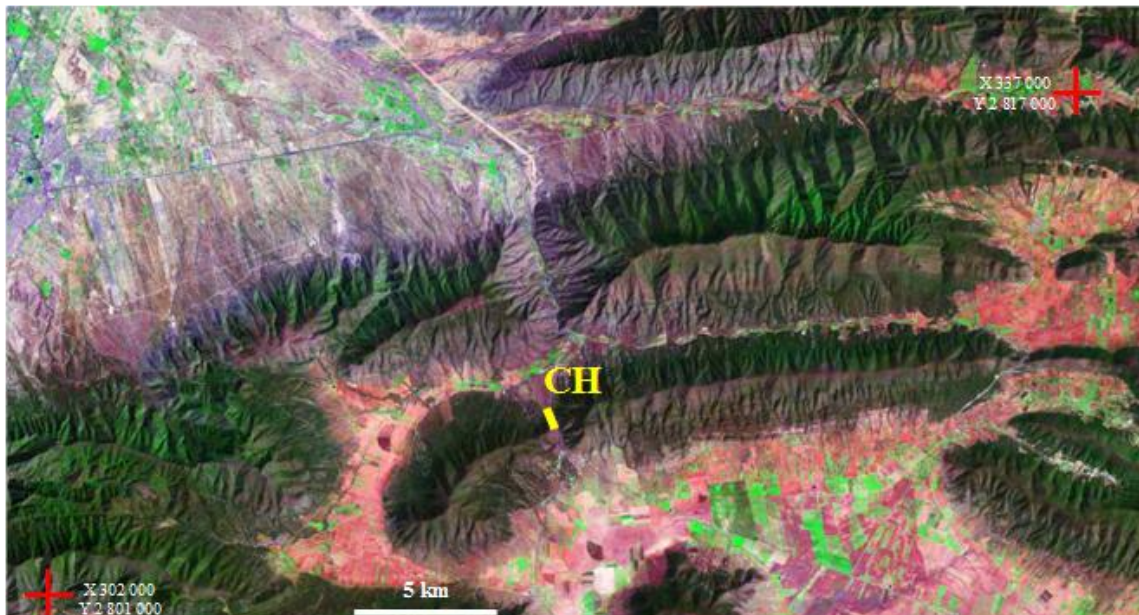


Fig. 2.6b. Thematic mapper satellite image of the Cañón de los Chorros area, showing the measured stratigraphic column location. Short line marks measured stratigraphic column at Cañón de los Chorros (CH). X and Y are coordinates in the Universal Transverse Mercator (UTM) Projection indicated by small crosses.

Plate III (Appendix 2.1) is a stratigraphic column from the backlimb of San Blas anticline in Cañón la Escalera (Fig. 2.6c). The column is about 206 m thick and represents the upper part of the Cupido Formation and probably the base of the Cupidito member. This stratigraphic column is composed of cyclic alternations of thin- to thick-bedded light gray algal mats, thin- to thick-bedded gray to light brown solution collapse breccias, thin- to thick-bedded gray dolostones, medium- to thick-bedded dark gray dolo-limestones, medium- to thick-bedded to massive gray rudist banks, and brown thick-bedded shaly limestones.

Plate IV (Appendix 2.1) modified in part from Ortega (2002) and is a stratigraphic column representing the upper part of Cupido Formation (64 m thick) and the bottom of Cupidito member (25 m thick) from the forelimb of San Blas anticline in Cañón Boquilla Corral de Palmas (Fig. 2.6c). This section is composed of sedimentary breccias, collapse solution breccias, limestones (wackestone/packstone of bioclasts), bivalve (rudist) banks, burrowed limestones (grainstones), dolostones, dolo-limestones and algal laminites. Thickness of these beds varies from 0.01 m (e.g., laminites) to 2 m (e.g., rudist bank).

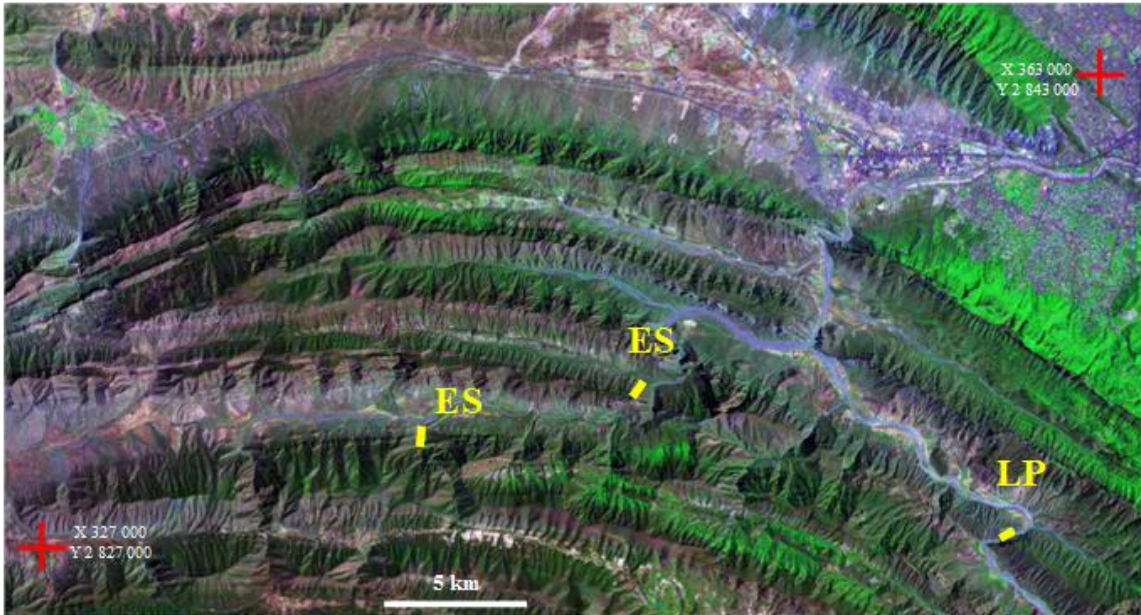


Fig. 2.6c. Thematic mapper satellite image of the Cañón Huasteca area, showing the measured stratigraphic columns locations. Short lines mark measured stratigraphic columns at Cañón la Escalera (ES) and Cañón Boquilla Corral de Palmas (LP) localities. X and Y are coordinates in the Universal Transverse Mercator (UTM) Projection indicated by small crosses.

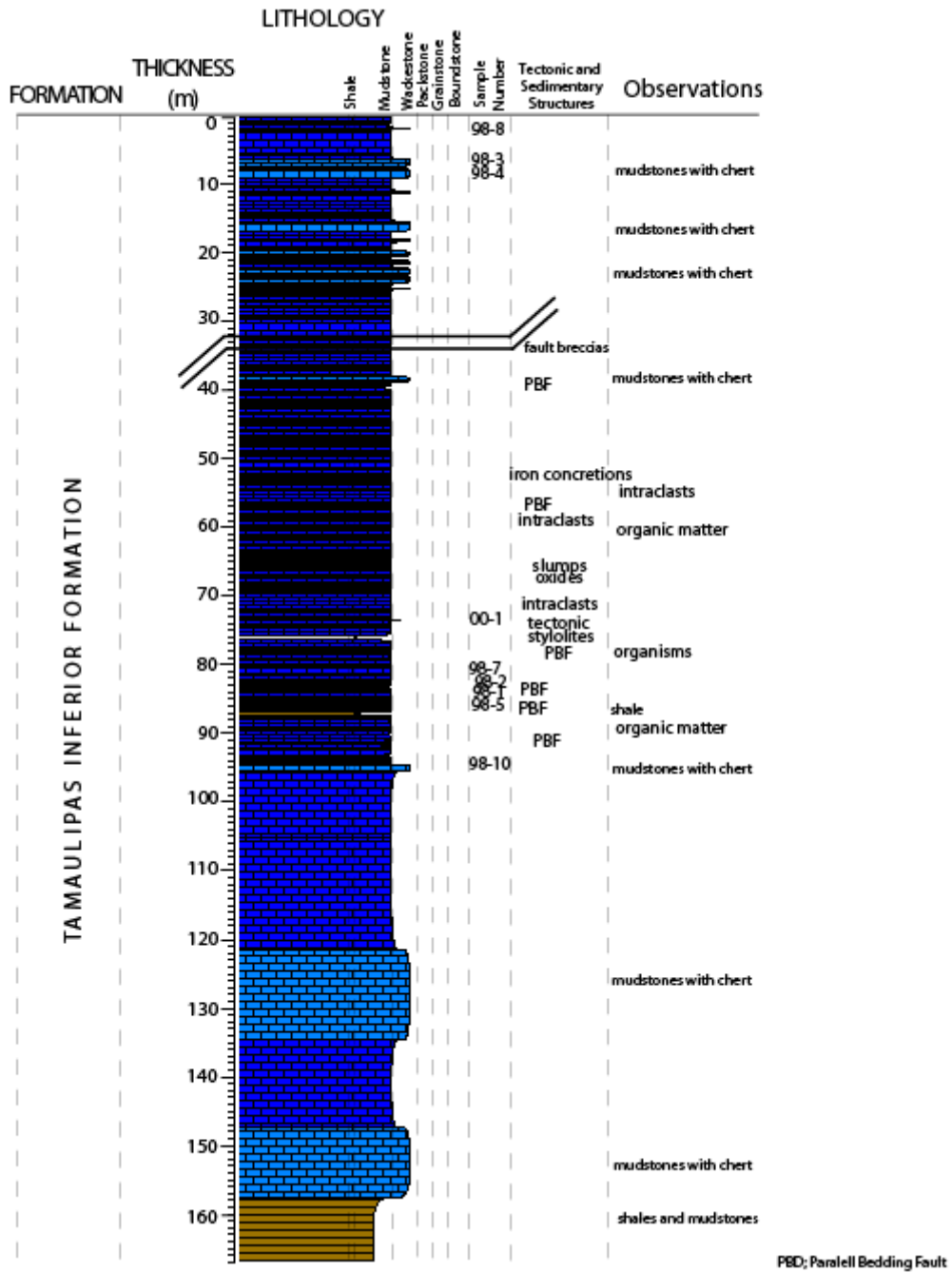


Plate I. Type Section of the Tamaulipas Inferior Formation at Santa Rosa-Iturbide locality

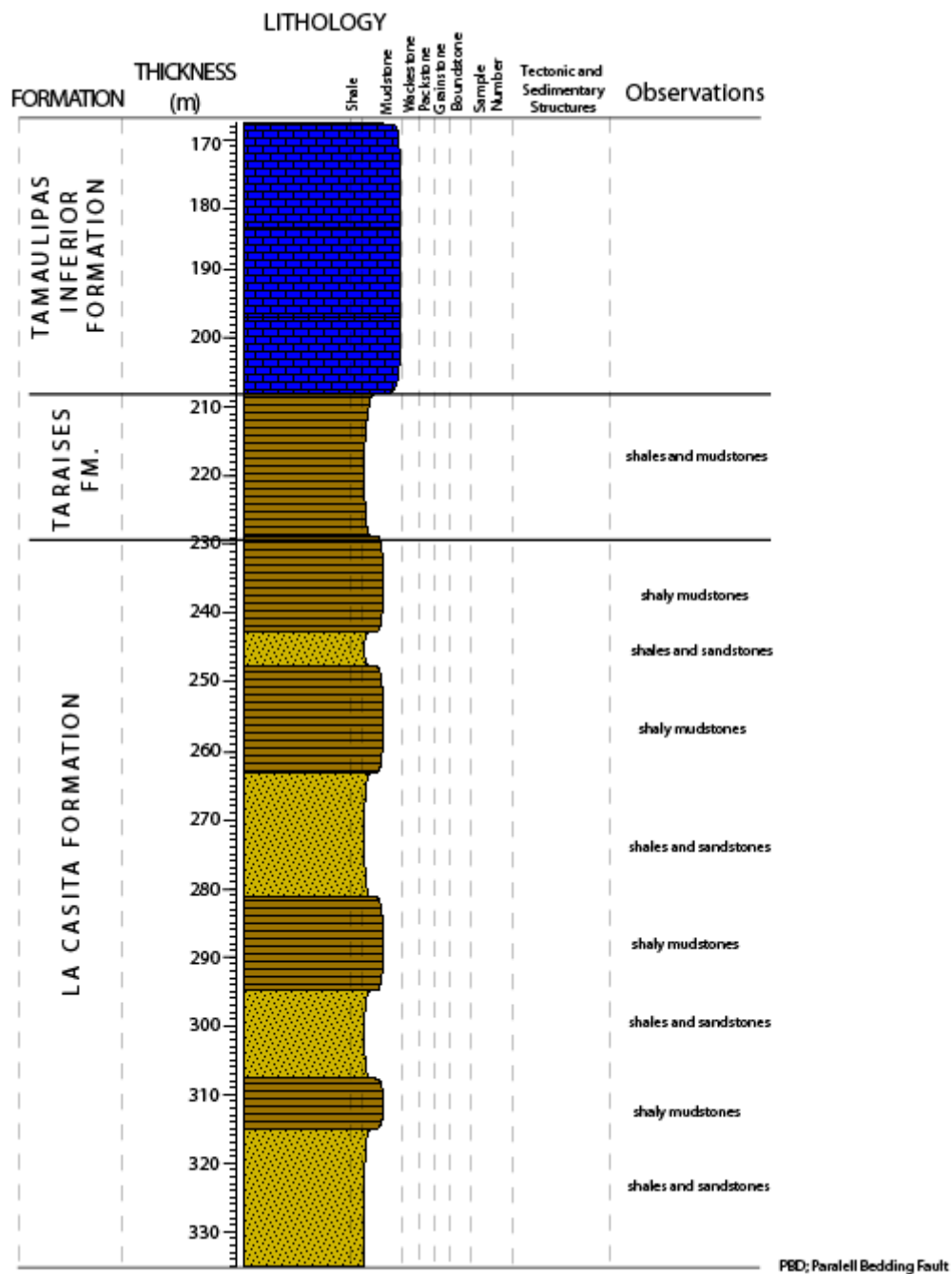


Plate I. Type Section of the Tamaulipas Inferior Formation at Santa Rosa-Iturbide locality (Continued)

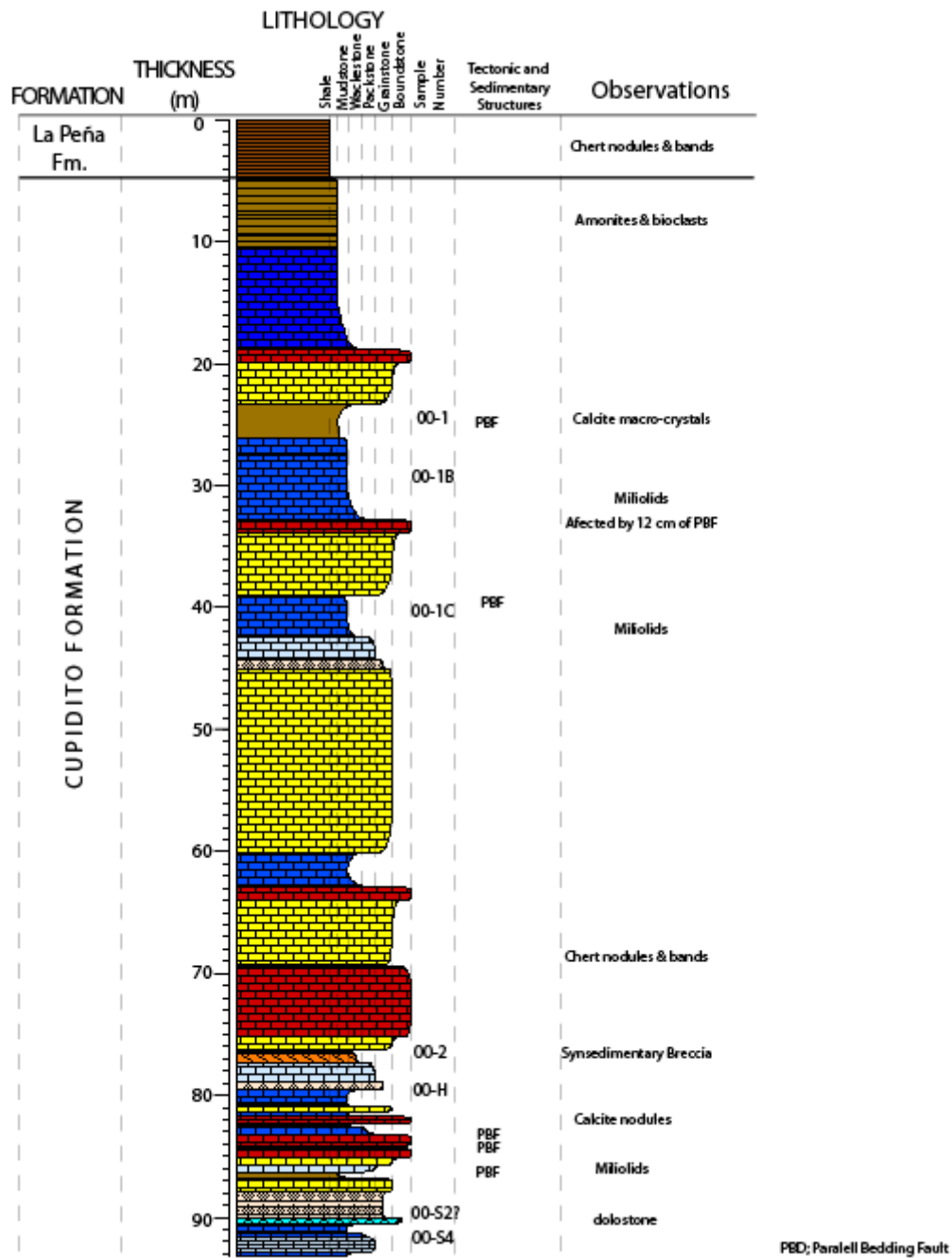


Plate II. Type Section of the Cupido and La Peña Formations at Los Chorros Locality

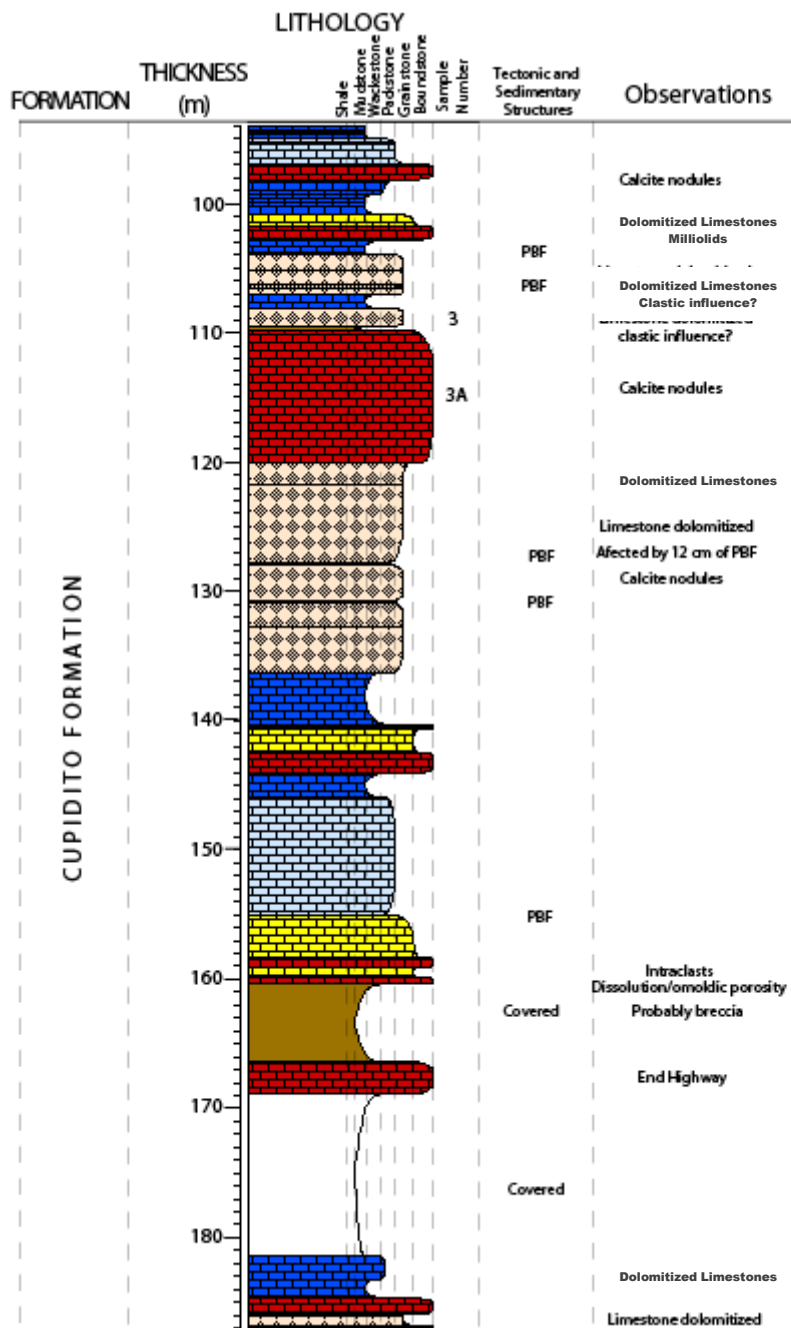


Plate II. Type Section of the Cupido and La Peña Formations at Los Chorros Locality (Continued)

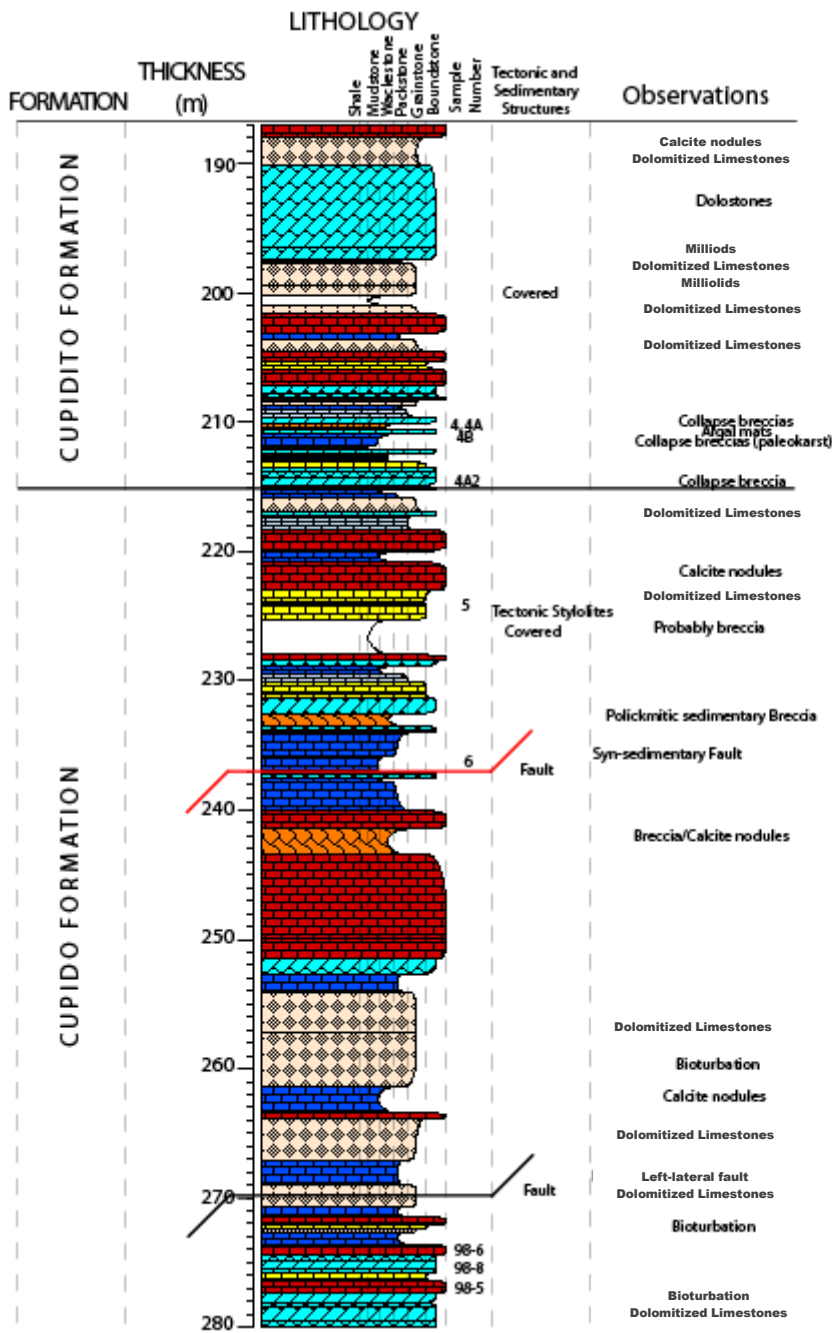


Plate II. Type Section of the Cupido and La Peña Formations at Los Chorros Locality (Continued)

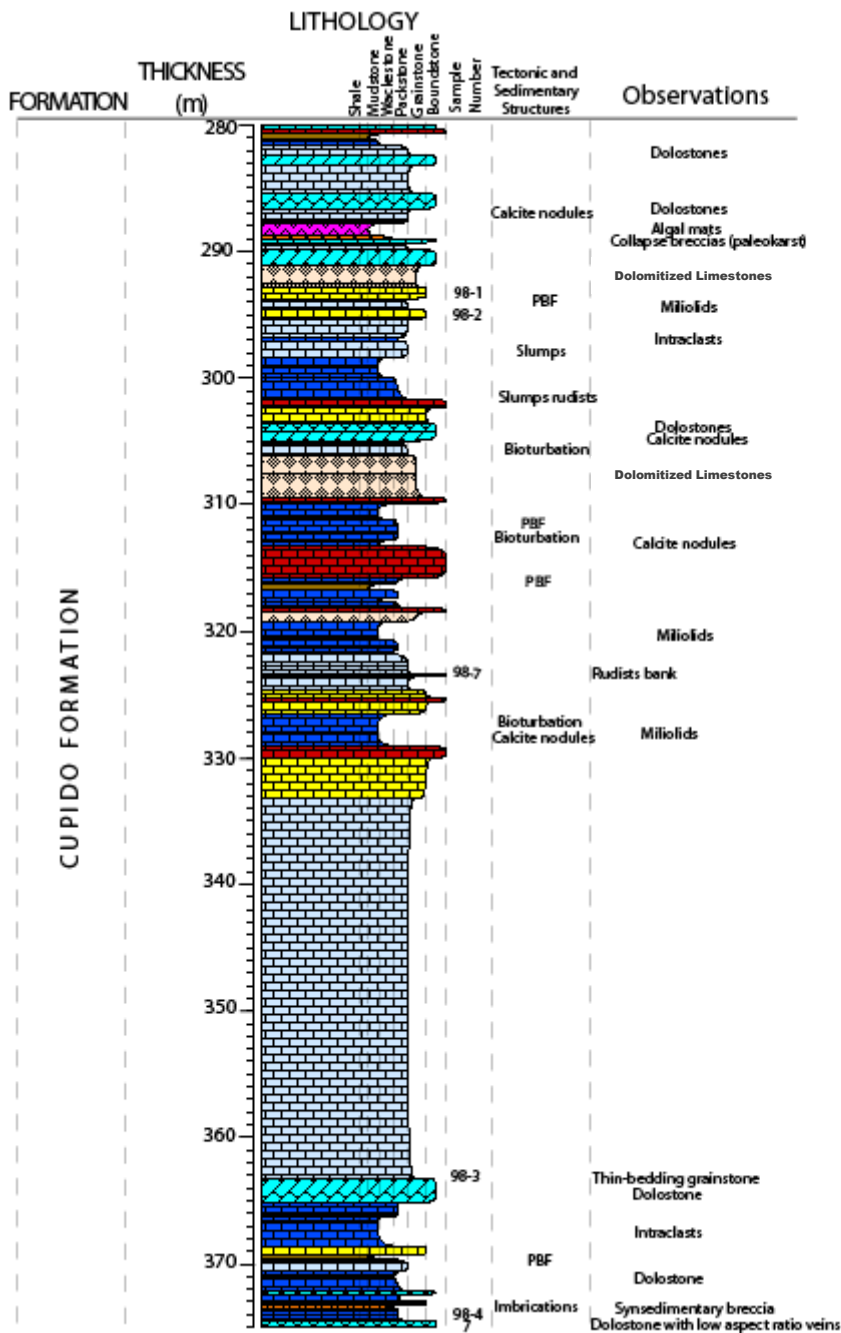


Plate II. Type Section of the Cupido and La Peña Formations at Los Chorros Locality (Continued)

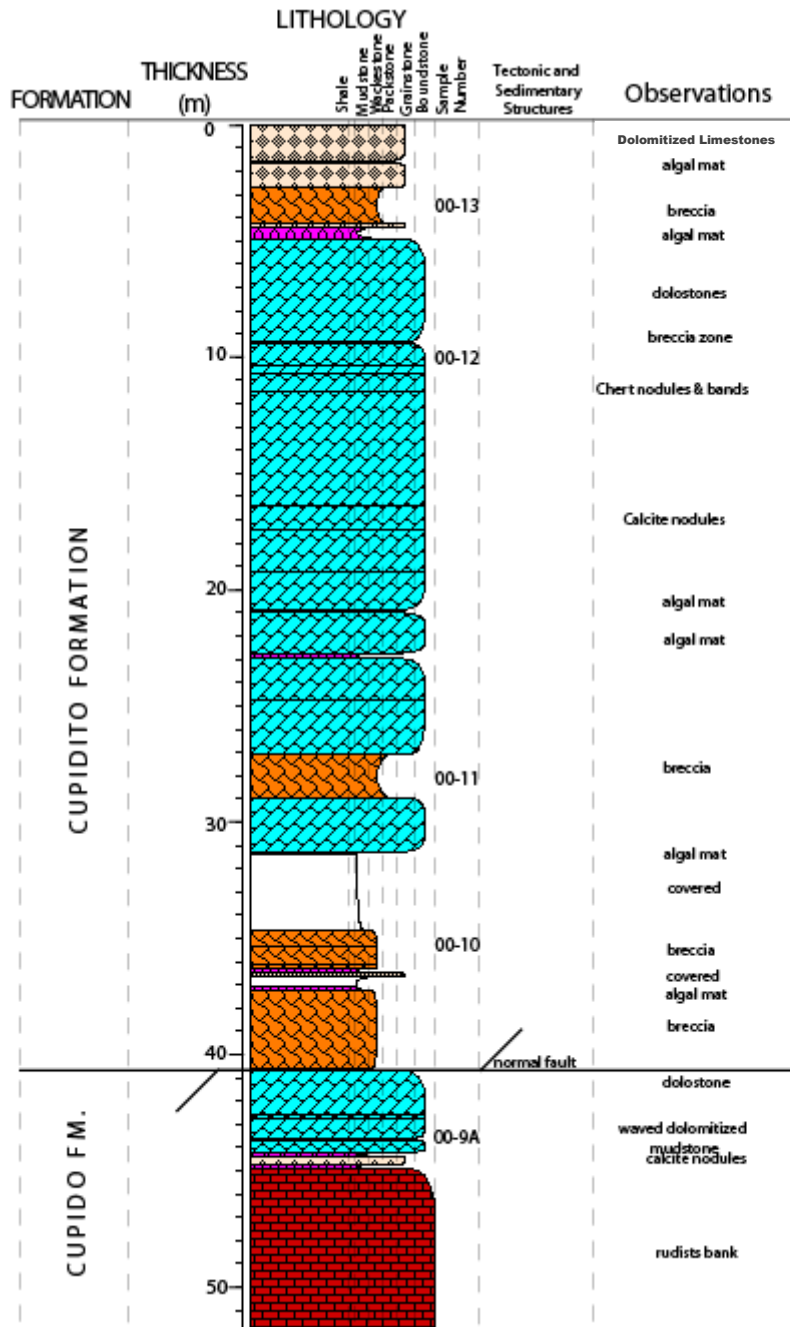


Plate III. Type Section of the Cupido and Cupidito Formations at La Escalera locality

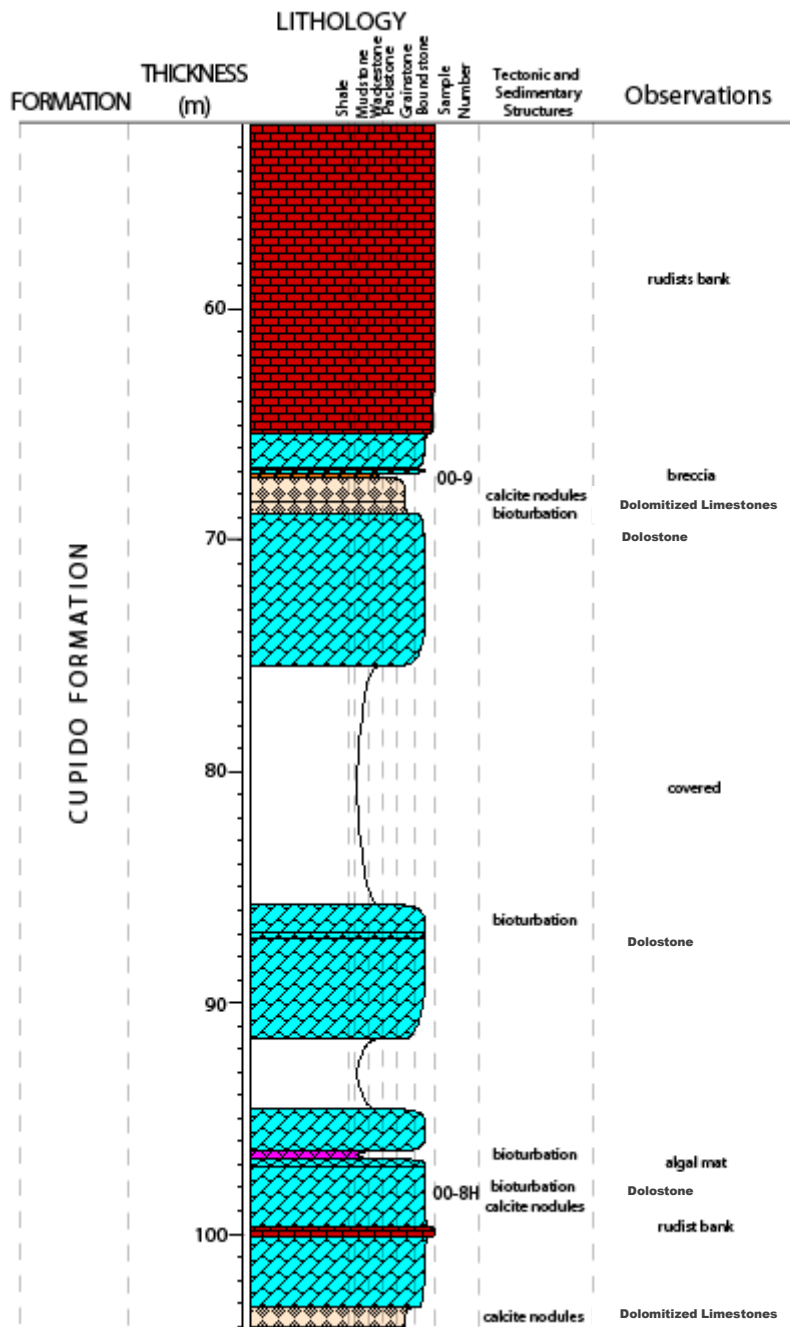


Plate III. Type Section of the Cupido and Cupidito Formations at La Escalera locality (Continued)

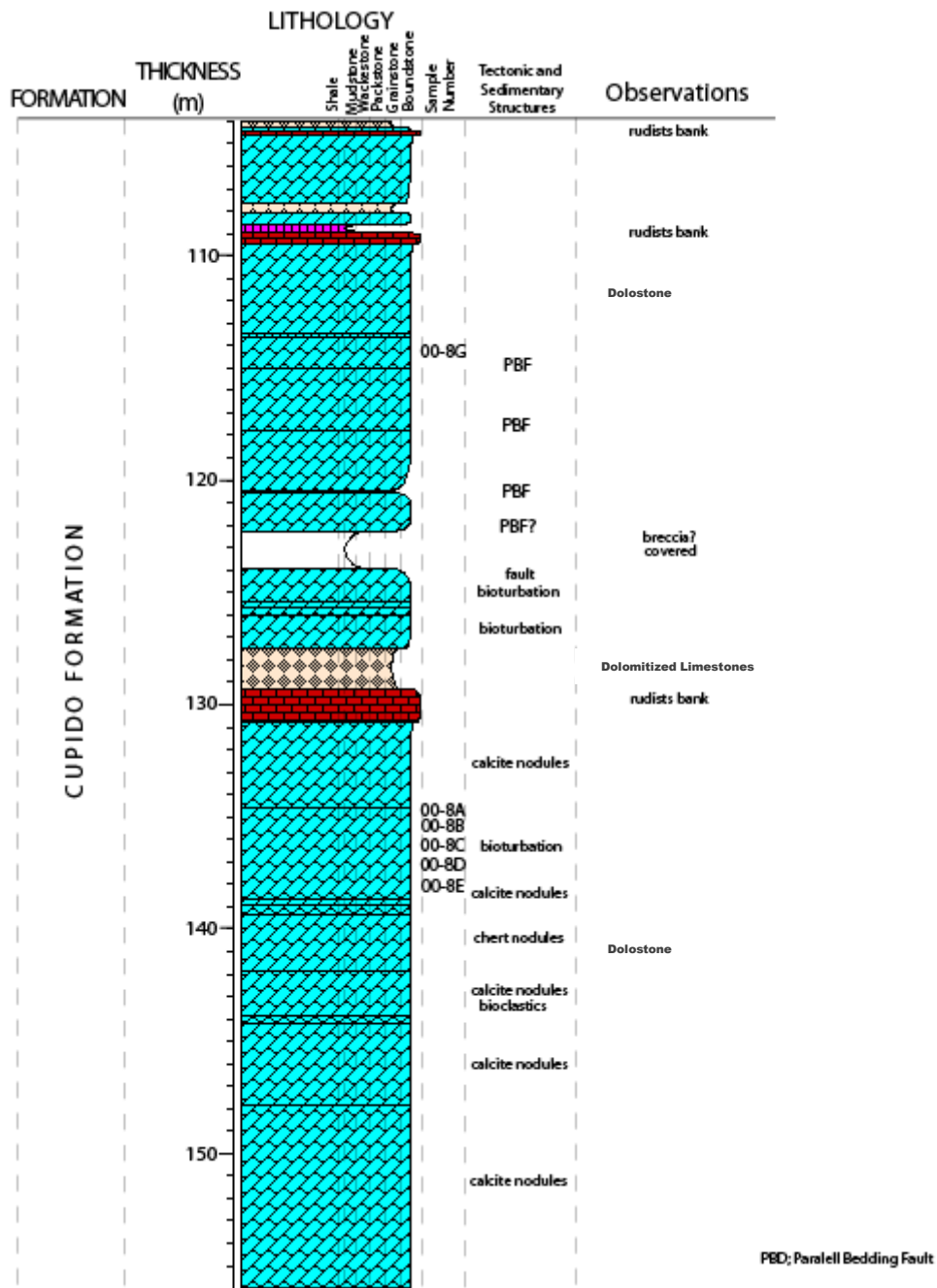


Plate III. Type Section of the Cupido and Cupidito Formations at La Escalera locality (Continued)

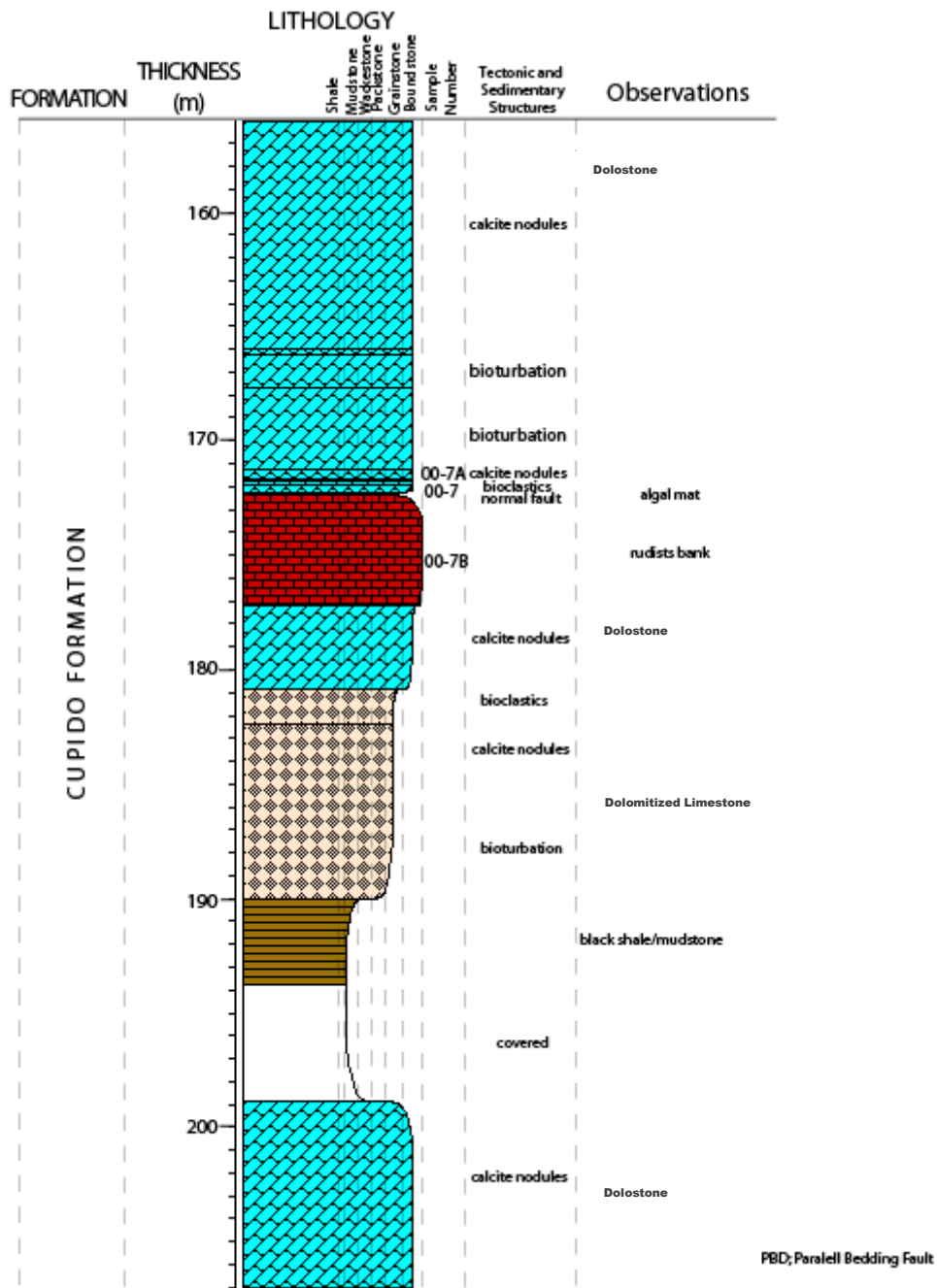
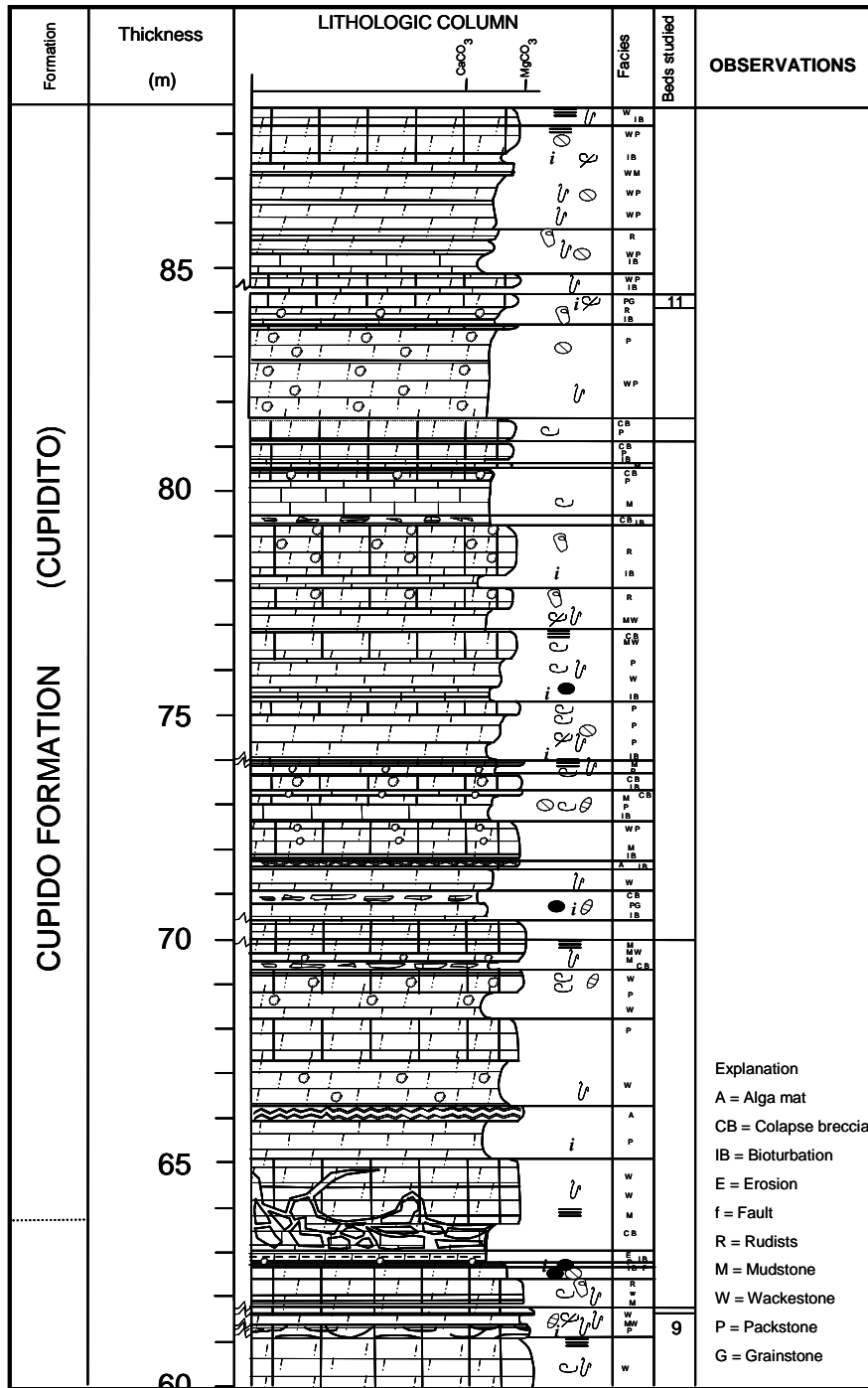


Plate III. Type Section of the Cupido and Cupidito Formations at La Escalera locality (Continued)



Explanation
A = Alga mat
CB = Colapse breccia
IB = Bioturbation
E = Erosion
f = Fault
R = Rudists
M = Mudstone
W = Wackestone
P = Packstone
G = Grainstone

Plate IV. Measured section of the Cupido and Cupidito Formations at Las Palmas Locality. Modified from Ortega (2002).

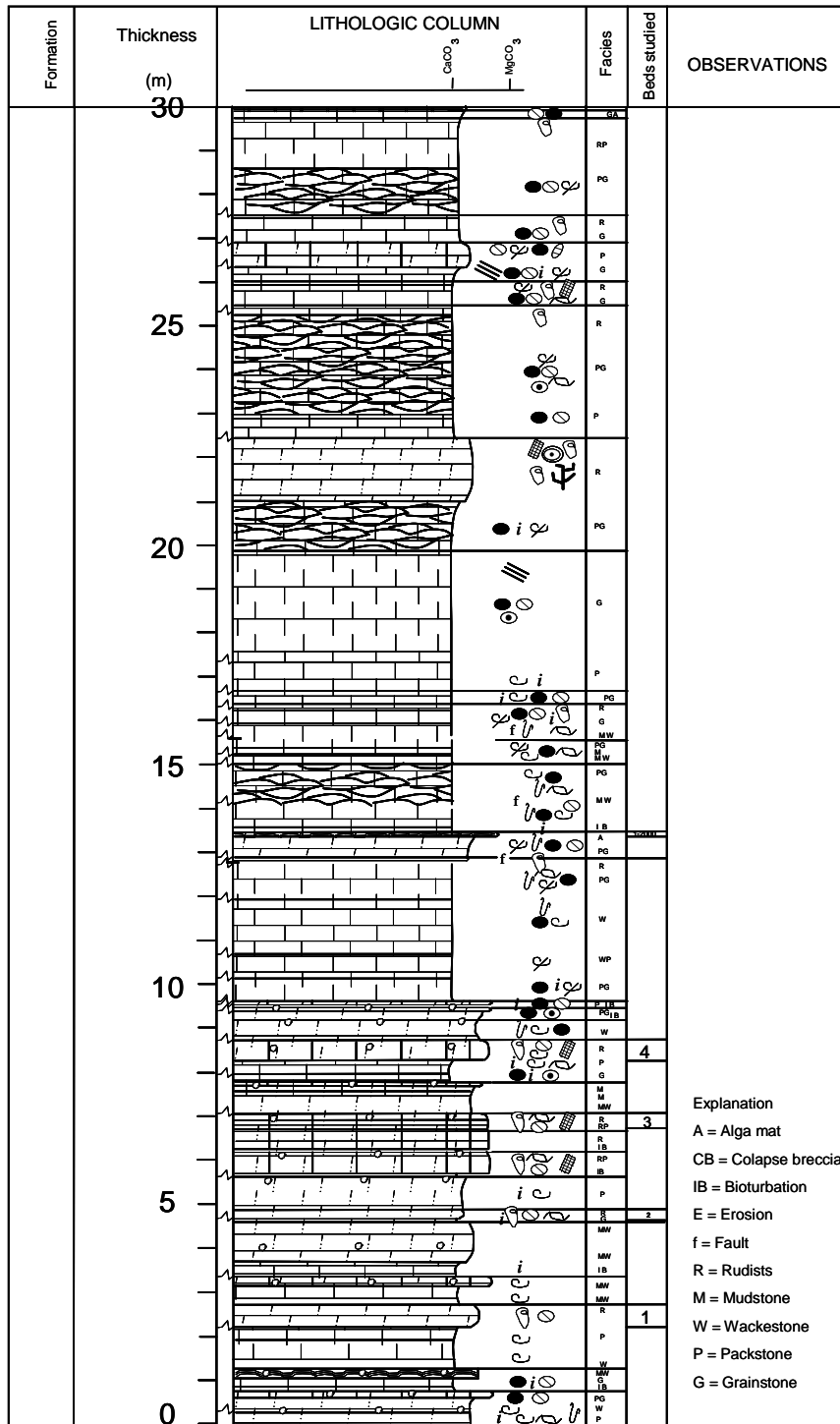


Plate IV. Measured section of the Cupido and Cupidito Formations at Las Palmas Locality (Continued). Modified from Ortega (2002).

Chapter 3. Lithofacies and Sedimentary Environments

INTRODUCTION: ROCK TYPES

Most textbooks on sedimentary geology define the term facies as a body of rock characterized by a particular combination of lithology, physical and biological structures that bestow an aspect (“facies”) different from the bodies of rock above, below and laterally adjacent (e.g., Walker and James, 1992; Tucker and Wright, 1990). A biofacies is a facies for which primary consideration is given to the biological content. If fossils are absent or of little consequence and emphasis is instead placed on the physical and chemical characteristics of the rock, then the term lithofacies (most widely used by sedimentologists) is appropriate (Reading, 1978). Because the outcrops of the Monterrey Salient are most feasibly distinguished on the basis of physical and chemical characteristics such as composition and texture, the concept of lithofacies is used in this study. Lithofacies are the subdivisions most readily comparable to the structural subdivisions of mechanical and fracture stratigraphy (Laubach et al., 2009). Based on field observations and petrographic analysis of more than fifty samples from six localities in the Monterrey Salient, six major lithofacies and their sedimentary environments were identified within the Cupido Formation and the correlative Tamaulipas Inferior Formation. These lithofacies are consistent with the generalized platform-basin facies model developed by previous workers (e.g., Conklin and Moore, 1977; Wilson, 1981). In addition, as a small contribution to the carbonate sedimentology of the Monterrey Salient, my work describes the main characteristics of evaporate solution breccias, which played a key role in the identification of early diagenetic and fracturing processes, as described below.

METHODOLOGY

Sedimentary lithofacies of Lower Cretaceous Cupido Formation and its depositional environments were interpreted from field observations and petrographic analyses. Samples of forty-four beds (Appendix 3.1) were collected from four localities in the study area: Cañón la Escalera, Cañón Santa Rosa-Iturbide, Cañón Boquilla Corral de Palmas, and Cañón de los Chorros (Fig. 2.3). Thickness, lithology, original texture, sedimentary environment and orientation of the beds were logged in the field (Appendix 3.1). The Dunham (1962) classification of carbonate rocks was used to categorize strata on the basis of textural characteristics for both outcrops and thin sections.

Approximately 106 large-sized (7 x 5 cm) thin sections (Appendix 3.2) and corresponding slabs were prepared for petrographic analyses. A thin section oriented parallel to stratification was prepared from each sample to observe sedimentologic characteristics. This sample configuration is also the most convenient for fracture analysis where fractures form high angles with bedding (further discussion and references in Gomez and Laubach, 2006). Identification of petrographic textures and fabrics was carried out with a standard transmitted light microscope and a scanning electron microscope (SEM). Thin sections were stained with Alizarin Red-S in a 0.2% HCl solution in order to distinguish calcite from dolomite using Friedman's (1959) method.

FACIES DISTRIBUTION AND ENVIRONMENT DEPOSITION

Previous workers (e.g., Conklin and Moore, 1977; Wilson, 1981) proposed that the Cupido Formation consists of six units constituted by several facies (Fig. 3.1). The vertical stacking pattern of the lowest five unit forms a large-scale shallowing-upward package (Goldhammer et al., 1991). In upward order these units are: unit A is composed

of medium- to thick-bedded, pelagic argillaceous, lime mudstones deposited in a basinal environment; unit B is composed of thick-bedded, lithoclastic-bioclastic lime wackestones to packstones deposited in ramp slope and fore-reef environments; unit C is massive rudist and coral-dominated packstones, grainstones and boundstones with stromatoporoids and marine cement deposited as a biostromal shelf margin; unit D is composed of crossbedded skeletal-peloidal, packstones-grainstones with ooids and oncolites of back-margin sand shoals; unit E is composed of cyclic thin-bedded, mudstones-packstones with cryptalgal laminites and evaporites deposited in a peritidal platform interior; and unit F is composed of thick-bedded, black, peloid-foram, wackestones-packstones with pelecypods and green algae fragments deposited in a back-margin subtidal lagoon (Fig. 3.1).

Unit A to the lower half of E compose the large-scale prograding and shallowing succession, and the upper half of E and unit F depict relative deepening and initiation of retrogradation back over the Cupido bank (Goldhammer, 1999). The boundary at the base of Cupidito is marked by a major evaporite solution breccia defining a sequence boundary (112 Ma) (Goldhammer, 1999). Unit F and upper half of unit E are roughly equivalent to the Cupidito unit (Goldhammer, oral communication).

The regional distribution of these facies in northeastern Mexico is shown in a Barremian to Lower Aptian paleogeographic map (Fig. 3.2). Shallow platform facies in general were deposited during this time in the northwestern part of the study area (Potrero García, Las Cortinas, La Escalera, Los Chorros and Corral de Palmas areas) passing toward the southeast into more deep-water open marine conditions (Iturbide-Santa Rosa area). More detail of sequence stratigraphy and paleogeographic evolution of

northeastern Mexico can be found in previous work (e.g., Wilson, 1981; Salvador, 1991; Goldhammer et al., 1991; Goldhammer, 1999; Lehmann et al., 1999).

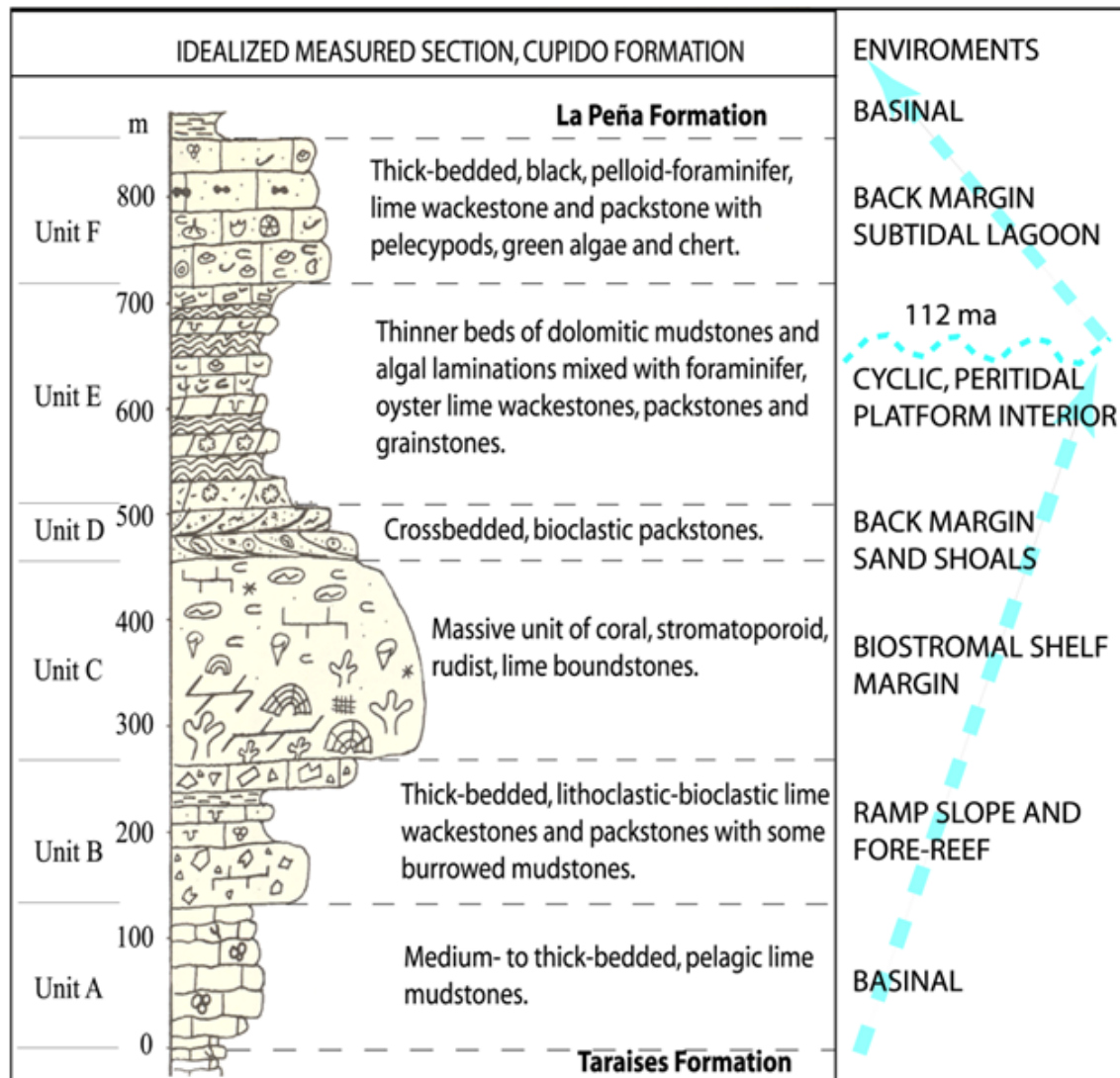


Fig. 3.1. Idealized vertical section of platform-basin facies model of Cupido Formation. Arrows indicate shallowing-upward from unit A to bottom half of unit E forming the Cupido Formation. The upper half of unit E and unit F constitute the initiation of a retrogradation event (after Conklin and Moore, 1977).



Fig. 3.2. Barremian to Lower Aptian paleogeographic map showing the Cupido platform developed around the Coahuila High, a positive element at that time. Outcrops used for this study included strata deposited in both shallow and deep water environments. PG, Potrero García; CT, Cañón de las Cortinas; CH, Cañón de los Chorros; ES, Cañón la Escalera; LP, Cañón Boquilla Corral de Palmas; IT, Cañón Santa Rosa-Iturbide; MO, Molano Fault; CP, Cañón Prieto; CI, Cienegas. X and Y are coordinates in the Universal Transverse Mercator (UTM) Projection indicated by small crosses. Square in inset map indicates the location of the map above. Modified from Goldhammer et al. (1991).

Lithofacies Description

Previous workers (e.g., Conklin and Moore, 1977; Wilson, 1981) identified six major lithofacies in the Cupido and Tamaulipas Inferior Formations, in a generalized platform-basin facies model. Part of my field work was verifying these six major lithofacies to have a sedimentological framework for my research. In terms of vertical sequence my observations are consistent with the generalized facies model. Below are the lithofacies that I recognized in the Monterrey Salient within the Cupido and Tamaulipas Inferior Formations:

Argillaceous pelagic, lime mudstone.

These mudstones are thin-to thick-bedded and light brown to gray (Fig. 3.3a). Intercalations of thin- to medium-bedded gray mudstones with nodules and bands of chert (Fig. 3.3b), and thin- to medium-bedded brown shales are also present. Microbioclastic content includes foraminifera, mainly coccolithophorids and calpionellids (Fig. 3.3c). Microfossils reported by previous work (e.g., Wilson, 1981; Goldhammer, 1999) in these limestones also include radiolaria, nannoconids, ostracods and echinoderms. The mudstones are scarcely bioturbated, partially dolomitized (affecting the rock from 3 to 10%) and recrystallized. Oxides associated with stylolites, organic material and detrital and replacement quartz are minor components. The organic matter and microfossils (Fig. 3.3c) indicate sedimentation under dysaerobic (oxygen-depleted) to anaerobic (anoxic) conditions. This lithofacies was deposited in water depths on the order of 150-500 m in slope to basinal conditions (Conklin and Moore, 1977) (Figs. 3.1 and 3.2). This lithofacies is present in Cañón Santa Rosa outcrops near Iturbide (Fig. 3.2, Appendix 2.1).



Fig. 3.3a. Outcrop photograph showing thin- to thick-bedded, basinal lime mudstones of Tamaulipas Inferior Formation. Cañón Santa Rosa locality. Individual on right hand side of image for scale.



Fig. 3.3b. Detail of Fig. 3.3a showing cherty basinal lime mudstone. Pen approximately 10 cm long. Tamaulipas Inferior Formation, Cañón Santa Rosa locality.

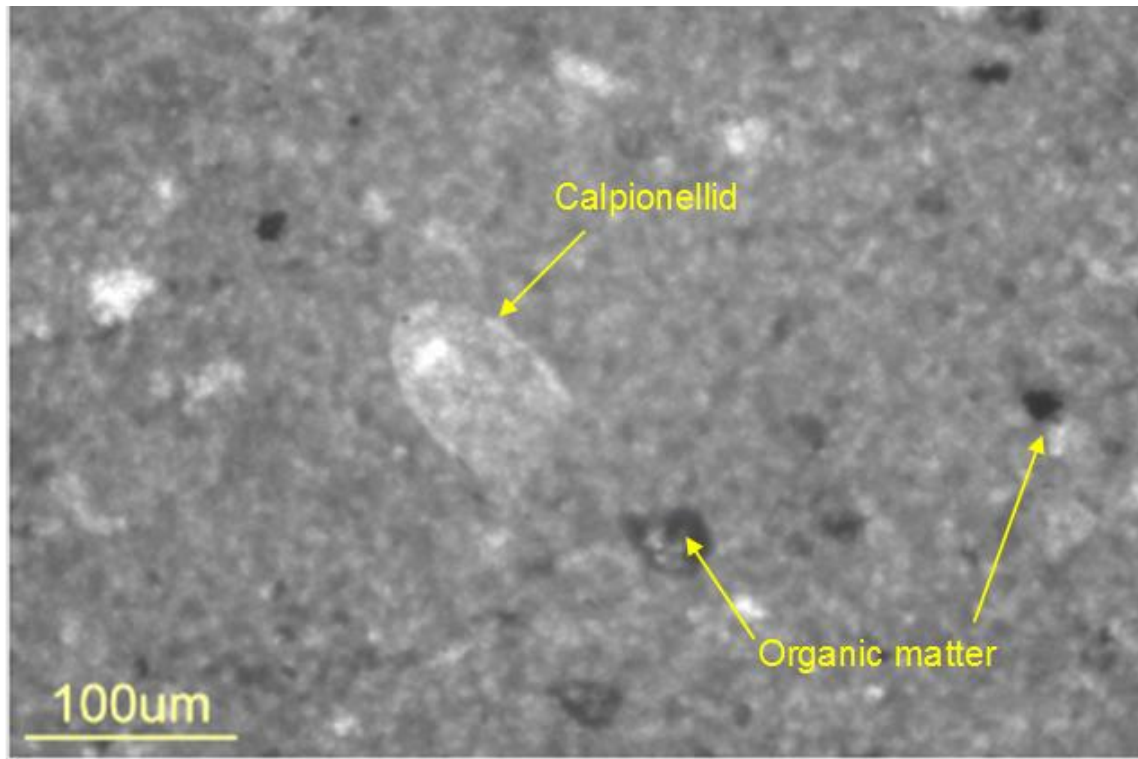


Fig. 3.3c. Photomicrograph illustrating cross section of a calpionellid and organic matter. Basinal lime mudstones of Tamaulipas Inferior Formation, Cañón Santa Rosa locality.

Intraclastic-bioclastic wackestone-packstone.

This lithofacies is represented by medium- to thick-bedded light brown wackestone-packstones. The allochem content includes bioclasts and intraclasts of pellets, peloids, and ooids (Fig. 3.4a). Syn-sedimentary breccia composed of clasts of wackestone-packstone of ooids and intraclasts in fine-grained dolomite matrix are also included in this lithofacies (Fig. 3.4b). These breccias are composed of 0.12 cm diameter clasts of wackestone of ooids and intraclasts in fine grained dolomite matrix. Fine grained

(5-12.5 μm) dolomite replaced both clasts and matrix (Fig. 3.4c). The intraclasts identified imply the sediment was reworked and redeposited before lithification took place, so during the sedimentation. This lithofacies represents ramp slope and fore-reef environments (Conklin and Moore, 1977) (Figs. 3.1 and 3.2), and is present in Cañón la Escalera, Cañón Boquilla Corral de Palmas and Cañón de los Chorros (Fig. 3.2, Appendix 2.1).

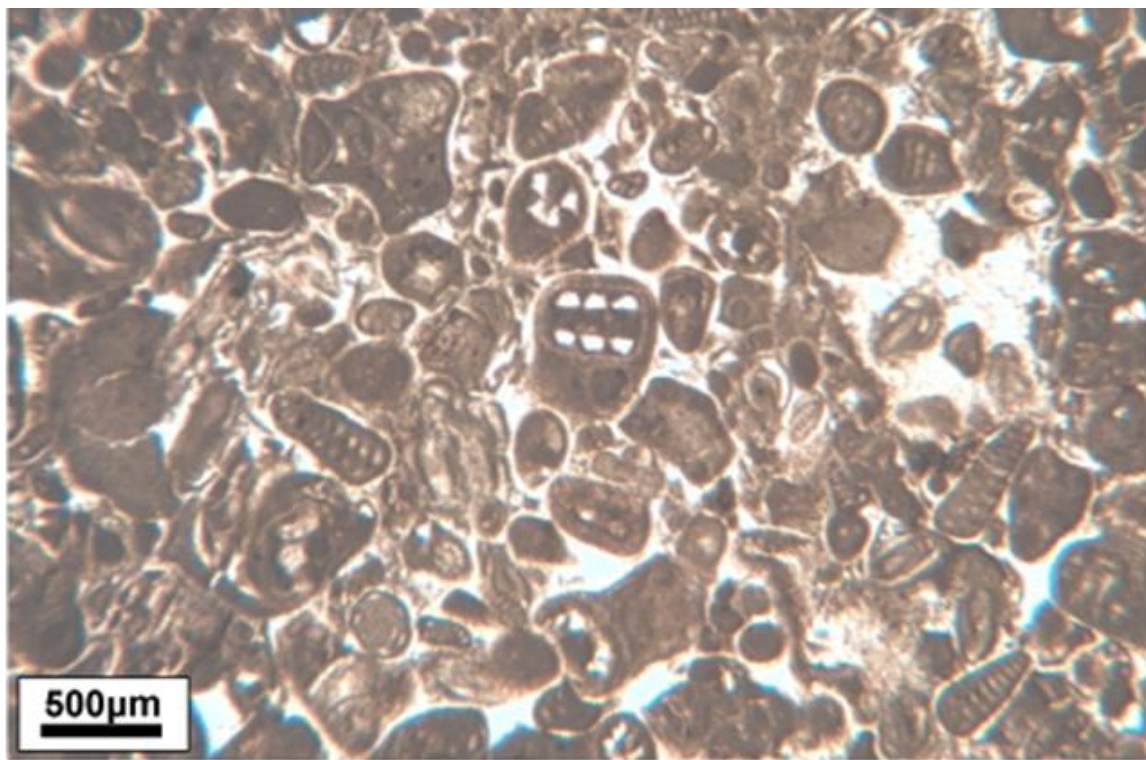


Fig. 3.4a. Photomicrograph illustrating fore-reef intraclastic-bioclastic packstone facies. Cupido Formation, Cañón de los Chorros locality.

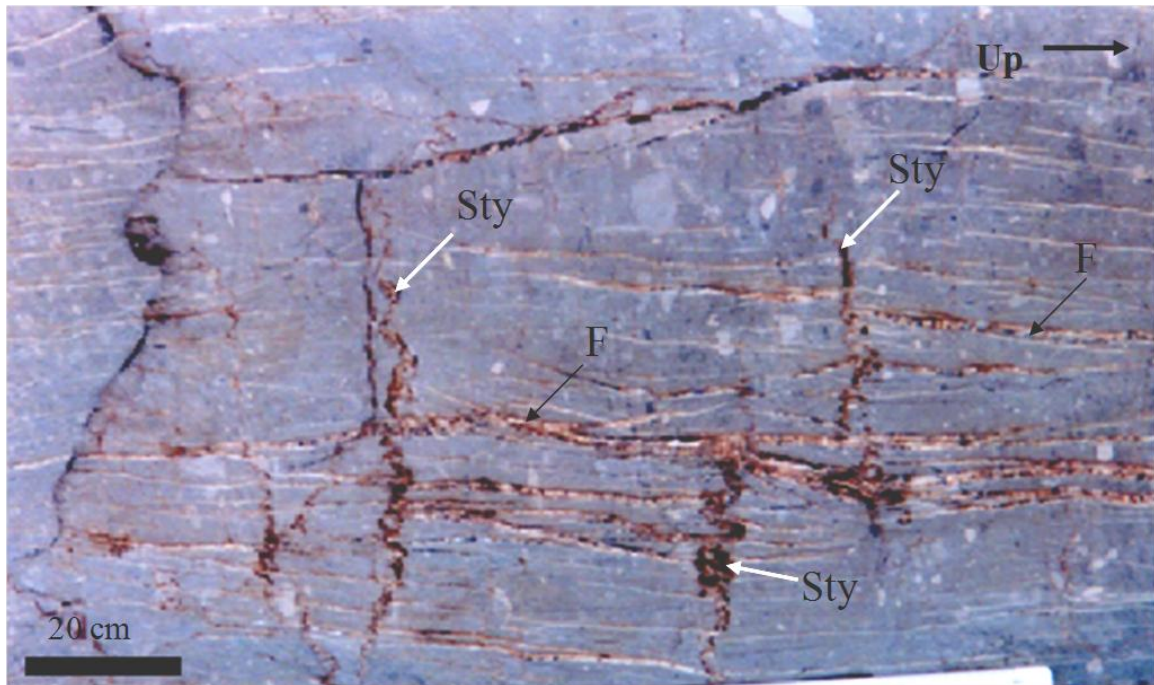


Fig. 3.4b. Outcrop photograph of syn-sedimentary breccia composed of subangular clasts that vary in size from 0.5 mm to 2 cm. Notice stylolites (Sty), perpendicular to bedding, cross cut clasts and also calcite-filled veins (F). Cupido Formation, Cañón de La Escalera locality.

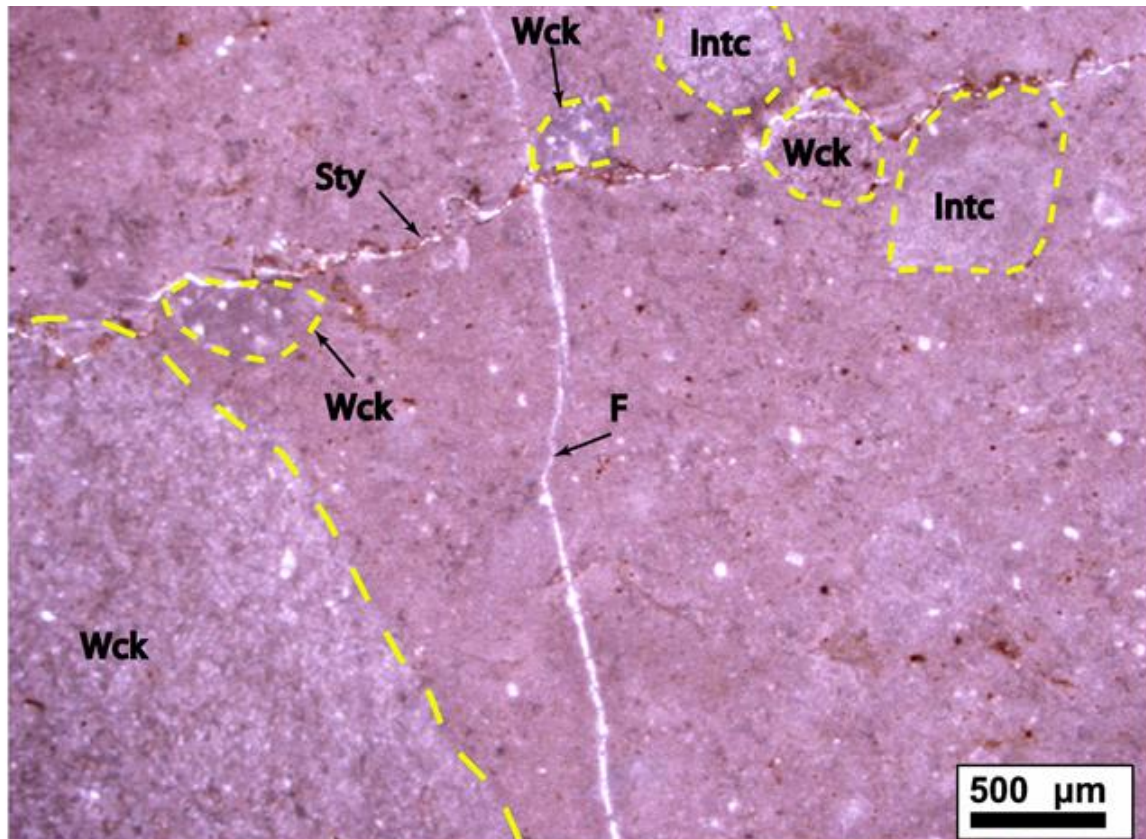


Fig. 3.4c. Syn-sedimentary breccia composed of clasts of wackestone (Wck) of ooids and intraclasts (Intc) in fine grained dolomite matrix. Notice stylolite (Sty) cross cuts clasts and also a calcite-filled vein (F). Cupido Formation, Cañón de La Escalera locality. Photomicrograph.

Rudist and coral-dominated packstones, grainstones and boundstones with stromatoporoids.

Rudist banks are thin to medium-bedded light brown to gray in color (Fig. 3.5a). At both Cañón la Escalera and Cañón de los Chorros areas this lithofacies consist of partially dolomitized packstones of rudists (Fig. 3.5b, Appendix 2.1). Bioclasts, ooids, intraclasts of pellets, and peloids are present in the packstones matrix (Fig. 3.5c). At

Cañón Boquilla Corral de Palmas (Appendix 2.1) rudist banks are less developed than in other areas, and they are medium- to thick-bedded and gray in color.

Dolomitization in these lithofacies varies from 5% to 70%, visual inspection in thin sections of these lithofacies shows that they are recrystallized (see Chapter 4). Recrystallization varies from 30% to 100%. Dedolomitization also affected these lithofacies, varying from 5% to 30%. This lithofacies represents biostromes that were deposited in shelf-margin environments (Conklin and Moore, 1977) (Figs. 3.1 and 3.2).

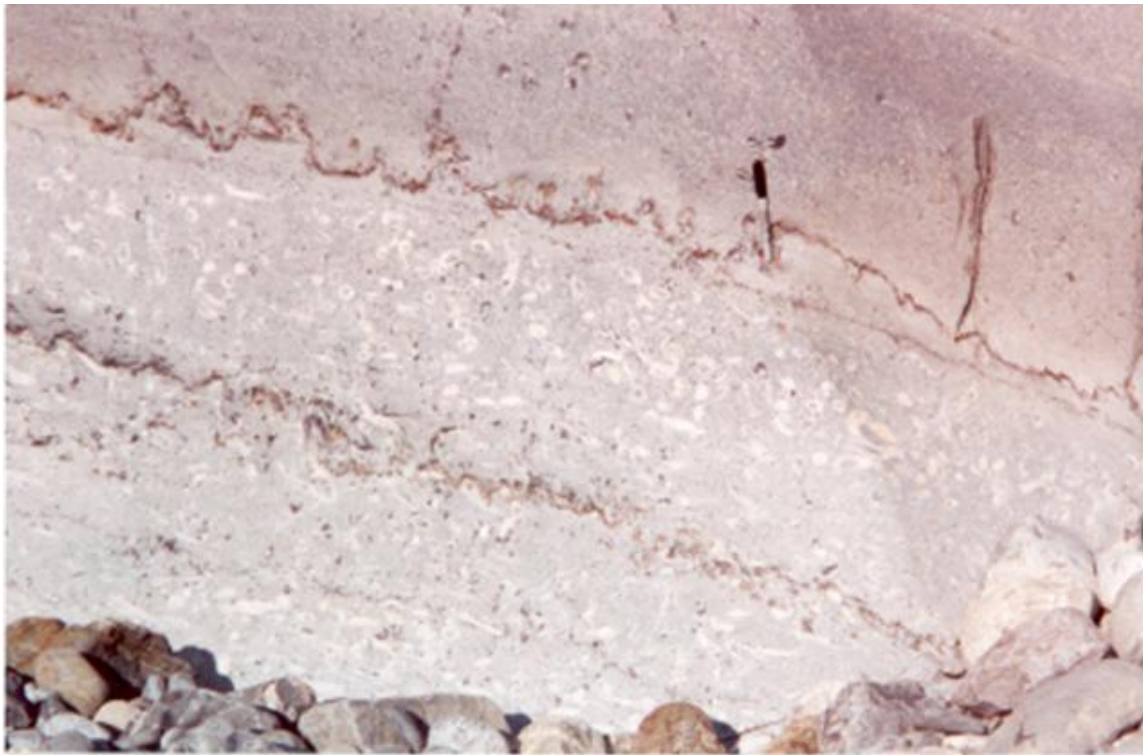


Fig. 3.5a. Abundant rudists in organic reef facies. Pen approximately 10 cm long. Cupido Formation, Cañón Boquilla Corral de Palmas locality. Outcrop photograph.



Fig. 3.5b. Reef facies showing abundant caprinid- type rudists. Cupido Formation, Cañón Boquilla Corral de Palmas locality. Outcrop photograph.



Fig. 3.5c. Partially dolomitized reef facies showing fragments of mollusk in a peloidal-packstone-grainstone matrix. Cupido Formation, Cañón de losChorros locality. Photomicrograph.

Crossbedded skeletal-peloidal, packstones-grainstones with ooids and oncolites.

At Cañón de los Chorros this lithofacies consists of medium- to thick-bedded light brown packstone-grainstones (Appendix 2.1). At Cañón Boquilla Corral de Palmas and Cañón la Escalera beds of this lithofacies are thinner, varying from thin- to medium-bedded (Fig. 3.6a, Appendix 2.1). This lithofacies is characterized by cross-laminations of ooids, bioclasts (foraminifera) and intraclasts (Fig. 3.6b). Dissolution features (microkarst and dissolved ooids) and calcitized anhydrite nodules are present in these

rocks. Dolomitization in this lithofacies varies from 5% to 95% and recrystallization is typically about 80% (see Chapter 4).. This lithofacies represents back-margin sand shoals (Conklin and Moore, 1977) (Figs. 3.1 and 3.2).



Fig. 3.6a. Back-margin sand shoals facies showing cross-bedding. Cupido Formation, Cañón la Escalera locality. Outcrop photograph.

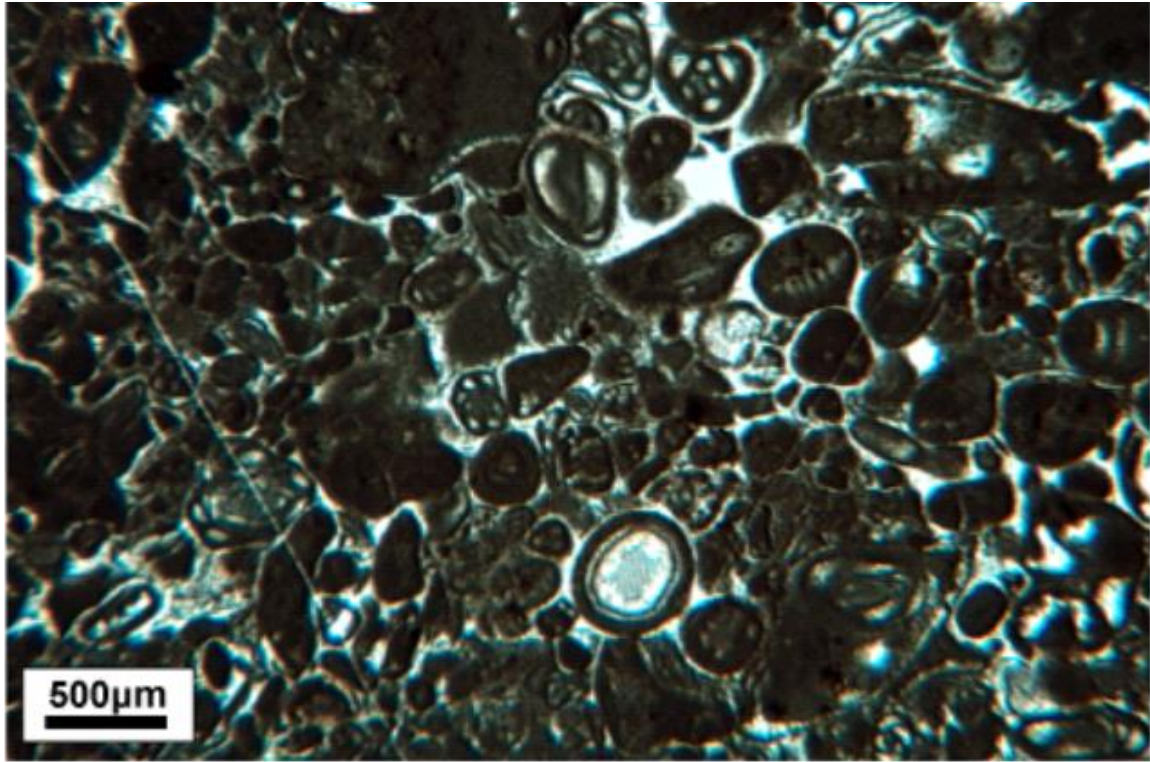


Fig. 3.6b. Sand shoal facies with bioclasts, ooids and peloids. Cupido Formation, Cañón la Escalera locality. Photomicrograph.

Mudstones-packstones with cryptalgal laminites and evaporites.

This lithofacies is characterized by mudstone-wackestones, which are intensively bioturbated (Figs. 3.7a and 3.7b) and dolomitized (affecting more than 90-95% of the rock volume), and algal mat laminations. At Cañón Boquilla Corral de Palmas (Appendix 2.1) this lithofacies consists of medium-bedded dark gray mudstones-packstones intercalated with algal mats. At Cañón la Escalera (Appendix 2.1) these mudstones-packstones are medium- to thick-bedded and dark gray to gray in color. Anhydrite

nodules and burrows filled with mudstone-wackestone of ooids and intraclasts are present. Algal mat beds are thin- to thick-bedded and light gray in color (Fig. 3.7c). Most algal laminations present convolute structures (Fig. 3.7d). Fine grained dolostones with partially dissolved ooids and stylolites with replacement and overgrowths of quartz are also present. Visual inspection in thin section shows that recrystallization affected these rocks up to 85% (see Chapter 4). This lithofacies represents peritidal platform interior areas where evaporation took place (Conklin and Moore, 1977) (Figs. 3.1 and 3.2).

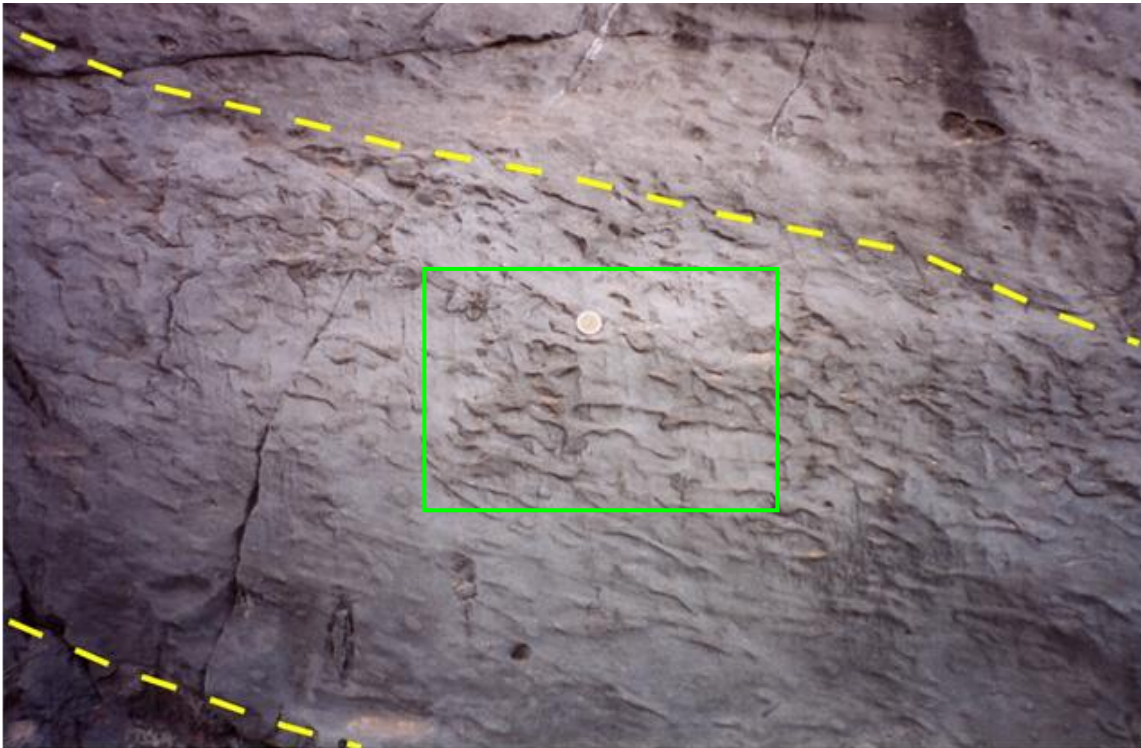


Fig. 3.7a. Cross-sectional view of burrows in shallow water marine carbonates. Burrows are partially filled with sediment. Dashed lines indicate bedding limits. Square indicates Fig. 3.7b location. Coin diameter is 2.0 cm. Cupido Formation, Las Palmas locality. Outcrop photograph.

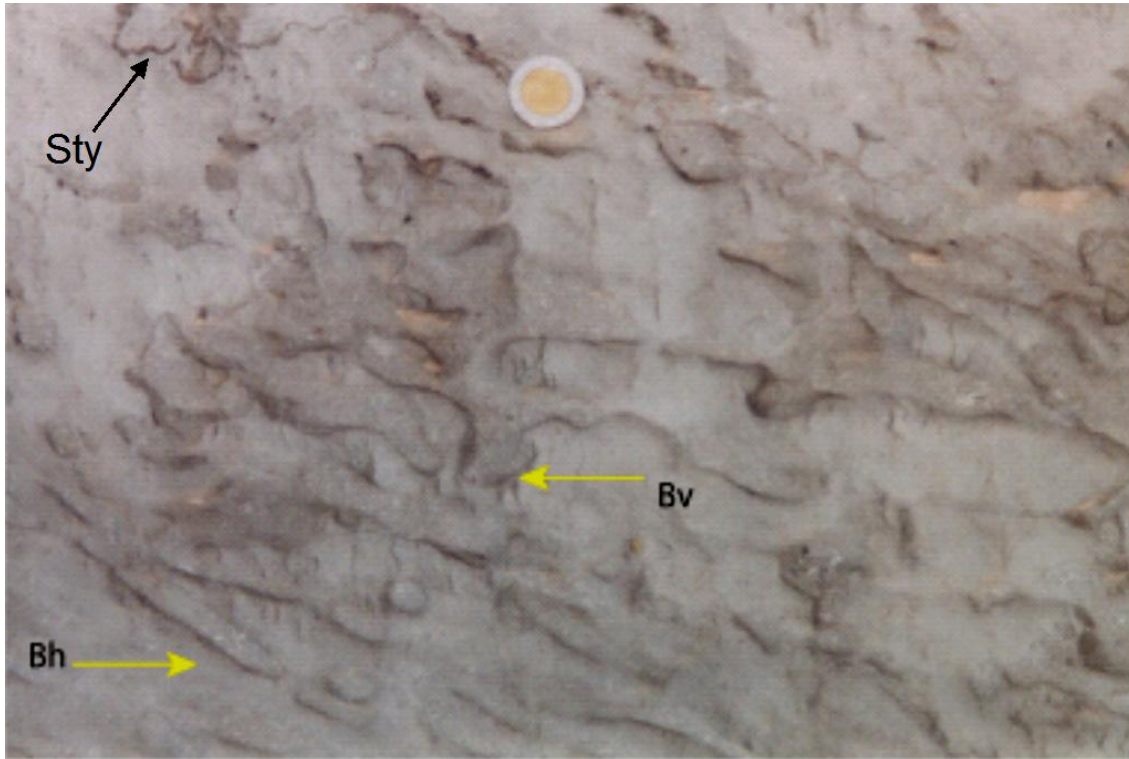


Fig. 3.7b. Detail of Figure 3.7a showing both bedding-perpendicular (Bv) and bedding-parallel (Bh) burrows in a dolostone bed. Burrows are partially filled with wackestone of bio- and intraclasts and probably were deformed by compaction. Notice stylolite (Sty) crosscuts some burrows. Coin diameter is 2.0 cm. Cupido Formation, Las Palmas locality.



Fig. 3.7c. Medium-bedded dark gray mudstones-packstones intercalated with light gray algal mats of peritidal platform interior facies. Cupido Formation, Cañón La Escalera locality. Outcrop photograph.

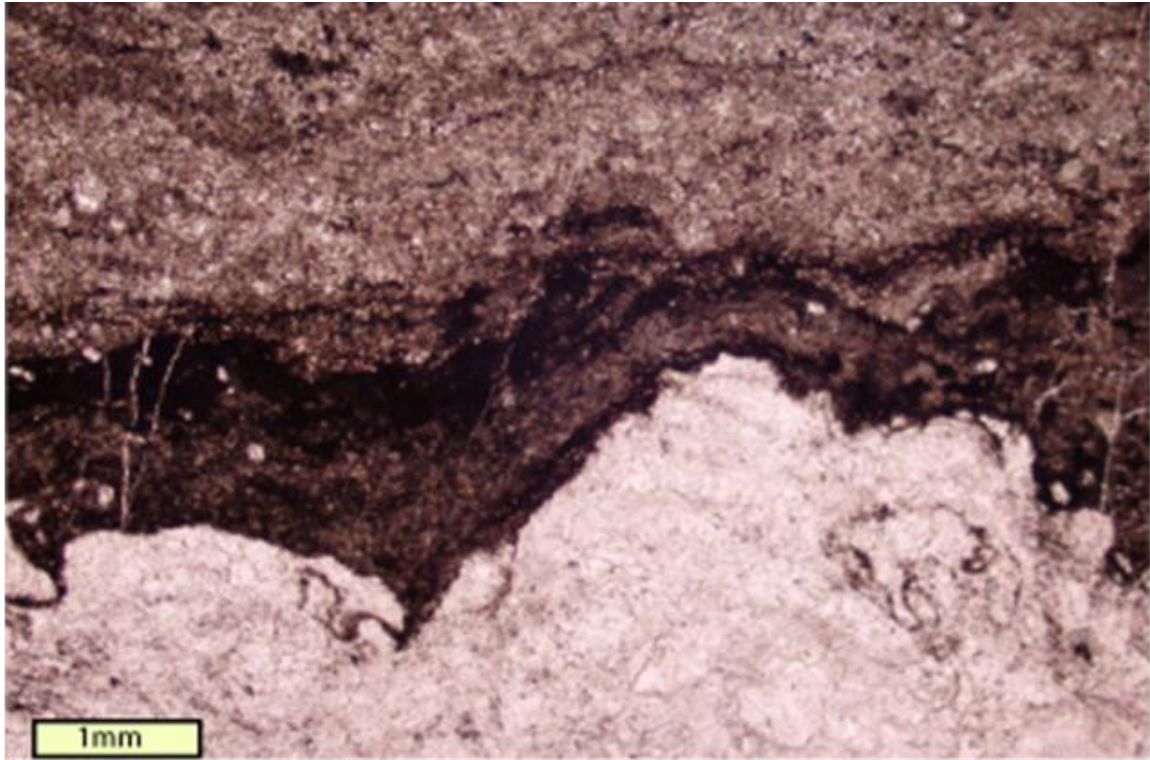


Fig. 3.7d. Convoluted algal laminations of peritidal platform interior facies. Cupido Formation, Cañón Prieto locality. Photomicrograph.

Peloid-foram, wackestone-packstones with pelecypods and green algae.

At Cañón Boquilla Corral de Palmas and Cañón de los Chorros this lithofacies consists of thin to medium-bedded brown wackestone-packstones of ooids with bioclasts (mainly algae fragments and miliolids), superficial oolites and grapestones of pellets (Fig. 3.8a, Appendix 2.1). Packstones of pellets, ooids, intraclasts and bioclasts are also present. Common components of this lithofacies are fecal pellets such as *Favreina*, sp. (Fig. 3.8b) and micritized bioclasts. At Cañón la Escalera this lithofacies consists of packstone-grainstones of ooids, intraclasts and bioclasts (miliolids, green algae, etc).

Dolomite has replaced both matrix and allochems (mainly pellets) up to 45%. These lithofacies are also partially recrystallized, petrographic visual inspection in thin sections shows that recrystallization varies from 40% to 95% (see Chapter 4). Based on the faunal content and allochems identified, this lithofacies represents lagoon deposits (Figs. 3.1 and 3.2).

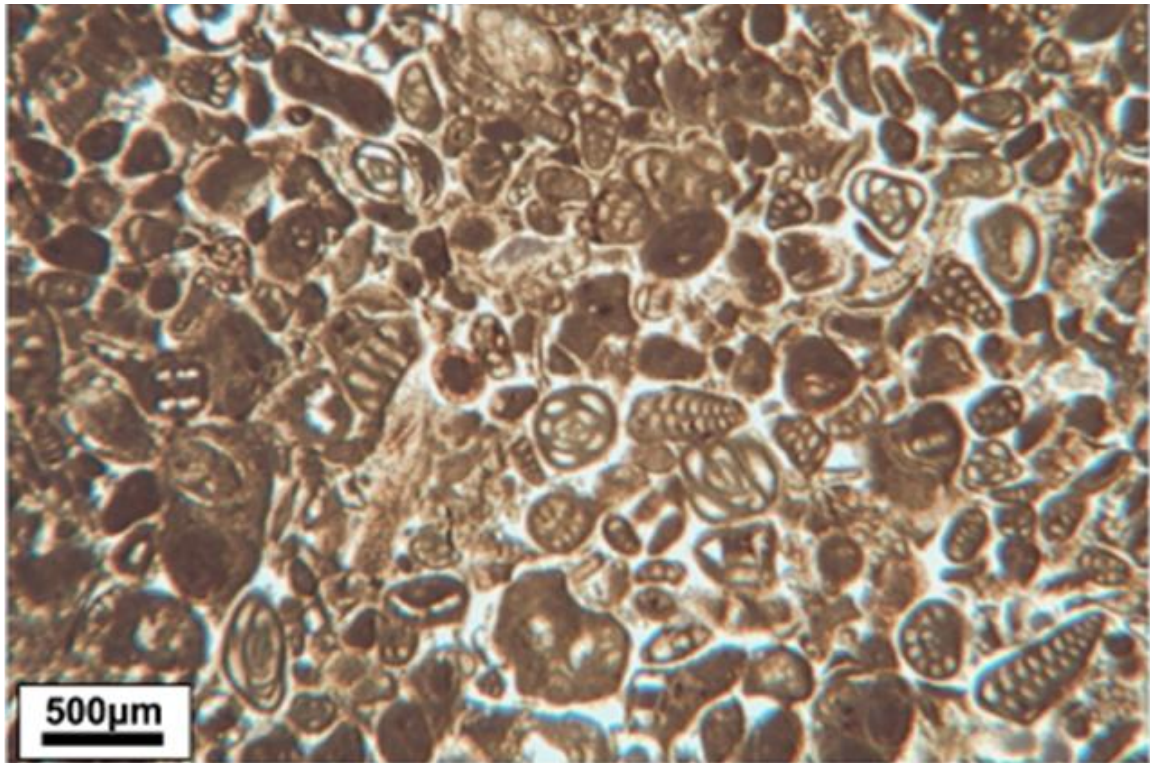


Fig. 3.8a. Back-margin lagoon facies of miliolid lime packstone with aggregate grains, gastropods, and green algae fragments. Cupido Formation, Cañón de los Chorros locality. Photomicrograph.

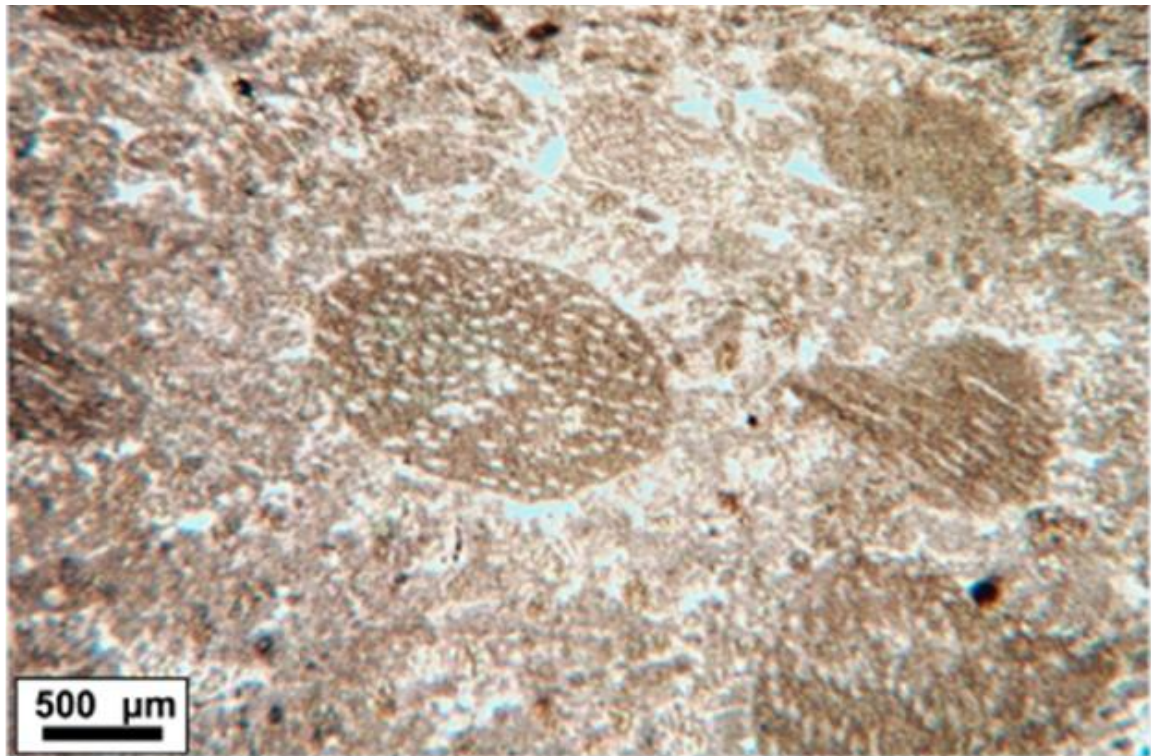


Fig. 3.8b. Pellet packstone showing *Favreina* sp. Cupido Formation, Cañón de los Chorros locality. Photomicrograph.

EVAPORITE SOLUTION BRECCIAS

Evaporite solution breccias (syn. evaporite collapse breccias) form when the subsurface removal of evaporite salts allows the intercalated or overlying rock to settle and become fragmented (Warren, 1999). The main breccia may be polymict or monomict (syn. oligomict) depending on the nature of the interbeds and the overburden (Warren, 1999). Breccias can be clast- or matrix- supported depending on the amount of residue entrained in the evaporitic interval prior to dissolution. According to Warren (1999), evaporite solution breccia beds typically have a planar to slightly irregular, continuous lower contact, which is often coated with insoluble residues. Unlike its lower contact, the upper contact of the main breccia interval is typically gradational, progressing from rubble breccia in the main body into mosaic, crackle then ultimately into unaltered overburden. The contrast between a sharp lower contact and a gradational upper contact is one of the most reliable characteristics of a solution breccia (Warren, 1999). It can be used both in outcrop and in the subsurface to separate a solution breccia from a depositional breccia or a tectonic breccia.

Evaporite solution breccias found in the Monterrey Salient are important keys to understanding the diagenetic history of the Cupido Formation. In addition, these breccias have been used as markers of sequence boundaries. The boundary at the base of Cupidito is marked by a major evaporite solution breccia named by Goldhammer (1999) SB-112 Ma.

Evaporite collapse breccias were identified at Cañón Corral de Palmas, Cañón la Escalera, and Cañón de los Chorros (See Appendix 2.1). These breccias were also identified in the Cañón de las Cortinas and outside of the Monterrey Salient in Potrero García, and in areas not reported before, for example at Cañón Prieto (Figs. 2.3 and 3.9a).

Fieldwork permitted recognition of two types of evaporite solution breccias at different stratigraphic levels (see Appendix 2.1): monomict and polymict clast-supported.

Monomict breccias at Cañón Prieto are stratiform and interstratal with sharp lower contact and irregular upper contact (Fig. 3.9a). Average thickness of this breccia is about 60 cm. Clasts are made up of 1-10 cm angular dolostone fragments and cemented by calcitized evaporites (Fig. 3.9b). Another good example of collapse breccia was identified at Las Palmas locality (Fig. 3.10). The breccia at this locality can be also classified as monomict clast-supported and it is characterized by content many calcite-filled veins in dolostones rotated blocks. Blocks in the breccia can be correlated with adjacent undisturbed layers; blocks that can be visually fitted together suggest in situ fragmentation and redeposition and thus local provenance (this study and Ortega, 2002). At the base of the collapse breccia at Las Palmas there is a layer of laminated evaporites replaced by calcite that pinches out laterally. This layer of evaporites and entire blocks of calcified anhydrite in the breccia suggest that the large collapse at Las Palmas is similar to smaller scale collapse features described in the literature (Goldhammer et al., 1991).

Polymict breccias are made up of algal mat, calcitized anhydrite, limestone (mainly packstone of ooids and pellets) and dolostone fragments. Clasts are angular and vary from a few mm to more than 10 cm long (Fig. 3.11a and 3.11b). These breccias are interbedded with dolostones and evaporites layers and have sharp lower contacts and irregular upper contacts (Fig. 3.11a). Because layers below the breccia are unaffected, clasts must have been derived from overlying strata. These breccias were also identified at Los Chorros, Potrero García and Las Cortinas localities.

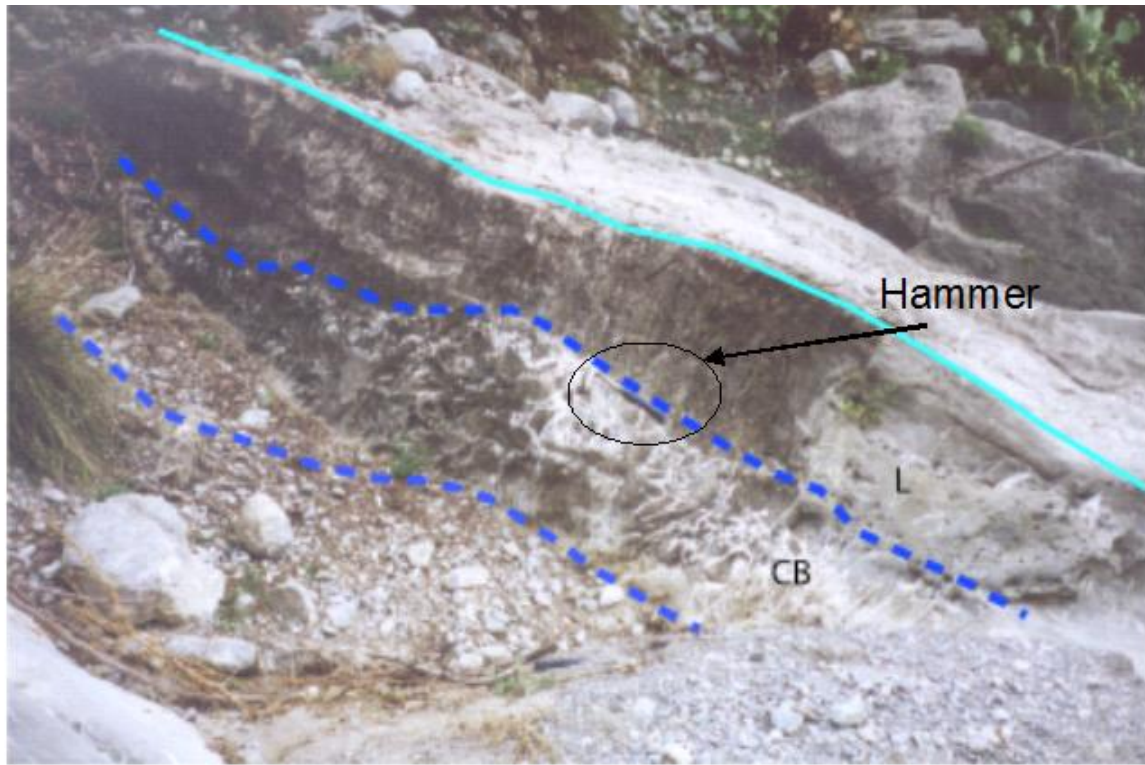


Fig. 3.9a. Monomict, clast-supported evaporite collapse breccia (CB) showing upper irregular contact. L, limestone; dashed lines indicate collapse breccia boundaries. Hammer (circled) is 30 cm long. Cupido Formation, Cañón Prieto locality. Outcrop photograph.

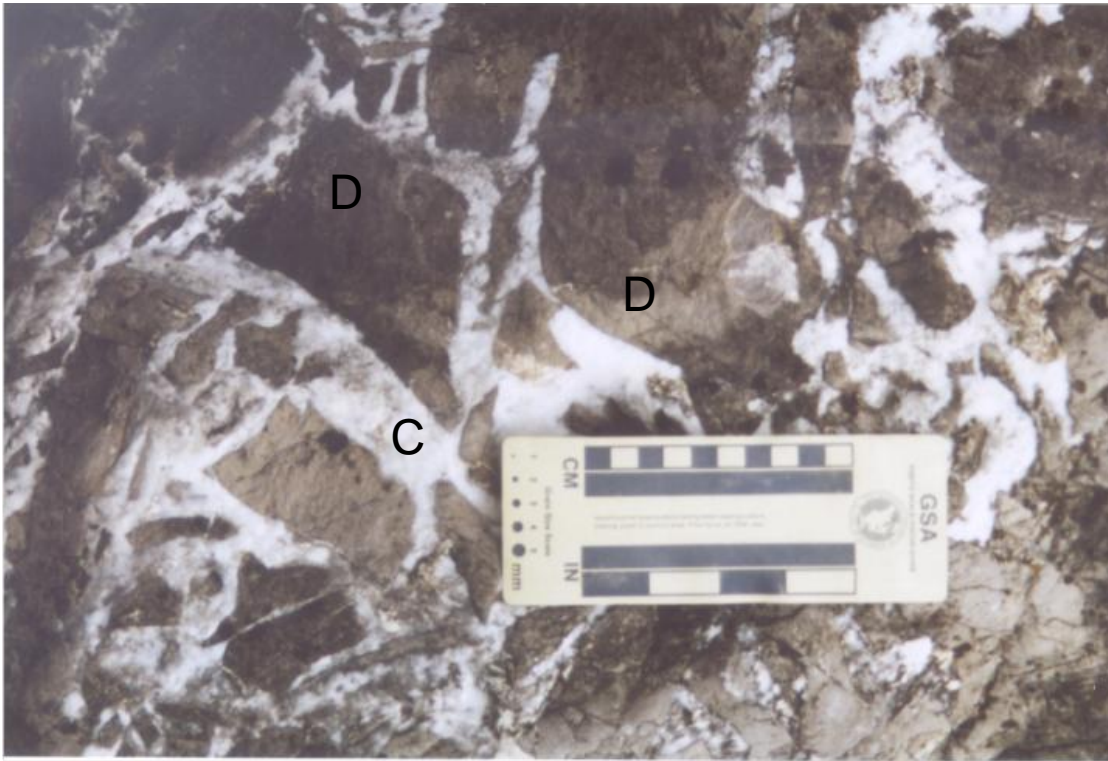


Fig. 3.9b. Detail of Figure 3.9a showing monomict evaporite solution breccia containing angular dolostone (D) clasts cemented with calcite (C). Cupido Formation, Cañón Prieto locality.

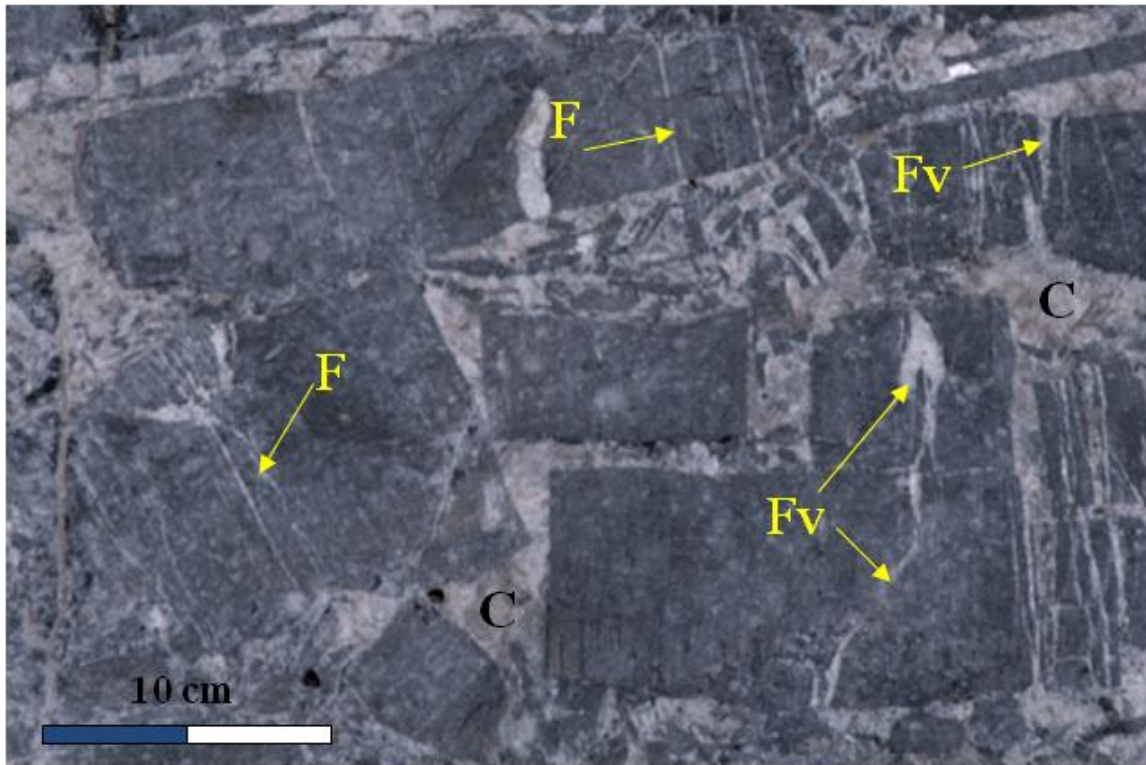


Fig. 3.10. Monomict, clast-supported breccia, showing rectangular shape blocks of dolostones. Notice that most of the calcite veins (F) affect only the blocks and restore to a common orientation if blocks are fitted back together, implying that these veins were already present at the time of brecciation (that is, they predate brecciation). Breccia is cemented with calcite (C). Fv; calcitized-evaporite-filled veins that crosscut F, probably formed during the time of brecciation. Photograph courtesy of Randall Marrett. Cupido Formation, Cañón Boquilla Corral de Palmas locality. Outcrop photograph.

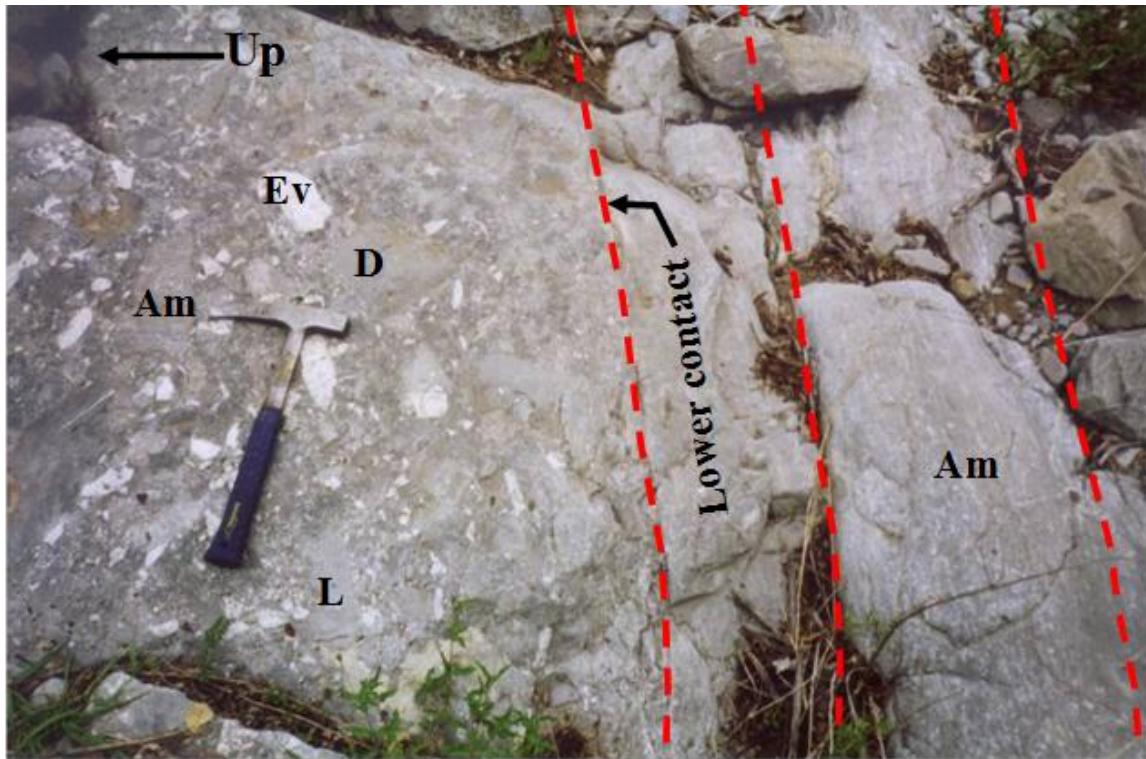


Fig. 3.11a. Polymict, clast-supported solution collapse breccia showing angular clasts and sharp lower contact, characteristic of these breccias. Clasts are made up of dolostone (D), limestone (L), calcitized anhydrite (Ev) and algal mat (Am) fragments. Beds at the bottom of collapse breccia are algal mat layers. Dashed lines indicate bedding. Cañón La Escalera locality. Note arrow marking stratigraphic up (facing) direction. Outcrop photograph.



Fig. 3.11b. Detail of Figure 3.11a showing a polymict, clast-supported evaporite solution breccia. Clasts consist of calcitized anhydrite (Ev), algal mat (Am), and dolostone (D) clasts. Notice that clasts are angular, indicating lack of transport. Cupidito (?), Cañón la Escalera locality.

Possible Origin and Timing of Evaporite Solution Breccias

A collapse breccia formed where soluble evaporites (halite, anhydrite, gypsum, etc.) have been partly or wholly removed by solution, therefore, the origin of these breccias can be analyzed in terms of solubility of evaporite beds. Evaporites can be dissolved and create cavities by percolating waters. Collapse breccias in Cupido Formation have been previously associated with fluctuations of sea level during the sedimentation of this unit (Goldhammer et al., 1991).

The field observations of the breccias identified at Cañón Corral de Palmas, Cañón la Escalera, Cañón de los Chorros, Cañón de las Cortinas, Potrero García, and Cañón Prieto, suggest the breccias in Cupido Formation were formed at or near the surface, under shallow-burial conditions, during the time-span of the Cupido Formation sedimentation.

Collapse breccias, identified in the Cupido Formation, are generally strata-bound, although sometimes collapse features extend up-section several meters suggesting the existence of an interconnected dissolution-induced cave-system (Ortega, 2002). Another line of evidence for the early origin of collapse breccias is that the breccias clearly occurred before burial stylolites (Ortega, 2002). Burial stylolites are often found at collapse breccia boundaries, and are absent in blocks within the breccia itself. Further support for the early origin of collapse breccias comes from the development of sedimentary fill deposits leveling the topography created by the collapse (Ortega, 2002).

Moreover, breccias composed of platy fragments of algal carbonate, anhydrite or mudstone cemented by evaporites, similar to those found in Cañón la Escalera (Figs. 3.11 a, 3.11b), have been documented as fairly common at and near the surface of modern sabkas and in equivalent ancient associations (Galloway and Hobday, 1983). They form

by in-situ dessication/infilling or by reworking of surficial algal mats by loading, bioturbation, root growth, channeling and other processes (Laznicka, 1988).

Another variety of breccias is formed by hydration expansion of anhydrite into gypsum. Breccias composed by trains of dolomite fragments in gypsum matrix, similar to those found in Cañón Prieto (Figs. 3.10 a, 3.10b), particularly conspicuous in tectonically undeformed associations (e.g., on carbonate platforms), probably formed by stretching and displacement of originally thin interbeds of dolomite in anhydrite (Laznicka, 1988). Finally, shrinkage caused by diagenetic dehydration of gypsum to anhydrite, uncompensated by compaction, produces brecciated anhydrite (Galloway and Hobday, 1983; Laznicka, 1988).

These stratigraphic and structural relations are important for understanding the fracture and diagenetic history of these rocks because evidence for syndimentary breccia specifies the age of some fractures (those that predate brecciation), and therefore of some of the diagenetic changes in the rock.

Chapter 4: Diagenesis and Implications for Porosity Evolution of Lower Cretaceous Cupido Formation, Monterrey Salient, Sierra Madre Oriental, Mexico.

SUMMARY

Studies of diagenetic processes in general and main fracture cement phases in particular constrain the diagenetic history and allow interpretation of the origin and evolution of the porosity in the Lower Cretaceous Cupido Formation carbonates, Monterrey Salient, Sierra Madre Oriental (SMO) Mexico. Early calcite cements occluded more than 85% of intergranular, intragranular and intercrystalline primary porosity in these carbonate rocks. Late dolomite, calcite, and in minor proportion quartz occluded almost 100% of secondary fracture porosity.

Four main calcite cements were identified. Relative timing was established by cement overlap and (in the case of cement in fractures) crosscutting relations. The first event (C1) precipitated thin isopachous fringe of fibrous calcite precipitated around allochems (i.e., ooids, peloids, oolites, and bioclasts). The second event (C2) is blocky calcite present as fill within remnant intergranular porosity. The third event (C3) calcite is blocky cement that replaced dolomite and fills remnant fracture porosity; it includes twinned calcite cement (C3t) that is present mainly in fault planes associated with bed-parallel flexural slip, suggesting the cement was deposited while Laramide-age folds grew. The last event termed C4 cement was precipitated during exposure and dissolution, due to exhumation of rocks in the SMO.

In addition, three main categories or types of dolomite cement were identified. The first dolomite precipitation event (D1) is characterized by millimeter-scale fine

laminations and fine grain size ($< 10 \mu\text{m}$) dolomite crystals. The second event (D2) dolomite is mainly a fabric-preserving phase that replaced both matrix and allochems and is characterized by fine to medium grain size (10-50 μm) anhedral crystals that postdate D1. Finally, baroque dolomite cement (D3) is present mainly as fracture fill and is characterized by undulatory extinction and subhedral to euhedral coarse crystals ($> 25 \mu\text{m}$) that postdate D2 dolomite.

Based on field observations and petrographic characteristics of the main cementation phases, six coupled fracturing-cementation events can be distinguished (see Chapter 5). Two fracture events named F1 and F2, characterized by synkinematic calcite cements that predate D2 dolomite precipitation, marked by at least four sets of fractures. Fractures of the third event (F3) are characterized by synkinematic dolomite fill, and are contemporaneous with D2 dolomite. The fourth event (F4) is characterized by synkinematic baroque dolomite and quartz, and is synchronous with D3. The fifth fracture event (F5) is characterized by synkinematic calcite (C3). Finally, flexural slip faults (F6) contain twinned calcite cement (C3t).

Crack-seal textures in dolomite bridges across fractures indicate that dolomite cements were deposited during fracture opening (synkinematic cement). The presence of synkinematic dolomite in the fractures suggests that fracturing and dolomitization are synchronous and therefore could be linked processes. Therefore, the most abundant cements, D2 dolomite, D3 baroque dolomite, and C3 calcite cements played the most important role in the evolution of the secondary porosity in the Cupido Formation rocks.

DIAGENESIS AND FRACTURE TIMING

Textbooks define *diagenesis* as all processes (chemical, physical, and biological) that affect sediments after deposition until incipient metamorphism is reached at elevated temperatures and pressures. Although diagenesis, *as defined*, includes both chemical and physical processes, much of the literature on postdepositional sediment alteration has focused on chemical processes without reference to mechanical processes that create structure (Milliken, 2003; Laubach et al., 2010). Much work has been done on chemical diagenesis of carbonate rocks (e.g., Folk, 1965; Fisher and Rodda, 1969; Bathurst, 1971; Zenger and Mazzullo, 1982; Land, 1985, 1987; Moore, 1989; Tucker and Wright, 1990; Land, 1992; Montañez et al., 1997; Lucia, 1999; Land, 1999), and there is a huge literature about diagenesis and its implications for the geological evolution of rocks. Commonly, six major processes are included in carbonate diagenesis: microbial micritization, neomorphism, dissolution, compaction (including pressure dissolution), dolomitization, and cementation (Tucker and Wright, 1990). Frequently fracturing has been ignored as a diagenetic process. Dolostones are recognized as fracture-prone rocks (Nelson, 1985) and dolomite localized along faults and fractures is a widely known phenomenon (Davies et al., 2006). Yet few studies describe pervasive, millimeter-scale fractures as an integral part of diagenesis. Where such fractures have been noted as part of the diagenetic process, fractures and the cement textures within them are commonly not described in detail or with structural rigor (Gaswirth et al. 2005; Montañez et al., 1997). Fracturing nevertheless is a common process that can modify rocks, starting early in diagenetic history and persisting through deep burial and eventual exhumation. Consequently, fracturing and other diagenetic processes commonly are broadly contemporaneous. Moreover, fracturing and diagenesis can be genetically coupled as this

study demonstrates and as is increasingly appreciated (Davies et al., 2006; Gale et al., 2010). Cementation in fractures is likely a critically important control on porosity, fluid flow attributes, and even sensitivity to effective stress changes (Laubach et al., 2004; Olson et al., 2009). Fractures are conduits for flow of fluids, which can modify rock composition and enhance diagenesis. For these reasons fracturing is considered as a diagenetic process in this study. Fracturing is commonly a key process in the origin of secondary porosity and, most importantly, in enhanced permeability in reservoirs. Consequently, it has economic implications for the mining and oil industries.

Excellent outcrops of the Lower Cretaceous Cupido and Lower Tamaulipas formations near Monterrey, Mexico, provide ideal sites to study relationships between diagenesis and fracture development. Several transverse canyons cut across the SMO folds and expose a partially dolomitized platform-to-basin carbonate system. Fracture patterns are well exposed in cross section and plan view. As will be demonstrated, the petrology of the fractures closely resembles the attributes of fractures found in core from the deep subsurface. This carbonate system can be used as analog in the subsurface for many oil and gas reservoirs.

Carbonate strata of Cupido Formation have been studied in detail from sedimentological and stratigraphic perspectives (Conklin and Moore, 1977; Wilson and Pialli, 1977; Wilson, 1981; Padilla y Sánchez, 1982, 1985; Suter, 1984; Selvius and Wilson, 1985; Campa, 1985; Aranda-García, 1991; Goldhammer et al., 1991; Goldhammer, 1999; and Lehmann et al., 1999; Ortega, 2002, Gomez, 2007) yet the relationship of diagenesis with the origin and evolution of fractures in these rocks has not been established.

In this dissertation, studies of diagenetic products and by inference processes in general and the precipitation sequence of the main cement phases in particular constrain the diagenetic history and allow interpretation of the origin and evolution of both primary and secondary porosity in the Cupido Formation. Petrographic delineation of cement volumes, textures and overlapping and crosscutting relations with fractures and microfractures from 44 sedimentary beds and 106 thin sections indicate that calcite cementation, dolomitization and fracturing were the main diagenetic processes that affected these carbonate rocks. From field and petrographic relationships I inferred the timing of cement deposition and fracturing and tested of the validity of these inferences using isotopic analyses (see Chapter 6). Understanding the origin and evolution of the porosity in general and the fracture porosity in particular in outcrops of the Monterrey Salient can help understanding other systems in the subsurface, where observations are limited to cores and indirect information such as well logs and seismic data.

To systematically develop a general paragenetic model for the Cupido Formation, this chapter is focused on the analysis of common diagenetic processes (cementation, dissolution, etc.), exclusive of mechanical processes that done fracturing. In contrast, in Chapter 5 I analyze the main fracture events, which are coupled with calcite and dolomite cementation, and combine the results with diagenetic analyses in order to articulate the paragenetic history of the Cupido Formation.

PREVIOUS WORK ON CUPIDO FORMATION DIAGENESIS

Only a few diagenetic and geochemical studies have been conducted in northeastern Mexico and adjacent areas, several of which are relevant to the present study. Moldovanyi and Lohmann (1984) conducted petrographic and stable isotopic analyses of the Cupido and Sligo Formations in northeastern Mexico and in South Texas, respectively, using cores from four wells located 100 km or more north of the Monterrey Salient: Anahuac # 6 in the Tamaulipas state of Mexico, and wells Shell-1 Brown, Gulf #1 Friedrichs, and Mobil # 1 in Texas. They identified four compositionally distinct cements in rock units ranging from approximately 1,500 to 5,500 m depth. The first two generations were interpreted as early calcite cement formed in a shallow, meteoric, phreatic environment. The third stage of calcite cement partly filled fractures. The results of fluid inclusion analysis indicate precipitation of late calcite (?) at minimum temperatures in the range of 60 to 80°C. The fourth stage generated coarsely crystalline calcite that occurs in fractures, moldic pores, and stylolitic seams. Fluid inclusion study of this fourth stage cements indicates precipitation at greater depths and higher temperatures than the third stage.

Similarly, Minero (1988) differentiated three diagenetic stages in the Cretaceous El Abra Formation along the eastern margin of the Valle-San Luis Potosi carbonate platform. The Valle-San Luis Potosi is located a more than 300 km southeast from Monterrey. According to Minero (1988), stage 1 encompasses early subaerial processes. Stage 2 corresponds to eogenetic processes dominated by equant calcite cement formed from karstic surface processes. Stage 3 is associated with Laramide-age deformation that resulted in gentle folding, fracturing, and karstification during the Cenozoic. Apart from these studies, however, little work has been done to address the interplay of diagenetic

processes with the origin and preservation of secondary porosity in the Cretaceous carbonate sequences of the SMO.

Two dissertations that were carried out partly concurrently with my work addressed aspects of cement deposits and fractures in the Cupido Formation. Ortega (2002) documented fracture size scaling for some fracture sets, whereas Gomez (2007) investigated fracture spatial arrangement for several outcrops. These studies relied in part on the diagenetic relations I documented (Monroy et al., 2001 and unpublished). Additionally, Gray et al. (2001) presented the thermal and thermo-chronological history of the SMO using fluid inclusions, K-Ar dating of illite, and apatite fission-track age analysis. These studies will be discussed later in the context of my results.

Some studies of vein cement compositions for rocks in northeastern Mexico were conducted concurrently or after my work was completed (Lefticariu, 2004; Lefticariu et al., 2005; Fischer et al., 2009). To the extent these results bear on my interpretations they are discussed below. Lefticariu (2004) documented the spatial and temporal evolution of a fluid rock system during the deformation of the evaporite-detachment Nuncios Fold Complex in the SMO, using field observations, stable and radioactive isotopes geochemistry of veins mineral and their host rock, trace element chemistry of vein minerals, and microthermometry of fluid inclusions in vein minerals.

Lower Cretaceous Cupido, Tamaulipas Superior, and Tamaulipas Inferior formations near Monterrey provide a well-known platform-to-basin carbonate system that has been the subject of a number of sedimentologic, stratigraphic and structural studies (e.g., Conklin and Moore, 1977; Wilson, 1981; Goldhammer et al., 1991; Lehmann et al., 1999; Padilla y Sánchez, 1982, 1985; and Aranda-García, 1991). Descriptions of sedimentary successions in the area are available from the literature, particularly for the

most accessible localities (e.g., Wilson et al., 1984; Goldhammer et al., 1991). This previous work provides the context for my study.

STUDY AREA: LOCATION OF SECTIONS ANALYZED

Stratigraphic sections selected for my study are located southwest of the city of Monterrey, southeast of Saltillo, and southeast of Galeana (Fig. 4.1a). A paleogeographic map of the Cupido carbonate platform system for Barremian-Aptian time in the area (Fig. 4.1b) shows that three localities selected for study are in dominantly shallow-water facies (e.g., evaporitic platform, lagoonal and grainstone shoals) of the Cupido Formation at Los Chorros, La Escalera, and Las Palmas, and one locality is in open-marine, deeper-water carbonates at Santa Rosa-Iturbide. In addition to these four localities used for this study, samples from five more areas were included: Potrero García, Cañón de las Cortinas, Cañón Prieto, Molano, and Cienegas in order to compare fracturing.

The localities chosen allow studying an array of sedimentary facies and depositional systems in order to establish the relationships between fracturing and diagenesis. Despite the intense deformation (upright isoclinal folding) experienced by these rocks during the Laramide orogeny, comparing different layers in the same structural domain of kilometer-scale folds can isolate the structural control on fracturing-diagenesis relationships. Isolating structural variables is also possible because most fracturing and diagenetic processes studied occurred before the main phase of the Laramide orogeny (my results and Marrett and Laubach, 2001).

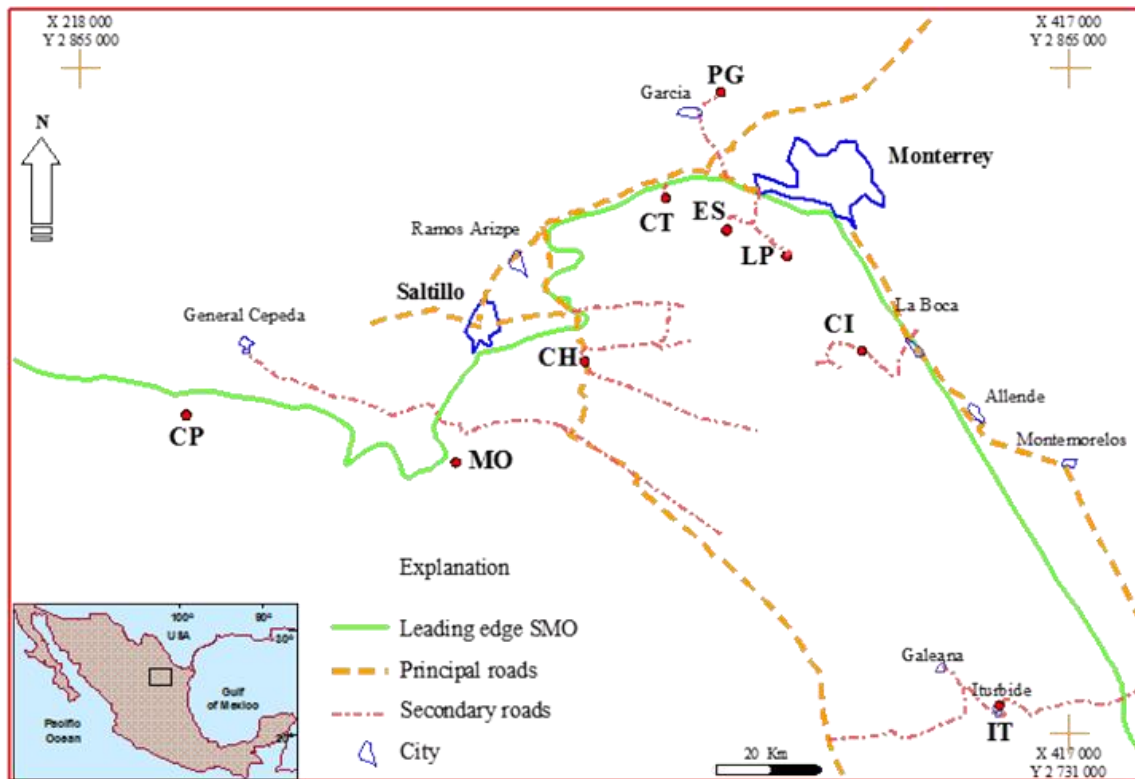


Fig. 4.1a. Location map of study localities, Monterrey Salient. Circles mark outcrop and sample localities: PG, Potrero García; CT, Cañón de las Cortinas; CH, Cañón de los Chorros; ES, Cañón la Escalera; LP, Cañón Boquilla Corral de Palmas; IT, Cañón Santa Rosa-Iturbide; MO, Molano Fault; CP, Cañón Prieto; CI, Cienegas. X and Y are coordinates in the Universal Transverse Mercator (UTM) Projection indicated by small crosses. Square in inset map indicates the location of the map above.

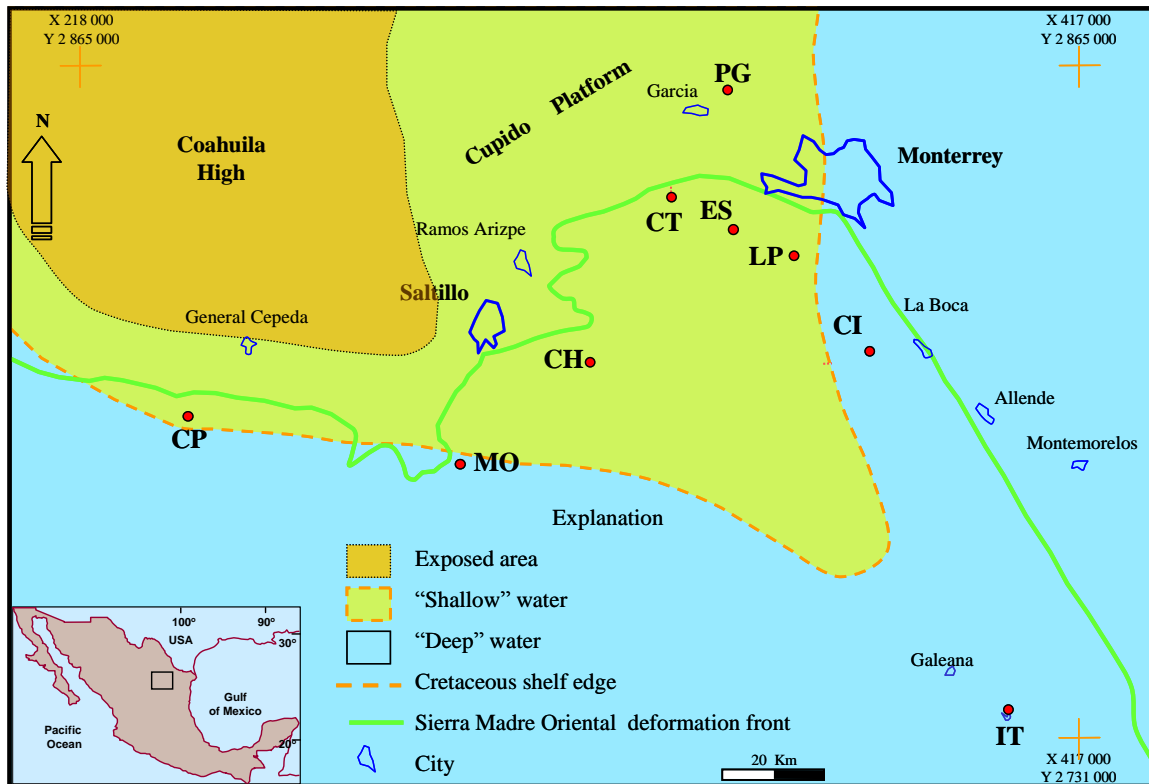


Fig. 4.1b. Barremian to Lower Aptian paleogeographic map showing the Cupido platform developed around the Coahuila High, a subaerial element at that time. Outcrops used for this study included strata deposited in both shallow and deep-water environments. PG, Potrero García; CT, Cañón de las Cortinas; CH, Cañón de los Chorros; ES, Cañón la Escalera; LP, Cañón boquilla Corral de Palmas; IT, Cañón Santa Rosa-Iturbide; MO, Molano Fault; CP, Cañón Prieto; CI, Cienegas. X and Y are coordinates in the Universal Transverse Mercator (UTM) Projection indicated by small crosses. Square in inset map indicates the location of the map above. Modified from Goldhammer et al. (1991).

STRUCTURAL-DIAGENETIC METHODOLOGY

Once I interpreted the sedimentary facies and measured fractures in the field, I did a structural-diagenetic petrographic study (SDPS). This approach consists of establishing a paragenetic sequence, taking fracturing as one additional diagenetic process that affected the rocks. In this way, I use petrographic analysis to identify and subdivide the main diagenetic processes and to establish a paragenetic sequence for each locality, in order to recognize the main cement phases and contemporaneous fracturing-cementation events. The use of textural observations from within the fractures, such as crack-seal texture and cements that overlap crack-seal texture, differentiates my approach from a few previous studies that listed cement-filled fractures in paragenetic sequences (Montañez et al., 1997). My paragenetic sequences allow me to uncover how chemical and mechanical processes are linked in the Cupido Formation.

Structural-Diagenetic Petrographic Study (SDPS)

Petrographic analysis

A methodology to prepare oriented thin sections from outcrop samples was created for structural-diagenetic petrographic study (SDPS). Samples of 44 sedimentary beds and 106 large-sized (7 cm x 5 cm) oriented thin sections (Appendices 3.1 and 3.2) and corresponding slabs were the main subjects for petrographic studies. Thin sections were oriented, and both layer-parallel and layer-perpendicular thin sections were cut. The former were prepared to observe mainly fracture characteristics and the latter to observe sedimentologic and diagenetic characteristics. Thin sections were stained with Alizarin Red-S in a 0.2% HCl solution in order to distinguish calcite from dolomite using Friedman's (1959) method.

Petrographic observations consisted of descriptions and identification of original rock textures, cement phases and matrix composition, and quantification of components (Appendix 4.1). Percent of dolomitization or dolomite cement volume was obtained by point counting (generally 200 counts) and visual estimation (Appendix 4.2), and measurements of dolomite crystal size (Appendix 4.3) were also included.

Identification of common diagenetic processes (microbial micritization, neomorphism, dissolution, compaction, including pressure or chemical dissolution, dolomitization, and cementation) in each thin section was carried out using standard transmitted light thin-section on stain, standard petrographic sections. Selected samples were imaged using scanning electron microscopy (SEM) and cathodoluminescence (CL) techniques.

In this study, I use the word event to encompass a period of time that a diagenetic or structural process affects a volume of rock, before and after which the process may have been inactive. For example, calcite cementation can affect the rock during multiple episodes of geologic time, separated in time by lapses of calcite cementation. To differentiate these periods of time, I numbered them in order from the first (the oldest, e.g. C1) to the most recent (the youngest, Cn), where n is the number of times that calcite precipitated in the rocks. This conceptualization of cement precipitation accords with standard practice (e.g., Montañez et al., 1997), but some of my results raise questions about this view of carbonate diagenesis that I return to later in my Discussion.

Because fracturing, in this study, was considered as part of paragenesis, identification of the main fracture sets (fractures sharing the same characteristics or attributes, such as orientation and mineral fill) was included in the diagenetic description. Fracture events were numbered following the same rule as other diagenetic events, but

relative timing was established by structural methods (Hancock, 1985). Fracture sets were characterized by their orientations, crosscutting relationships and cement types and kinematically significant textures (for example, crack-seal texture) both in the field and from inspection of oriented thin sections. Attributes described for fracture-filling cements include composition, crystal size, presence and character of crack-seal texture, overlap relations, mineral cleavage, extinction, presence and degree of twinning, and evidence of transection by later fractures. Appendix 4.1 includes 36 petrographic summary sheets based on 106 thin section descriptions. Note that the presence or absence of a particular mineral phase in a fracture is, by itself, insufficient evidence to subdivide fractures into separate categories. Field photographs and photomicrographs were taken to document the petrographic observations.

Table 4.1 shows an example of a petrographic summary sheet of Appendix 4.1, based on the description of two thin sections (CulPa 9-98p and CulPa 9-98So). The rock sample, in this example, is a dolostone (100% dolomite). The main diagenetic processes identified in thin sections were: dolomitization that replaced 95 to 100 % of the original rock texture, three fracture events (one characterized by calcite cement fill only and the other two by both dolomite and calcite cement). The last two fracture sets were differentiated because they have different orientations. The replacing dolomite phase is constituted by very fine-grained crystal sizes (0.015-0.020 mm). Dolomite cement in fractures is constituted by euhedral meso-crystals. In this example, stylolites cut the fracture set with only calcite cement and one of the fracture sets with calcite and dolomite cement, so stylolites postdate these first two fracture sets and predate the other fracture set with calcite and dolomite cement.

Structural-diagenetic Petrographic Summary Sheet					
Hand sample description: CulPa-9-98.					
Dolostone. There are at least three main fracture sets. All fractures are perpendicular to the stratification plane. Fractures present both fibrous and blocky cements. At the bottom of the sample CulPa9-98 there are two sets of fractures. One presents fibrous dolomite cement and calcite. The second one cuts the first and is composed by blocky calcite cement and dolomite.					
Thin Section:					
Number	Formation	Facies	Age	Polish Quality	Location
CulPa-9-98p CulPa-9-98So	Cupido	Peritidal Platform	Lower Cretaceous	Ok	Las Palmas, SMO Mexico
Outcrop quality	Rock Type		Sampled Date	Date description	
Good	Dolostone		January, 2000	July, 26, 2001	
Oriented?	Notch?	North?	Macrofractures?	Location?	
Yes	Yes (3)	Yes	Yes	Everywhere in thin section	
Description: Dolostone formed by matrix with very fine grain micro-dolomite crystals. Probably the primary texture was mudstone. Culpa 9-98So Most of the rock is affected by dolomitization and also most of the fractures.					
Diagenetic Processes:					
	Processes	%	Description (size, etc)		
D	dolomitization	95-100	very fine euhedral crystals (0.015-0.20 mm). Replacement phase.		
Ps	pressure-solution		Stylolites		
Paragenesis: D (very fine crystals) – F1 (calcite cement) – F2 (calcite and dolomite cement) – PS (stylolites) – F3 (calcite and dolomite)					
Fracture Description: Culpa-9-98So sample presents two fractures sets. The first one is a microfracture set with calcite cement. The second set cuts the first one and is composed by fibrous euhedral meso-crystals of dolomite and blocky calcite cement. Stylolites cut F1 and F2, but not F3. Because in some cases stylolites cut F1 and F2 fractures and vice versa probably both events were developed at the same time. Note: SEM studies for this sample. P, sample perpendicular to stratification; So, sample parallel to stratification.					

Table 4.1. Sample of petrographic summary sheet of a thin section description.

PARAGENETIC SEQUENCE

The relative chronology (paragenetic sequence) of diagenetic processes was determined based on cross-cutting relationships, petrographic evidence among diagenetic features, and field observations. Table 4.2 shows the diagenetic processes (cementation, dissolution, etc.) and the evidence (field and petrographic observations, and effects on older and younger features) that supports interpretation of their relative chronology. Fracture diagenetic analysis is exhaustively described in Chapter 5.

The events are described in order of their relative chronology. However, it is important to clarify that 1) some events probably occurred simultaneously, 2) others, like compaction, likely occurred during protracted periods in the history of these rocks, and 3) a few events, like cementation and possibly some fracturing, probably occurred during comparatively brief periods of time. This provisional interpretation of the likely duration of events agrees with conventional wisdom (for example, McBride, 1989; Nelson, 1985); on the other hand some recent work in siliciclastic rocks suggests that some cement precipitation processes (Lander et al., 2008) and fracture growth histories (Becker et al., 2010) are extremely protracted, lasting tens of millions of years. The tables refer to figure numbers from Chapters 3 (field evidence) and this chapter (petrographic evidence) to evidence the information described in more detail in the following pages.

Process	Field Observations	Petrographic Observations	Evidence of older or synchronous features	Evidence of younger features	Localities
Micritization		Micrite in form of envelopes on carbonate grains (Fig.4.6). Bioclasts completely altered. Original skeletal nature of grains difficult to determine (Fig.4.2a).	Allochrem and mud deposited.	Calcite overlapping and filling space among micritized ooids implies micritization predates calcite cementation. Replacement dolomite overlaps micrite, so postdates it (Fig. 4.4a).	Los Chorros Las Palmas
Dolomitization (D1) (fine grained & laminated)	Laminations of dolomite and evaporites. Dolomite fragments are components in solution breccias. (Fig. 4.3c).	Laminations of different size dolomite crystals (Fig. 4.3a). D1 dolomite is composed of fine-grain (< 50µm) crystals and form millimeter-scale fine laminations. Different crystal sizes distinguish the laminations. Dolomite in solution breccias fragments are similar in crystal size, texture and color to laminated dolomite.	Laminations of dolostones and evaporites imply simultaneous deposition (Fig. 4.3a).	D1 dolomite fragments in solution breccias imply D1 predates brecciation (Fig. 4.3c). Probable desiccation fractures cut D1 laminations (Fig. 4.3a). Both calcite veins and bedding-parallel stylolites cut D1 dolomite laminations (Figs. 4.3a, 4.3b).	Cienegas, Cañón Prieto, Potrero García, La Escalera, Los Chorros Las Palmas.
Calcite cementation (C1)		Thin isopachous fringe or fibrous crystals around ooids and peloids (Figs. 3.6b, 4.2a).	C1 calcite around micritized ooids (Fig. 4.2a) implies C1 postdates micritization.	Calcite veins cross-cut C1 (Fig. 3.6b, 4.2a).	Los Chorros Las Palmas
Dissolution		Ooids cores dissolved and oomoldic porosity. (Figs. 3.6b, 4.2a).	C1 around micritized ooids partially dissolved implies dissolution postdates C1 (Figs. 3.6b, 4.2a).	Oomoldic porosity (Fig. 3.6b) filled by C2 calcite implies dissolution predates C2.	Los Chorros Las Palmas

Table 4.2. Diagenetic processes and evidence used to determine relative timing.

Process	Field Observations	Petrographic Observations	Evidence of older or synchronous features	Evidence of younger features	Localities
Evaporite solution/breccias	Two types of evaporite solution breccias at different stratigraphic levels were recognized. Monomict breccias are stratiformal and interstratal with sharp lower contacts and irregular upper contacts, and show rectangular shape blocks of dolostones (Figs. 3.9a, 3.9b, 3.10, 3.11a). Polymict clast-supported solution breccias are constituted by algal mat, calcitized anhydrite, limestone and dolostone fragments and have sharp lower contact. Clasts are angular and vary from a few mm to more than 10 cm long (Figs. 3.11a and 3.11b). Algal mat layers present at the bottom of solution breccias (Fig. 3.11a).	Breccias cemented by blocky calcite (Figs. 3.10, 4.2b). Breccia cemented by two types of calcite: non-isopachous equant calcite spar, as first generation cement around dolostone clasts, and by poikilotopic twinned calcite spar (Fig. 4.2b).	D1 dolostone clasts in breccias imply brecciation postdates D1 dolomite (Figs. 4.2b, 5.5b). In monomict breccias some calcite veins affect only the fragments, implying veins were already present at the time of brecciation (Figs. 3.10, 4.2b). Breccias are cemented with calcite that also fills veins, so these veins probably were formed during the time of brecciation (Fig. 3.10, 5.5b).	Compaction truncates both fracture types, pre-brecciation and synbrecciation, so compaction postdates brecciation (Fig. 5.5b).	Las Palmas, La Escalera, Potrero García, Las Cortinas, Los Chorros
Calcite cementation (C2)		C2 calcite is equant spar drusy mosaic and clear anhedral calcite that fills oomoldic porosity and pore-space between grains (Figs. 3.6b and 4.2a). C2 includes also non-isopachous equant calcite spar cement around clasts in solution breccias (Fig. 4.2b).	C2 calcite fills oomoldic porosity (Fig. 4.2a), so postdates dissolution. C2 calcite around D1 dolomite fragments implies C2 postdates D1 and also brecciation (Fig. 4.2 b).	Calcite filled veins and stylolites cross-cut C2 calcite (Figs. 3.6b, 4.2a).	Los Chorros Las Palmas
Compaction, bedding parallel stylolites	Stylolites are preferentially developed along stratigraphic planes or at the boundaries of mechanical layers (Figs. 4.7b, 5.3). Some stylolites present large teeth and are most common at dolostone/limestone contacts. Most of fractures form high angle with these stylolites (Fig 4.7b, 5.3).	Flattened and aligned anhydrite nodules (Fig. 4.3b). Pellets and bioclasts with tangential contacts and sutured contacts between grains (Fig. 4.7a).	Sutured contacts between pellets dissolved C1 calcite cement (Fig. 4.7a), so calcite cementation predates compaction. Sutured contacts between clasts in solution breccias truncates both fracture sets identified, so compaction postdates both fracturing and the brecciation (Fig. 5.5b)	Calcite veins (F2 or F5) crosscut bedding parallel stylolites, so compaction predates calcite veins.	Las Palmas, Potrero García, Las Cortinas, La Escalera, Los Chorros

Continuation Table 4.2.

Process	Field Observations	Petrographic Observations	Evidence of older or synchronous features	Evidence of younger features	Localities
Pervasive dolomitization (D2)	Outcrops of carbonate sequence at Las Palmas and La Escalera localities are formed mainly by thin to medium bedded dolostones (Fig. 4.4b).	Plane-light photomicrographs show limestones partially replaced by idiopathic mosaic of anhedral dolomite rhombs (Fig. 4.4a) called here D2. D2 is characterized by fine to medium grain size (10-50 μm anhedral crystals that replaces both matrix and grains (Figs. 4.4a). Dolomite replaces from 5 to 100% of the rocks.	Because D2 dolomite replaces host rocks, processes like micritization, C1 and C2 calcite, predate D2 dolomitization (Figs. 3,5c, 4.4a). Dolomite bridges in F3 fracture have petrographic characteristics that are similar to D2 matrix dolomite, so both are contemporaneous. (Fig. 5.6b).	Fractures with both baroque dolomite (F4) and calcite cements cross cut D2 dolomite. (Fig. 5.7b).	Las Palmas, La Escalera
Baroque dolomite (D3)	Outcrops of carbonate sequence at Las Palmas, La Escalera and Los Chorros localities are formed by thin to medium bedded dolostones with fractures present fibrous dolomite crystals cement.	Baroque dolomite is characterized by undulatory extinction and sub- to euhedral fibrous/elongated coarse crystals (> 25 μm) (Fig. 4.5a, 5.7b). Dolomite crystals are elongate at high angle to fracture walls (Fig. 5.7b). Calcite in fracture cross-cuts both quartz and dolomite.	Fractures with baroque dolomite have straight paths that cut and postdate D2 dolomite (Figs. 5.7b, 5.7c).	Incomplete and irregular baroque dolomite crystal borders are overlapped by calcite (Fig. 5.7b, 5.7c, 5.7d), thus dolomite predates calcite in fractures.	Las Palmas, La Escalera, Los Chorros
Dolomitization (Ferroan dolomite)		Fe-dolomite found in open marine facies is characterized by isolated euhedral crystals with external iron rich zone (Fig. 4.5b).	No evidence	No evidence	Las Palmas, La Escalera, Los Chorros Santa Rosa
Calcite cementation (C3)	Calcite fills fracture porosity and is also present as cement and filling microfractures in some fault breccias.	C3 includes all calcite cement that postdates both D2 and D3 dolomite and is characterized by blocky cement that partially replaces dolomite cements in fractures and fills remnant porosity (Fig. 4.2c, 5.7b, 5.7c, 5.7d, 5.7e). C3 is also present as cement and filling microfractures in some fault breccias (Fig. 4.7a). C3 is distinguished from C1 because the last one is restricted to around ooids as thin isopachous fringe of fibrous crystals, and from C2 because C3 is mainly present as fracture fill.	D2 and D3 dolomite bridges in fractures are partially overlapped by calcite, indicating calcite is partially replacing both D2 and D3 dolomite (Figs. 5.7b, 5.7c, 5.7e).	Karst dissolution affects C3 calcite.	Los Chorros, Las Palmas

Continuation Table 4.2.

Process	Field Observations	Petrographic Observations	Evidence of older features	Evidence of younger features	Localities
Recrystallization		Aggrading calcite crystals in the matrix, fossils, and ooids. Uniform crystal size in allochems and matrix (Fig. 4.8). Where recrystallization is present, it affects from 5 to 100% of the rock.	Uniform crystal size in allochems and matrix (Fig. 4.8) is indicative of recrystallization, so processes like micritization, bioturbation, calcite cementation (C1, C2), and dolomitization predate recrystallization.	Bedding oblique stylolites cut recrystallized rock so, recrystallization predates pressure solution.	Las Palmas, La Escalera, Santa Rosa
Dedolomitization		Dedolomitization is shown by "corroded" and incomplete dolomite crystals, partly replaced by calcite (Fig. 4.9). Some calcite rhombs might have been dolomite crystals now completely replaced by calcite during dedolomitization.	D2 pervasive dolomite crystals are "corroded" and incomplete imply that D2 dolomite predates dedolomitization (4.9).	No evidence	Santa Rosa, Los Chorros, La Escalera, Las Palmas
Pressure-solution (bedding oblique stylolitization)	Outcrops at La Escalera and Corral de Palmas show inclined or high angle stylolites with respect to bedding (Fig. 4.7d). Most fractures form low angle with stylolites.	Stylolites partially dissolved matrix and grains in both dolostones and limestones (Fig. 4.8). Bedding oblique stylolites present quartz cement along their paths, and they dissolved partially F4 fractures (Fig. 5.7d).	Stylolites cross cut F4 fractures (synkinematic baroque dolomite cement), so postdate F4 fracturing and baroque dolomite cementation. Quartz cementation in stylolites, implies that both are synchronous (Fig. 5.7d).	Calcite cement replaced quartz cement in stylolites, so postdates pressure solution (Fig. 5.7d).	Las Palmas, La Escalera,
Silica cementation (quartz)	Outcrops of carbonate sequence at Las Palmas, La Escalera and Los Chorros localities are formed by thin to medium bedded dolostones with fractures that contain quartz and fibrous dolomite cements. At Santa Rosa and Los Chorros localities chert nodules and silica bands are common (Fig. 3.3b).	Quartz is present as authigenic along bedding oblique stylolites, in F4 fracture cement, and as chert nodules in basinal facies rocks (Fig. 3.3b). Quartz in F4 fractures has aligned fluid inclusions possibly indicating crack seal texture (Figs. 4.10d). Inclusions are also aligned in trends approximately perpendicular to macrofracture orientation (Figs. 4.10d). Quartz crystals typically contain carbonate inclusions that probably were dolomite crystals originally (Figs. 4.10c).	Quartz cementation in stylolites (Fig. 4.10a) implies that both events are synchronous. Dolomite inclusions in quartz imply simultaneous precipitation of both minerals (Fig. 4.10b).	Quartz crystals are overlapped by C3 calcite crystals thus quartz predates C3 (Fig. 4.10c).	Santa Rosa, Los Chorros, La Escalera, Las Cortinas, Las Palmas

Continuation Table 4.2.

Process	Field Observations	Petrographic Observations	Evidence of older features	Evidence of younger features	Localities
Twinned calcite (C3t)	Thick fibrous calcite sheets are present in most flexural slip planes and in some cases a reddish zone marking a layer-parallel breccia between carbonate beds (Figs. 5.9a, 5.9b).	Flexural slip planes contain fibrous calcite cement. This calcite is characterized by thick twins with sharp edges in large crystals (Fig. 5.9c). C3t twinned calcite is also found in fault breccia planes, and occasionally as cement in some fractures.	Flexural slip planes affected most of the identified diagenetic processes in the Cupido Fm., so most are pre-flexural.	Karst dissolution affects flexural slip faults and C3t calcite.	Los Chorros, Las Palmas, Las Cortinas
Dissolution (karst) and precipitation of calcite and travertine (C4)	Calcite fills fracture porosity and is also present as cement and filling microfractures in some fault breccias. Caves are present in several places at the Monterrey Salient (e.g., Potrero García), (Fig. 4.11).	Dissolution affects the whole rock (Fig. 4.11). Calcite precipitation due to subaerial exposure and dissolution of the carbonate sequence in the SMO is called C4 and is postkinematic cement in some of the fracture sets identified in this study, filling remaining porosity. I found no petrographic diagnostics to distinguish C3 from C4. However, isotopic analysis (see Chapter 6) shows that these two phases of calcite cement represent different events. For that in this Chapter I named as C3 (excluding C3t) cement all calcite that postdate D3 baroque dolomite	Presence of caves in the Monterrey Salient (e.g. Potrero García, La Huasteca), demonstrates dissolution and precipitation is currently acting in rocks of the SMO (Fig. 4.11). Caves are located in high areas in the SMO, so postdate structural deformation. Joints and travertine are present in the SMO.	No evidences.	All localities

Continuation Table 4.2.

DESCRIPTION OF DIAGENETIC PROCESSES

According to the results of the petrographic studies and field observations, summarized in Tables 4.2a to 4.2f, six major diagenetic processes affected the carbonate sequence of the Cupido Formation: microbial micritization, dissolution, cementation, compaction, dolomitization and fracturing. These processes can yielded at least 22 distinct events during the history of these rocks. However, dolomite and calcite are the most abundant cements in both matrix rock and fractures, and therefore these phases played the most important role in the evolution of porosity of the Cupido Formation. The following sections first describe calcite and dolomite cements and other secondary processes. The second part of this section discusses the paragenetic sequence by localities, and infers some regional patterns. The associated fracture sets (fractures with dolomite and calcite synkinematic cement) are analyzed in next chapter.

Calcite Cement

Four main calcite cementation events were identified in carbonates of the Cupido Formation:

C1 and C2 calcite cement

C1 includes thin isopachous fringes of fibrous calcite precipitated around allochems (i.e., ooids, peloids, oolites, and bioclasts) (Fig. 4.2a). The presence of C1 around micritized ooids implies that C1 postdates micritization. C2, for practical purposes, includes equant spar, drusy mosaic, and clear anhedral calcite that fills oomoldic (from dissolved ooids) and intergranular porosity (Fig. 4.2a), and non-isopachous equant calcite spar around clasts in evaporite solution breccias (Fig. 4.2b).

Because C1 cement is present around grains as thin envelopes and C2 calcite is in the spaces between those grains, I infer that C2 filled the porosity after C1 precipitation (Fig. 4.2a). Thin sections show grains in point contact suggesting a low degree of compaction (Fig. 4.2a), probably due to the early timing of these cements, so C1 and C2 likely predate significant compaction. These cements are best developed in non- or partially dolomitized shallow water limestones (e.g., oolitic grainstone, evaporite solution breccias, etc.) where primary porosity commonly is high (James, 1990). However, they are also present in lower concentration in other facies. Based on their fabrics and morphologies (James, 1990), C1 and C2 cement can be interpreted as marine in origin. Marine cement usually forms fringes up to a few hundred microns thick and shows polygonal boundaries between fringes (Tucker and Wright, 1990), and occurs in reef cavities, but also is particularly common in grainstones (Fig. 4.2a). Calcite precipitated in the zone of aeration above the water table, i.e., vadose zone, are blocky and fibrous-needle calcites; below the water table, calcite cements commonly form rims of bladed to equant crystals that completely encircle the grains (Bathurst, 1971; Milliman, 1974; Scholle, 1978; Longman, 1980). Although most C1 and C2 calcite have a marine origin, some C2 calcite around clasts in evaporite solution breccias (Fig. 4.2b) probably precipitated due to fresh water percolation or meteoric water influence (Folk, 2002, oral communication). C1 and C2 calcite cements are evident in most of the non-dolomitized beds in Cañón de los Chorros, Cañón Boquilla Corral de Palmas, and Cañón de la Escalera.

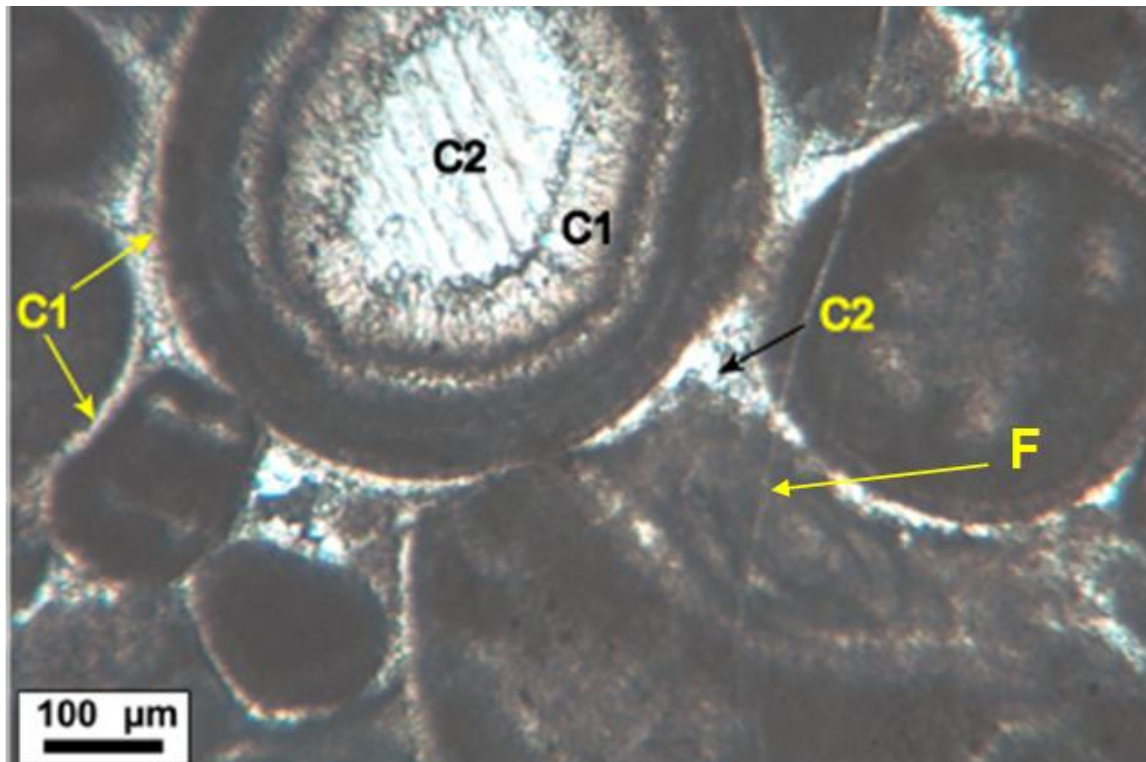


Fig. 4.2a. Grainstone showing two generations of calcite cement. C1 is thin isopachous fringe of bladed calcite around ooids and C2 is equant spar totally filling the intergranular porosity. Dissolved ooid space is filled with fibrous and C2 poikilotopic calcite cements. C1 cement probably prevented mechanical compaction of this grainstone which has only grains in point contact. Notice a thin calcite veins cross-cutting ooids and both C1 and C2 cements. Cupido Formation, sample CulCh3-98, Los Chorros locality. Photomicrograph.

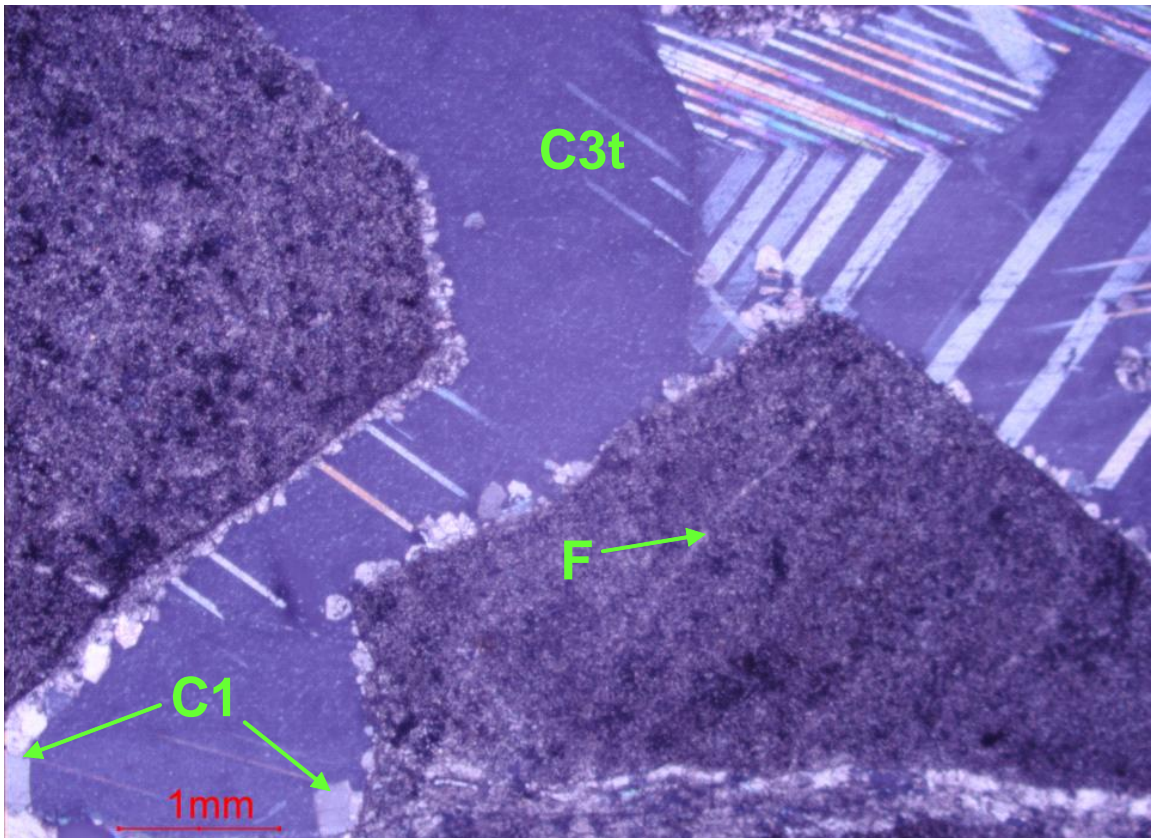


Fig. 4.2b. Solution breccia showing non-isopachous equant calcite spar (C2), first generation cement around dolostone clasts, and later poikilotopic twinned calcite spar (C3t) occluded the porosity. Dolostone fragments are composed by microcrystalline dolomite. It is inferred that dolostones were eroded to produce fragments, and because dolomitization did not affect calcite cements, dolomite predates C1 and C3t calcite. Notice a calcite-filled vein (F) that affected only a dolomite clast, implying that this vein predates brecciation. Cupido Formation, sample CulPa1-01, Cañón Las Palmas locality. Photomicrograph.

C3 calcite cement

In this Chapter I classified as C3 (excluding C3t and C4) all calcite that postdates dolomite cementations (see dolomitization below). Blocky C3 calcite cement partially replaced dolomite in fractures (Fig. 4.2c) and filled remnant porosity. C3 also filled microfractures in some fault breccias (see C3t twinned calcite below). C3 is distinguished from C1 by not being restricted to thin isopachous fringes around grains, and from C2 by mainly being present as fracture fill. The timing of C3 also differs from C1 and C2 because it postdates the replacement dolomite phase.



Fig. 4.2c. Veins in a dolostone. Matrix is composed by replacement phase dolomite. Calcite (in red) overlaps dolomite, indicating that C3 calcite postdates dolomite cementation. Thin section stained to differentiate dolomite (brown, grey or white) from calcite (red). Thin section is parallel to bedding. Cupido Formation, sample CulPa8-98, Cañón Las Palmas locality.

C3t twinned calcite

C3 also includes twinned calcite, referred as C3t. C3t is twinned calcite cement found mainly on flexural slip fault planes (see Chapter 5), and occasionally in solution breccias (Fig. 4.2b).

C4 calcite cement (“modern calcite”)

Calcite precipitation due to subaerial exposure and dissolution of the carbonate sequence in the SMO is called C4 and is postkinematic cement in some of the fracture sets identified in this study, filling remnant porosity. I found no petrographic evidence to distinguish C3 from C4. However, isotopic analysis (see Chapter 6) shows that these two phases of calcite cement represent different events

Dolomite Cement

Dolomite is a widespread, rock-forming, rhombohedral mineral consisting of $\text{CaMg}(\text{CO}_3)_2$ (Land, 1980). In ideal dolomite, there are an equal number of Ca and Mg ions, and these are arranged in separate sheets, with CO_3^{2-} planes in between (Tucker and Wright, 1990). Dolomite is formed in different environments with a wide range of crystal sizes, forms, and fabrics. Dolomite can originate as a primary precipitate from seawater and as a replacement phase of pre-existing carbonates, but dolomite is also commonly present as cement, filling voids and fractures.

Three main types of dolomite recognized in the carbonate sequence of Cupido Formation are: fine grained and laminated dolomite, fine to medium grained replacement dolomite, and coarse grained baroque dolomite. Additionally, a few crystals of medium grained ferroan dolomite were found in basal facies as mentioned at the end of this section. As explained below, these types of dolomites were differentiated based on petrographic characteristics such as crystal size, extinction form, and cross-cutting relationships with other diagenetic features.

Fine grained and laminated dolomite (D1)

Dolomite characterized by fine-grained ($< 10 \mu\text{m}$) and anhedral crystals, which form millimeter-scale laminations that are distinguished by different grain sizes (Fig. 4.3a), is named D1 in this study. Dolomite laminations are interbedded with evaporite layers (Fig. 4.3b), algal mats, and evaporite solution breccias (see Appendix 2.1). D1 dolomite was affected by compaction and by calcite-filled veins that crosscut laminations (Fig. 4.3a), so D1 dolomitization predates desiccation, compaction and calcite fractures. An evaporite solution breccia in the Potrero García locality is composed of dolostone

clasts with a matrix of limestone that lacks evidence of dolomitization (Fig. 4.3c). Because dolomite in these clasts has characteristics in size and texture of D1 dolomite, and because beds composed of D1 dolomite laminations overlie solution breccias, I infer that the clasts were derived from D1 dolostones. If this inference is correct, then D1 dolomitization partly predates and partly postdates brecciation.

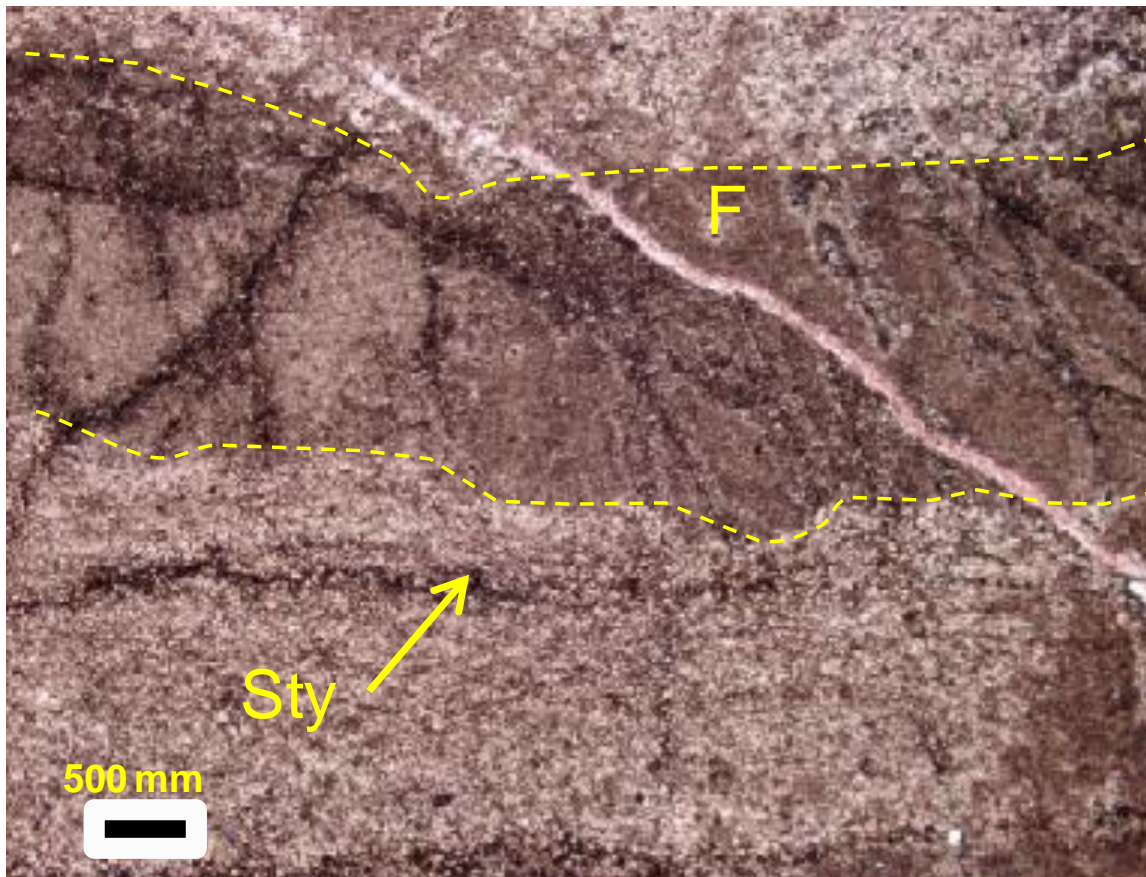


Fig. 4.3a. Photomicrograph of D1 dolomite. Three different crystal sizes distinguish the laminations. Notice the bedding parallel stylolites (Sty) affecting the laminations. F is a calcite-filled fracture that crosscut the laminations. Therefore, D1 predates both compaction and fracturing. Dashed lines indicate lamination boundaries. Cupido Formation, sample CP2-01, Cañón Prieto locality.

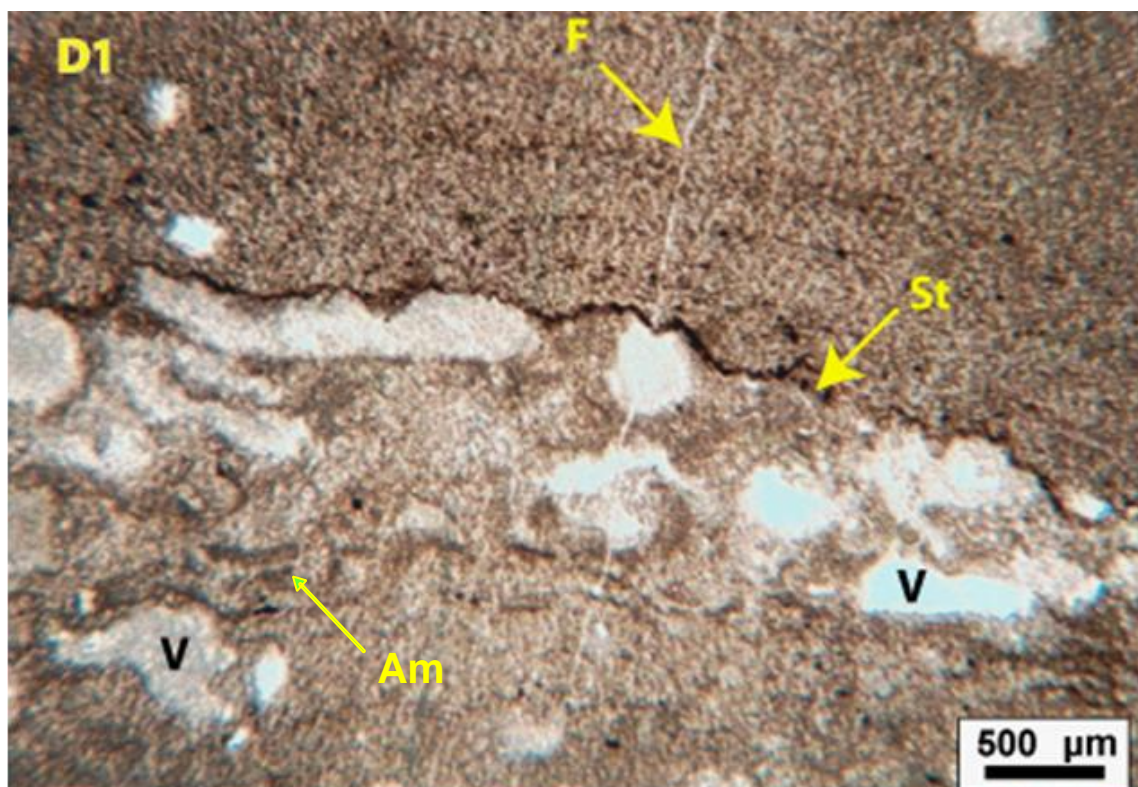


Fig. 4.3b. Plane-light photomicrograph of laminated dolostone (D1) and algal mats (Am) with calcitized evaporite nodules (V). The boundary between D1 and Am is marked by a bedding-parallel stylolite (St), with teeth amplitudes less than 250 microns, that dissolved evaporite nodules. Notice that stylolite cuts cross a calcite-filled vein (F), so compaction postdates F fracturing. The interlaminations of D1 dolomite, algal mats and evaporites imply simultaneous deposition. Cupido Formation, sample CuEsc3-98, Cañón la Escalera locality.

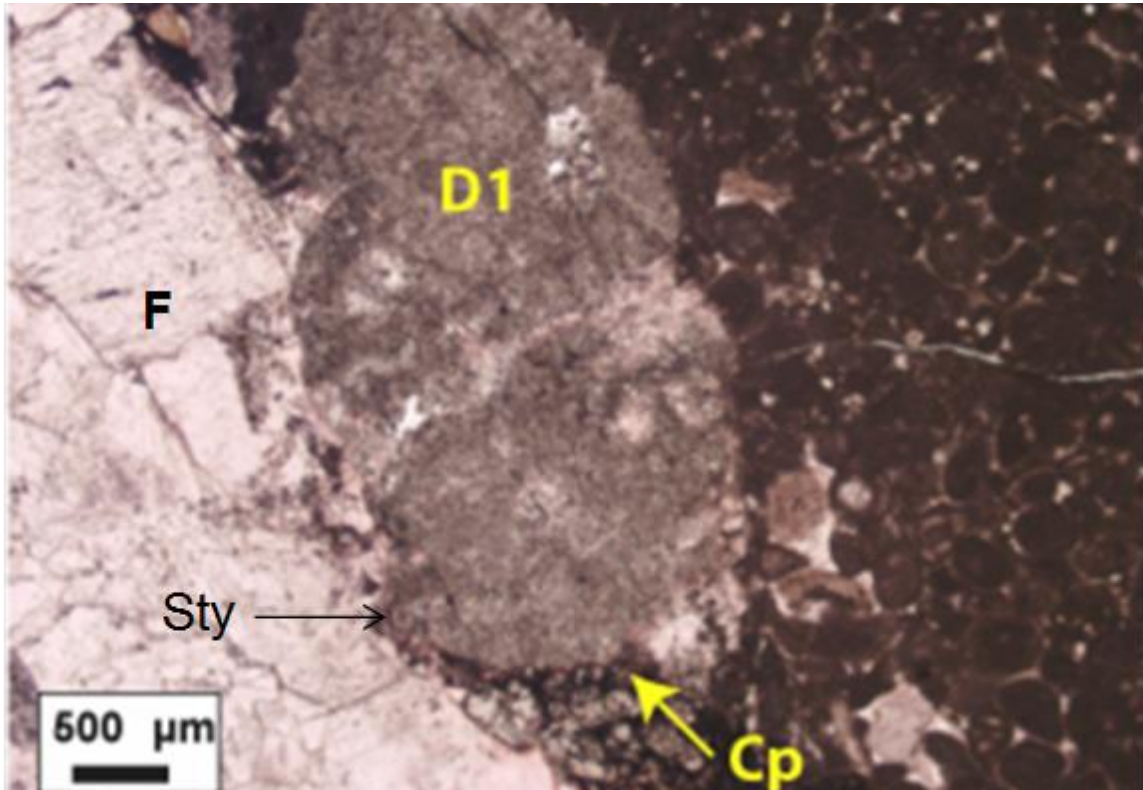


Fig. 4.3c. Photomicrograph of evaporite solution breccia showing a calcite-filled vein (F) and a microcrystalline dolostone clast (D1) in a pellet wackestone-packstone matrix (W-Pm). Because matrix is not dolomitized, it is interpreted that the clast was dolomitized before brecciation. Dolomite clast is interpreted as a product derived from D1 dolostones, because the dolomite textures are identical and beds composed of D1 dolomite laminations overlie this solution breccia. Notice also that a bedding-oblique stylolite (Sty) affects both clast and vein, so postdates both D1 dolomitization and the vein. Cupido Formation, sample PG2-01, Potrero García locality. Cp, compaction.

Replacement dolomite (D2)

Another type of dolomite found in the Cupido Formation is characterized by fine to medium grain size (10-50 μm) euhedral to sub-euhedral crystals, and is named D2 dolomite because of textural evidence that it postdates D1. D2 dolomite is mainly differentiated from D1 on the basis of its crystal size, and from baroque dolomite on the basis of its crystal size and the lack of undulatory extinction. D2 dolomite crystals are the dominant components in dolostones and dolomitized limestones of the Cupido Formation, and in minor proportion as fracture cement. Original rock textures of dolostones can be recognized with the aid of standard petrographic microscopy (e.g. examples from Cañón de los Chorros), and indicate that the host rocks were originally shallow marine carbonates (wackestones-packstones and grainstones) (Fig. 4.4a) that were later affected by D2 dolomite. Therefore, D2 dolomite is considered as a phase that replaced both matrix and grains of original limestones, including solution breccias. D2 dolomite replaced micritized grains, and calcite cements (C1 and C2), so it postdates micritization, calcite cementation (Fig. 4.4a), and brecciation.

In terms of rock volume affected by dolomitization in the study area, D2 dolomite is the most abundant compared with the other two dolomite types (laminated D1 and baroque D3 dolomite). D2 replaced from 3 to 100% of the rock volume, and in the extreme case forms an idiomorphic mosaic of euhedral dolomite rhombs. D2 dolomite replacement affected the Cupido Formation on a regional scale (see Chapter 2, Appendix 2.1). The degree of dolomitization increases upward within the parasequences (Ortega, 2010). Moldovanyi and Lohman (1984) described similar distributions of dolomite content in the Sligo Formation sequences that are lateral correlatives of Cupido Formation. D2 dolomite affected about 90% of the entire Cupido column at Cañón de la

Escalera (Fig. 4.4b), about 70% at Cañón Boquilla Corral de Palmas, and between 12% and 70% in other localities inside of the SMO (i.e. Cañón de las Cortinas, Cañón de los Chorros, and Cienegas), although less than 12% at Cañón Santa Rosa-Iturbide.

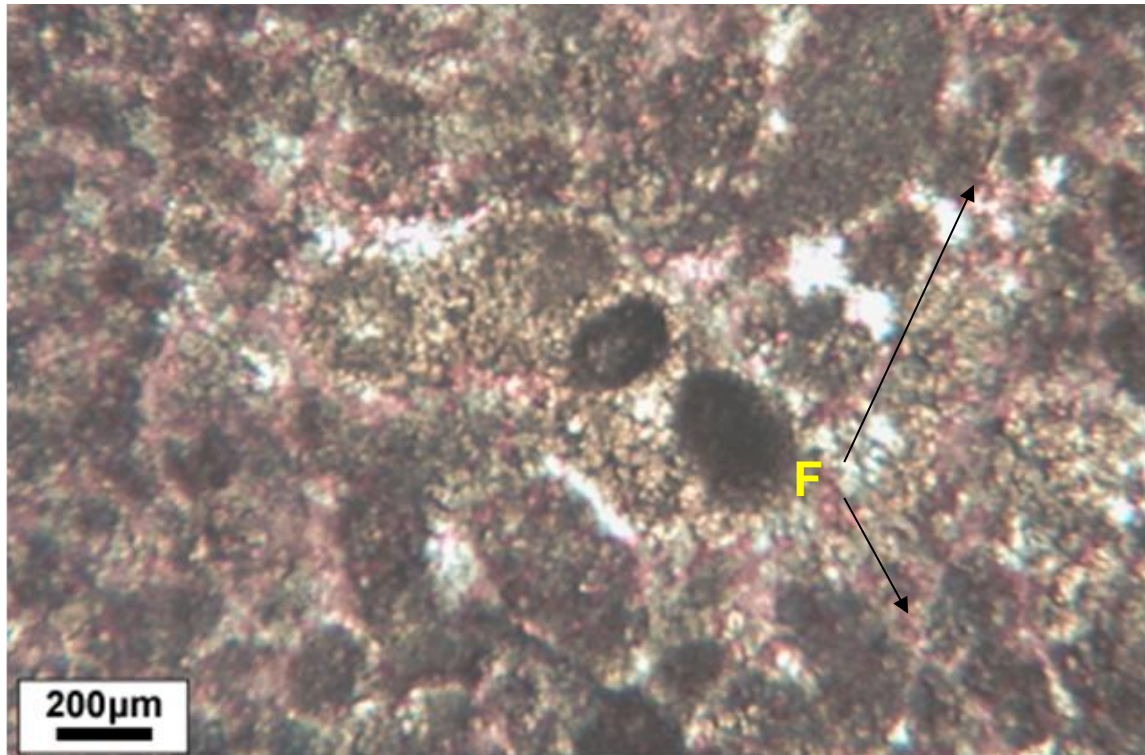


Fig. 4.4a. Packstone of ooids partially replaced by idiomatic mosaic of sub-euhedral D2 dolomite rhombs. Notice that medium-grained D2 dolomite replaced the matrix (including C1 and C2 calcite), and grains (micritized grains, ooids, intraclasts, etc.). Notice also two thin calcite veins (F) replaced by D2 dolomite. Thin section stained to differentiate dolomite (brown and grey) from calcite (red). Cupido Formation, sample CulCh8-98, Cañón de los Chorros locality. Plane-light photomicrograph.



Fig. 4.4b. Thin (<8 cm) to thick (1.8 m) bedded dolostones. About 90% of the entire column exposed in this place is dolomitized by D2 dolomite phase. Arrow indicates top of bedding; bedding dips to right. Cañón La Escalera locality, Cupido Formation. Outcrop photograph.

Baroque dolomite (D3)

Another type of dolomite found in the Cupido Formation is present as either a replacement phase or as cement in fractures. It can be classified, according its petrographic characteristics, as baroque or saddle dolomite (Radke and Mathis, 1980), and here I call it D3 dolomite. Baroque dolomite is typically characterized by a warped crystal lattice, so that it has curved crystal faces, curved cleavage planes and markedly undulose extinction, opaque white color and relatively large crystal size (Radke and Mathis, 1980). D3 baroque dolomite found in the carbonate sequence of Cupido Formation is characterized mainly by non-ferroan dolomite with curved crystal faces and undulatory extinction and occurs as clear to brown or white euhedral to sub-euhedral coarse crystals that range from 0.025 mm to more than 2 mm in size. D3 dolomite is differentiated from D1 and from D2 by its curved crystals, undulatory extinction and large crystal sizes, and overlap textures that indicate relative timing with respect to other cements.

D3 replaced the host rock and occluded some remnant fracture porosity (Fig. 4.5a). Because distinguishing D2 from D3 replacement phase is difficult using standard microscopy, this type of dolomite was also included for isotopic analysis (see Chapter 6). Petrographically, timing between D2 and D3 was difficult to establish, however fractures containing D3 baroque dolomite crosscut D2 dolomite (see Chapter 5), evidence that D3 postdates D2. D3 dolomite as a replacement phase was found in a few dolostones at the Potrero García locality, outside of the Monterrey Salient.

Ferroan dolomite

A few crystals of ferroan dolomite were found in basinal facies at the Iturbide-Santa Rosa locality. Petrographic characteristics of this dolomite are external iron-rich zones (Fig. 4.5b) and medium size euhedral crystals ($> 40 \mu\text{m}$).

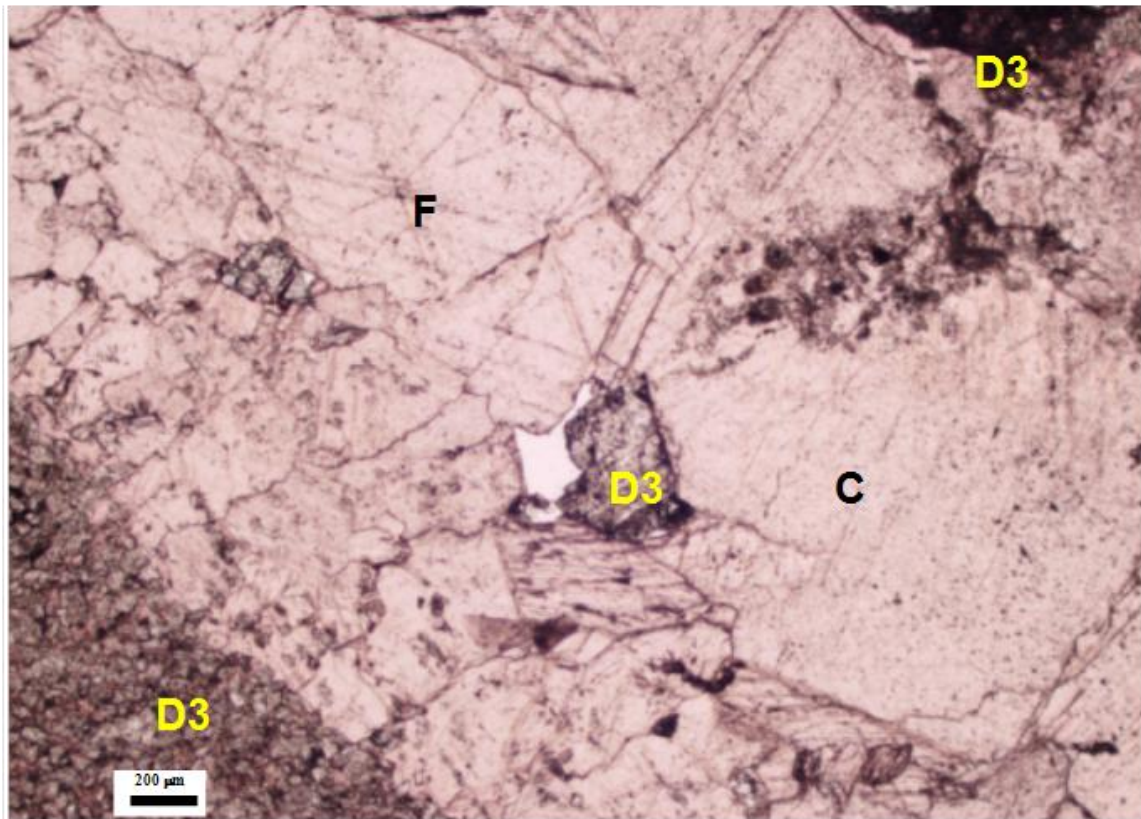


Fig. 4.5a. Calcite-filled vein (F) in a dolostone. D3 dolomite replaces rock matrix. Notice dolomite crystals overlap calcite (C) in vein walls and partially fill remnant porosity, evidence that dolomite replaced calcite and consequently that the fracture predates D3 dolomite. Notice that the dolomite crystal size filling the remnant porosity in the fracture exceeds 0.5 mm, one characteristic of this type of dolomite. Thin section stained to differentiate dolomite (brown and grey) from calcite (red). Cupido Formation, sample PG2-01, Potrero García locality. Plane-light photomicrograph.

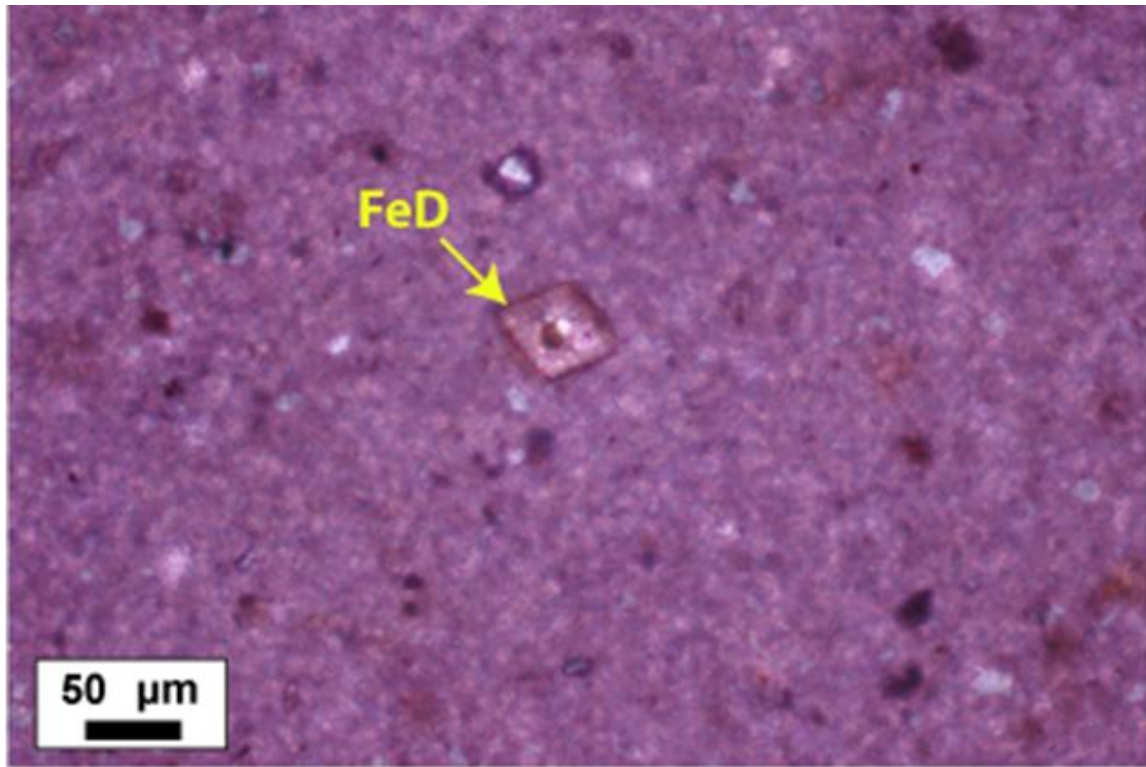


Fig. 4.5b. Photomicrograph of euhedral possible Fe-dolomite crystal (FeD) in a basinal mudstone. Notice external iron rich zone in the crystal. Tamaulipas Inferior Formation, sample CuStR1-98, Cañón Santa Rosa-Iturbide locality.

Other Diagenetic Processes

In addition to dolomite and calcite cement, which played the most important role in the evolution of fracture porosity, evidence of other diagenetic processes is also apparent in Cupido Formation textures. Although these additional processes are insignificant to fracture porosity evolution in this carbonate sequence, the following section briefly describes evidence for these processes.

Microbial micritization

Microbial micritization is a process whereby bioclasts are altered while on the seafloor or just below by endolithic algae, fungi and bacteria. The skeletal grains are bored around the margins and the holes filled with fine-grained sediment or cement. Micritic envelopes are produced in this way (Tucker and Wright, 1990). Micrite envelopes on carbonate allochems are common in the Cupido Formation. This process mainly affected bioclasts (Fig. 4.6) and is most evident in shallow water carbonates of the Los Chorros and Las Palmas localities.

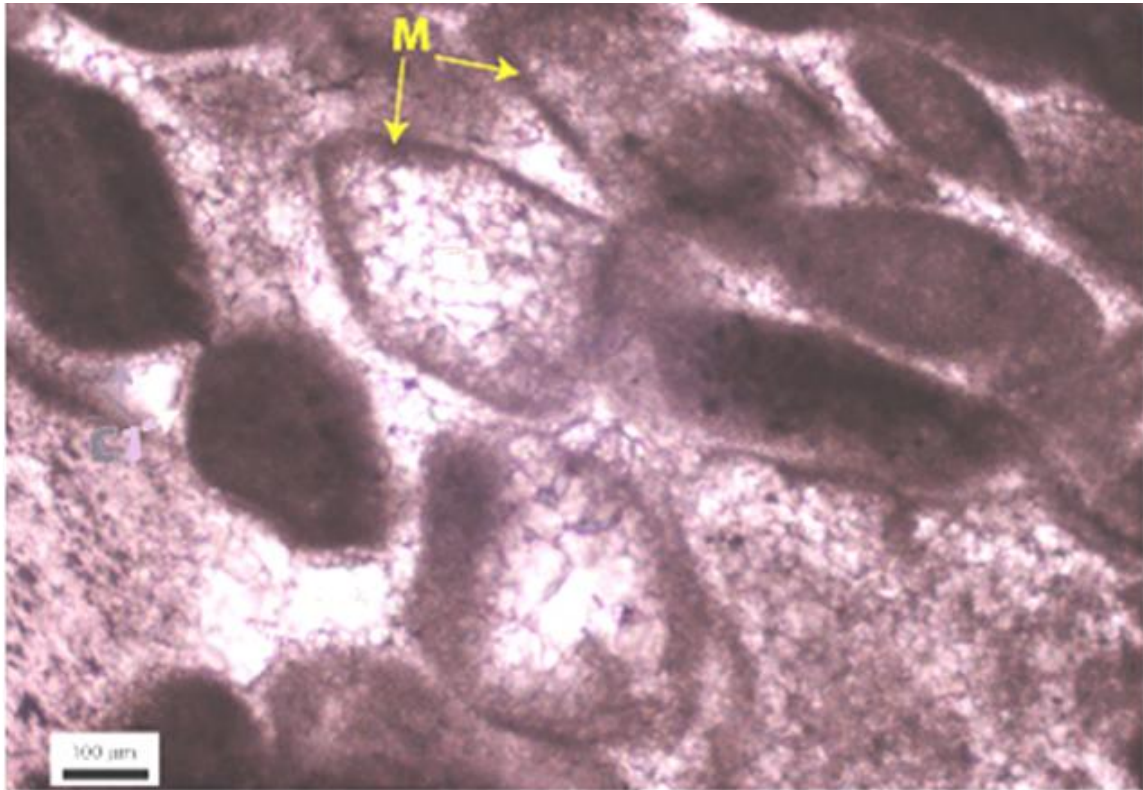


Fig. 4.6. Grainstone of bioclasts and ooids showing crushed micrite (M) rims around former fossils and ooids. Cupido Formation. Cañón Las Palmas locality. Photomicrograph.

Compaction and pressure solution

Compaction includes both mechanical and chemical effects (Bjorlykke, 1999). Evidence of mechanical compaction include fluidized structures in fine-grain carbonates, ooid splints, broken shells impinged by other allochems, cracked flat pebbles, and flattened burrows (Fig. 4.7a). The main features as result of chemical compaction are sutured and concavo-convex grain contacts. Partially dissolved grains at sutured and concavo-convex contacts identified in thin sections of non-dolomitized limestones are

interpreted as effects of chemical compaction. Dissolution of thin isopachous C1 calcite around ooids at sutured grain contacts suggests compaction took place after C1 cementation (Fig. 4.7a). Pressure solution refers to the interpenetration of adjacent grains in contact under the influence of pressure and in the presence of solution (Tomson, 1959). Evidence for penetrative chemical and pressure solution (interpenetrations on grain scale) is mostly limited in coarse grained Cupido Formation deposits, but is likely a pervasive phenomenon in carbonate mudrocks, as marked by widespread bed-parallel foliation in these rock types. Much more common are bed-parallel stylolites, marking spaced bed-parallel chemical compaction. Stylolites at a high angle to bedding are locally found, particularly in fine grained rock types in or near fold hinges. Locally these fabrics are penetrative and can be considered to be tectonic cleavage, probably formed shortly before or during folding (Marshak and Engelder, 1985).

Burial stylolites

At Cañón la Escalera and Las Palmas localities bedding-parallel stylolites are common features that can be identified in both outcrops and thin sections. The amplitudes of stylolite teeth vary from less than 250 microns, appreciable in thin sections (Fig. 4.3b), to centimeters at outcrop scale (Figs. 4.7b and 4.7c). These stylolites are interpreted as burial stylolites because they are developed along stratigraphic planes or at the boundaries of mechanical layers, and interpenetrating stylolite teeth are oriented perpendicular to layering. Some burial stylolite amplitudes suggest that appreciable amounts (~10 percent) of rock have been dissolved.

Burial stylolites crosscut calcitized anhydrite nodules, some calcite veins (Fig. 4.3b and 4.7c), indicating that the stylolites at least locally postdate those veins.

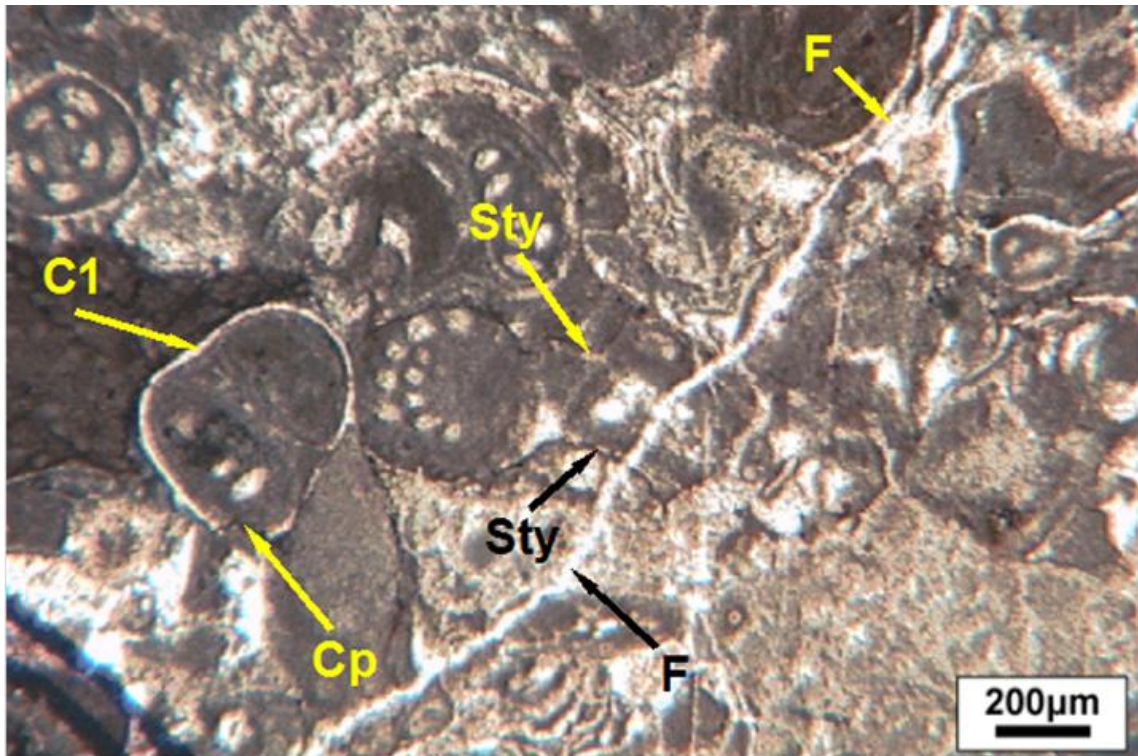


Fig. 4.7a. Bio- and intraclastic wackestone showing effects of chemical compaction (Cp) at sutured and concavo-convex grain contacts. Notice stylolites (Sty) that crosscut everything else, including a calcite vein (F1 or F2), and partially dissolved grains. Notice also C1 calcite cement around intraclasts. Cupido Formation, sample CulCh3-98, Cañón de los Chorros locality. Photomicrograph.



Fig. 4.7b. Bedding-parallel stylolites at bed boundaries. Notice that burial stylolites are better developed along stratigraphic planes or at the boundaries of mechanical layers. Hammer is 30 cm long. Cupido Formation, Cañón Las Palmas locality, beds dip to right. Note stylolite amplitude. Outcrop photograph.

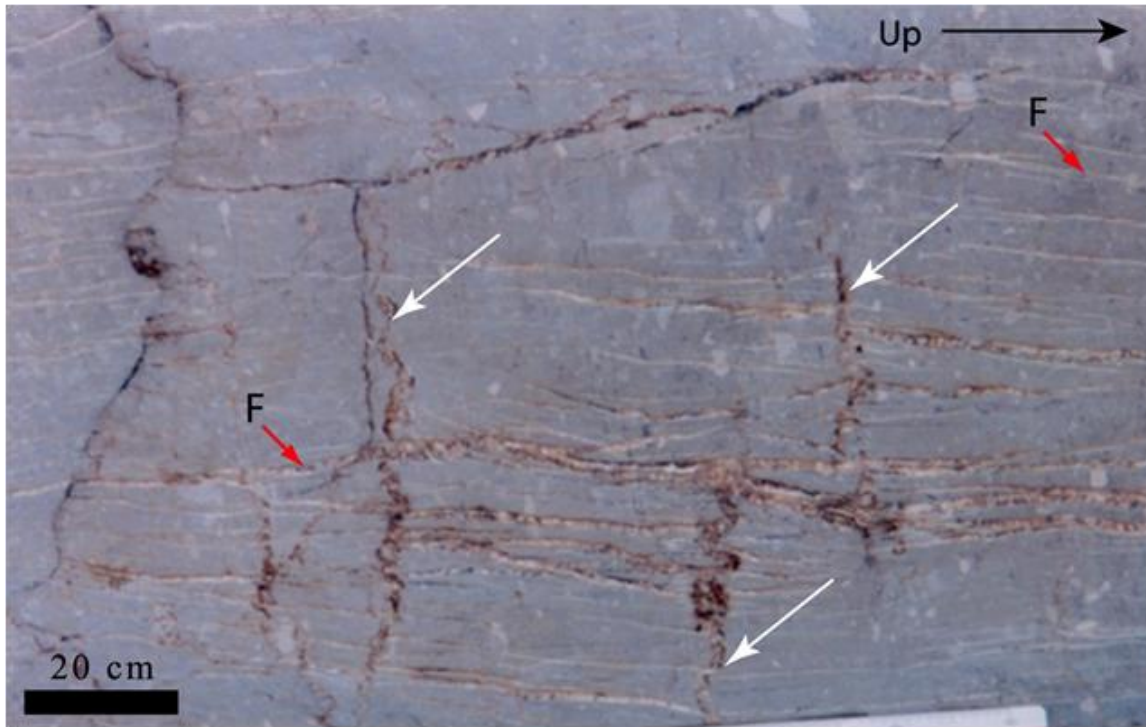


Fig. 4.7c. Dolomitized sedimentary breccia showing burial stylolites indicated by white arrows cross-cutting some fractures (F), implying that bedding-parallel stylolites postdate these fractures. Fractures are perpendicular to the stratification. Cupido Formation, Cañón La Escalera locality. Up; top of stratification. Close-up outcrop photograph.

Tectonic stylolites

Stylolites at high angle to bedding occur at most of the localities (Fig. 4.7d); such structures are typically interpreted to have a tectonic origin (for example, Marshak and Engelder, 1985). Spaced tectonic stylolites are bed-bound, and developed preferentially in dolostones at most of localities. No clear examples of tectonic stylolites cross-cutting burial stylolites were found, however a few large tectonic stylolites abut burial-stylolite surfaces (Fig. 4.7d), suggesting, but not proving, that tectonic stylolites postdate burial

stylolites. However, in thin section it is clear that bedding-perpendicular stylolites (Sty) cut all features described above (including fractures), indicating that these stylolites are among the youngest structures. Both calcite and quartz cements were found along tectonic stylolites (see quartz cement below).

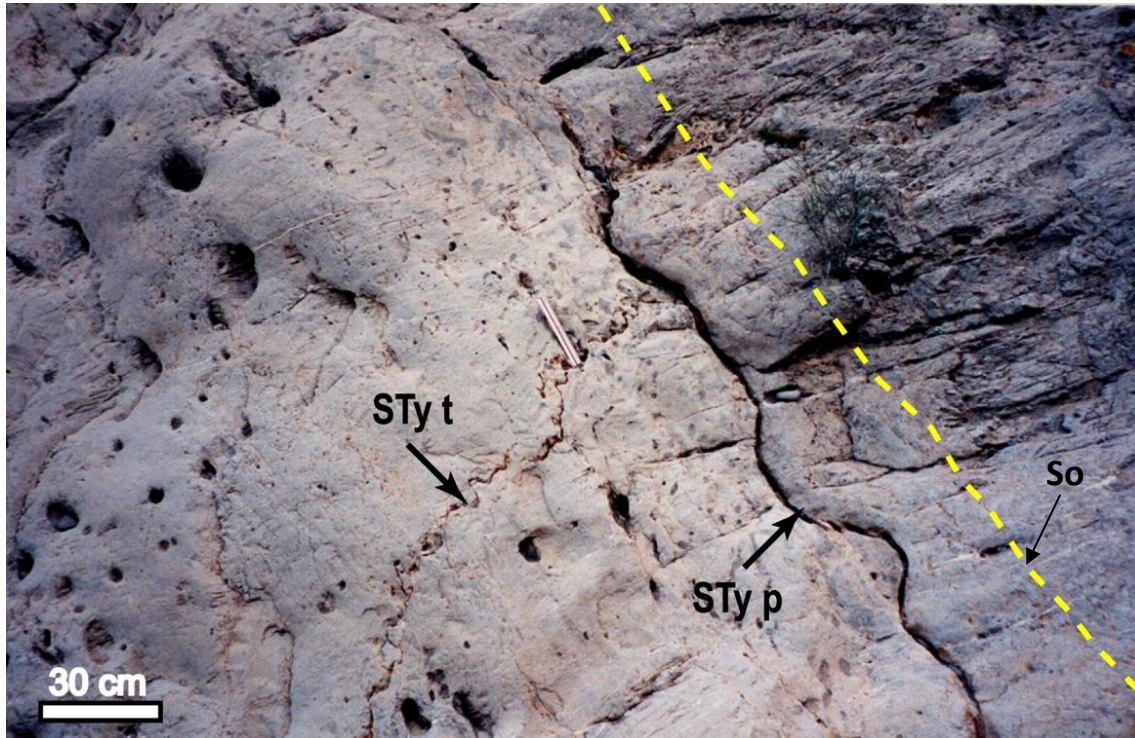


Fig. 4.7d. High-angle (Sty t) and bedding-parallel (Sty p) stylolites in a dolostone bed. Bed dips to the right of the photograph. Note amplitude of stylolites marking where rock has been dissolved. Bedding-parallel stylolites are interpreted to have formed during burial and they are preferentially developed along stratigraphic surfaces or at the boundaries of mechanical layers. Stylolites at high angle to bedding are interpreted as tectonic in origin. Dashed line indicates stratification surface (So). Cupido Formation, Cañón la Escalera locality. Outcrop photograph.

Recrystallization

Much of the Cupido Formation rock volume was recrystallized at some point in its history, generating larger calcite crystals from carbonate mud (aggrading recrystallization, Folk, 1965), and locally destroying internal allochem structures. Figure 4.8 is a photomicrograph showing rock with uniformly sized calcite crystals. Some fibrous structures in bivalve shells and ooids are visible because micrite envelopes remain as evidence of the original allochems (Fig. 4.8), however both matrix and ooids present the same size calcite crystals. This indicates that recrystallization took place and increased calcite crystal size in matrix, fossils, ooids and other allochems. Recrystallization affected from 50 to 90 percent of the rocks at Cañón la Escalera and locally those in Cañón Boquilla Corral de Palmas.

Dedolomitization

Corroded, incomplete and irregular dolomite crystal borders and overlaps of calcite over dolomite indicate calcite partially replaced dolomite, producing a degree of dedolomitization (Fig. 4.9). Dedolomitization is a diagenetic process that changes dolomite into calcite (Katz, 1971; Land and Prezbindowski, 1981). Characteristic features of dedolomite are dolomite-shaped, rhombohedral crystal forms occupied by calcite pseudomorphs. Although widespread, dedolomite is not abundant. Textural evidence for the relative timing of dedolomite is ambiguous in the samples examined in this study.

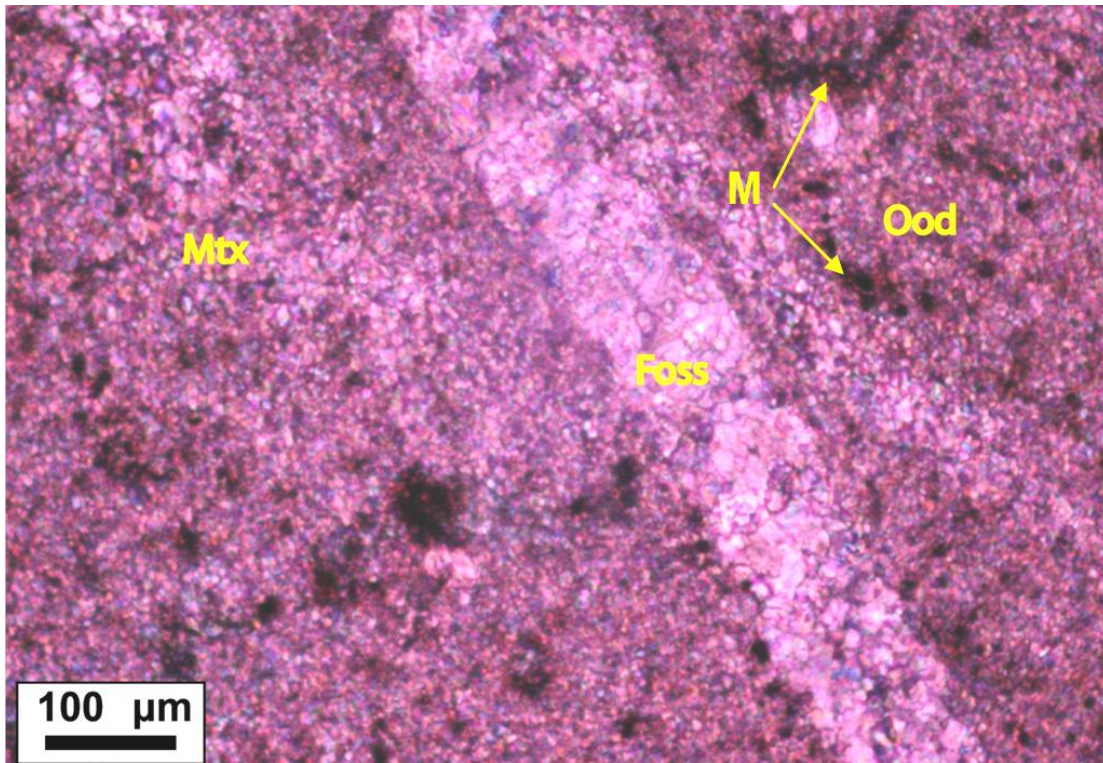


Fig. 4.8. Recrystallized limestone, Cañón Las Palmas. The whole rock was affected by a high degree of aggrading recrystallization, including matrix (Mtx), fossils (Foss) and ooids (Ood), producing almost uniform crystal sizes in the rock. Notice micrite envelopes (M) remain as evidence of the original allochems. Cupido Formation, sample CuLPa6-98, Cañón Las Palmas locality. Photomicrograph.

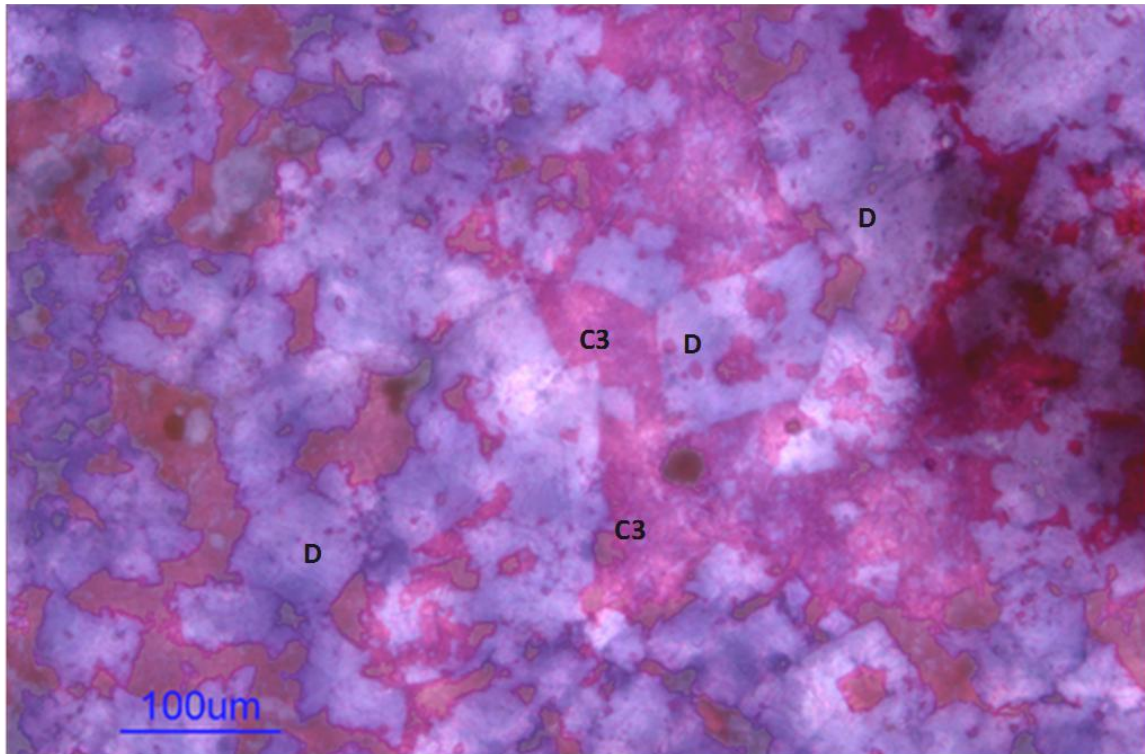


Fig. 4.9. Corroded dolomite crystals. Notice irregular D2-D3 dolomite crystals (D) borders partially replaced by C3 calcite cement producing dedolomite. Notice the penetrative replacement of dolomite by calcite in these rocks. Thin section stained to differentiate dolomite (grey or white) from calcite (red). Cupido Formation, sample CuEsc2-98, Cañón la Escalera locality. Photomicrograph.

Quartz cement

Quartz occurs along bedding-perpendicular stylolites (Fig. 4.10a). Although nowhere abundant in the rock mass, trace amounts of authigenic quartz (Figs. 4.10b and 4.10c) and chert nodules are widespread. Quartz is also present in some fractures and locally within the rock mass. Fluid inclusion trains in quartz cement deposits within fractures mark crack-seal texture in the fracture cement phase. Crack-seal texture shows that quartz cement is probably a synkinematic fracture fill cement (Figs. 4.10d).

Bedding-perpendicular stylolites with quartz crosscut fractures containing synkinematic baroque (D3) dolomite cement (Fig. 4.10a), implying that quartz at least locally postdates D3 dolomite. Thin sections show that some authigenic quartz crystals have fluid and solid inclusions, probably of dolomite (McBride, 2001, pers. com.), that imply simultaneous precipitation of these two minerals (Fig. 4.10b). Thin sections also show that quartz crystals are overlapped by C3 calcite crystals, implying C3 calcite postdates quartz cementation (Fig. 4.10c).

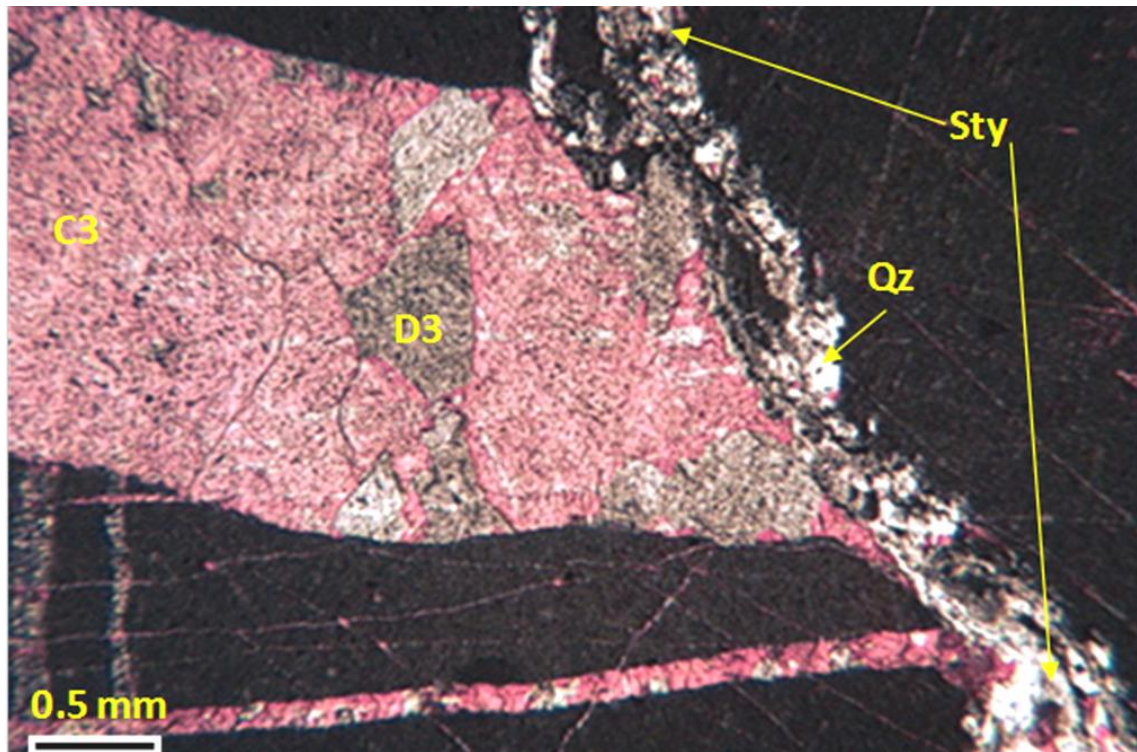


Fig. 4.10a. Detail of bedding-perpendicular stylolite (Sty) with quartz (Qz) cement along its path that cuts a macro-fracture, containing D3 baroque dolomite and C3 calcite crystals, indicating that both stylolites and quartz postdate fracturing. Thin section stained to differentiate dolomite (D3) (grey) from calcite (red). Cañón Boquilla Corral de Palmas locality. Thin section is parallel to bedding. Photomicrograph.

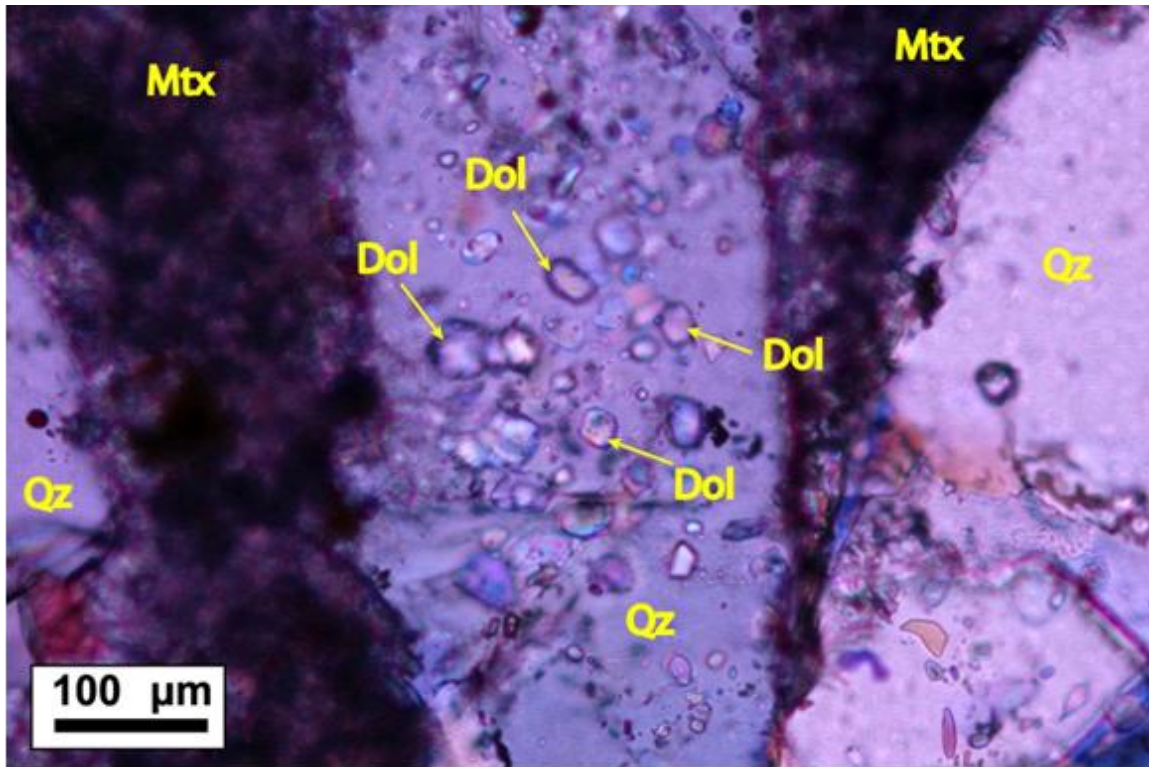


Fig. 4.10b. Authigenic quartz (Qz) in fracture showing primary fluid and solid inclusions of probable dolomite (Dol), implying simultaneous precipitation. Mtx, matrix. Thin section stained to differentiate dolomite (grey or white) from calcite (red). Cupido Formation, CuEsc2-98, Cañón La Escalera locality. Photomicrograph.

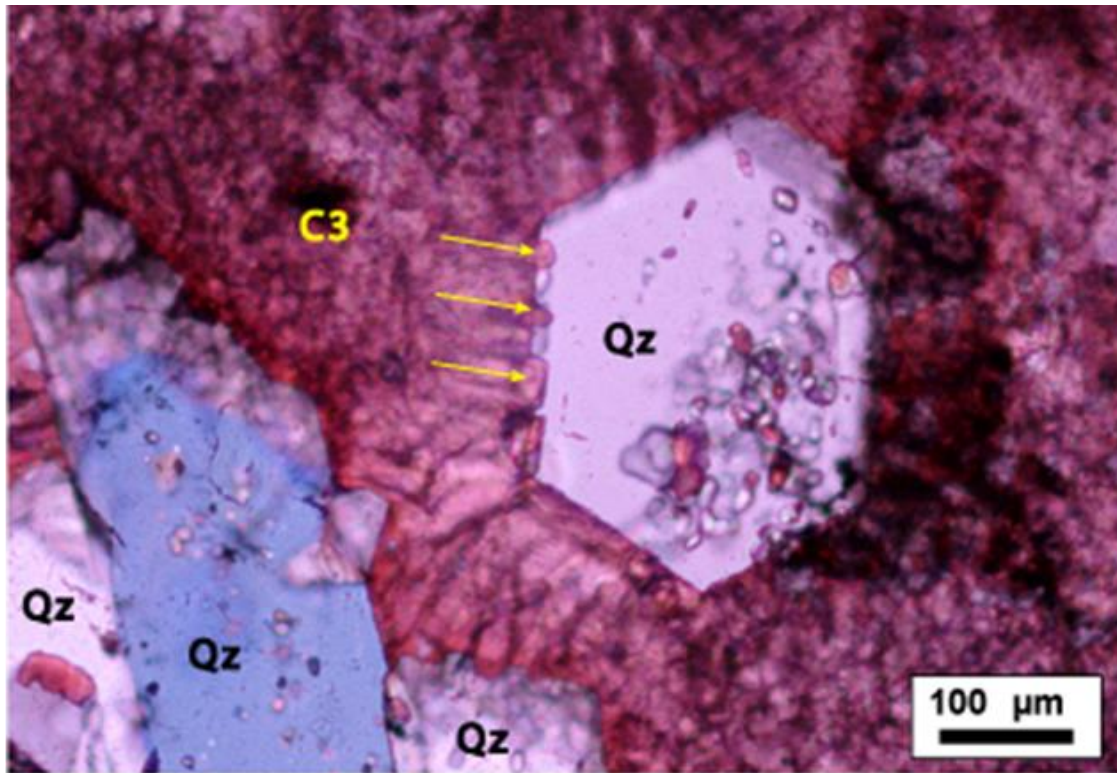


Fig. 4.10c. Authigenic quartz crystals (Qz). Notice that quartz crystals are overlapped by C3 calcite crystals, thus Qz predates C3 calcite. Arrows indicate calcite crystals that partially replaced quartz. Thin section stained to differentiate dolomite (grey or white) from calcite (red). Cupido Formation, CuEsc2-98, Cañón La Escalera locality. Photomicrograph.

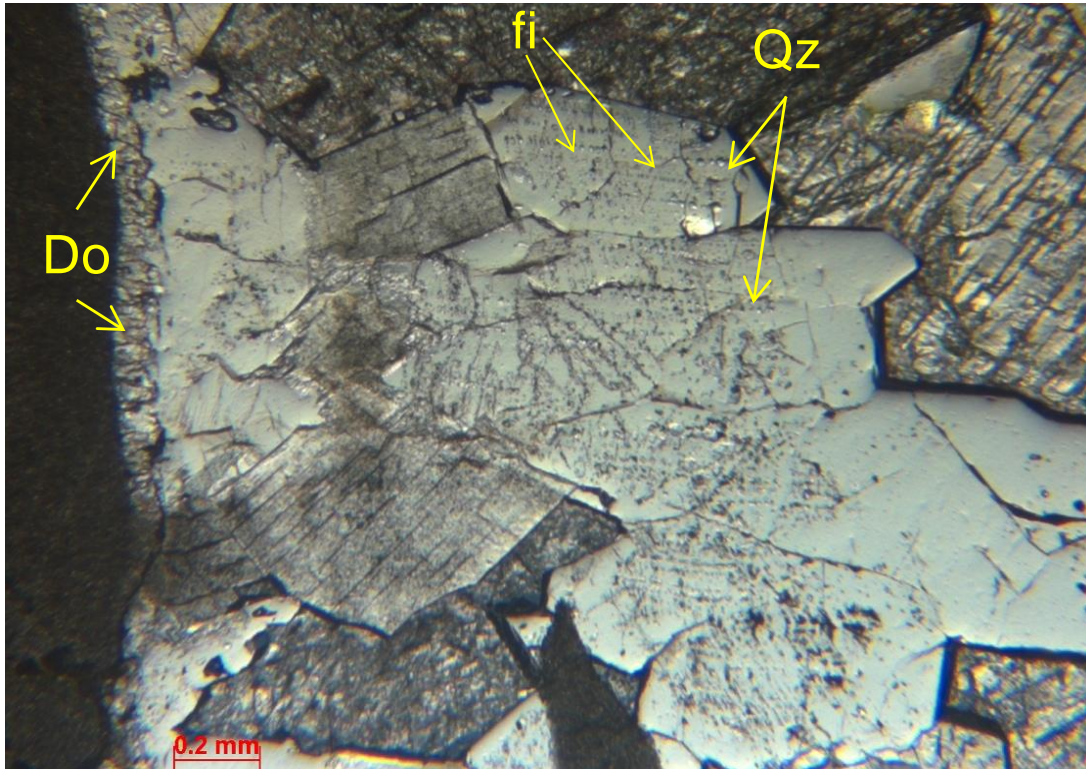


Figure 4.10d. Quartz crystals in macrofracture. Quartz crystals (Qz) have aligned fluid inclusions (fi). Fluid-inclusion planes that parallel the fracture wall probably mark crack-seal texture. Notice fibrous/elongated dolomite next to fracture wall. Dolomite precipitated first but quartz was deposited as fracture grew. C3 calcite fills in space between quartz bridges and is therefore a later deposit, probably after fracture growth ceased (modified from Gómez, 2006). Thin section 02LG11-2, stained for calcite, 3.125X, plane light.

Dissolution

Dissolved cores of ooids, oomoldic porosity, solution breccias (see Chapter 3), and karstification in the Cupido Formation are evidence that dissolution took place more than once during the geological history of these rocks. Partially dissolved fossils and ooids indicate at least one dissolution event took place before C2 calcite cement

precipitation. Therefore, this dissolution is interpreted as an early process in the diagenetic history of Cupido Formation rocks (see Chapter 3). Solution breccias also support at least one dissolution event early in the diagenetic history. Because of the location of these features in the stratigraphic sequence (see Chapter 3), I infer that evaporite layers were dissolved to create space for solution (collapse) breccias development.

Caves in the Monterrey Salient (e.g., Potrero García) are evidence of modern karstification affecting carbonate rocks in the Monterrey Salient (Fig. 4.11). This modern karst is evidence that dissolution and calcite precipitation is a modern process in rocks of the SMO.



Fig. 4.11. Potrero García caves. Dissolution takes place in Cupido Formation rocks forming a karst landscape. A cave is visible in the center of the image.

ORIGIN AND DISTRIBUTION OF DOLOMITES

Because the textural evidence indicates dolomite cementation and fracturing are coupled (see Chapter 5), here I briefly speculate on what these patterns imply about the possible origin and distribution of the dolomite types found in this study. Figure 4.12 shows interpretation from selected thin sections for the three main dolomite types identified in the Cupido Formation.

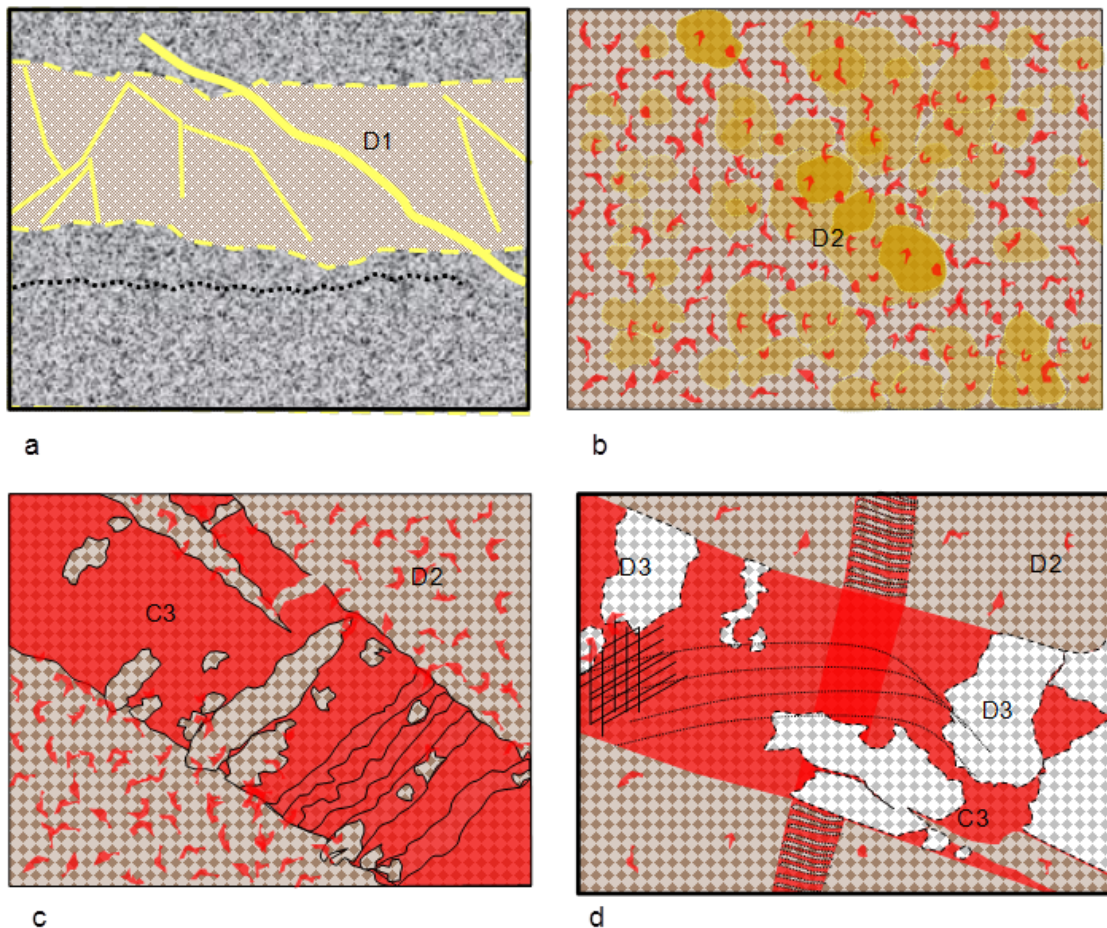


Fig. 4.12a. Sketch for the three main dolomite types identified in the Cupido Formation. a) Fine grained and laminated D1 dolomite, showing some probable desiccation fractures; b) D2 replacement dolomite in rock matrix; c) D2 replacement dolomite in rock matrix and in C3 calcite fill of fractures; d) D3 baroque dolomite in fractures.

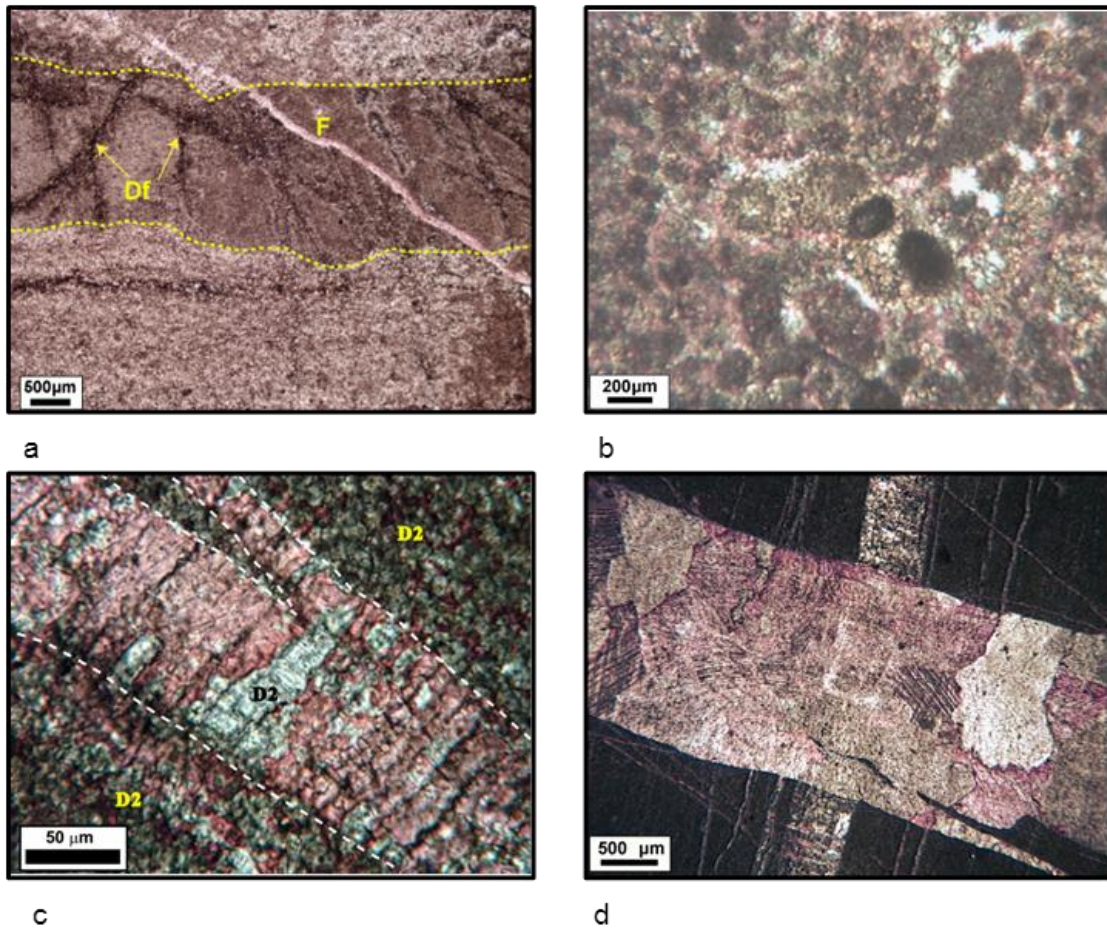


Fig. 4.12b. Selected thin sections for sketch of Figure 4.12a.

D1 Dolomite

Fine grained and laminated D1 dolomite forms thin beds of dolostone. These are frequently found at the top of parasequence cycles in the Cupido Formation, and are intercalated with evaporites and algal mats. This association commonly is taken to indicate early and near surface dolomitization (Allan and Wiggins, 1993). D1 dolomite probably formed by direct precipitation from seawater in a subtidal to supratidal setting

as part of the sea level cycles that governed the Cupido depositional sequences. According to Moore (1989), dolomite that originates during subtidal to supratidal cycles has microcrystalline textures, is usually stratiform, and preserves sedimentary structures (e.g., laminations). In arid depositional settings, early dolomite is associated with sedimentary features characteristic of the sabkha environment, e.g., algal mats, rip-up clasts, nodular anhydrites, and evaporite solution breccias (Allan and Wiggins, 1993). This dolomite can often be seen to precede compaction and may have diagnostic early diagenetic textures and be spatially associated with other early cements (Allan and Wiggins, 1993). D1 has these attributes of early dolomite. D1 dolomite is present outside of the Monterrey Salient in Cienegas, Cañón Prieto, and Potrero García, and elsewhere within the salient, for example at the La Escalera locality. D1 dolomite might also be present in Los Chorros and Las Palmas. These observations suggest that D1 formed during deposition and early burial across a regional area.

D2 Dolomite

D2 replacement dolomite ranges from fabric destructive to retentive and from selective to pervasive. The shapes of dolomite crystals in replacement mosaics vary from anhedral to euhedral rhombs. Partially dolomitized limestones and dolostones are also frequently found at the top of parasequence cycles, intercalated with intertidal and supratidal deposits having calcitized evaporite nodules. Several models have been proposed to explain the replacement dolomitization type. In order to dolomitize a limestone, two requirements must be met (Adams and Rhodes, 1960; Land, 1980; Tucker and Wright, 1990): (1) a source of Mg sufficient to dolomitize the limestone must exist;

and (2) a transport mechanism must be available to carry the Mg to the site of dolomitization. In most cases, the source of Mg is seawater or seawater-derived formation water or brine (Lucia and Major, 1994). A model for early dolomite replacement is that of hypersaline water circulation from evaporative environments (King, 1947; Adams and Rhodes, 1960; Lucia and Major, 1994). Dolomitization associated with hypersaline flux occurs at shallow burial depths and early in the diagenetic history of the rocks. In the Lucia and Major (1994) dolomitization model, hypersaline reflux characterized by high concentration of magnesium promotes the dolomitization of beds immediately below the evaporative environments. This model has potential application to shallow-water facies of the Cupido Formation that is characterized by cyclic occurrence of dolostone and limestone layers and absence of shales (Ortega, 2002).

D2 dolomite, forming dolostone beds, is volumetrically the most important dolomite in the Cupido Formation. Figure 4.13 shows a regional map of D2 dolomite distribution in the Monterrey Salient. D2 dolomite increases in rock volume from Cañón de los Chorros, where the percentage of rock volume dolomitized in the stratigraphic column is lower than 20%, to Cañón de la Escalera where almost 90% of the column consists of dolostones (see Appendix 2.1, Chapter 2); and from low amounts in Cañón Santa Rosa-Iturbide, with less than 10%, to high amounts in Cañón de la Escalera. The contour of 10% is influenced by the amount of dolomite from Cañón Santa-Rosa-Iturbide. If the other contours follow this one, then the dolomite content in the map approximately follows the former Cupido platform shape, supporting a possible hypersaline flux dolomitization model. This map is the first that attempts to quantify the relative volume of dolomitized limestones in the Cupido Formation of the Monterrey

Salient. Recognizing and documenting these patterns could have application to using these outcrops as an analog to subsurface fractured and dolomitized oil and gas reservoirs. My results and previous studies of fracture intensity in the Cupido Formation suggest that dolomite content and fracture abundance (intensity) are systematically related, with higher dolomite content corresponding to greater fracture abundance (this study and Ortega, 2002).

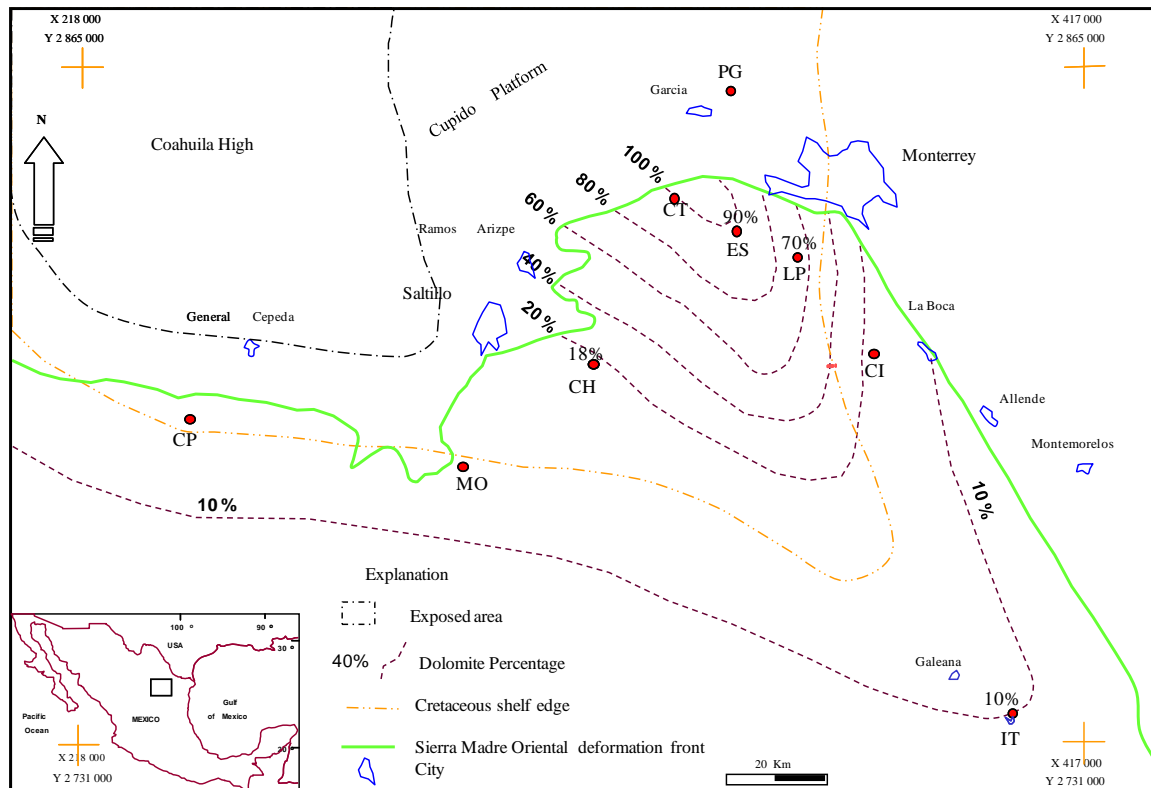


Fig. 4.13. Map showing regional distribution of D2 dolomite in the Monterrey Salient (this study). Notice dolomitization increases from Cañón de los Chorros (CH), where the percentage of rock volume dolomitized in the stratigraphic column is lower than 20%, to Cañón de la Escalera (ES) where almost 90% of the column consists of dolostones, and from Cañón Santa Rosa-Iturbide (IT) with less than 10% dolomite to the ES. Average values of dolomite percentage were estimated from field observation along the stratigraphic columns (Appendix 2.1) and from petrographic analysis of dolomite percentage (Appendix 4.2). Dashed contour lines indicate percent of dolomite. Red circles mark sampled outcrop localities: PG, Potrero García; CT, Cañón de las Cortinas; LP, Cañón Boquilla Corral de Palmas; MO, Molano Fault; CP, Cañón Prieto; CI, Cienegas. X and Y are coordinates in the Universal Transverse Mercator (UTM) Projection indicated by small crosses. Square in inset map indicates the location of the map above.

D3 Dolomite

D3 baroque dolomites found in the Cupido Formation are possibly associated with relatively deep burial conditions and high temperatures, such as those documented for other baroque dolomites (Morrow, 1982). Oil inclusions are commonly found in baroque dolomite, suggesting that this dolomite forms within the oil-gas maturation window, at temperatures of 60 to 150°C (Radke and Mathis, 1980). Burial dolomitization normally occurs after deposition and lithification, therefore baroque dolomite typically crosscuts depositional facies and formation boundaries as well. D3 dolomite in fractures was identified mainly at the Cañón de la Escalera and Cañón Boquilla Corral de Palmas localities. The limited areal extent of this cement suggests that, unlike the conditions for D2, the conditions for baroque dolomite precipitation were not widespread.

Finally, ferroan dolomite, more than 2 mole % FeCO₃ (Tucker and Wright, 1990), is present as scattered rhombs in argillaceous lime-rich basinal mudstones in the Santa Rosa locality. Although ferroan dolomite is a common late diagenetic precipitate, the limited extent of these deposits suggest that whatever conditions led to ferroan dolomite precipitation, they were not widespread in the Monterey Salient.

ORIGIN AND EVOLUTION OF POROSITY SYSTEM

Based on the paragenetic sequence, the origin and evolution of the porosity system in Cupido rocks can be interpreted and separated into four main stages: the depositional and shallow burial stage, the prograde burial stage, the tectonic (folds and faults active) stage and the uplift and exhumation stage.

After deposition, early in the diagenetic history (~Barremian-Early Aptian) grainstones and packstones originally had high porosity (~ 35%), and facies distribution controlled the porosity system. However, before mechanical compaction took place primary inter- and intragranular porosity was partially occluded by C1 calcite cement. Later on, probably during shallow burial conditions, C2 calcite occluded almost all remnant porosity. Therefore, these grainstones and packstones had very low porosity (probably less than 4%) during this stage of diagenesis. However, during the later stages of shallow burial conditions the replacement dolomite phase D2 took place. This led to an increase in porosity (probably to more than 8% locally) mainly in beds close to evaporite layers, such as mudstones and packstones-grainstones. Some of the most prominent fractures also formed at this time.

During prograde burial and deep burial conditions (probably more than 1 km deep) Cupido rocks experienced protracted burial loading (Late Aptian-Maestrichtian). During this time several fracturing events took place, affecting mainly dolostone beds (mudstones and packstone-grainstones that had preferentially been dolomitized) accompanied by D3 baroque dolomite precipitation. However, the rate of dolomite precipitation probably decreased with time. In fact, the oldest fracture sets (see Chapter 5) are more occluded by dolomite cement whereas younger fracture sets are only cemented by calcite. Possibly this phenomenon resulted from progressive Mg depletion (or at least

diminishing Mg supply). At the beginning of burial the seawater source of Mg was more accessible and possibly larger (connate water) than when the last fractures formed. However, in these later stages of fracture the main secondary porosity developed in both fractures and matrix. Presence of dolomite inclusions in authigenic quartz indicates contemporaneous cementation of minor quartz and dolomite at the time of the last fractures. Cements such as ferroan dolomite and baroque dolomite, while not volumetrically important in fractures and typically only a few volume percent of the rock, if present, likely formed while some of these fractures were still open and could therefore serve as conduits for long distance fluid flow. During this stage of burial these rocks possessed high secondary porosity (probably a range between 9 and 10%) in both pores in the rock mass and in fractures.

C3 calcite fracture cement locally replaced quartz and dolomite cements. Late in the diagenetic history, probably during Laramide (Early Tertiary) tectonic folding and local fault slip, twinning took place in thrust faults, tectonic veins and flexural slip faults. Eventually, nearly all fracture porosity was occluded by C4 calcite cement. Judging from the lack of crack-seal texture in this calcite, fold-related deformation had ceased when this fill was emplaced. Despite the presence of this soft calcite cement in fractures in various structural positions around folds, C4 is itself undeformed and thus probably formed after folding, possibly during uplift and exhumation of these rocks (~20 Ma-Present). Today these rocks have low porosity (less than 3 %) in the rock mass and negligible open pore space in fractures; the only locally high porosity is due to dissolution related to modern karstification.

Chapter 5: Fracture Analysis of Lower Cretaceous Cupido Formation, Monterrey Salient, Sierra Madre Oriental, Mexico

SUMMARY

This chapter demonstrates new field and petrographic evidence to support the idea that most of the fractures in carbonate rocks of the Lower Cretaceous Cupido Formation in the Monterrey Salient, Sierra Madre Oriental (SMO), formed at shallow (near surface) to intermediate burial depths before late Cretaceous-Tertiary Laramide-age folding took place in this area. Structural-diagenetic petrographic analysis was carried out and integrated with field observations, allowing recognition of six fracture events (F1, F2, F3, F4, F5, and F6, in order from the oldest to the youngest). The relative timing of fracture sets was ascertained from crosscutting and abutting relations; timing relative to burial history was estimated using the pattern of cement fills.

Correlation of fracture attributes at outcrop scale to microscopic scale was possible. Four regional opening-mode fracture sets W, X, Y, and Z, in order from the oldest to the youngest, were previously established for Cupido Fm. in the Monterrey Salient. Currently these are all dolomite and calcite filled veins, but evidence outlined in this chapter shows that the filling history of these fractures was intermittent and that fractures likely retained open pore space for parts of their history. Several sets of fractures can be correlated regionally, and in some cases proximal or continuous outcrop allowed event correlation with greater confidence. F1 fracture event includes fractures most clearly expressed in differential compaction boudinage structures and evaporite solution-collapse breccias. These fractures have inconsistent orientations (in part owing to their presence within rotated solution collapse blocks). Geometric relations of rotated

fractures in solution breccia blocks imply that F1 is related to near-surface process that developed in pre- and syn-brecciation times. The second event (F2) includes fractures characterized by synkinematic C2 calcite cement. These fractures are found in limestone and partially dolomitized limestone beds at all study localities; these also have inconsistent orientations (no systematic preferred orientation). F2 predates D2 regional dolomitization and, based on the inference that D2 dolomitization is a shallow burial phenomenon, these fractures also probably originated under shallow burial conditions. The third event (F3) includes fractures characterized by synkinematic dolomite. These fractures were found in partially dolomitized limestone and dolostone beds at all study localities and it shares characteristics (orientation, fracture cements, and morphology) of a set locally correlated as set W at the Los Chorros, Las Palmas, and La Escalera localities. Synkinematic dolomite cement in F3 is similar to D2 regional dolomite, a correlation that implies that F3 and D2 dolomitization are broadly synchronous, and originated under shallow burial conditions. The fourth event (F4) includes, at microscopic scale, fractures characterized by synkinematic baroque dolomite and quartz; these fractures postdate D2 dolomite. F4 fractures occur in partially dolomitized limestone and dolostone beds at all study localities and have similar characteristics of locally correlated as set X at the Los Chorros, Las Palmas, and La Escalera localities. Cross cutting relationships indicate that synkinematic D3 baroque dolomite cement in F4 postdates D2 regional dolomite. F4 originated under burial conditions after regional dolomitization took place and at least in part during D3 baroque dolomite cementation. Event five (F5) includes fractures characterized by synkinematic C3 calcite fill. These fractures are found in limestone and partially dolomitized rocks, and they have similar characteristics to fractures locally correlated as set Y at the Santa Rosa, Los Chorros, Las Palmas, and La

Escalera localities. Cross cutting relationships suggest that fracture set Y is older than burial stylolites, and in some places crosscutting relations imply that this set also predates tectonic stylolites. Fracture set Y crosscuts locally correlated sets W and X, as observed in several beds in the field and in thin section. F5 originated under moderate to deep burial conditions after regional dolomitization took place, and probably before folding or during an early state of folding (tectonism), since these structures are cut by fractures of F6. Event six (F6) includes all flexural slip faults associated with synkinematic twinned calcite cement. These faults are found in limestone and partially dolomitized rocks, and are equivalent to locally correlated set Z at Santa Rosa, Los Chorros, Las Palmas and La Escalera localities. Fracture set Z is at a high angle to tectonic stylolites, but the alignment of these fractures orthogonal to the stylolites means these two types of structure are kinematically compatible with each other and with formation of folds. Fracture set Z crosscuts sets W, X, and Y. The mineralogy of synkinematic quartz and dolomite in F6 fractures suggests that the F6 fracture event originated under deep burial conditions during folding of the SMO.

FRACTURE TERMINOLOGY

Since this chapter describes fractures and their relationships with each other and with diagenetic cements, the basic concepts and terms used in this chapter are here defined.

Fracture Classification

Based on the relative displacement of the material on opposite sides, fractures can be divided in two types (Twiss and Moores, 1997) (Fig. 5.1a): a) Opening mode, extension, or mode I, fractures have relative displacement that is perpendicular to the fracture wall, so the walls move apart. b) Faults or shear fractures (mode II or III or mixed mode) that involve an important component of movement parallel to the fracture wall, with or without a component of fracture-perpendicular (opening or closing) movement. At mode II tip lines, the relative displacement is perpendicular to the tip of the fracture. At fault (shear mode III) tip lines, the relative displacement is parallel to the tip of the fracture.

The terminology displacement mode I/II/III is usually used in experimental or theoretical situations where displacement can be observed or specified (National Research Council, 1996). Following Pollard and Aydin (1988) the more general term opening mode is more appropriate for field observation, but microscopic observations in some cases allow greater certainty. Here I use opening mode (mode I) for most of the fractures described. Some widely used fracture terms are also not well suited to circumstances where mineral deposits are present in the fractures and the sequence of fracture infill is of interest. For example, most Cupido Formation fractures are now filled with cement, and so could be termed veins. Yet these structures may have been open

fractures for much of their history. Cupido Formation outcrops also contain opening-mode fractures that lack any cement deposits; such barren fractures are termed joints. Although some of these joints have regular patterns (systematic joints) they are outside the scope of this study. Because they are barren (no cement) and also because they cross cut all cement phases and other diagenetic fabrics, they must postdate other processes in the diagenetic history of Cupido rocks. Moreover, the spatial arrangement of many of these fractures suggests they are a response at least in part to modern topography.

Veins are tabular mineral deposits (not necessarily fractures). Veins derived from fractures may fill with crystalline material after opening or during progressive opening (Ramsay and Huber, 1983) or in some combination. Depending on whether cement filled fractures that were static or spanned fractures while they were opening (or between opening increments), as well as the type of cement and the fracture wall composition (Gale et al., 2010), morphology of cement deposited in carbonate rock veins commonly is euhedral (idiomorphic), laminated or fibrous. A fibrous habit is indicative of cement precipitated during fracture opening (Ramsay and Huber, 1983) where fibers have not been deformed significantly after their growth (Cox, 1987). A fibrous habit is distinct from the faceted habit shown by crystal growth into an open space (euhedral crystals) and the long axis of a fiber may have arbitrary orientation with respect to the crystallographic directions of the crystal making up the fiber (Ramsay and Huber, 1983).

Fibrous crystals in a vein may be straight or curved. Based on fiber geometry we can infer the movement history of fracture opening, however, there are some types of fibrous microstructures which do not track an incremental displacement path (Cox, 1987). Two simple rules can be applied in the analysis of fibrous crystals: 1) fibers link points on opposite walls that were once in contact, and 2) fibers grow in the direction of

contemporaneous displacement. If the displacement pattern is simple, then the fibers are straight, whereas if the net displacement is the result of a sequence of changing opening directions, then the fibers will be curved (Ramsay and Huber, 1983). The fibrous crystals in veins included in this study are perpendicular to the vein walls and have not been deformed.

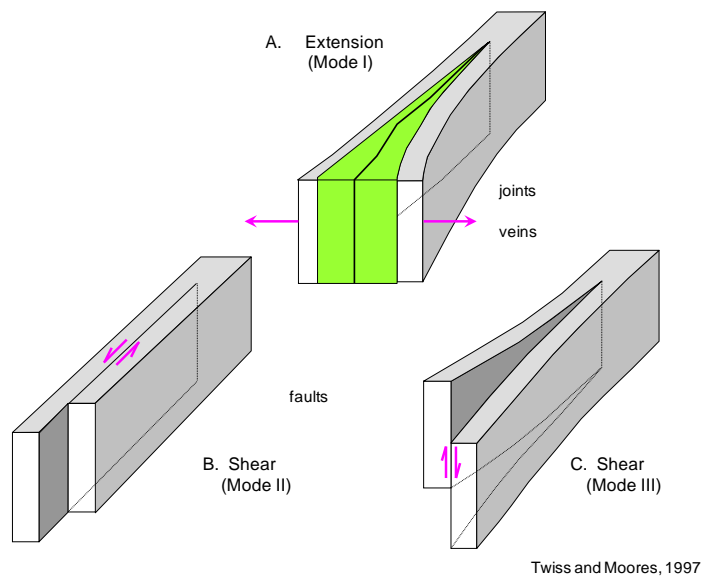


Fig. 5.1a. Fracture classification based on the relative displacement of the material on opposite sides of the fracture: In extension or mode I, the relative displacement is perpendicular to the fracture, so the walls move apart. Shear fractures involve movement parallel to the fracture plane, but there is no perpendicular movement. In mode II the relative displacement is parallel to the fracture plane and perpendicular to the tip line of the fracture. In shear fracture mode III the relative displacement is parallel to the fracture plane and to the fracture tip. Veins can be extension fractures (mode I) filled with mineral deposits (cements).

Fracture Set

A fracture set is a family of fractures that shares the same attributes or characteristics, such as strike and dip direction, mineral fill composition and texture, etc., and that usually are interpreted to share the same genesis. Not all fractures in a set are necessarily identical, however. For example, fractures in a set may have a wide range of sizes (Fig. 5.1b).

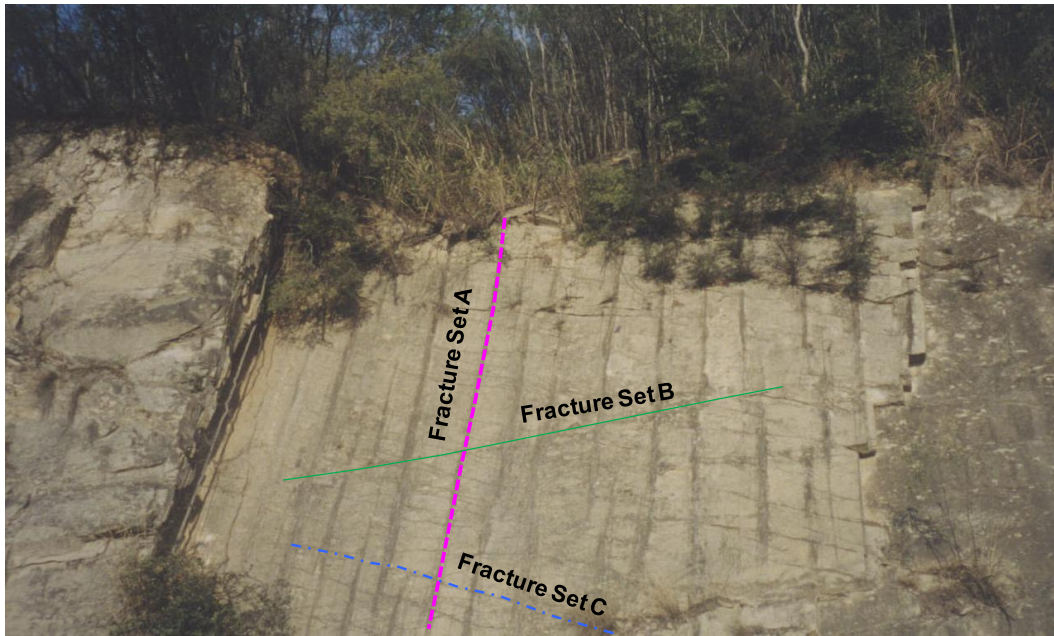


Fig. 5.1b. Outcrop photograph showing three main fracture sets or families. Outcrop photograph area is about 5 m x 3m long.

Fracture and Diagenetic Event

As used here, a fracture and diagenetic event, based on textural relations showing that a fracture set was opening (growing) while a cement phase was precipitating, indicates a period of time that structural and diagenetic processes affected a volume of rock. Implicit but rarely explicitly stated in both the older structural literature (e.g., Hancock, 1985; Engelder, 1985; Pollard and Aydin, 1988) and the diagenesis literature (McBride, 1988; Dutton and Land, 1988; Milliken, 2003) is the inference that, respectively, fracture sets and cement phases form in relatively short, discrete events. Thus, a fracture event can be ascribed to a period of tectonism (tectonic event) or folding; cements can be assigned to a paragenetic sequence and placed on a paragenetic sequence diagram. The duration of these events is rarely documented or defended, but by placing a relative timing sequence of events (fractures or cement) on a time line tends to imply the processes are punctuated. Recent work on fracture cements in sandstones demonstrates that this portrayal can be misleading, and that fractures can grow continuously over long time periods, on time scales compatible with diffusion processes (Becker et al., 2010). Similarly, recent work in diagenesis has tended to emphasize the continuity and long duration of diagenetic processes, where apparent events are the result of competing rates of chemical reactions and varying temperature history (Lander et al., 2008). In brief, events may be, in some respects, misleading ways of grouping fracture sets or cement mineral phases in a paragenetic sequence. With this caveat in mind, however, the linked fracture set and cement phase usage defined here has value because it captures special relations that arise from joint action of chemical and mechanical processes.

Fracture Cement

Cements in fractures (commonly also present in host rock) can be classified by crack-seal texture, crosscutting or overlapping relations as pre-, syn- or postkinematic depending on whether cements precipitated before, during, or after fractures of a particular set opened (Laubach 1988; 2003). Fractures in the subsurface can be partially sealed by both synkinematic and postkinematic, however remnant porosity can be present (Fig. 5.1c).

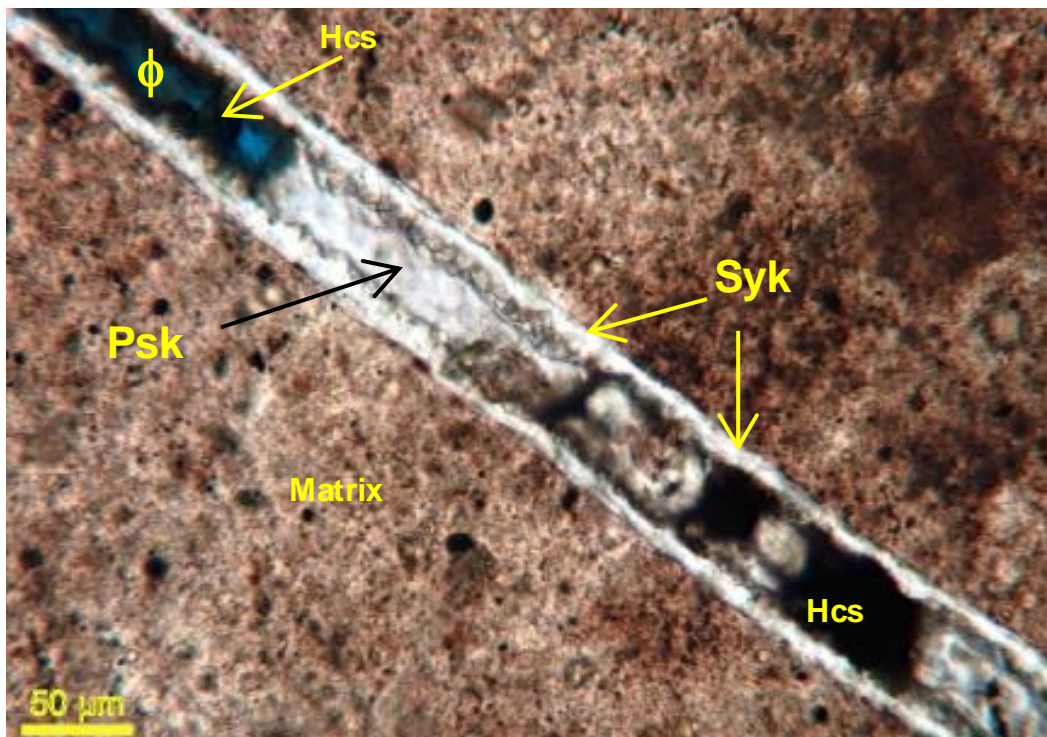


Fig. 5.1c. Detail of fracture in a limestone from an oil reservoir. Cements partially filled the fracture are both quartz: synkinematic (Syk) and postkinematic (Psk). Notice the remnant porosity and oil stain (Hcs) in black. ϕ , porosity. Photomicrograph.

Bridges and Pillars

Bridges (similar to structures called stretched crystals by Ramsay, 1980, although bridges differ from textures formed in completely mineral filled veins) are defined as “cement deposits [containing crack-seal texture] that span fractures and that are surrounded by fracture porosity (Fig. 5.1d) or by later cements” (Laubach et al., 2004), whereas the term pillar is used to describe cement deposits that are elongated transverse to a fracture but do not connect the two walls. Some pillars are probably bridges that are incompletely exposed due to the thin section or outcrop surface not being precisely parallel to the bridge. Others may be bridges that at some point in their history failed to span fractures during progressive opening and ceased to grow. The progressive development of such structures need not be simple (Laubach et al., 2004; Becker et al., 2010; Gale et al., 2010).

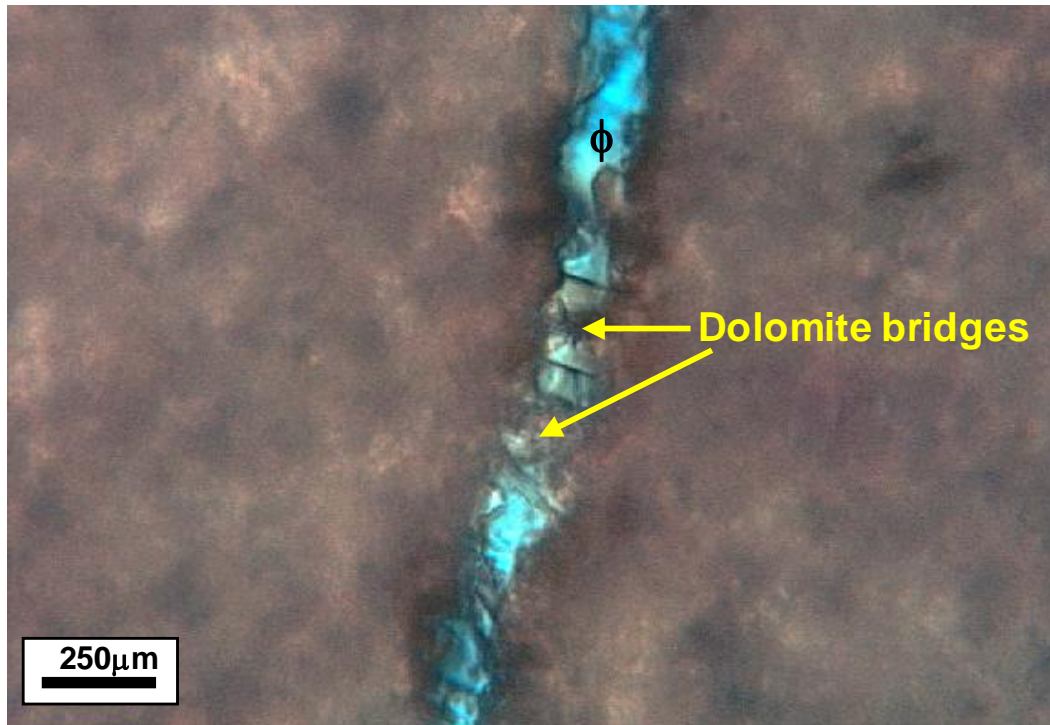


Fig. 5.1d. Detail of fracture in a limestone from an oil reservoir. Dolomite bridges cement partially filled fracture porosity (ϕ). Photomicrograph.

Crack-seal Texture

Intracrystalline crack-seal texture (Ramsay, 1980) is “marked by lamination parallel to fracture walls defined by wall-rock inclusions, broken cement inclusions, cement zoning cut by fractures and fluid inclusion planes” (Laubach, 2003) (Fig. 5.1e). Crack-seal texture is interpreted as the result of repeated fracturing with cement at least locally filling in the fracture (or part of the fracture) between opening increments; cement deposits having crack-seal texture in sedimentary rocks can co-exist with otherwise mostly open (porous) fractures (Laubach et al., 2004), probably as a result of faster cement accumulation rates on freshly broken fracture surfaces compared to those on

idiomorphic crystals (Lander et al. personal communication, 2002; Lander et al., 2008; Gale et al., 2010).

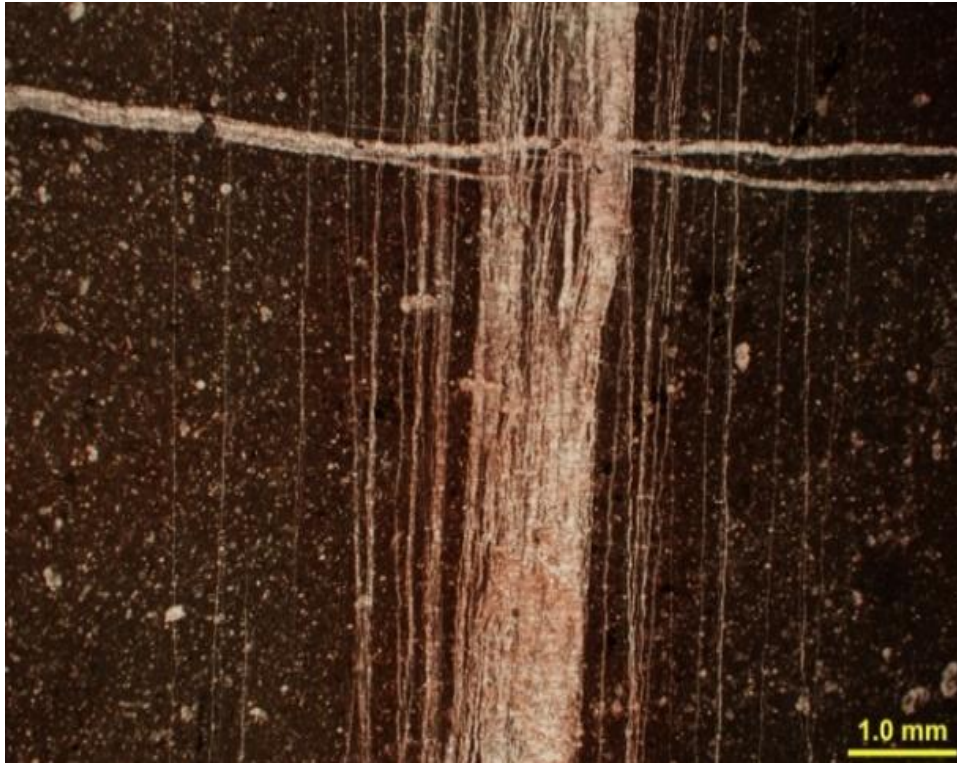


Fig. 5.1e. Detail of sealed fracture calcite cement in a limestone, with a crack seal texture. Photomicrograph.

Emergent Threshold

Emergent threshold is defined as the fracture size marking transition from small (commonly microscopic) fractures that are mostly filled with synkinematic cement to larger fractures in which synkinematic cement merely lines or bridges fractures and abundant porosity or postkinematic cement fills the remaining fracture volume (Laubach, 2003). An emergent threshold results in fractures (or segments of fractures) with less

complete fill by synkinematic cement (and therefore higher porosity or postkinematic cement) than in slightly smaller fractures (Laubach, 2003). Because opening-mode fractures tend to have elliptical shapes (narrow tips), emergent threshold systematically reduces fracture network connectivity and average open fracture length and thus dramatically reduces the capacity of fracture networks to conduct fluids, even if most parts of the fracture system remain open (Philip et al., 2005; Olson et al., 2009).

CHARACTERIZING AND PREDICTING FRACTURES

Subsurface fracture characterization is a key issue in exploration, development and exploitation of fractured oil and gas reservoirs (Nelson, 1985; Lonergan et al., 2007). Due to the high cost of wells, effort must be focused on predicting open natural fracture attributes and abundance prior to drilling. However, prediction is challenging mainly because data from the subsurface commonly are limited and direct detection with seismic methods is not feasible (Marrett et al., 2007). One way to approach subsurface fracture prediction is to understand how geologic parameters control fracture characteristics and their distributions. For example, open fractures in a sedimentary succession can be controlled by structural position, diagenesis, facies, rock composition, or a combination of one or more of these or other parameters (National Research Council, 1996). Some fracture sets can be distinguished in outcrops by systematic attitude and systematic crosscutting relationships (Hancock, 1985; Pollard and Aydin, 1988), but microscopic characterization is necessary in all cases to understand timing relationships and genesis.

In order to determine the geologic controls over fracturing in a study area, it is useful to begin by identifying and characterizing fracture sets (groups of fractures sharing the same characteristics or attributes, such as orientation, relative timing or mineral fill). Fractures are grouped in sets because fractures sharing attributes may be genetically related. However, there are some problems with this approach. Because opening-mode fractures in isotropic materials propagate in directions perpendicular to the local least compressive stress (Lawn and Wilshaw, 1975; Pollard and Aydin, 1988), a common assumption behind the categorization of fractures based on orientation is that each fracture set represents one fracturing event (Bai et al., 2002). However, even a homogeneous stress field can generate multiple fracture sets at the same time if one or

more sets include a shear component of motion. In addition, two different fracture events, occurring at different geologic times and under different geological conditions, can share the same orientation. These problems can be resolved in part by structural-diagenetic petrographic study (DSPS), because the deposits of cement provide an independent way to separate or differentiate fractures. Petrographic study provides additional criteria to separate different fracturing events that produced fractures sharing common orientation, and to recognize fractures with different orientations but that formed contemporaneously.

In this chapter, I illustrate an approach of combining basic field observations of fracture orientation together with the results of structural-diagenetic petrographic analysis (Chapter 4) to fully characterize fracture sets in a carbonate sequence. Full fracture characterization should include identification of the component fracture sets, classification of mineral fills, establishment of fracture events, determination of relative timing among fracture events and other diagenetic processes, and interpretation of a possible genesis for each fracture event. Using this full characterization approach facilitates identification of the geologic controls over fracturing, and thus could help improve prediction of fracture distribution in a carbonate sequence in the subsurface.

PREVIOUS FRACTURE WORK IN NE MEXICO

Several attempts have been made to interpret the origin and distribution of fractures in the SMO (e.g., Camerlo, 1998; Rico, 1999; Fischer and Jackson, 1999; Lu, 2000; Marrett and Laubach, 2001, Ortega, 2002). Both syn-folding and pre-folding times of fracture formation have been interpreted for the most abundant fractures.

Camerlo (1998) studied the geometry and kinematic evolution of the San Juan Bautista and San Blas anticlines of the Monterrey Salient, using vein geometry and other kinematic indicators in Cupido and Tamaulipas Superior Formations. Orientations and structural positions of fractures within anticlines showed a strong preferred orientation at high angles to fold axes and a slight increase in abundance near fold axial surfaces. This slight increase in abundance in parts of folds was interpreted as evidence that most veins are related to folding (Camerlo, 1998). Rico (1999) found similar relationships in the San Miguel anticline of the San Julian uplift. Two of three vein sets in the San Miguel anticline were interpreted to result from bed-parallel contraction, flexural slip, or focused bending during the folding process. Such an interpretation of fracture orientations and abundance patterns is in line with conventional thinking about the likely relationship of fractures and folds (Hancock, 1985; Nelson, 1985), approaches that rely heavily on the geometry of fractures patterns with respect to folds (in this case)(e.g., Stearns, 1967) or, more broadly, the idea that the fractures should be in some expected alignment with the putative loading conditions (Engelder, 1985)--kinematic compatibility--to infer the relationship between cause and effect.

Crosscutting relations with other structures can also shed light on the origins of fractures. Lu (2000) analyzed vein and stylolite orientations and crosscutting relationships in Cupido and Tamaulipas Inferior Formations from seven anticlines on the

northern and eastern sides of the SMO Salient. Layer-parallel stylolites can be reasonably ascribed to shortening perpendicular to bedding and thus to burial conditions of nearly flat lying beds. The oldest veins in six of the study localities are at a high angle to but kinematically linked with or cross cut by layer-parallel burial stylolites, and thus probably predate tilting of beds (stylolites would no longer be bed normal) and folding.

Relations to other near-surface or sedimentary structures provide fracture timing evidence. Marrett and Laubach (2001) interpreted many veins and faults as contemporaneous with Cupido deposition. After bedding is restored to horizontal, these veins indicate opening directions that agree across fold limbs and vary systematically around the SMO in a pattern that coincides with paleogeographic down-dip directions at the time strata were deposited (Marrett and Laubach, 2001).

Indirectly, mechanical stratigraphy casts some light on fracture timing. Ortega (2002; Ortega et al., 2006; 2010) studied the variation of fracture abundance as a function of sedimentological facies, composition, and layer thickness in the Cupido and Tamaulipas Inferior Formations of the Monterrey Salient. He found that dolomite content was the strongest predictor of fracture abundance (intensity), and that layer thickness and facies did not exert significant control. This pattern suggests that fractures must be contemporaneous with or postdate dolomitization.

Gómez (2007) studied the relationships between fracture diagenesis and how fractures are spatially arranged in the Cupido Formation. His work focused mainly on nine localities from La Escalera, Las Palmas and la Huasteca canyons. He found three fracture categories with different degrees of roughness, fracture cements and timing with respect to the regional D2 dolomitization (Monroy, 2001). Fractures with irregular traces are interpreted to have developed before the regional D2 dolomitization event. Fractures

with straight traces were developed after D2 dolomitization, whereas other fractures are interpreted to have developed simultaneously with D2 dolomitization and to have enhanced flow of the diagenetic fluids that caused D2 dolomitization.

In fact, many of the fractures in all areas are kinematically linked with layer-parallel burial stylolites and with D2 regional dolomitization as well. Thus, many of the fractures probably predate folding. In this study I establish that the majority of outcrop-scale fractures in the Cupido Formation are characterized by synkinematic dolomite cement and therefore are contemporaneous with D2 regional dolomite precipitation or baroque dolomite cementation. One interpretation from petrographic characteristics of these synkinematic dolomites is that they formed at shallow to moderate burial depths, and that fractures were in place prior to deepest burial of the SMO, that is, before folding commenced.

FRACTURE STUDY AREA

The study area encompasses four main localities in the SMO: Cañón de los Chorros, Cañón la Escalera, Cañón Boquilla Corral de Palmas, and Cañón Santa Rosa-Iturbide. Samples from five more localities were also included: Cañón de las Cortinas, Cañón Prieto, Molano Fault, Cienegas, and Potrero García (Fig. 5.2).

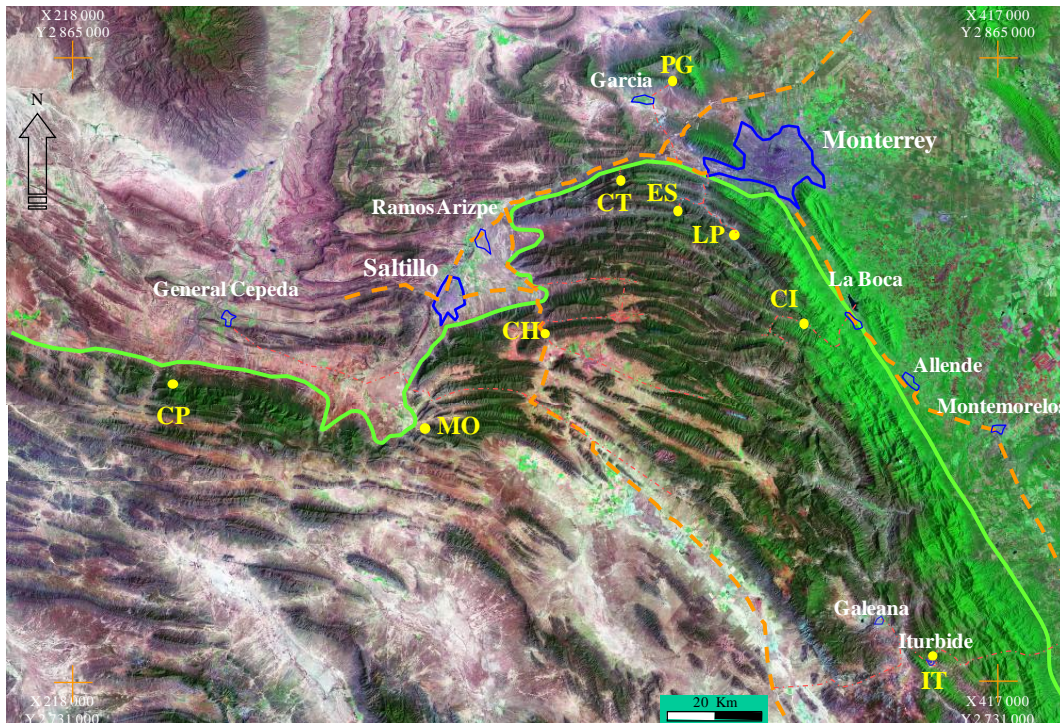


Fig. 5.2. Landsat TM satellite image of part of the SMO, showing the Monterrey Salient. Circles mark outcrop and sample localities: PG, Potrero García; CT, Cañón de las Cortinas; CH, Cañón de los Chorros; ES, Cañón la Escalera; LP, Cañón Boquilla Corral de Palmas; IT, Cañón Santa Rosa-Iturbide; MO, Molano Fault; CP, Cañón Prieto; CI, Cienegas. X and Y are coordinates in the Universal Transverse Mercator (UTM) Projection indicated by small crosses. Main cities and towns are labeled. Continuous line approximates the thin-skinned deformation front, as delimited by lateral continuous exposure of Jurassic-Cretaceous carbonate strata. Dashed lines show main roads. X and Y are coordinates in the Universal Transverse Mercator (UTM) Projection indicated by small crosses. Foreland is to the north and northeast.

CHAPTER ORGANIZATION

This chapter is divided in four parts. First part explains the methodology used to identify fracture sets in the field and to collect oriented samples for petrographic analysis, and presents a summary of the results of the fracture set analyses of field data from the Cupido Formation in the Monterrey Salient, as reported by Ortega (2002). The second part presents a description of fracture events and fracture sets, and their correlations from outcrop to microscopic scale (as defined in the structural-diagenetic petrographic study). The third part justifies my interpretation of the chronology of fracture sets relative to other diagenetic features (complete paragenetic sequence), based on the evidence shown in Chapter 4 that supports fracture differentiation in the Cupido Formation. The fourth part is a discussion of the benefit of using data at different scales to fully characterize fractures in a carbonate sequence, and the implications of the links between fractures at a range of scales and their associated cement deposits for oil and gas reservoir characterization.

FRACTURE METHODOLOGY

Identification of fractures sets, based on strike and dip, fracture filling cements (observed at outcrop scale with the aid of a hand lens), and cross-cutting relationships is the first step to make a fracture classification. Equal area, lower hemisphere stereographic projections were used to represent fracture set orientations in each locality. Once fracture sets were identified, their strikes and dips can be used to select scanline (line of observation) direction for each fracture set in order to collect data for fracture aperture or length analysis. For my study, the key objectives are identification and differentiation of fracture sets at different scales, and their correlation with diagenetic events. The relative

chronology of fracture sets at each sample locality was determined in the field based on crosscutting relationships among fractures and stylolites. This field work yielded local correlations of sets, based on strike and dip patterns, in some areas. Oriented rock samples containing fractures of each set were collected for laboratory analysis. Those samples were used to characterize petrographically each fracture set. Correlation between fracture sets identified in the field and fracture events interpreted petrographically yielded a complete characterization of fracturing in the Cupido Formation rocks. Although I contributed to collecting a large fracture aperture size data set by scanline methods, the full analysis of fracture aperture size scaling patterns is beyond the scope of my dissertation. Fracture aperture analyses in these rocks are reported by Ortega (2002) and more data are in my Appendix 5.2. This information is important in the context of my study because of the size dependency of gradual cement infill in fractures and the interaction of that infill pattern on evolving fracture porosity and permeability.

Fracture Size Data

Fracture data collected from outcrops represent more than 12,700 fractures, measured along a total of 286 m of scanlines in 41 carbonate beds (Appendix 5.1). Bed-parallel exposures are very limited in the canyons of the Monterrey Salient and mostly bed-perpendicular exposures along canyon walls were used for fracture measurement. Forty-nine oriented rocks samples were taken for petrographic analysis (Appendix 5.2). For the purposes of this study, an ideal rock sample should satisfy two conditions. The first condition is the sample should be obtained along the outcrop scanline, which allows petrographic study of the same fractures measured along the outcrop. If a rock sample could not be obtained along the outcrop scanline, the sample should be collected close to

it. The second condition is to ensure that the rock sample contains fractures measured along this scanline. The sample is labeled with a consecutive number and the locality name, and the sample must be marked with geographic north, stratification (So) orientation (strike and dip), and identification of the fracture set or sets measured in the scanline. Appendix 2.1 (Chapter 2) shows the locations of the beds studied in detailed stratigraphic columns of Cañón de los Chorros, Cañón la Escalera, Cañón Boquilla Corral de Palmas, and Cañón Santa Rosa-Iturbide localities. Two basic criteria were used to select beds for study. The first criterion was the presence of macrofractures in the bed and the second the existence of enough surface exposure for collection of representative fracture data along scanlines. Stratification (So), fracture plane orientation, fracture aperture, fill cement composition, bed thickness, lithology, sedimentary facies, and structural features were described in the field.

FIELD IDENTIFICATION OF FRACTURE SETS

In all localities, at least four fracture sets were identified, but size analysis focused on three of these sets as reported by Ortega (2002) (Appendix 5.2). Most fracture sets are distinguished by systematic attitude with respect to bed surfaces and systematic crosscutting relationships with both types of stylolites, bedding parallel (referred to as burial stylolites) and bedding transverse (referred as tectonic stylolites, a kind of spaced cleavage). A similar nomenclature was used for local fracture set identification (W, X, Y, and Z) in each locality. However, identification names at different localities indicate similarities in relative timing but do not imply that fracture sets with the same label have same attributes (orientation, fill, etc.), in each locality. The significance of this can be

appreciated by recalling that one of the early sets may change strike drastically around the SMO; defining and naming sets with regional designations (in part based on local strike patterns) might obscure such a relationship. One objective of this Chapter is to demonstrate that it is possible to recognize which fracture sets share effectively similar attributes from locality to locality. Sets W and X are the oldest sets of fractures, set Y is the next youngest fracture set, and set Z is the youngest at all localities. The following section describes the field observations used to separate the four main fracture sets of the Cupido Formation in the Monterrey Salient. These designations agree with and are in large part the basis of those designations used by Ortega (2002).

Burial and Tectonic Stylolites

Burial and tectonic stylolites are key features to interpret relative timing and cross-cutting relations among different fracture sets. La Escalera, Las Palmas, Los Chorros and Santa Rosa localities present both burial and tectonic stylolites, and their characteristics and crosscutting relationships are discussed in Chapter 4.

Stylolite attributes vary within the study area. Large teeth on burial stylolites at La Escalera and Las Palmas are most common at dolostone/limestone contacts (Fig. 5.3). Burial stylolites are also common at the boundaries of mudstones at Santa Rosa. The amplitudes of stylolites teeth in this locality are smaller than for bed-parallel stylolites in other localities and range from less than a millimeter to a couple of centimeters. At Los Chorros burial stylolites follow bedding plane surfaces and are not as well developed as at Las Palmas or at La Escalera. However, isolated outcrops of dolostones down section from the section studied at El Chorro show abundant tectonic stylolites, suggesting fold-

axis parallel contraction similar to San Blas Anticline at La Escalera locality (Ortega, 2002).

Tectonic stylolites are also present at all localities. At La Escalera and Las Palmas tectonic stylolites form a high angle with bedding and poles to stylolite surfaces are aligned with fold perpendicular to axes; the intersection of bedding and spaced stylolite surfaces parallels the regional fold axis. At Santa Rosa tectonic stylolites are also present, but they are less abundant (more widely spaced) than at the La Escalera locality (Fig. 5.3). Attitudes of tectonic stylolites suggest bed-parallel contraction subperpendicular to the fold axial surface (Ortega, 2002).

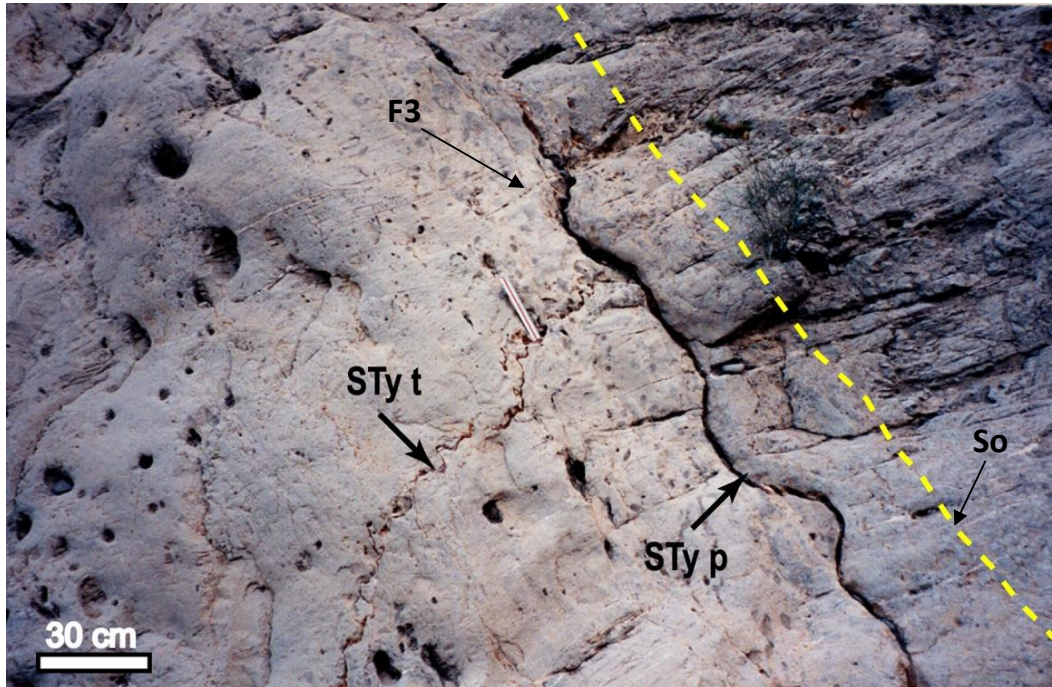


Fig. 5.3. High-angle (Sty t), bedding-parallel (Sty p) stylolites, and fractures (F3) in a dolostone bed. Sty p are interpreted as burial stylolites preferentially developed along stratigraphic planes or at the boundaries of mechanical layers. Stylolites (Sty t) at high angle to bedding (So) are interpreted as tectonic in origin. Sty t and Sty p are perpendicular each other. Fractures (F3) form high angles with Sty p and low angles with Sty t. Orientation of F3 fractures is parallel to the tectonic stylolites and thus kinematically incompatible with them. Orientation and relationships with both burial and tectonic stylolites suggest that F3 fractures belong to set W measured in this outcrop. Development of tectonic stylolites along the walls of fracture set W confirms that set W is older than tectonic stylolites. Bed dips to the right of the photograph. Dashed line indicates stratification surface (So). Cupido Formation, Cañón la Escalera locality. Outcrop photograph.

FRACTURE SETS W, X, Y, AND Z.

Based on their orientation (strike and dip), attitude with respect to bedding or cross cutting relationships, four fracture sets were identified at all localities, named from the oldest to the youngest: Sets W, X, Y, and Z. Figure 5.4 shows equal area, lower hemisphere stereographic projections of fracture orientation at four localities studied.

Crosscutting relationships among fractures permitted, at outcrop scale, the determination that sets W and X are the oldest fractures in the study area. These sets were identified mainly in dolostones beds at Las Palmas, La Escalera and Los Chorros. Set W are fractures with irregular or jagged paths and contain fibrous dolomite and calcite cement. Set X fractures are characterized by millimeter-scale dolomite crystals (cement), calcite and a minor percent of quartz. The presence of these coarse crystals facilitates outcrop-scale differentiation of these fractures from others. At La Escalera sets W and X can be separated because W fractures are systematically oblique to bedding whereas fractures from set X are nearly perpendicular to bedding for all bed attitudes (Fig. 5.4 a), suggesting that set W is older than X. Set W and X fractures at Las Palmas locality have similar orientations but fractures from set W strike more northerly than set X and fracture set X is slightly oblique to bedding (Fig. 5.4 b). At Los Chorros, set W fractures form a higher angle with bedding than fracture set X. Set W attitude is also closer to vertical than set X (Fig. 5.4 c). Both sets W and X are slightly oblique to the fold axis at the Iturbide locality (Fig. 5.4 c). Fractures from sets W and X are parallel to tectonic stylolites and therefore are kinematically incompatible with them. Development of tectonic stylolites along the walls of fracture sets W and X confirms that sets W and X are older than tectonic stylolites. Moreover, these crosscutting relationships with tectonic stylolites suggest that fracture sets W and X are unrelated to folding, inasmuch as the

tectonic stylolites are probably fold related. Such stylolite structures commonly begin to form slightly prior to and during folding (Marshak and Engelder, 1985; Engelder and Marshak, 1985). Furthermore, considerable overlap in orientation exists for fracture sets W and X when fracture orientations from all beds are plotted in the same stereographic projection (Fig. 5.4). Sets W and X were considered as a single set by Ortega (2002), but separate petrographic analyses for sets W and X indicate that these sets mark different events.

Set Y fractures in general are scarce but more abundant than set Z fractures at outcrop scale. These fractures cross cut sets W and X, are thin (microfractures) and contain calcite cement. Field observations at La Escalera, Los Chorros, Las Palmas and Iturbide indicate that fracture set Y crosscuts fracture sets W and X, suggesting that fracture set Y is younger than sets W and X. Tectonic stylolites along fracture walls suggests that fracture set Y predates tectonic stylolites. Fracture set Y lacks a well-defined orientation with respect to the fold axis, in some places such as La Escalera, Las Palmas, and Iturbide set Y is oblique to the fold axis, while in other places such as Los Chorros set Y is parallel to the fold axis (Fig. 5.4). Also, the attitude of this set with respect to bedding varies, from slightly oblique with respect to bedding at La Escalera and Las Palmas, to perpendicular to bedding at Los Chorros. According to Ortega (2002), set Y orientation is broadly consistent with simple models of fold axis-perpendicular contraction and fold axis-parallel extension, but the patterns could also fit a scenario where the fractures are superposed on a pre-existing fold (Narr, 1992).

Set Z fractures are long, narrow, and filled with calcite cement. Fractures are arranged in swarms (qualitatively defined clusters) with common en echelon trace geometry. At La Escalera and Iturbide Set Z fractures are roughly parallel to bedding and

also form a high angle with tectonic stylolites (Figs. 5.4 a and 5.4 d), and consequently are kinematically compatible with them and with folding, suggesting that fracture set Z may be tectonic in origin (Ortega, 2002). At Cañón de los Chorros- Set Z crosscuts sets W, X and Y. Set Z is formed by conjugate mixed mode vein sub-sets. One of the groups of fractures defining a subset is oblique to the fold axis and forms a low angle with bedding; the other subset is parallel to bedding and to the fold axis (Fig. 5.4 c), suggesting bed-perpendicular extension and bed-parallel contraction. At Iturbide fracture set Z is orthogonal to bedding and to the fold axis (Fig. 5.4 d), suggesting bed-parallel extension and fold axis-perpendicular contraction. At Los Chorros and La Escalera set Z fractures are similar in morphology and geometric relationships. This similarity between fracture sets in separate folds suggests a common formation mechanism and timing (Ortega, 2002).

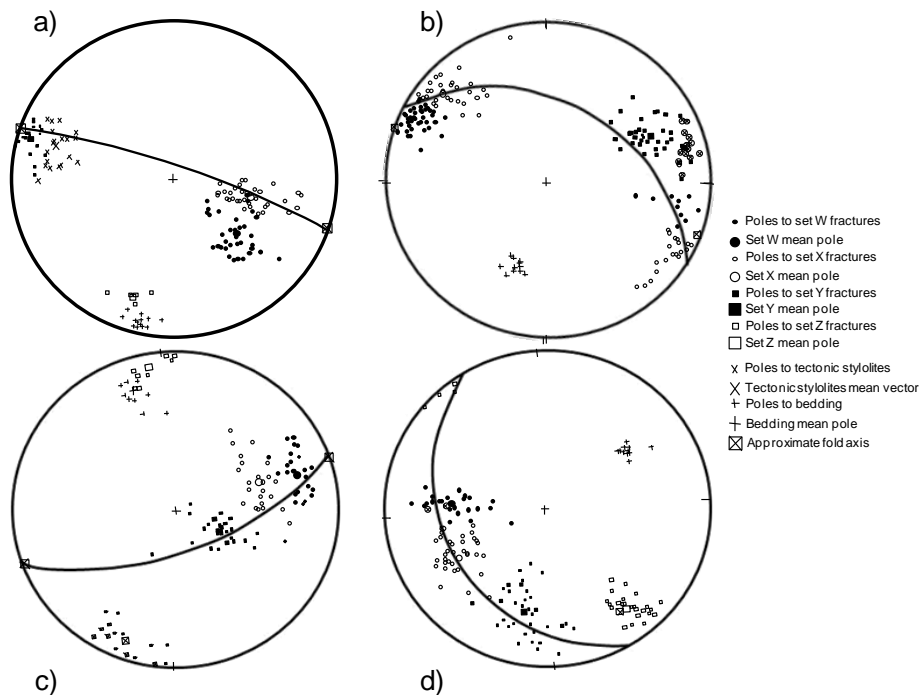


Fig. 5.4 . Equal area, lower hemisphere stereographic projection of fracture orientation at four localities studied. (a) Cañón de La Escalera; (b) Cañón Boquilla Corral de Palmas; (c) Cañón de Los Chorros (d) Santa Rosa-Iturbide. At La Escalera, sets W and X are oblique to the fold axis; set Y forms a high angle with respect to the fold axis; and set Z is subparallel to bedding and forms a high angle with tectonic stylolites. At Las Palmas, most fracture sets display considerable orientation dispersion and overlapping, however fracture sets are distinguishable in the field based on systematic crosscutting relationships, attitude with respect to bedding, fracture morphology and fracture fill. Most fracture sets are oblique to the fold axis. At Los Chorros locality, fracture sets W and X, form high angles with bedding, but are oblique to the fold axis. Set Y is roughly parallel to the fold axis which plunges WSE. These sets partly overlap and show considerable orientation dispersion, but their attitudes with respect to bedding and crosscutting relationships are systematic on a bed by bed basis. Fracture set Z is roughly vertical, crosscut other sets, and is interpreted as formed by two conjugate mixed-mode vein sets. At Iturbide locality, all fracture sets form high angles with respect to bedding. Fracture sets W, and X are slightly oblique to the fold axis. Fracture set Y is oblique to the fold axis. Fracture set Z is roughly perpendicular to the fold axis. Tectonic stylolites are parallel to fracture sets W and X. Larger symbol is the mean vector to a particular group of surfaces. From Ortega (2002).

FRACTURE EVENTS

Next section describes the fracture events (F1 to F6) identified in the Cupido and Tamaulipas Inferior Formation: their relationships with cementation stages, their order in the general paragenesis and their possible origins.

F1-F2 Fracture Event

Fractures that predate D2 and D3 dolomites are classified as F1 or F2. Evidences for the F1 fracture event was found in differential compaction boudinage structures and evaporite solution collapse breccias at the Las Palmas and La Escalera outcrops (Figs. 5.5a and 5.5b). F1 fractures are thin veins (<0.05 mm width) present in solution breccias clasts and wide fractures with C1 calcite and D1 dolomite cement present in boudin necks. Fractures have differing orientations in adjacent breccia blocks, but the orientations become congruent when the rotated breccia blocks are restored. These observations indicate thin F1 fractures predate brecciation and their origin is related to surface exposure. Wide veins, marking the boundaries of breccia blocks, have similar mineralogy, and in some cases similar strike, to rotated thin fractures, suggesting that these two groups of F1 fractures are related and perhaps broadly synchronous. Compaction stylolites truncate both fracture sets, implying that bed-perpendicular shortening postdates both groups of early fractures. Some thin (<0.1 mm) calcite veins cross-cut C1 and C2 calcite (Fig. 4.2a and 4.7a, Chapter 4), and so at least partly postdate both cements..

F2 fractures are characterized by an irregular or jagged path (fracture trace) with synkinematic calcite cement. Calcite-bearing fractures are present, varying from very thin (<0.05 mm width) to less than 1 mm; these fractures are locally difficult to identify at

outcrop scale. However, at petrographic scale they are visible in both limestones and dolomitized limestones. D2 dolomite partially replaced calcite in F2 fractures (Fig. 5.5c), showing that dolomite postdates F2. Therefore, F2 fractures predate D2 regional dolomitization and these fractures probably originated under shallow burial conditions due to basinward extension and vertical loading.

Orientations are locally inconsistent and no preferred orientation is evident, so they are excluded from veins sets W-Z. These fractures are found at all localities.

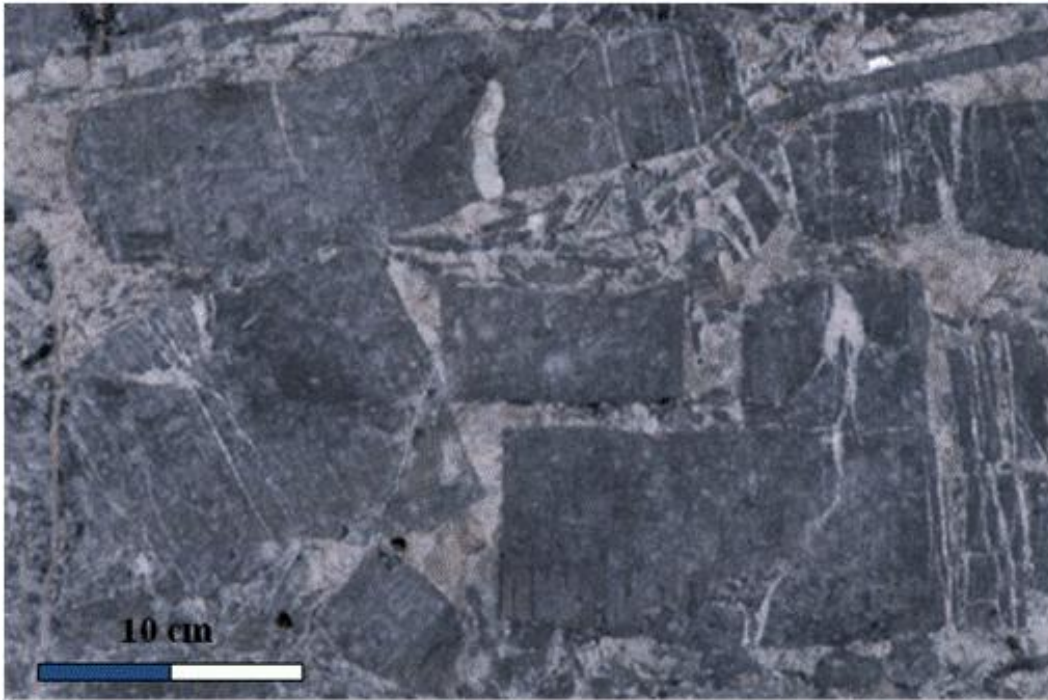


Fig. 5.5a. Monomict, clast-supported breccia, showing rectangular shaped blocks. Note rotated veins in adjacent clasts. Cross-cutting relations show most of the calcite veins (F1 fractures) affect only the fragments, implying that these veins were already present at the time of brecciation. Breccia is cemented with calcite. Photograph courtesy of Randall Marrett. Cupido Formation, Cañón Boquilla Corral de Palmas locality. Outcrop photograph.

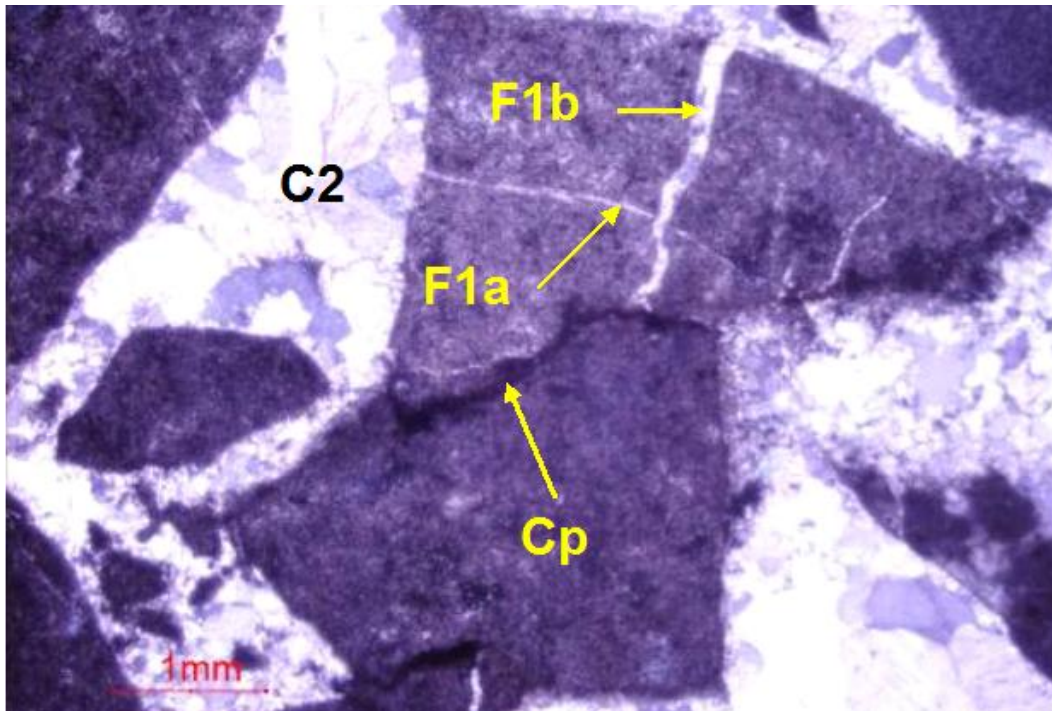


Fig. 5.5b. Solution breccia constituted of dolostones clasts and showing two fractures: Thin calcite filled vein (F1a) is only present within the clasts, implying that this vein predates brecciation. Wide calcite vein (F1b) cross cuts the thin vein and contains cement that is continuous with the breccia cement, indicating that brecciation and F1b fractures were synchronous. The breccia is cemented by C2 blocky calcite. Notice compaction feature (Cp) truncates both veins, implying that Cp postdates both events. Cupido Formation, sample CulPa1-01, Cañón Las Palmas locality. Photomicrograph.

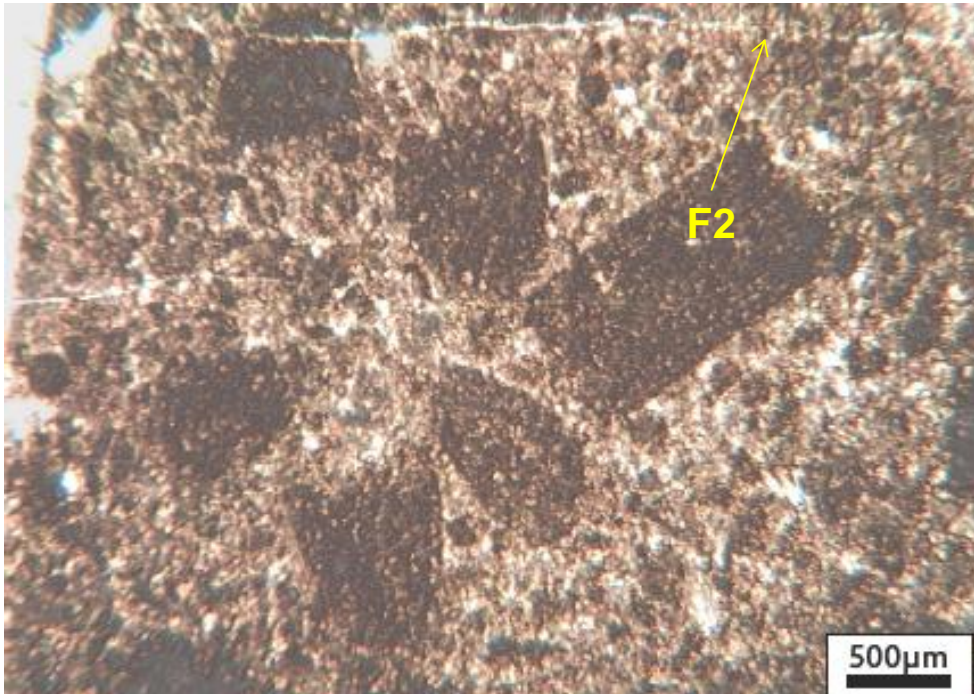


Fig. 5.5c. Dolomitized pellet packstone showing F2 calcite fractures partially replaced by fine grained D2 dolomite matrix. Cupido Formation, Cañón de los Chorros locality. Photomicrograph.

F3 Fracture Event

Faceted dolomite crystals, with petrographic characteristics that resemble D2 dolomite, are found as cement in some fractures. Those fractures are termed F3 because crosscutting relations indicate they postdate F2. F3 fractures are the most abundant at both the Las Palmas and La Escalera localities; they are developed preferentially in dolostone layers (Fig. 5.6a). Fracture traces are characterized by irregular or jagged paths. Pillar-shaped D2 dolomite and bridges of rhombohedral dolomite crystals in F3 fractures likely indicate synkinematic precipitation of dolomite (Fig. 5.6b), so D2 dolomite is synchronous with F3 fractures. F3 fractures also contain postkinematic C3 calcite cement.

D2 dolomite lines fracture walls and is overlapped by the calcite, implying D2 dolomite predates calcite in fractures. This calcite cement was named C3 because of the timing relations implied by crosscutting relations with post-F2 calcite and overlapping relations with D2 dolomite. Thin sections stained to differentiate dolomite (grey) from calcite (red) show some dolomite bridges partially stained in red, suggesting that C3 calcite also replaced D2 dolomite (Fig. 5.6b). From these observations I infer that D2 dolomite crystals grew in open fractures. These dolomite-lined fractures were later filled with C3 calcite that also is found in the matrix pore space (intra-crystalline volume) (Fig. 5.6b). F3 fractures probably originated under moderate burial conditions due to basinward extension and vertical loading. They have characteristics of orientation, fracture cements, and morphology of set W measured at Los Chorros, Las Palmas and La Escalera.

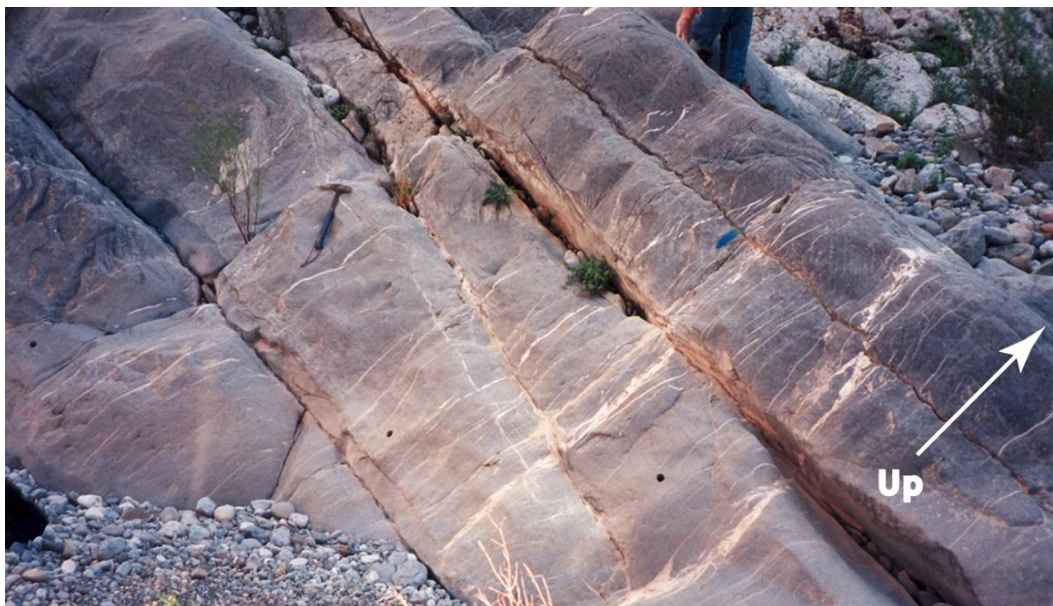


Fig. 5.6a. Dolostone beds showing F3 fractures cross cutting several carbonate beds (dolostone). These fractures are filled with synkinematic dolomite and postkinematic calcite cements; local Set W fractures. Cupido Formation, Las Palmas locality. Arrow indicates top of bedding (up section); hammer is ~ 30 cm long. Outcrop photograph.

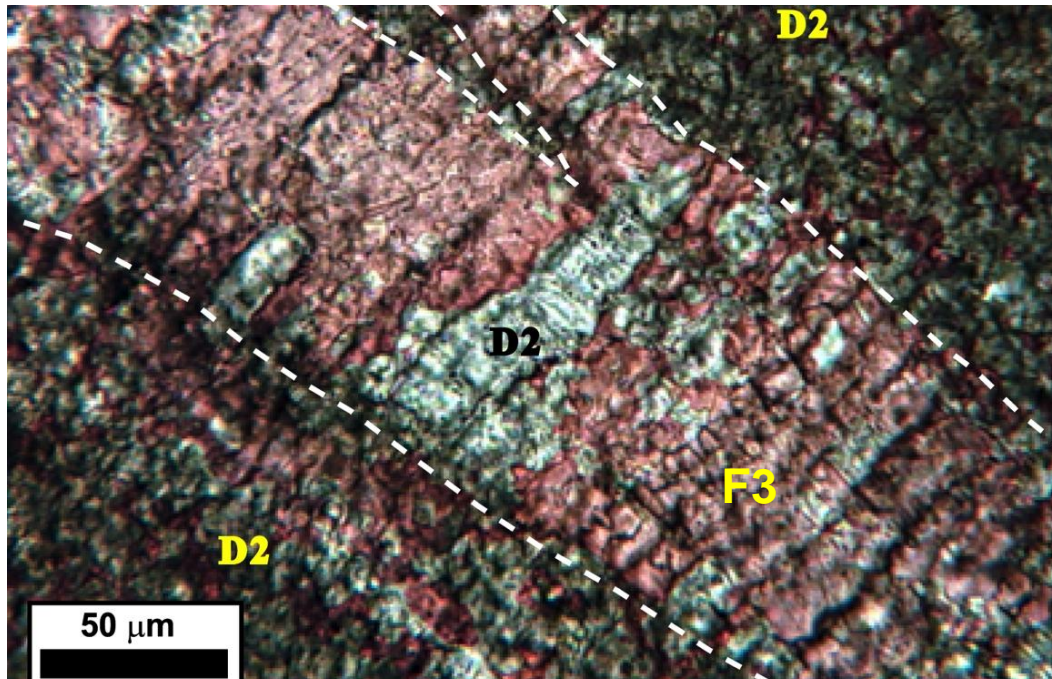


Fig. 5.6b. F3 fracture with dolomite and calcite fill. F3 fractures are characterized by irregular or jagged boundaries (dashed lines). Characteristics of color and form of dolomite in F3 fracture resemble D2 dolomite in matrix. Dolomite crystals that cross from wall to wall inside of the fractures are bridges. Notice that in some places matrix dolomite crystals apparently cross fracture walls, but also some bridges apparently pass into the matrix. These observations support the interpretation that both matrix dolomitization and dolomite precipitation in fractures are synchronous events, and belong to the D2 dolomite phase. Pillar-shaped dolomite bridges likely indicate synkinematic precipitation of dolomite because crystal morphology probably arose from crack-seal processes. Bands of inclusions that parallel fracture walls likely mark crack-seal texture. Dolomite bridges that are partially overlapped by calcite (bridges stained in red) indicate that calcite postdated and partially replaced D2 dolomite. Calcite that postdated D2 dolomite is C3. Thin section stained to differentiate dolomite (grey) from calcite (red). Crystal shapes suggest that dolomite crystals grew in open fractures, which later were filled with postkinematic calcite that partially replaced dolomite; calcite also precipitated in matrix porosity. These fractures have similar characteristics (orientation, fracture cements, and morphology) of set W measured in the field. These fractures likely originated synchronously with D2 regional dolomitization. Thin section is parallel to bedding. Cupido Formation, sample CuEsc3-98, La Escalera locality. Cross-polarized light photomicrograph.

F4 Fracture Event

F4 fractures are characterized by low aspect ratio (length/width), straight paths, and large fibrous baroque dolomite crystals (D3) that bridge the fractures. Most of these fractures are perpendicular to bedding and are restricted to beds of a given lithology (height is restricted by bed boundaries). Calcite and a minor percent of quartz are present as postkinematic cements; these compositional contrasts make it possible at outcrop scale to differentiate these fractures from other sets (Fig. 5.7.a). F4 fractures crosscut and thus postdate F3 fractures. D3 baroque dolomite fills, bridges or lines F4 fractures (Fig. 5.7b). D3 dolomite bridges in F4 fractures (Fig. 5.7c) indicate that dolomite was deposited during fracture opening (synkinematic cement), so D3 and F4 are synchronous. Straight paths of F4 fractures cross-cut replacement D2 dolomite (Figs. 5.7b), and indicate that F4 fractures postdate D2 dolomite.

Because both calcite and quartz cements are found in F4 fractures, their relative timing with respect to D3 dolomite can be established. Incomplete and irregular D3 dolomite crystal borders and overlaps of calcite over baroque D3 dolomite in F4 fractures (Figs. 5.7b and 5.7c) indicate that calcite partially replaced D3 dolomite, and must postdate D3. Because calcite that postdates D3 has the same petrographic characteristics as C3, I interpret it as C3 calcite.

Tectonic (non-bedding parallel) stylolites that locally contain quartz cement cut D3 within F4 fractures, indicating that stylolites and quartz postdate D3 (Fig. 5.7d). F4 fractures have multiple orientations that show mutually crosscutting relations. Since individual fractures from F4 fracture event crosscut each other (Figs. 5.7d), it is possible that a multiplicity of D3 dolomite cements is present, as has been documented in other dolomites through CL zoning patterns and other methods (for example, zoned dolomite

described by Montañez et al., 1997). However, scanning electron microscope-based cathodoluminescence (SEM-CL) studies show indistinct (poor) zonation in Cupido Formation dolomites (Fig. 5.7e). These fractures also probably originated under moderate burial conditions due to basinward extension and vertical loading. F4 fractures have characteristics (orientation, fracture cements, and morphology) of set X measured at Los Chorros, Las Palmas and La Escalera.



Fig. 5.7.a. Dolostone bed showing bedding perpendicular F4 fractures. Fractures are filled with baroque dolomite, quartz and calcite. Calcite cement presents negative relief due to outcrop-related dissolution while dolomite and quartz are well preserved due to resistance to dissolution. These fractures have characteristics of set X measured at other localities. Dashed lines indicate bedding. Pen is 15 cm long. Cupido Formation, Cañón Las Palmas locality. Outcrop photograph.

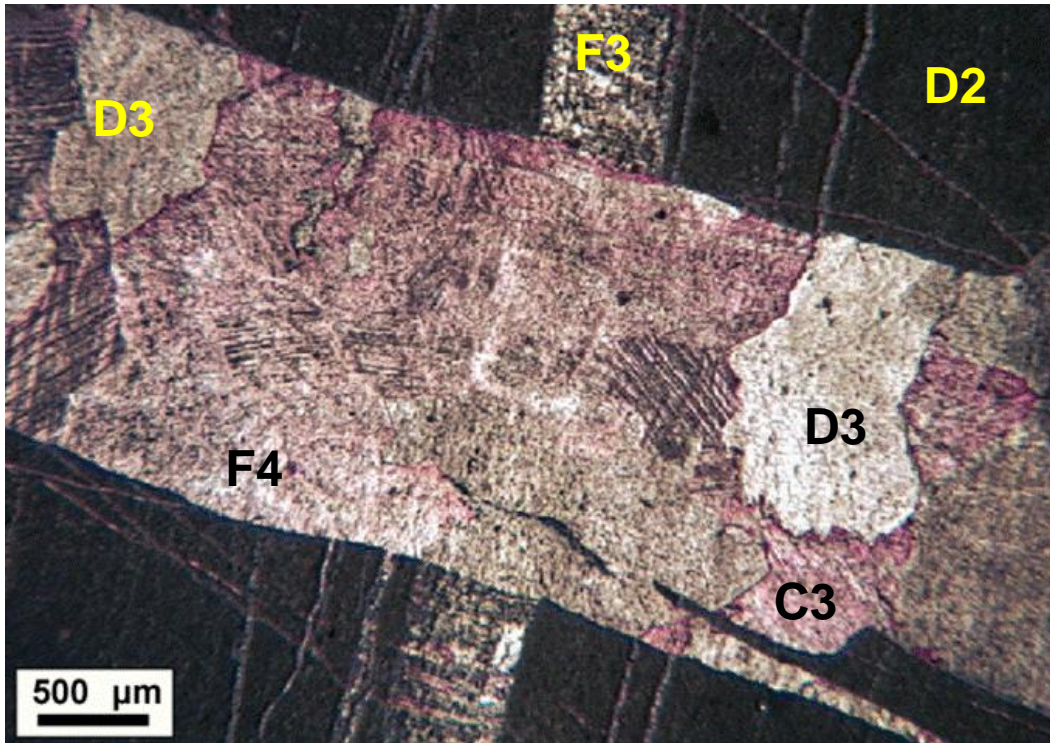


Fig. 5.7b. Wide vein in a dolostone. Matrix is composed by replacement phase D2 dolomite. Fracture has straight path that indicates that it cuts D2 dolomite. Dolomite in fracture is composed by crystal sizes bigger than 1 mm and presents twins, curved crystal faces, and undulatory extinction characteristic of D3 saddle or baroque dolomite. The pillar-shaped dolomite bridges likely indicate synkinematic precipitation of dolomite. Fractures with synkinematic baroque dolomite cement are named F4. Baroque dolomite crystals are incomplete and have irregular borders. Calcite (in red) overlaps D3 dolomite, indicating that C3 calcite postdates D3. F4 vein cross cuts F3. Thin section stained to differentiate dolomite (brown, grey or white) from calcite (red). Thin section is parallel to bedding. Cupido Formation, sample CulPa8-98, Cañón Las Palmas locality.

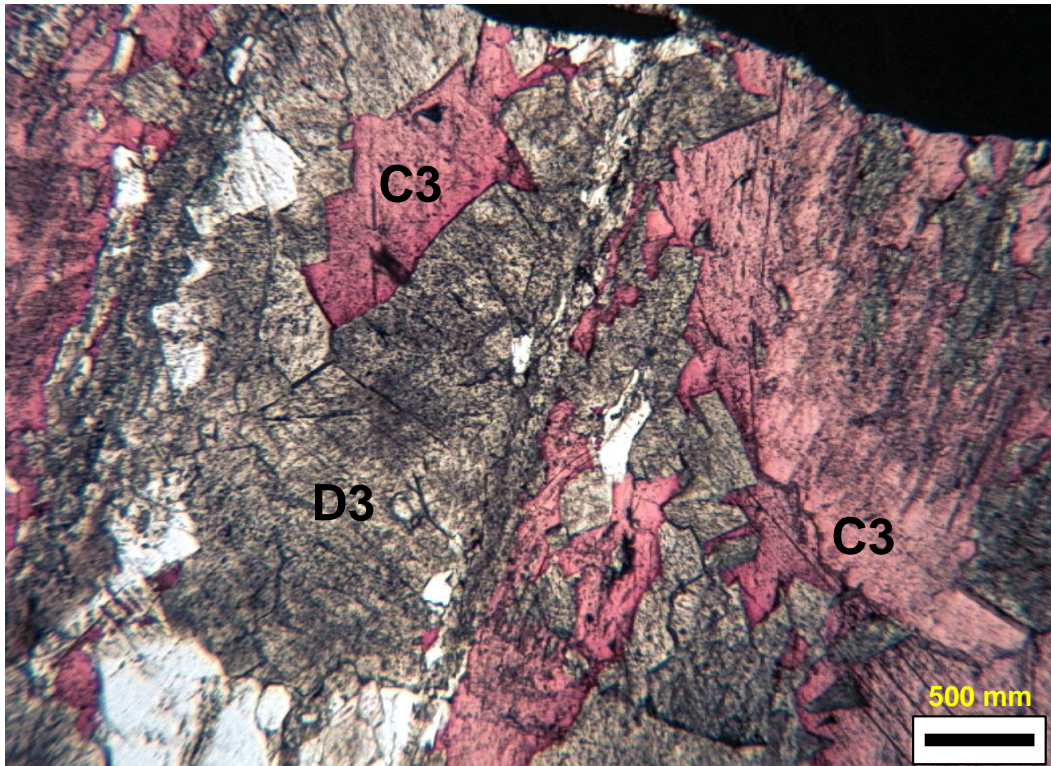


Fig. 5.7c. F4 fracture showing baroque dolomite (D3) bridges. D3 dolomite lines fracture walls and forms bridges that cross from wall to wall inside of the fracture. D3 crystals are overlapped by C3 calcite, thus D3 dolomite predates C3 calcite. Thin section stained to differentiate dolomite (brown, grey or white) from calcite (red). Thin section is parallel to bedding. Cupido Formation, sample CuEsc1-98, Cañón Las Palmas locality. Plane-light photomicrograph.

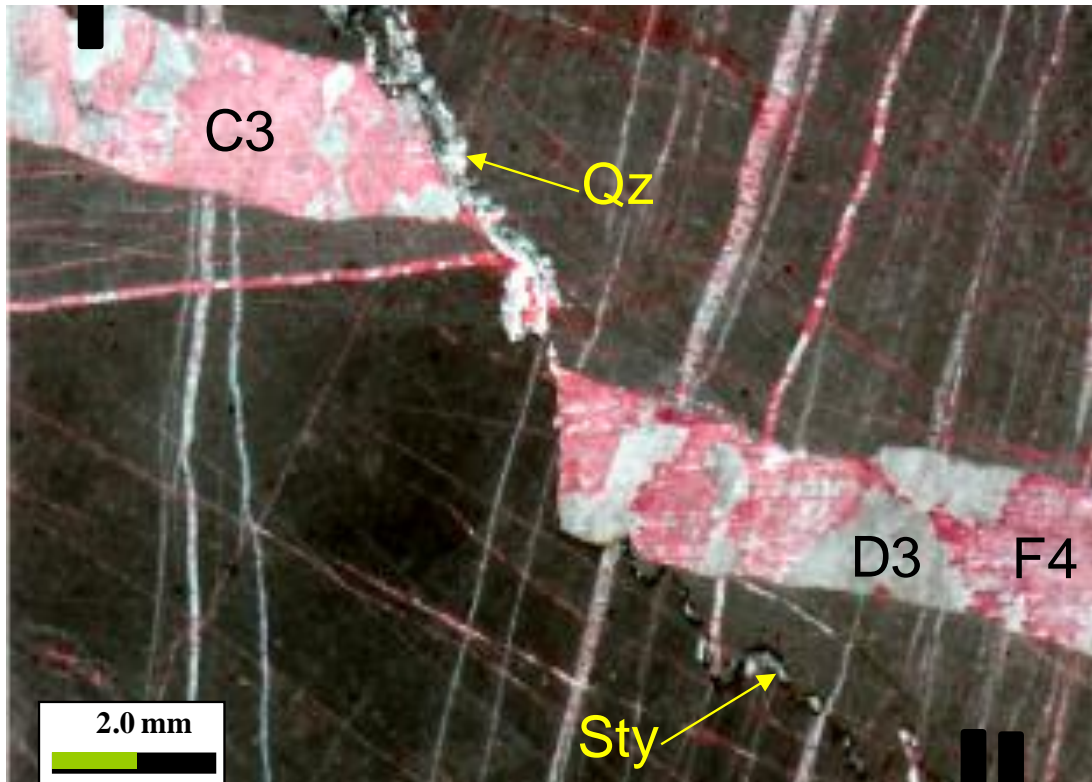


Fig. 5.7d. Detail of F4 fracture petrographic characteristics: straight paths, large baroque dolomite crystals (D3) bridge the fracture, and calcite is textureless postkinematic cement (C3). Incomplete and irregular D3 dolomite crystal borders and overlaps of calcite over dolomite indicate that calcite postdates dolomite and partially replaced D3. Notice subvertical stylolite (Sty) with quartz (Qz) cement along its path cuts all fractures and D3 dolomite crystals also in F4, indicating that both stylolites and quartz postdate fracturing and D3 dolomite. Thin section stained to differentiate dolomite (D3) (grey) from calcite (C3) (red). Thin section is parallel to bedding, notches indicate north. Cupido Formation, sample CulPa8-98, Cañón Boquilla Corral Las Palmas locality. Plane-light photomicrograph.

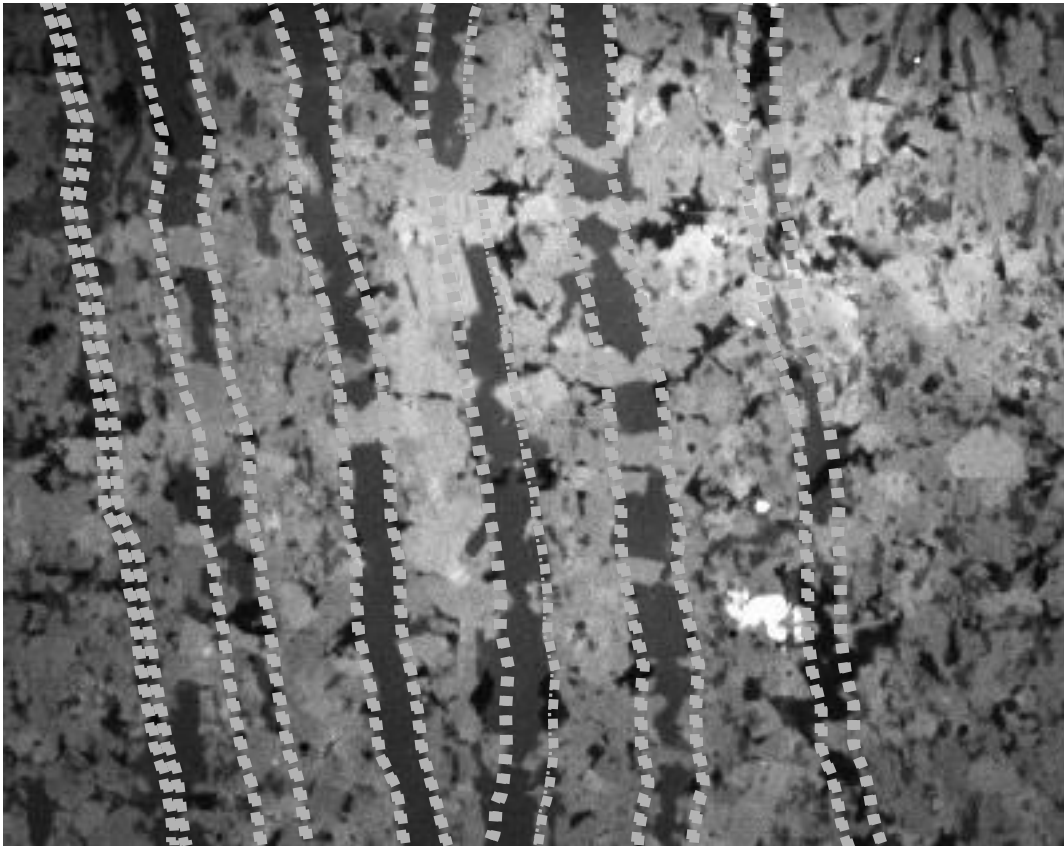


Fig. 5.7e. SEM-CL image showing F4 fractures with synkinematic D3 dolomite (light grey) and postkinematic C3 calcite (dark grey) cements. Notice euhedral to subhedral D3 dolomite crystals showing poor zonation that fill, bridge (indicated by arrows) and line fractures. Calcite cement (C3) precipitated in remnant porosity between D3 dolomite crystals and in the matrix also. Dashed lines indicate fracture walls. N, north. Cupido Formation, sample CulPa9-98, Cañón Las Palmas locality.

F5 Fracture Event

Fractures containing synkinematic C3 calcite are named F5 fractures. Fractures from the F5 event postdate F4 fractures, D2 replacement dolomite and D3 baroque dolomite. Fracture shape (morphology) generally is long and narrow. In other words, the aspect ratio of these fractures differs from older sets, which tend to be shorter and wider. Fractures of F5 are arranged in swarms with common en echelon geometry (Fig. 5.8a).

Since there are many examples of C3-filled veins having different orientations that cross cut each other, it is possible that multiple events of petrographically indistinguishable C3 calcite precipitation occurred. This interpretation is also consistent with one interpretation of the isotopic data (see Chapter 6). However, for this section I provide textural evidence that C3 calcite postdates both D2 replacement dolomite and D3 baroque dolomite. Evidence that C3 calcite replaced D2 and D3 dolomite fracture fill was found in several veins (Figs. 5.8b and 5.8c). One line of evidence is the incomplete and irregular baroque dolomite crystal borders that are overlapped by calcite, but also I found some corroded dolomite crystals, producing dedolomitization texture (see Chapter 5). In addition, some D3 dolomite crystals are broken and cut by F5 microfractures (Figs. 5.8b and 5.8c). Because I found no petrographic differences between calcite in F5 microfractures and C3 calcite elsewhere, these relations are most simply interpreted to mean that dolomite crystals were broken and later filled by C3 calcite.

Fractures from the F5 event share characteristics of set Y measured in the field (Fig. 5.8a). Some tectonic stylolites nucleated along F5 fracture walls suggesting that the F5 event predates tectonic stylolites. However, petrographic evidences and a few crosscutting relationships suggest that F5 fractures and tectonic stylolites could be synchronous events (Fig. 5.8d). Therefore F5 fractures were originated under deep burial

conditions due to vertical loading and probably incipient tectonics. Fractures with large aperture in set Y are preferentially affected by tectonic stylolites. These fractures are developed in the most dolomitized beds at Cañón de la Escalera, Cañón de los Chorros, Cañón Boquilla Corral de Palmas and Cañón Santa Rosa-Iturbide.



Fig. 5.8a. En echelon F5 fractures in a dolostone bed. Arrows indicate relative movement and the sense of slip that would have ensued if a fault had eventually formed. Cupido Formation, La Escalera locality. Outcrop photograph.

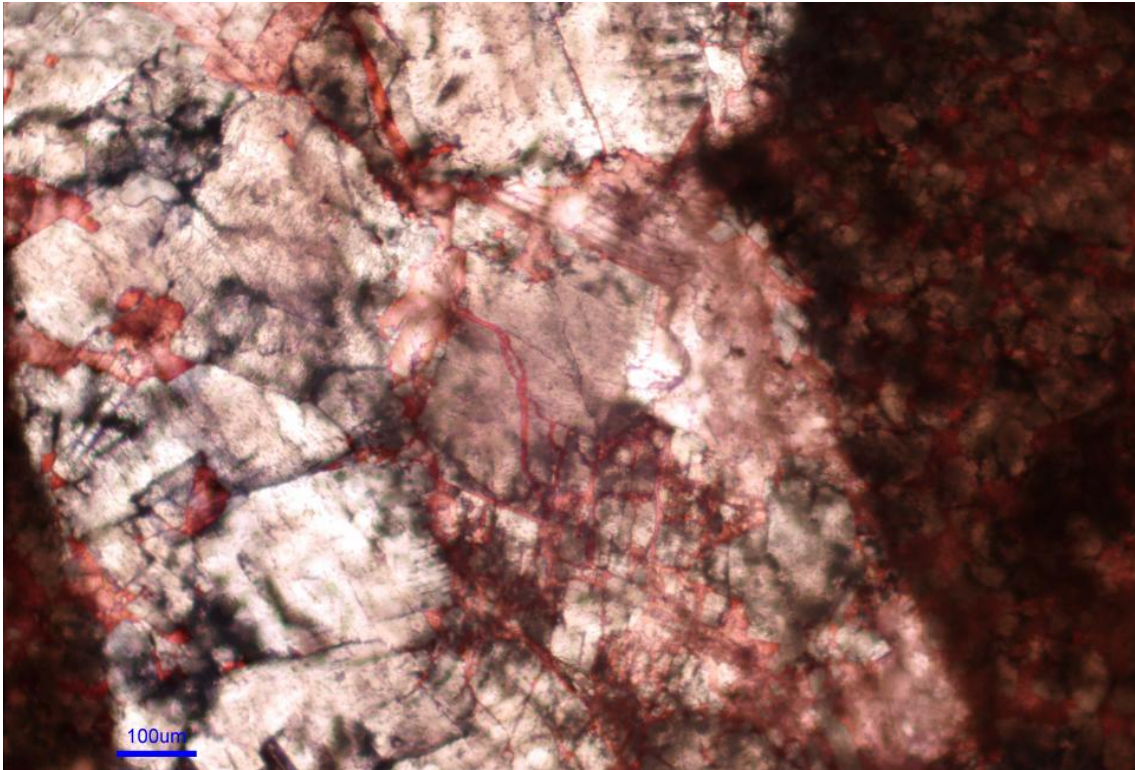


Fig. 5.8b. F4 macrofracture filled with D3 baroque dolomite and C3 calcite. Notice D3 dolomite crystals are incomplete and have borders that are irregular. Some dolomite crystals are broken and cut by microfractures filled with C3 calcite (see Fig. 5.8c). Thin section stained to differentiate dolomite (brown, grey or white) from calcite (red). Cupido Formation, sample CulCh8-98, Cañón de los Chorros locality. Photomicrograph.

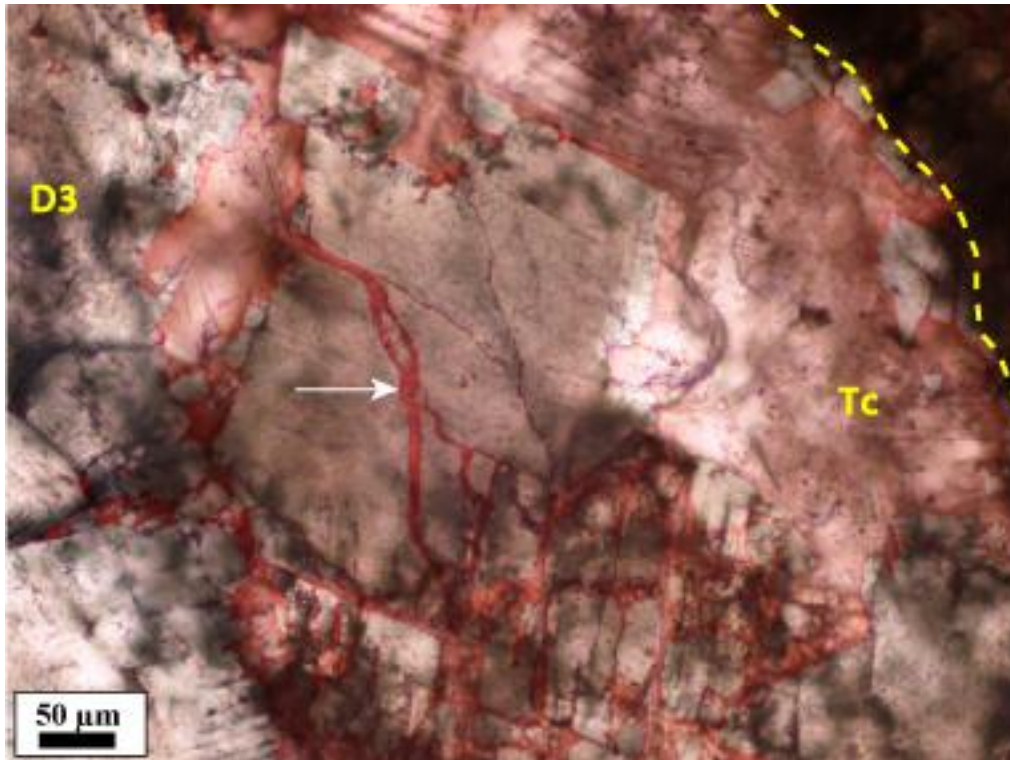


Fig. 5.8c. Detail of Fig. 5.8b showing broken D3 baroque dolomite crystals. Microfractures (indicated by arrow) are filled with calcite. These microfractures are named F5 and cross-cut dolomite crystals. Because there are no differences between calcite in microfractures and C3 calcite elsewhere, dolomite crystals probably were broken prior to C3 and later filled by C3 calcite. Incomplete and irregular D3 dolomite crystal borders and overlaps of calcite over dolomite indicate that calcite partially replaced D3. Thin section stained to differentiate dolomite (brown, grey or white) from calcite (red). Cupido Formation, sample CulCh8-98, Cañón de los Chorros locality. Photomicrograph.

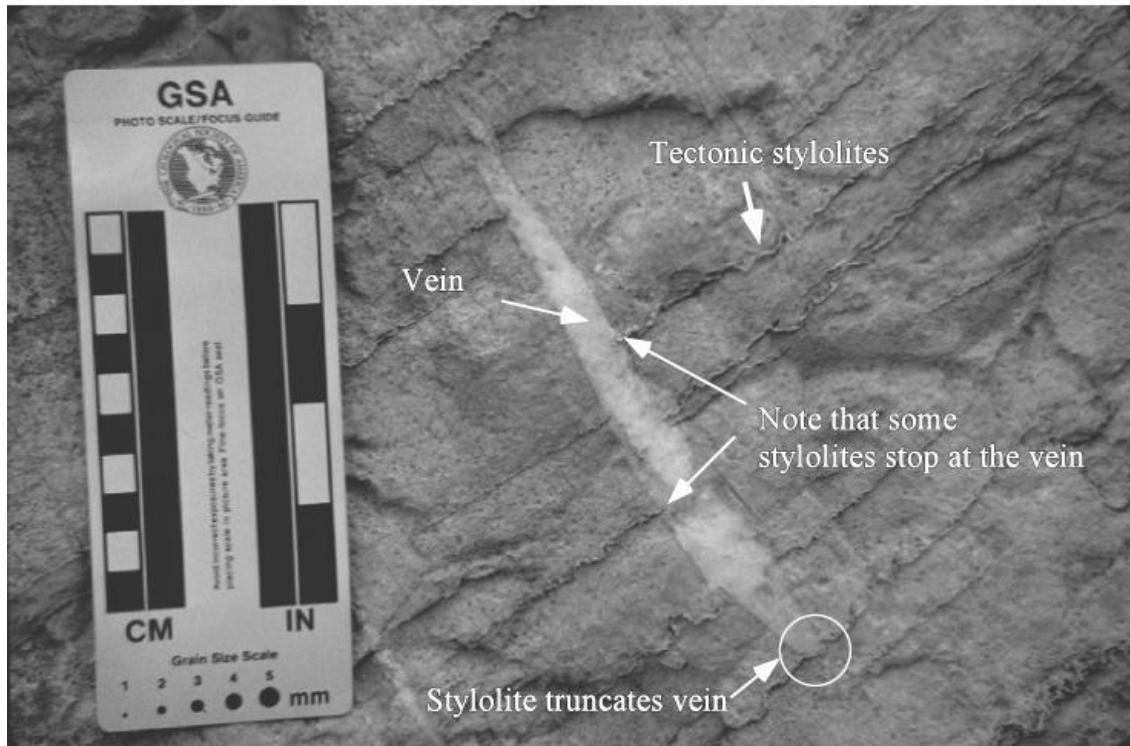


Fig. 5.8d. View of the base of a carbonate mudstone bed showing relationship between F5 fracture (vein) and tectonic stylolites in Tamaulipas Inferior Formation. Mutually cross-cutting relations between the vein and stylolites include stylolites that stop at the vein walls or a few millimeters inside the vein and do not have a continuation on the other side of the vein, and a stylolite that truncates one tip of the vein (circle). El Mural, Santa Rosa Canyon, near Iturbide (from Ortega, 2002).

F6 Fracture Event

F6 fractures are mainly flexural slip faults developed along stratigraphic limits or at the boundaries of mechanical layers (Figs. 5.9a and 5.9b). Most flexural slip planes show thick fibrous calcite sheets (C3t) and in some cases a reddish zone marking a layer-parallel breccia between carbonate beds (Figs. 5.9b and 5.9c).

Common C3t calcite twins in flexural slip planes are thin and straight to slightly curved with undulose extinction (Fig. 5.9d). Twinning is a post-crystallization deformation mechanism, and does not have any direct relationship with the genesis of the cement. Nevertheless, twinned calcite cement is found on fault breccia planes that have fibrous mineral lineations (Fig. 5.9b). These have configurations and slip sense that is consistent with an origin through flexural slip during Laramide-age folding of the Cupido Formation.

Many authors have concluded that the thickness and shape of calcite twins are mainly governed by the temperature of deformation (e.g., Ferrill, 1991; Burkhard, 1993). Thick twins develop at elevated temperatures and thin twins develop at temperatures below 200°C. Camerlo (1998) analyzed calcite twinning in samples collected in the San Blas (Cañón Boquilla Corral de Palmas) and San Juan Bautista anticlines in the SMO. Common calcite twins in these anticlines were classified by Camerlo (1998) as type I and type II, and were interpreted as having formed at low temperature (<200°C) according to Burkhard's 1993 classification. However, significant numbers of twins greater than 1 μm thickness were also identified and were interpreted to have developed within the type II temperature regime of 150 to 300°C. The majority of calcite twins were interpreted to have developed around 200°C. Although hardly conclusive, these observations are suggestive that some twins formed during or after folding.

F6 fractures share characteristics of set Z measured in the field, are the youngest fractures, and probably are associated with formation of folds. Flexural slip faults were identified at Cañón las Cortinas, Cañón Boquilla Corral de Palmas, Cañón de la Escalera and Cienegas.



Fig. 5.9a. Chevron fold showing flexural slip planes (Flx) containing twinned C3t calcite cement. Notice some of these flexural slip planes are thicker than 15 cm. These flexural slip faults belong to set Z. Set Z is interpreted as tectonic-related fractures, based on their orientation and the kinematic indicators of movement and because they are parallel to bedding and to the fold axis, suggesting fold axis-perpendicular contraction (Ortega, 2002). Hammer is ~30 cm long. Tamaulipas Inferior Formation, Cienegas locality. Outcrop photograph.



Fig. 5.9b. Outcrop of bedding-parallel fault (F6 fractures). Bedding is approximately horizontal. The sheet of white fibrous calcite (Fig. 5.9c) and reddish breccia mark a layer-parallel breccia between two carbonate beds. Square indicates Fig. 5.9c; hammer is 30 centimeters long. Cupido Formation, Cañón de las Cortinas locality.



Fig. 5.9c. Detail of Fig. 5.9b showing a thick fibrous calcite sheet. Because this sheet marks the contact between two carbonate layers and the calcite contains slickenside lineations, this is interpreted to have formed by flexural slip during Laramide-age folding of the Cupido Formation. Arrow indicates slip direction of hanging wall (eroded away) relative to footwall.

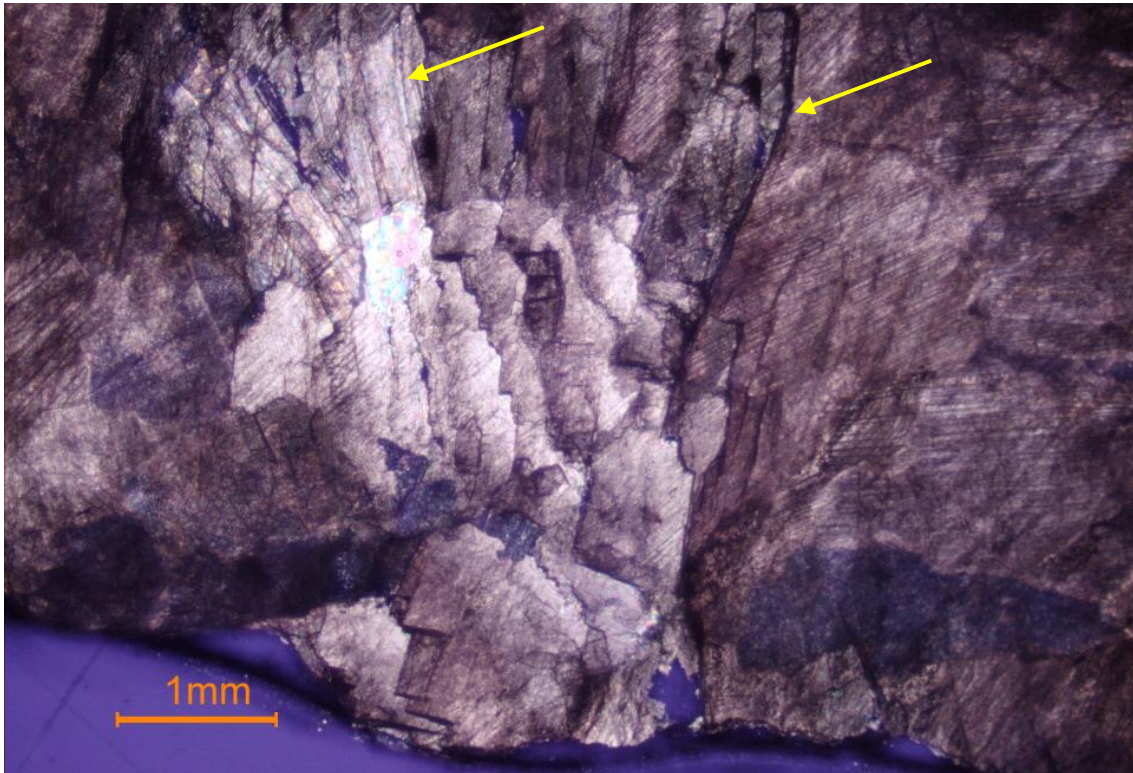


Fig. 5.9d. Fibrous calcite from sample of Fig. 5.9c showing twins with sharp edges in large crystals. Notice twins are thin and straight to slightly curved (indicated by arrows) with undulose extinction (Type I according to Burkhard's 1993 classification). Cupido Formation, Cañón de las Cortinas locality. Photomicrograph.

Travertine-filled Fractures and Joints

Among the last formed structures are travertine-filled and caliche-filled fractures, and barren joints. Although commonly non-systematic, opening-mode fractures that lack cement deposits, or joints, locally have regular orientation patterns (systematic joints). The spatial arrangement of many of these fractures adjacent to and aligned with modern escarpments suggests they are a gravitational response at least in part to modern

topography. Because they crosscut calcite (except for caliche deposits) and dolomite, they are late structures in the diagenetic history of the Cupido Formation.

DIAGENETIC PROCESSES AND EVIDENCE TO DETERMINE RELATIVE TIMING

Table 5.1 lists the evidence from field and petrographic observations that support interpretation of relative chronology of diagenetic and fracturing events. This table is similar to Table 4.2 from Chapter 4, the difference being that in this case the main fracture events described above are included.

Process	Field Observations	Petrographic Observations	Evidence of older or synchronous features	Evidence of younger features	Localities
Micritization		Micrite in form of envelopes on carbonate grains (Fig. 4.6). Bioclasts completely altered. Original skeletal nature of grains difficult to determine (Fig. 4.2a).	Allochem and mud deposited.	Calcite overlapping and filling space among micritized ooids implies micritization predates calcite cementation. Replacement dolomite overlaps micrite, so postdates it (Fig. 4.4a).	Los Chorros Las Palmas
Dolomitization (D1) (fine grained & laminated)	Laminations of dolomite and evaporites. Dolomite fragments are components in solution breccias. (Fig. 4.3c).	Laminations of different size dolomite crystals (Fig. 4.3a). D1 dolomite is composed of fine-grain (< 50 μ m) crystals and form millimeter-scale fine laminations. Different crystal sizes distinguish the laminations. Dolomite in solution breccias fragments are similar in crystal size, texture and color to laminated dolomite.	Laminations of dolostones and evaporites imply simultaneous deposition (Fig. 4.3a).	D1 dolomite fragments in solution breccias imply D1 predates brecciation (Fig. 4.3c). Probable desiccation fractures cut D1 laminations (Fig. 4.3a). Both calcite veins and bedding-parallel stylolites cut D1 dolomite laminations (Figs. 4.3a, 4.3b).	Cienegas, Cañón Prieto, Potrero García, La Escalera, Los Chorros Las Palmas.
Calcite cementation (C1)		Thin isopachous fringe or fibrous crystals around ooids and peloids (Figs. 3.6b, 4.2a).	C1 calcite around micritized ooids (Fig. 4.2a) implies C1 postdates micritization.	Calcite veins cross-cut C1 (Fig. 3.6b, 4.2a).	Los Chorros Las Palmas
Dissolution		Ooids cores dissolved and oomoldic porosity. (Figs. 3.6b, 4.2a).	C1 around micritized ooids partially dissolved implies dissolution postdates C1 (Figs. 3.6b, 4.2a).	Oomoldic porosity (Fig. 3.6b) filled by C2 calcite implies dissolution predates C2.	Los Chorros Las Palmas

Table 5.1. Diagenetic processes and evidence used to determine relative timing including fracturing.

Process	Field Observations	Petrographic Observations	Evidence of older or synchronous features	Evidence of younger features	Localities
Evaporite solution/breccias	Two types of evaporite solution breccias at different stratigraphic levels were recognized: monomict and polymict clast-supported. Monomict breccias are stratiformal and interstratal with sharp lower contacts and irregular upper contacts, and show rectangular shape blocks of dolostones (Figs. 3.9a, 3.9b, 3.10, 3.11a). Polymict clast-supported solution breccias are constituted by algal mat, calcitized anhydrite, limestone and dolostone fragments and have sharp lower contact. Clasts are angular and vary from a few mm to more than 10 cm long (Fig. 3.11a and 3.11b). Algal mat layers present at the bottom of solution breccias (Fig. 3.11a).	Breccias cemented by blocky calcite (Figs. 3.10, 4.2b). Breccia cemented by two types of calcite: non-isopachous equant calcite spar, as first generation cement around dolostone clasts, and by poikilotropic twinned calcite spar (Fig. 4.2b).	D1 dolostone clasts in breccias imply brecciation postdates D1 dolomite (Figs. 4.2b, 5.5b). In monomict breccias some calcite veins affect only the fragments, implying veins were already present at the time of brecciation (Figs. 3.10, 4.2b). Breccias are cemented with calcite that also fills veins, so these veins probably were formed during the time of brecciation (Fig. 3.10, 5.5b).	Compaction truncates both fracture types, pre-brecciation and synbrecciation, so compaction postdates brecciation (Fig. 5.5b).	Las Palmas, La Escalera, Potrero García, Las Cortinas, Los Chorros
Fracturing (F1) pre- and synbrecciation, also present in boudin necks.	Fractures are present in solution breccias: thin (<0.05 mm width) calcite filled veins are only present in the clasts. Wide calcite veins cross cut the first ones and fragments (Fig. 5.5a). Wide fractures with calcite and dolomite cement present in boudin necks.	Calcite filled veins only present in clasts. Calcite in wide veins has petrographic characteristics similar to the breccia cement (Fig. 5.5b). Fracture cement in boudinage is constituted by blocky calcite and fine grained dolomite with petrographic characteristics similar to D1 dolomite (Figs. 5.5a).	Calcite filled veins only present in clasts indicates it predates brecciation (Figs. 5.5a, 5.5b). Calcite, in wide veins, with petrographic characteristics similar to the breccia cement indicates these two events were synchronous (Figs. 5.5a, 5.5b).	Compaction features truncate both fracture sets, implying that it postdates both events (Fig. 5.5b). Bedding parallel stylolites cross cut fractures in boudinage, so postdate fracturing.	Las Palmas, La Escalera
Calcite cementation (C2)		C2 calcite is equant spar drusy mosaic and clear anhedral calcite that fills oomoldic porosity and pore-space between grains (Figs. 3.6b and 4.2a). C2 includes also non-isopachous equant calcite spar cement around clasts in solution breccias (Fig. 4.2b).	C2 calcite fills oomoldic porosity (Fig. 4.2a), so postdates dissolution. C2 calcite around D1 dolomite fragments implies C2 postdates D1 and also brecciation (Fig. 4.2 b).	Calcite filled veins and stylolites cross-cut C2 calcite (Figs. 3.6b, 4.2a).	Los Chorros Las Palmas

Continuation Table 5.1.

Process	Field Observations	Petrographic Observations	Evidence of older or synchronous features	Evidence of younger features	Localities
Compaction, bedding parallel stylolites	Stylolites are preferentially developed along stratigraphic planes or at the boundaries of mechanical layers (Figs. 4.7b, 5.3). Some stylolites present large teeth and are most common at dolostone/limestone contacts. Most of fractures form high angle with these stylolites (Fig 4.7b, 5.3).	Flattened and aligned anhydrite nodules (Fig. 4.3b). Pellets and bioclasts with tangential contacts and sutured contacts between grains (Fig. 4.7a).	Sutured contacts between pellets dissolved C1 calcite cement (Fig. 4.7a), so calcite cementation predates compaction. Sutured contacts between clasts in solution breccias truncates both fracture sets identified, so compaction postdates both fracturing and the brecciation (Fig. 5.5b)	Calcite veins (F2 or F5) crosscut bedding parallel stylolites, so compaction predates calcite veins.	Las Palmas, Potrero García, Las Cortinas, La Escalera, Los Chorros
Fracturing (F2) with synkinematic C2 calcite	Calcite fractures are present, vary from thin (<0.05 mm width) to less than 1mm width sometimes visible at outcrop scale.	Thin calcite veins crosscut laminations, rock matrix and grains (Figs. 4.3a, 4.3b, 4.7a, and 4.11a, 3.4c). F2 fractures are characterized by irregular or jagged path with calcite cement. Calcite fractures present remnant porosity partially filled by dolomite cement.	Thin calcite veins cross cut D1 dolomite (Fig. 4.3a, 4.3b), and both C1 and C2 calcite (Fig. 4.7a), so postdate all of these events.	D2 dolomite partially filled remnant porosity in F2 fractures shows dolomite postdates F2 (Fig. 5.5c).	Los Chorros
Fracturing (F3) with synkinematic dolomite (D2) and postsynkinematic calcite	Outcrops of carbonate sequence at Las Palmas, La Escalera and Los Chorros localities are formed by thin (< 8 cm) to medium (1.8 m) to medium bedded dolostones with at least four fracture sets (Fig. 5.6a).	Fractures with irregular or jagged path. Calcite is most prominent cement in fracture. Faceted dolomite crystals are locally present on fracture walls. Presence of bridges of rhombohedral dolomite crystals in macrofracture. Pillar-shaped dolomite bridges and pillars likely indicate synkinematic precipitation of dolomite because crystal morphology in bridges is suggestive of crack-seal processes. Calcite cement precipitated both in fracture and in matrix. Dolomite in fractures has similar petrographic characteristics than D2 dolomite (Fig. 5.6b).	Dolomite lines fracture walls and is overlapped by calcite, thus dolomite predates calcite in fractures (Fig. 4.3d).	Fractures with irregular or jagged path in pervasive D2 dolomite matrix indicate fractures occurred first. At least two fracture sets (from F4 and F5) cross cut F3 fractures (Fig. 5.7b).	Las Palmas, La Escalera

Continuation Table 5.1.

Process	Field Observations	Petrographic Observations	Evidence of older or synchronous features	Evidence of younger features	Localities
Pervasive dolomitization (D2)	Outcrops of carbonate sequence at Las Palmas and La Escalera localities are formed mainly by thin to medium bedded dolostones (Fig. 4.4b).	Plane-light photomicrographs show limestones partially replaced by idiopathic mosaic of anhedral dolomite rhombs (Fig. 4.4a) called here D2. D2 is characterized by fine to medium grain size (10-50 μm anhedral crystals that replaces both matrix and grains (Figs. 4.4a). Dolomite replaces from 5 to 100% of the rocks.	Because D2 dolomite replaces host rocks, processes like micritization, C1 and C2 calcite, predate D2 dolomitization (Figs. 3,5c, 4.4a). Dolomite bridges in F3 fracture have petrographic characteristics that are similar to D2 matrix dolomite, so both are contemporaneous. (Fig. 5.6b).	Fractures with both baroque dolomite (F4) and calcite cements cross cut D2 dolomite. (Fig. 5.7b).	Las Palmas, La Escalera
Fracturing (F4) synkinematic baroque dolomite (D3) & quartz; postkinematic calcite	Outcrops of carbonate sequence at Las Palmas, La Escalera and Los Chorros localities are formed by thin to medium bedded dolostones with fractures present fibrous dolomite crystals cement (Fig. 5.7a).	F4 fractures are characterized by baroque dolomite fill, calcite and a minor percent of quartz. Crack-seal textures in dolomite bridges in fractures indicate that baroque dolomite was deposited during fracture opening. Quartz crystals have aligned fluid inclusions parallel to fracture walls possibly indicating crack seal texture (Figs. 4.10d). Some inclusions were identified as small and irregularly shaped dolomite crystals (Figs. 4.10b). Calcite in fracture cross-cuts both quartz and dolomite (Figs. 5.7c).	F4 fractures in dolostones have straight paths that indicate they cut and postdate D2 dolomite (Figs. 5.7b, 5.7c). Calcite fills in spaced between quartz bridges and is therefore a later deposit, probably after fracture growth ceased. F4 fractures cross cut F3 fractures (Fig. 5.7b).	Calcite microfractures, cross-cut baroque dolomite in macrofractures (Fig. 5.8b, 5.8c). Tectonic stylolites cross-cut F4 (Fig. 4.10a, 5.7d) indicating stylolites post-date F4 fractures.	Las Palmas, La Escalera, Los Chorros
Baroque dolomite (D3)	Outcrops of carbonate sequence at Las Palmas, La Escalera and Los Chorros localities are formed by thin to medium bedded dolostones with fractures present fibrous dolomite crystals cement.	Baroque dolomite is characterized by undulatory extinction and sub- to euhedral fibrous/elongated coarse crystals (> 25 μm) (Fig. 4.5a, 5.7b). Dolomite crystals are elongate at high angle to fracture walls (Fig. 5.7b). Calcite in fracture cross-cuts both quartz and dolomite.	Fractures with baroque dolomite have straight paths that cut and postdate D2 dolomite (Figs. 5.7b, 5.7c).	Incomplete and irregular baroque dolomite crystal borders are overlapped by calcite (Fig. 5.7b, 5.7c, 5.7d), thus dolomite predates calcite in fractures.	Las Palmas, La Escalera, Los Chorros

Continuation Table 5.1.

Process	Field Observations	Petrographic Observations	Evidence of older features	Evidence of younger features	Localities
Dolomitization (Ferroan dolomite)		Fe-dolomite found in open marine facies is characterized by isolated euhedral crystals with external iron rich zone (Fig. 4.5b).	No evidence	No evidence	Las Palmas, La Escalera, Los Chorros Santa Rosa
Fracturing (F5) synkinematic calcite (C3) microfractures	En echelon F5 fractures are visible in a dolostone beds (fig. 5.8a).	Several fault breccias are cemented by baroque dolomite and calcite. F5 are calcite filled microfractures cross cut baroque dolomite crystals present in both fault breccias and F4 fractures (Figs. 5.8b, 5.8c). Calcite in microfractures is petrographically identical to the calcite cement in fault breccias.	Calcite filled microfractures cross cut D3 baroque dolomite crystals, so microfractures postdate D3 (Figs. 5.8b, 5.8c).	Calcite filled fractures are cross cut by bedding oblique stylolites, so predate stylolitization.	Las Palmas, La Escalera, Los Chorros Santa Rosa
Calcite cementation (C3)	Calcite fills fracture porosity and is also present as cement and filling microfractures in some fault breccias.	C3 includes all calcite cement that postdates both D2 and D3 dolomite and is characterized by blocky cement that partially replaces dolomite cements in fractures and fills remnant porosity (Fig. 4.2c, 5.7b, 5.7c, 5.7d, 5.7e). C3 is also present as cement and filling microfractures in some fault breccias (Fig. 4.7a). C3 is distinguished from C1 because the last one is restricted to around ooids as thin isopachous fringe of fibrous crystals, and from C2 because C3 is mainly present as fracture fill.	D2 and D3 dolomite bridges in fractures are partially overlapped by calcite, indicating calcite is partially replacing both D2 and D3 dolomite (Figs. 5.7b, 5.7c, 5.7e).	Karst dissolution affects C3 calcite.	Los Chorros, Las Palmas
Recrystallization		Aggrading calcite crystals in the matrix, fossils, and ooids. Uniform crystal size in allochems and matrix (Fig. 4.8). Where recrystallization is present, it affects from 5 to 100% of the rock.	Uniform crystal size in allochems and matrix (Fig. 4.8) is indicative of recrystallization, so processes like micritization, bioturbation, calcite cementation (C1, C2), and dolomitization predate recrystallization.	Bedding oblique stylolites cut recrystallized rock so, recrystallization predates pressure solution.	Las Palmas, La Escalera, Santa Rosa

Continuation Table 5.1.

Dedolomitization		Dedolomitization is shown by "corroded" and incomplete dolomite crystals, partly replaced by calcite (Fig. 4.9). Some calcite rhombs might have been dolomite crystals now completely replaced by calcite during dedolomitization.	D2 pervasive dolomite crystals are "corroded" and incomplete imply that D2 dolomite predates dedolomitization (4.9).	No evidence	Santa Rosa, Los Chorros, La Escalera, Las Palmas
Pressure-solution (bedding oblique stylolitization)	Outcrops at La Escalera and Corral de Palmas show inclined or high angle stylolites with respect to bedding (Fig. 4.7d). Most fractures form low angle with stylolites.	Stylolites partially dissolved matrix and grains in both dolostones and limestones (Fig. 4.8). Bedding oblique stylolites present quartz cement along their paths, and they dissolved partially F4 fractures (Fig. 5.7d).	Stylolites cross cut F4 fractures (synkinematic baroque dolomite cement), so postdate F4 fracturing and baroque dolomite cementation. Quartz cementation in stylolites, implies that both are synchronous (Fig. 5.7d).	Calcite cement replaced quartz cement in stylolites, so postdates pressure solution (Fig. 5.7d).	Las Palmas, La Escalera,
Silica cementation (quartz)	Outcrops of carbonate sequence at Las Palmas, La Escalera and Los Chorros localities are formed by thin to medium bedded dolostones with fractures that contain quartz and fibrous dolomite cements. At Santa Rosa and Los Chorros localities chert nodules and silica bands are common (Fig. 3.3b).	Quartz is present in three forms: authigenic along bedding oblique stylolites, in F4 fracture cement, and as chert nodules in basinal facies rocks (Fig. 3.3b). Quartz in F4 fractures has aligned fluid inclusions possibly indicating crack seal texture (Figs. 4.10d). Inclusions are also aligned in trends approximately perpendicular to macrofracture orientation (Figs. 4.10d). Quartz crystals typically contain numerous carbonate inclusions that probably were dolomite crystals originally (Figs. 4.10c).	Quartz cementation in stylolites (Fig. 4.10a) implies that both events are synchronous. Dolomite inclusions in quartz imply simultaneous precipitation of both minerals (Fig. 4.10b).	Quartz crystals are overlapped by C3 calcite crystals thus quartz predates C3 (Fig. 4.10c).	Santa Rosa, Los Chorros, La Escalera, Las Cortinas, Las Palmas
Flexural slip faulting (F6) (twinned calcite cement, (C3t))	Flexural slip planes are developed along stratigraphic limits or at the boundaries of mechanical layers. Most flexural slip planes show thick fibrous calcite sheets and in some cases a reddish zone marking a layer-parallel breccia between carbonate beds (Figs. 5.9a, 5.9b).	Flexural slip planes contain fibrous calcite cement. This calcite is characterized by thick twins with sharp edges in large crystals (Fig. 5.9c). C3t twinned calcite is also found in fault breccia planes, and occasionally as cement in some fractures.	Flexural slip planes affected most of the identified diagenetic processes in the Cupido Fm., so most are pre-flexural.	Karst dissolution affects flexural slip faults and C3t calcite.	Los Chorros, Las Palmas, Las Cortinas

Continuation Table 5.1.

<p>Dissolution (karst) and precipitation of calcite and travertine</p> <p>(C4)</p>	<p>Calcite fills fracture porosity and is also present as cement and filling microfractures in some fault breccias.</p> <p>Caves are present in several places at the Monterrey Salient (e.g., Potrero García), (Fig. 4.11).</p>	<p>Dissolution affects the whole rock (Fig. 4.11).</p> <p>Calcite precipitation due to subaerial exposure and dissolution of the carbonate sequence in the SMO is called C4 and is postkinematic cement in some of the fracture sets identified in this study, filling remaining porosity. I found no petrographic diagnostics to distinguish C3 from C4. However, isotopic analysis (see Chapter 6) shows that these two phases of calcite cement represent different events.</p> <p>For that in this Chapter I named as C3 (excluding C3t) cement all calcite that postdate D3 baroque dolomite</p>	<p>Presence of caves in the Monterrey Salient (e.g. Potrero García, La Huasteca), demonstrates dissolution and precipitation is currently acting in rocks of the SMO (Fig. 4.11). Caves are located in high areas in the SMO, so postdate structural deformation. Joints and travertine are present in the SMO.</p>	<p>No evidences.</p>	<p>All localities</p>
---	--	---	---	----------------------	-----------------------

Continuation Table 5.1.

PARAGENETIC SEQUENCE BY LOCALITIES

Chapter 4 focused on the analysis of common diagenetic processes (cementation, dissolution, etc.), while the previous section of this Chapter was focused on the analysis of the main fracture events and their timing relative to calcite and dolomite cementation. The next section unifies the relative chronology (paragenetic sequence) of diagenetic processes in all studied localities, including timing of fracturing.

Cañón Santa Rosa-Iturbide

Table 5.2a shows the main diagenetic processes identified at Santa Rosa-Iturbide. The rocks are mainly deep water carbonate mudstones. Eleven rock samples and twenty thin sections (Appendix 3.2, Chapter 3) were studied from this locality. Nine diagenetic processes were identified in the field and in thin sections. The sequence is at most weakly dolomitized (< 15%). Dolomite is present as sparse isolated euhedral microcrystals in the matrix. This dolomite is petrographically similar to D2 dolomite identified in the other localities. Crosscutting relationships between dolomite cement and fractures indicate that here four fracture events exist. Two events are characterized by synkinematic C1 and C2 calcite cement fill (F1 and F2 fractures) that predates dolomitization, and two more events, with C3 calcite cement fill that postdates dolomitization (F5 and F6 fractures). Tectonic stylolites cut most of the fractures. Quartz was identified in chert nodules and along bed-perpendicular stylolite traces. Recrystallization was one of the last diagenetic processes that affected the whole rock. In some cases 90% of the rock is recrystallized (Table 5.2a). The analysis of these rocks shows some ambiguities in the relationships

between diagenetic events and fracture development. Finally, due to negligible variation in facies at this locality, it is impossible to recognize any facies-specific variations here.

GENERAL PARAGENESIS FROM SANTA-ROSA LOCALITY													
Sample	Lithology	← Earliest PROCESSES Latest →											
		CuStR1-98	mudstone		F2 cal	F2 cal	C2	D2 10%	Fe-D 2%		Styl-?	Rx 85%	
CuStR2-98	mudstone					D2 8%	F5 cal	F5 cal	C3	Rx 82%			
CuStR3-98	mudstone		F2 cal	F2 cal			Sty						
CuStR4-98	mudstone		F2 cal	F2 cal	C2	D2 5%	Sty			Rx 2%		qrzt 1%	
CuStR5-98	mudstone	Sty		F2 cal	C2	D2 10-15%	Fe-D 2%		Dd	F6 cal	C3t	qrzt 1%	
CuStR6-98	Mudstone-Wackestone					D2 1%	F5 cal		C3				
CuStR7-98	mudstone					D2 5%	F5 cal	C3	Sty ?	F6 cal	C3t	Sty ?	
CuStR8-98	mudstone												
CuStR9-98	mudstone		F2 cal	F2 cal	C2	D2 10-15%	F5 cal	F5 cal	C3	Styl-?		qrzt <1%	
CuStR10-98	mudstone						F5 cal	C3	Sty	F6 cal	C3t		
CuStR11-98	Mudstone		F2 cal	F2 cal	C2	D2 <10%	Fe-D 2%		Sty ?	Rx 90%		qrzt 1%	
LEGEND													
		Sty	Bedding parallel stylolites				Sty	Bedding inclined stylolites					
		F cal	Calcite filled vein				Rx	Recrystallization					
		C	Calcite cementation				Dd	Dedolomitization					
		D2	Pervasive dolomitization				Qz	Quartz cementation					
		D3 (FeD)	Ferroan dolomite										
Note: Numbers indicate percentage based on petrographic estimation													

Table 5.2a. Diagenetic and fracturing processes identified at Cañón Santa Rosa-Iturbide locality. Nine main diagenetic processes were identified that can be arranged into at least 13 diagenetic events. Notice that these rocks are only slightly dolomitized (dolomite lower than 15%). Two events of F2 cal (fractures with synkinematic calcite cement) developed before dolomitization and two sets (F5 and F6) after dolomitization.

Cañón de los Chorros

Table 5.2b shows the main diagenetic processes identified at the Cañón de los Chorros. Eight rock samples and sixteen thin sections (Appendix 3.2, Chapter 3) were studied from this locality. Nine diagenetic processes were identified: Bedding-parallel stylolites are common in these shallow water carbonates (wackestone, packstone,

grainstones and boundstones). More than half of the rocks are partially dolomitized (5 to 90% dolomitized). Where dolomite is present it is mainly as euhedral macrocrystals replacing the matrix.

In slightly to undolomitized rocks three fracture events (F2, F5 and F6) are present with synkinematic calcite fill. The relationship between replacement dolomite and these events of fractures is similar to those found in the Santa Rosa locality. F4 fracture event is characterized by fractures with synkinematic D3 baroque dolomite fill cement that postdates D2 dolomitization. F5 fractures filled with C3 calcite crosscut D3 dolomite crystals. Dedolomitization was identified in less than 20% of samples. Both bedding parallel and high angle stylolites are present. Analysis of these rocks shows a clear relationship between D2 dolomitization and fracture development. Rocks with more than 80% dolomite (dolostones) developed at least one more fracture event (D3 dolomite-calcite filled fractures, Table 5.2b) than other rocks, and the fractures from that event are in part contemporaneous with D3 dolomite precipitation.

C2 synkinematic calcite fill that predates D2 dolomitization. F5 calcite fractures postdate D2.

Dolostone rocks (with more than 90% dolomite) developed two fracture events that postdate or are synchronous with D2 dolomite: F3 fractures with synkinematic D2 dolomite, and F4 fractures with synkinematic D3 baroque dolomite. Fractures from both events have C3 calcite postkinematic cement. Tectonic stylolites have quartz cement along their traces and crosscut all fractures. Dedolomitization is more abundant in this locality than elsewhere.

Analysis of these rocks shows a relationship between D2 dolomitization and the number of fracture events developed and fracture mineralogy. Rocks with more than 95% dolomite developed four events of dolomite-calcite filled fractures (Table 5.2c).

D2 dolomite is present mainly as euhedral macrocrystals replacing the matrix and is also the most abundant cement. Crosscutting relationships between D2 dolomite and fractures, in partially (10-15%) dolomitized rocks, indicate that two fracture events (F2 fractures) exist characterized by synkinematic C2 calcite fill cement that predates D2 dolomite, and one fracture event (F5) that postdates D2.

Dolostone and partially (> 15%) dolomitized rocks are characterized by two or more fracture events. D2 dolomite is the most abundant cement in these rocks. F3 fractures are characterized by irregular or jagged traces and dolomite fill petrographically similar to D2 dolomite. These fractures also contain postkinematic C3 calcite cement. F4 fractures are characterized by straight paths and synkinematic D3 baroque dolomite cement. Recrystallization affected the whole rock, in some cases reaching 100%. Quartz was identified in chert nodules and along bed-perpendicular stylolites traces (Table 5.2d).

GENERAL PARAGENESIS FROM LA ESCALERA LOCALITY											
Sample	Lithology	← Earliest PROCESSES Latest →									
		CuEsc1-98	Dolostone (breccia)		D2 100%	F3 (D2,C3)			F5 cal	SiO ₂ 1%	C3t
CuEsc2-98	Dolostone		F1 cal	F2 cal	D2 75-80%	F3 dc (D3,30%)		Qz 3%	C3t	Dd 30%	
CuEsc3-98	Mudstone-packstone	Dfg	Ev	F2 cal	D2 40-70%	F3 (D2,C3)	Dissolution?	Rx 40%			
CuEsc4-98	Dolostone		Dis	F2 cal	D2 95-100%	F3 (D2,C3)	F5 cal		Qz 3%	Sty	F6
CuEsc5A-98	Packstone			F2 cal	F2 cal	D2 <10-15%					
CuEsc5C-98	Mudstone-wackestone			F2 cal	F2 cal	D2 <10-15%		Rx 85-90%			
CuEsc6A-98	Packstone		Sty	F2 cal		D2 60%	F5 cal		Sty	Rx 100%	
CuEsc6B-98	Grainstone		C1	F2 cal	F2 cal	D2 90-95%	F5 (C3,D4)		Sty	F6	
CuEsc6C-98	Packstone					D2 40-45%			Rx 100%		
CuEsc7-98	Dolostone				F3dc (d,qz)	D2 100%	F5 cal				
CuEsc8-98	Dolostone					D2 100%					
CuEsc9-98	Dolostone		F2 cal			D2 90%	F5 cal		Rx 90%	Qz 3%	
CuEsc10-98	Grainstone		F2 cal			D2 10%			Rx 90%		
CuEsc-Yeso	Gypsum Nodule		F2 cal								
LEGEND											
	C	Calcite cementation		Fdcqz	Dolomite-calcite-quartz filled vein						
	Dfg	Fine grain laminated dolomite		FeD	Ferroan dolomite						
	Dis	Dissolution		Sty	Bedding inclined stylolites						
	Ev	Evaporites dissolution		Rx	Recrystallization						
	Fb	Fracturing synbrecciation		Dd	Dedolomitization						
	Sty	Bedding parallel stylolites		Qz	Quartz cementation						
	F cal	Calcite filled vein			Flexural slip, faults						
	D2	Pervasive dolomitization			Karst dissolution						
Note: Numbers indicate percentage based on petrographic estimation											

Table 5.2d. Diagenetic and fracturing processes identified at La Escalera locality. Sixteen diagenetic processes in these rocks were identified. Notice that rocks with less than 25% dolomite present two sets of fractures (F2 fractures) with synkinematic C2 calcite fill cement that predate D2 dolomitization, and an event with fractures calcite fill cement (F5) that postdates D2. Dolostone (higher than 90% dolomite) rocks have two F2 fracture events and a F3 (fractures with synkinematic dolomite and postkinematic calcite cements) that is synchronous with D2.

REGIONAL PARAGENETIC SEQUENCE

The paragenetic and fracture sequences were established for each locality to ascertain if the main diagenetic processes, coupled with fracturing events, are present in all areas and to document their regional distribution. A consistent regional pattern indicates that regional, rather than local, geochemical and structural influences predominate.

Regionally pervasive processes are more likely to be applicable to dolostone sequences that have only experienced basin scale subsidence and only subtle regional deformation. In other words, such patterns would suggest that we can apply the experience from this outcrop example, at least paragenesis predating large upright folds, as an analog in subsurface oil and gas fields where no such folds exist. Regionally consistent structural and diagenetic patterns, rather than patterns that vary with structural position around folds or between different folds, is also predicted by the hypothesis of Marrett and Laubach (2001) that many if not most of the fractures in the study area predate orogenic folding. Comparison of patterns between localities therefore provides a test of this hypothesis.

Table 5.3 shows the regional diagenetic and fracturing processes identified in the Cupido Formation in the Monterrey Salient. Comparison of the four field areas shows a total of six fracture events associated with eighteen texturally separable diagenetic patterns. Table 5.3 shows that shallow marine facies (e.g. Las Palmas) were more affected by diagenesis in the sense that they have more complex patterns than basinal facies (e.g. Santa Rosa). Fractures are developed better (more sets; closer spacing) in dolostones than in slightly to moderately dolomitized rocks and limestones.

The implication of these patterns is that several regionally consistent fracture and cement precipitation events affected the Cupido Formation. Although not rigorously documented, the similarity of these patterns in disparate structural settings around the Monterrey Salient suggests that the causative loading and geochemical conditions operated on a regional scale rather than on the scale of a fold or a segment of a fold, or these processes/patterns are insensitive to structural (fold) position.

Table 5.4 summarizes diagenetic assemblages and processes and their paragenetic sequence (relative order of occurrence). This table also shows the different inferred diagenetic stages and the approximate timing of occurrence of each diagenetic event. The relative timing of fracturing events can be referenced to the pervasive dolomite (D2) replacing cement phase, because the similarity of D2 composition, texture and distribution suggests that this was, apparently, a regional event. In other words, by taking the D2 dolomite as a reference, the numerous local fracture events can be distinguished and correlated regionally. Two fracturing events (F1, F2) predate D2 dolomite, and three more (F4, F5 and F6) postdate D2. Evidence of dolomite in crack-seal texture shows that F3 development was synchronous with D2 dolomite, while F4 development was simultaneous with D3 baroque dolomite precipitation. All of these coupled structural-geochemical events influenced evolution of fracture porosity in the Cupido Formation.

Field and petrographic observations suggest that D1 dolomite is responsible for less than 10 % of whole-rock dolomite volume, whereas D2 makes up more than 85 % of dolomite. D3 makes up no more than 5% because it is mainly sparse fracture cement. Nevertheless, distinguishing D1 and D2 dolomite in the fine-grained rock mass is problematic. However, D1 is commonly found intercalated with algal mat laminations and mud limestones in peritidal facies. Owing to the fine grain size of much of the

dolomite host rock, this authigenic dolomite is generally obscure under transmitted light magnification (~100x), but it is apparent under scanning electron microscope CL imaging (200x and higher). D2 dolomite replacement phase percent decreases downward, away from the evaporites.

LOCALITY	PROCESSES																								
	Micritization	Dolomitization (D1) (fine grained & laminated)	Calcite Cementation (C1)	Dissolution	Calcite Cementation (C2)	Evaporites dissolution (breccias)	Fracturing (F1) pre- and synbrecciation	Compaction (bedding-parallel stylolites)	Fracturing (F2) synkinematic calcite	Fracturing (F3) (synkinematic D dolomite)	Dolomitization (D2) (pervasive dolomite)	Fracturing (F4) (synkinematic D3 dolomite)	Dolomitization (D3) (fracture an pervasive)	D4 ferroan Dolomitization (FeDo)	Fracturing (F5) (synkinematic calcite)	Calcite Cementation (C3)	Pressure-solution (bedding-inclined stylolitization)	Recrystallization	Dedolomitization	Pressure-solution (quartz, bedding-inclined stylolites)	Silica Cementation	Flexural slip faulting (F6) (twinned calcite cement)	Calcite Cementation (C3)	Dissolution (karst) and C4 calcite cementation	
Las Palmas																									
Los Chorros																									
Escalera																									
Santa Rosa																									
Fracture Event							F1	F2	F3	F4	F5	F6													
Fracture Set							W	X	Y	Z															
LEGEND		Micritization	Fine grain laminated dolomite	Calcite cementation	Dissolution	Evaporites dissolution	Fracturing synbrecciation	Bedding parallel stylolites	Calcite filled veins	Pervasive dolomitization	Dolomite-calcite-quartz filled veins	Baroque dolomite	Ferroan dolomite	Bedding inclined stylolites	Recrystallization	Dedolomitization	Quartz cementation	Flexural slip, faults	Karst dissolution						

Table 5.3. Regional diagenetic and fracturing processes identified in the Monterrey Salient, based on the four localities: Santa Rosa, Los Chorros, Corral de Palmas and La Escalera. Six fracture groupings (F1 to F6 events) associated with eighteen, texturally separable diagenetic patterns, were found in these rocks of Cupido and Tamaulipas Inferior Formations. Each process is indicated by a particular color and patterns. Fracture sets (W, X, Y and Z) are correlated with fracture events F3 to F6.

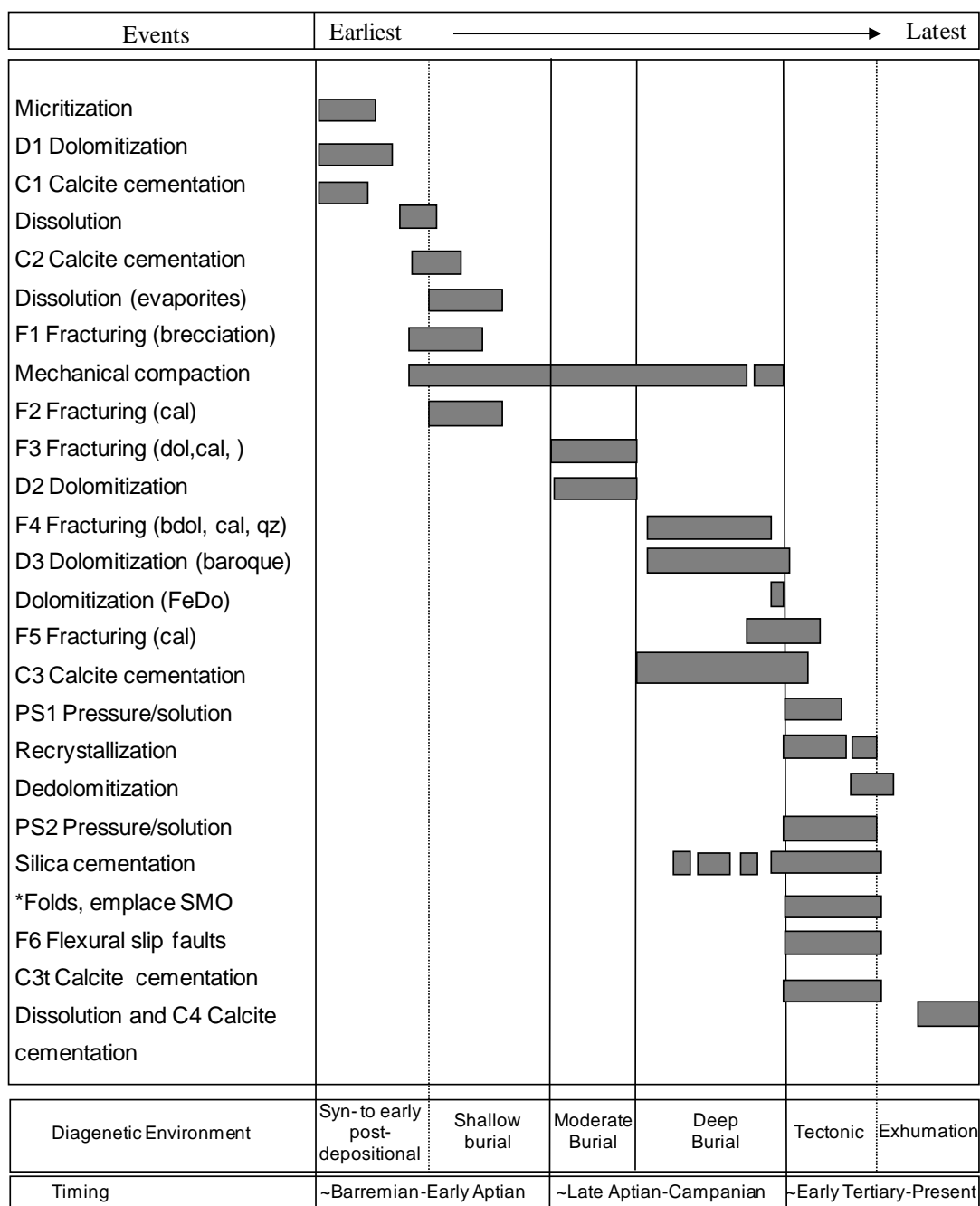


Table 5.4. Generalized paragenetic sequence, relative duration of diagenetic events and inferred diagenetic stages. Bars represent diagenetic processes, including fracture events and main cementation stages. Relative timing is from cement and fracture overlapping and crosscutting relations. Absolute start-stop times are conjectural.

FRACTURE-CEMENTATION COUPLED EVENTS

Fig. 5.10 synthesizes the relationships between the main fracturing events and the dolomite and calcite cementations in the Cupido Fm. Each fracture event was recognized by a combination of field observations and carefully petrographic observations. Timing of fracture events was determined by their synkinematic and postkinematic cements, and the cross cutting relationships between fractures. F1 and F2 fractures predate D2 and originated during C1 and C2 calcite precipitation, respectively. Two samples of D1 dolomite cement were found in F1 boudin necks. F3 is characterized by pillar-shaped D2 dolomite and bridges of rhombohedral dolomite crystals, indicating synkinematic precipitation of dolomite, so D2 dolomite is synchronous with F3 fractures. F3 fractures also contain postkinematic D3 dolomite and C3 calcite cement. F4 fractures are characterized by large fibrous baroque dolomite crystals (D3) that bridge the fractures. C3 calcite and a minor percent of quartz are present as postkinematic cements. D3 dolomite bridges in F4 fractures indicate that dolomite was deposited during fracture opening, so D3 and F4 are synchronous. F5 fractures contain synkinematic C3 calcite indicating that both events are synchronous. F5 fractures have both postkinematic C4 calcite and quartz cements. Finally, F6 fractures show thick fibrous synkinematic C3t calcite cement, and C4 postkinematic cement.

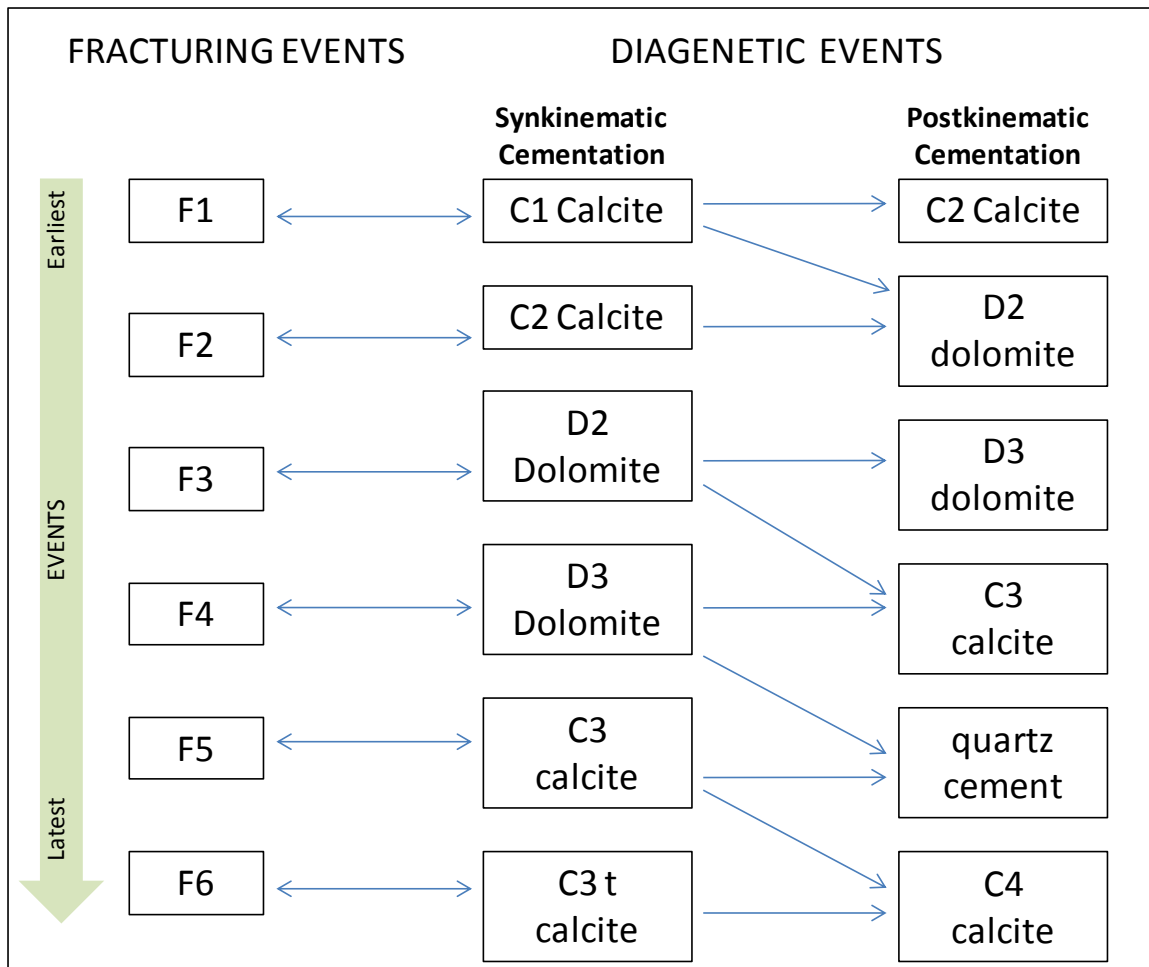


Fig. 5.10. Fracture events and their corresponding cements in the Cupido Formation. Presence of synkinematic cements in fractures indicates that these cements precipitated during opening of these fractures. For example F3 and F4 fractures originated simultaneously with D2 and D3 dolomite respectively. Postkinematic cements precipitate after fracture opening and after synkinematic cement. C3 and C4 calcite were the most important postkinematic cement in fractures, reducing their remnant porosity. Single-end arrows indicate correlation; double-end arrows indicate contemporaneous events.

OUTCROP SCALE FRACTURE CORRELATION TO MICROSCOPIC SCALE

This section presents the correlation between fractures at two different scales: regional fracture sets identified in outcrops, and those fractures related with each fracture event defined based on the structural-diagenetic petrographic study discussed in Chapter 4 and part of this Chapter.

Table 5.5 shows the correlation between fracture events determined from structural-diagenetic petrographic study and regional sets measured in the field at the four localities analyzed in the Monterrey Salient (Table 5.3). There is a good correlation between fracture sets W to Z with F3 to F6 fracture sets. W fracture set corresponds to F3 fracture event, X set to F4 event, Y set to F5, and Z set to F6 fracture event, respectively. The table also notes synkinematic and postkinematic cements for each fracture set. These are the key characteristics to correlate fractures across scales.

Fracture Events	Fracture Sets	Fracture set orientation in the field (strike current day)				Fracture cements identified petrographically		Where found	Timing	Comments
		Santa Rosa Iturbide	Los Chorros	Las Palmas	Escalera	Syn-kine matic	Post-kine matic			
F1		<i>Not measured</i>	<i>Not measured</i>	<i>Not measured</i>	<i>Not measured</i>	C1	C2/D1	breccia clasts and boudin necks breccias	predates brecciation syn-brecciation	Fractures not measured in the field because of inconsistent orientations
F2		<i>Not measured</i>	<i>Not measured</i>	<i>Not measured</i>	<i>Not measured</i>	C2	D2	partially and not dolomitized limestones	pre-D2 dolomitization	Fractures not measured in the field because of inconsistent orientations
F3	W	N-S	NE-SW	NE-SW	NE-SW	D2	C3, D3	dolomitized limestones and dolostones	syn-D2 dolomitization	Set W is oblique to bedding
F4	X	NW-SE	NE-SW	NE-SW	NE-SW	D3	C3, Qz, C4	dolostone and dolomitized limestones	syn-D3 dolomitization; post-D2 burial dolomitization	Set X is perpendicular to bedding
F5	Y	NW-SE	NE-SW	NE-SW	NE-SW	C3	Qz, C4	limestones and fault planes	post-D3 dolomitization; burial-tectonic	Set Y is slightly oblique with respect to bedding. Perpendicular to the fold axis.
F6	Z	NE-SW	NW-SE	<i>Not measured</i>	NW-SE	C3t	C4	flexural slip and fault planes	tectonic	Z forms high angle with tectonic stylolites

Table 5.5. Correlation between fracture events determined from the structural-diagenetic petrographic study and fracture sets measured in the field in four localities of the Monterrey Salient. Notice the good correlation of fractures at outcrop scale to microscopic scale. Regional pattern consists of four main outcrop scale fracture sets W, X, Y, and Z. W fracture set corresponds to F3 fracture event, X set to F4 event, Y set to F5, and Z set to F6 fracture event. F1 and F2 orientations are undefined because these categories of fracture have inconsistent orientations and lack preferred orientation. Sets W, X, Y, and Z were distinguished in the field by fracture crosscutting relations and crossing relationships between fractures and tectonic and burial stylolites. Fracture events were determined petrographically based on crosscutting relations among fractures and other diagenetic features. Cements were determined from petrographic analyses. D2, dolomite replacement cement; D3, baroque dolomite; C1 and C2, calcite cements pre-D2 dolomite; C3, C3t and C4, calcite cement post-D2 dolomite; qz, quartz cement.

IMPLICATIONS OF THE CEMENT PATTERNS

In summary, six fracture events can be delineated based on crosscutting relations. These fractures currently are mostly or entirely filled and thus constitute veins. The main mineral phase filling the fractures is calcite, but because calcite in early fractures is cut by later fractures, these otherwise nearly identical looking calcite deposits cannot all be the same age. Moreover, textural evidence in the form of dolomite bridges containing possible crack-seal textures and dolomite on fracture walls suggests that in each of at least the younger F3-F4 fractures, dolomite, but not calcite, precipitated while fractures were opening. Fracture space between dolomite crystals was later filled by postkinematic calcite. Two inferences follow from this. First, geochemical conditions must have changed from favoring dolomite to favoring calcite precipitation during and/or after fracture growth and the pattern of changing cement type was the same for each of these two F3-F4 fractures, possibly implying some sort of cyclic process. One possibility is that dolomitization drove fracturing. Second, because dolomite deposits in fractures fill a very limited volume (usually less than 10 percent) of the wider (> 0.5 mm) fractures, these fractures must have been substantially open during and probably for some time following progressive opening of fractures.

The presence of dolomite more completely filling narrow fractures and the narrow tips of wide fractures suggests size dependence to the infill of fractures by concurrent dolomite precipitation and thus an emergent threshold can be defined at about 0.1 mm for these fractures. By analogy with processes documented in sandstones (Laubach et al., 2004; Becker et al., 2010), such a size dependency likely primarily reflects temperature dependent dolomite accumulation rates rather than processes intrinsic to fracture opening (like crack seal) or fluid flow (Gale et al., 2010).

Fracture porosity (open fracture pore space) increases with the opening displacement of fractures and decreases with infill by cement. For fracture systems in the Cupido Formation that exhibit power-law fracture size distributions (Ortega et al., 2006), fracture volume and surface area are concentrated in the numerous smaller fractures (Marrett, 1996). Thus, dolomite was the most important cement for reducing overall fracture porosity even though this phase did not fully occlude the large fractures. Calcite, on the other hand, was responsible for ultimate filling of the large fractures. Together these phases have eliminated fracture porosity for F1-F6 fractures.

DISCUSSION: STRUCTURE AND DIAGENESIS

Petrographic structural-diagenetic study (PSDS) combined with systematic field observations allow understanding the diagenetic history of rocks such as the Lower Cretaceous limestones and dolostones of the Monterrey Salient. Petrographic and textural characteristics of Cupido Formation limestones contain the imprints of their initial marine genesis, as well as their shallow and burial diagenetic alterations in a hydrodynamic system. Solution breccias and associated fractures, calcite and dolomite cement, and fracturing events can be sequenced based on crosscutting relations. The fractures are key elements in understanding the origin and evolution of the porosity system in these rocks.

Evaporite solution breccias and their residual pore spaces are important keys in understanding the syn-depositional and early post-depositional history of these rocks and they are also evidence of former presence of evaporite units. The stratigraphic position of these solution breccias and relationships between overlying and underlying beds indicate that dissolution of evaporite beds produced these solution breccias and also are the Mg/Ca rich fluids source for D2 dolomitization. Dolomitization associated with hypersaline flux occurred at shallow burial depths and early in the diagenetic history of the rocks. The hypersaline reflux dolomitization model is characterized by high concentration of magnesium that promotes the dolomitization of beds immediately below the evaporative environments (Lucia and Major, 1994).

D3 baroque dolomite and C3 calcite cements are also important keys to understanding fracture porosity evolution. As D3 baroque dolomite cement is present mainly as F4 fracture cement, it is inferred that at least F4 fractures developed at moderated to deep burial conditions. The iron content of dolomite may be related to the lithology (shales) of the surrounding rock. Baroque dolomite from facies with high

content of shales tends to have higher iron content than baroque dolomite from facies with little or no shale material, such as the Cupido Formation. Ferroan dolomite is minor cement in these rocks. Most crystals replace matrix cements. In general, the amount of ferroan dolomite is variable, with the least and most iron-rich baroque dolomite found at the Iturbide-Santa Rosa locality where basinal facies dominate. Burial diagenesis has not significantly dolomitized these limestones. Owing to low host rock porosity, at this stage it is likely that faults and fractures controlled the movement of formation waters in the Cupido system and determined the location and intensity of late stage diagenetic processes.

Previous diagenetic studies of these rocks include fracturing as just one event and ascribe fractures to tectonics and uplift of the SMO (example: Moldovanyi and Lohmann, 1984, and Minero, 1988). However, integration of diagenetic processes and fracturing events shows that it is possible to distinguish more than a single fracturing event in this paragenetic sequence. In fact, six fracturing events were identified, each with distinct diagenetic characteristics including textural evidence that cements precipitated simultaneously during fracturing. F3-F5 events produced the most abundant fractures in Cupido rocks. F3 through F5 fractures are locally arranged in patterns that suggest the fractures and bed-parallel stylolites formed with kinematic compatibility, implying that these structures are broadly contemporaneous. Elsewhere, bed-parallel stylolites crosscut these fractures, showing that bed-normal compaction at least partly postdated F3-F5 fractures.

Finally textural relations show that calcite precipitation occurred in some new fracture void space created when F3-F5 fractures were reactivated. Crosscutting relations among F3-F5 calcite veins suggests that polyphase precipitation of C3 calcite is possible.

In general, in the samples examined, a generation of calcite was among the latest, if not the last, cement to precipitate.

DISCUSSION: FRACTURE HISTORY

Although crosscutting relationships do not directly constrain an absolute time of fracture formation, they can be used to separate groups of fractures that formed approximately synchronously and probably under similar remote loading (stress) conditions. Crosscutting relationships can be confusing in the field, however, under microscopic inspection it is easier to recognize these relationships. In this chapter I show how petrographic data can supplement and strengthen relative timing arguments based on field data.

In Chapters 4 and 5, I demonstrated that in a thick carbonate sequence, such as the Cupido Formation, it is possible to differentiate fractures having different origins based on careful observation of outcrops and samples under the microscope. Overlap relations of cements in fractures, kinematically significant textures in those cements, such as crack seal texture (for synkinematic cements) and massive texture (for postkinematic cement) allow the timing of fracture opening to be specified relative to the formation of rock mass cements (diagenetic events). Integrated structural and diagenetic analysis allows delineation of events related to these fractures. The textural results alone do not yield unique depth ranges or precise start-stop times for structural events. To obtain such information requires direct dating of synkinematic cements, which is yet impractical given the small volumes of cement and the lack of good dating methods for the phases involved (quartz, calcite, and dolomite). In this study, the broad depth ranges were inferred by taking, at face value, broad temperature ranges for some of the diagenetic

processes (such as regional dolomitization) from the literature and from other sources. If the accumulation of some of these cements is temperature dependent, as has been proposed for dolomite in dolostone fractures (Gale et al., 2010), then this analysis could be taken further with a data set that includes a well-defined burial (or thermal) history, fluid inclusion data, and dolomite cement accumulation volumes, as has been done for quartz cement in sandstone fractures (Becker et al., 2010).

In the following chapter I use isotopic analyses data from fracture cements to more closely constrain fracture timing and to test the broad inferences proposed in this chapter. The postulate is that fractures that formed under shallow burial conditions may show cement fills with isotopic signatures indicative of low temperatures at the time of cementation. Certain fracture cement mineralogies might also suggest deep burial cementing conditions during fracture formation. For example, in the literature baroque dolomite or quartz cements are associated with deep burial conditions and hot deep basin brines. For these reasons I carried out an isotopic study to characterize both synkinematic and postkinematic fracture cements, and matrix cement as well, to interpret precipitation conditions and to calibrate the paragenetic sequence determined in the petrographic study (see Chapter 6).

This chapter also demonstrates that it is possible in this area to effectively characterize the large scale (outcrop scale) fractures using hand samples and microscopy. This result demonstrates that deformation of these carbonate rocks is to an extent penetrative. The presence of penetrative deformation is consistent with the occurrence in this area of structures like tectonic stylolites (spaced cleavage; Marshak and Engelder, 1985), a style of deformation that is not usually equated with oil field geology. Nevertheless, the types of fractures found do not differ significantly from those found in

nearby oilfields, implying that penetrative style deformation may be more prevalent in reservoir type rocks than hitherto expected.

Results in this chapter suggest a way to circumvent challenges of sampling subsurface fractures, using the penetrative aspects of the fracture and diagenetic fabrics. The methodology needed to conduct a combined fracture and cement analysis requires good representative, oriented samples. Based on oriented samples from each studied bed in the field, I was able to characterize the same fracture sets at different scales: macro-scale (field) and micro-scale (thin sections). Correlations between these two different scales are important because in the oil industry, for example, subsurface fracture data at macro-scale are scarce, but we can obtain equivalent information if we use micro-scale fracture data to characterize conductive fracture sets important for the fluids flow in oil and gas reservoirs.

Chapter 6: Stable Isotope Analyses of Fracture Cements in the Cupido Formation, Monterrey Salient, Sierra Madre Oriental, Mexico

SUMMARY

This study investigates the stable isotope geochemistry of opening-mode fractures (veins) from carbonate rocks of the Cupido Formation in the Monterrey Salient, Sierra Madre Oriental (SMO), Mexico, to characterize the environments in which fracture cementation occurred and to constrain the origin and development of fracture systems. Fifty-eight samples collected for isotopic analyses, mainly from fracture cements, are the basis of this study. D2 and D3 synkinematic dolomite cements associated with F3 and F4 fractures, respectively, and postkinematic C3 and C4 calcite cements are the main fracture-filling phases in the most abundant fractures of the Monterrey Salient area. These cements and their associated fractures are the object of the analysis presented in this chapter.

D2 and D3 synkinematic dolomite composition (PDB) $\delta^{13}\text{C}$ values range from +1.59 ‰ to +3.43 ‰ and $\delta^{18}\text{O}$ values from -2.31 ‰ to -5.15 ‰. These isotopic compositions are depleted in $\delta^{18}\text{O}$ with respect to Cretaceous marine carbonate material indicating precipitation at higher temperatures than those at the surface. Dolomite isotopic composition displays a progressive trend toward lower $\delta^{18}\text{O}$ values in the fill of younger fractures. This supports the idea the probable evolution of fluids from original marine composition and increasing temperatures of dolomite precipitation during progressive burial. Assuming a geothermal gradient of 23 °C/km, and the temperature of baroque dolomite precipitation of ~60 to ~150 °C (from published data), D3 dolomite precipitated between depths of ~1.4 to ~4.8 km, shallower than the maximum burial

depth of more than 5 km that has been inferred for part of the SMO based on structural restoration, vitrinite reflectance and other data (Pottorf et al., 1997).

C3 calcite synkinematic calcite with respect to F5, presents $\delta^{13}\text{C}$ values range from +2.38 ‰ to +2.78 ‰, and $\delta^{18}\text{O}$ values from -5.904 ‰ to -6.27 ‰. The $\delta^{18}\text{O}$ values are depleted with respect to Cretaceous marine carbonate material and host rock isotopic values, suggesting precipitation at higher temperature than the surface. In contrast, C4 postkinematic cement from F3, F4 and F5 fractures, ranges from +0.30 ‰ to +2.89 ‰ and from -2.21 ‰ to -4.13 ‰ $\delta^{18}\text{O}$, indicating precipitation from cool waters.

The genetic interpretation that synkinematic dolomite cement formed during relatively shallow (but possibly progressively deeper) to deep burial conditions, between depths of ~1.4 to ~4 km, implies that fractures were in place prior to deepest burial of the SMO, that is, before folding commenced. In contrast, much of the calcite cement in fractures formed late, after folding, possibly during exhumation and breaching of the SMO folds. This hypothesis is supported by the geochemical data presented here. The results and interpretations of this study are consistent with burial and thermal histories and timing of tectonic folding inferred for the SMO from fluid inclusion thermometry and thermochronology reported before.

INTRODUCTION

Stable isotope measurements have been used mainly to constrain cement environment and diagenetic history in sedimentary carbonate rocks. However, little work has been done using stable isotope measurements to help characterize fracture history and associated authigenic cements. Isotopic compositions from fracture cements and host-rock samples can be used to constrain conditions of fracture development.

Cements in fractures and in host rock can be defined as pre-, syn- or postkinematic depending on whether they precipitated before, during, or after fractures of a particular set opened (Laubach and Milliken, 1996; Laubach, 1997). One benefit of this subdivision of cements is that it encompasses cements in fractures and host rock. The most important cement to interpret origin of fractures is synkinematic, however postkinematic cement is, in many cases, the most abundant in fractures and its amount is critical in the evolution of fracture porosity, yet it has little or nothing to do with fracture formation, having been precipitated after fractures were created. This distinction was critical for interpretation of isotopic composition of vein-filling minerals from the Lower Cretaceous Cupido Formation.

Integration of stratigraphic and diagenetic studies, and carbon and oxygen isotopic data for the carbonate succession of the Cupido Formation, provides insight into the origin and history of fractures in these rocks. Cement-filled opening-mode fractures (namely, veins) are abundant in the Cupido Formation. A protracted fracture history mostly pre-dating folding (Marrett and Laubach, 2001) is consistent with results of isotopic measurements of this study. Moreover, dramatic shifts in fracture porosity and connectivity are indicated, from extremely low values currently to very high values in the past. Interpretation of isotopic analysis of this study are consistent with burial and

thermal histories and timing of tectonic folding inferred for the SMO from fluid inclusion and thermochronology (e.g. Gray, 2001) results as described below.

STUDY AREA

The field area for this study is located in the Monterrey Salient, SMO, northeast of Mexico. Source data for this study come from Lower Cretaceous Cupido and Tamaulipas Inferior Formation rocks, based on field observations and sample studies of nine localities: Potrero García, Cañón de las Cortinas, Cañón Prieto, Cañón Los Chorros, Cañón La Escalera, Cañón Boquilla Corral de Palmas, Molano Fault, Cienegas and Cañón Santa Rosa-Iturbide (Fig. 6.1). The good exposures of the rocks, in several transverse canyons cut the SMO folds, make the ideal sites to study the relationships between lithofacies, diagenesis and fractures.

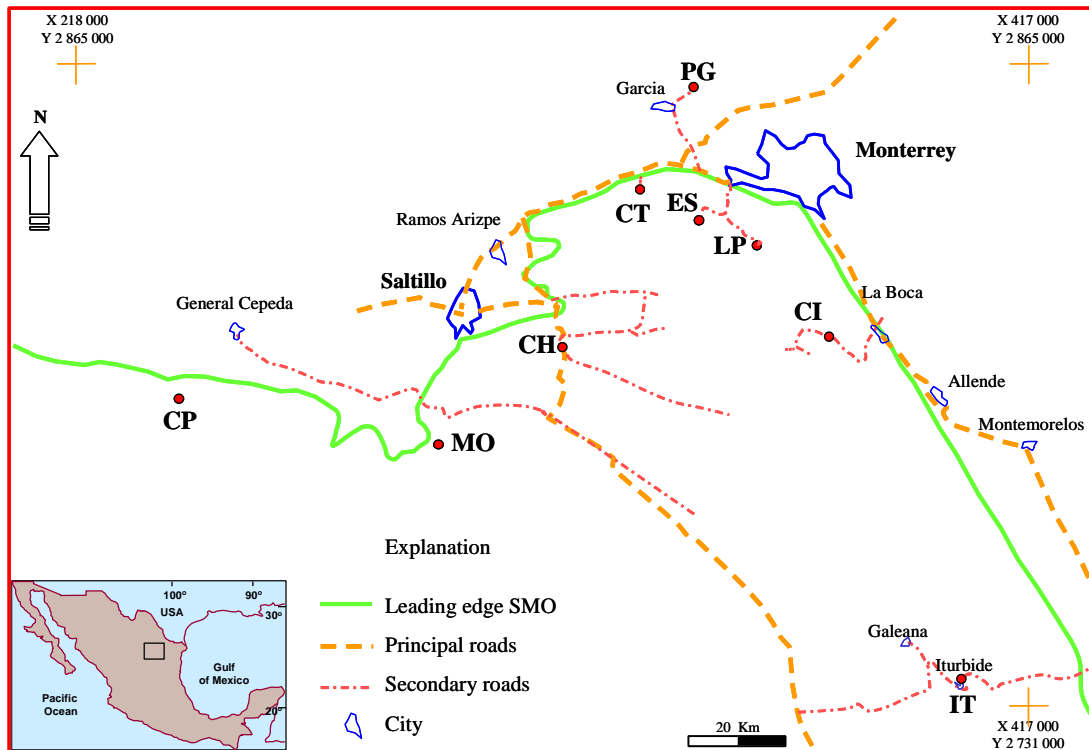


Fig. 6.1. Location map of study localities, Monterrey Salient. Circles mark Outcrop and sample localities: PG, Potrero García; CT, Cañón de las Cortinas; CH, Cañón de los Chorros; ES, Cañón la Escalera; LP, Cañón Boquilla Corral de Palmas; IT, Cañón Santa Rosa-Iturbide; MO, Molano Fault; CP, Cañón Prieto; CI, Cienegas. X and Y are coordinates in the Transverse Mercator Projection (UTM) indicated by small crosses. Square in inset map indicates the location of the map above.

PREVIOUS GEOCHEMICAL WORK

Stable isotopic analyses have been used previously to constrain sedimentary environments, chronostratigraphic relations and diagenetic sequences of the Sligo and Cupido Formations in northeastern Mexico and in South Texas. Where studied these units are at over 5 km depth and outside of the SMO. Moldovanyi and Lohmann (1984) defined four generations of cements based on petrographic and stable isotopic analyses of equant cements, within reefal facies of the Lower Cretaceous Sligo and Cupido Formations. The two first generations of equant early calcite cements were interpreted to have formed in a shallow, meteoric, phreatic environment. The third, which occurs as a void-filling spar and in fractures, was interpreted to have formed in a burial-phreatic environment. Fluid-inclusion analyses indicate calcite precipitation at elevated temperatures. The fourth stage of cementation produced coarsely crystalline calcite in fractures and stylolites. Baroque dolomite is also present and it was included in the fourth stage. Fluid inclusion study of fourth stage cements indicates precipitation at even greater depths and elevated temperatures. Calcite and dolomite isotope data indicate some pore water enriched in ^{18}O , perhaps produced from dehydration of evaporites or dewatering of other stratigraphic units.

Minero (1988) differentiated three diagenetic stages in the Cretaceous El Abra Formation along the eastern margin of the Valle-San Luis Potosí platform, within the SMO but 400 km south of the Monterrey Salient. Stage 1 encompasses early subaerial processes. Stage 2 corresponds to eogenetic processes dominated by equant calcite cement formed by karstification. Stage 3 occurred during Laramide-age deformation that resulted in folding and fracturing during the Paleogene. Lehmann et al., (1999) integrated biostratigraphic data with carbon and strontium isotopic stratigraphy to clarify

chronostratigraphic relations across northeastern Mexico. Leticariu, et al., (2005) analyzed oxygen, carbon, and strontium isotope variations in vein-filling calcite and quartz cements and their host rocks to elucidate the origin, spatial and temporal evolution, and migration pathways of fluids in the detachment Nuncios fold complex, northeastern Mexico, which is the Laramide-age frontal structure of the Monterrey Salient. They defined that the fluid history of the Nuncios fold complex evolved two main stages: (1) burial diagenesis and early folding, during which fluids were confined within individual units, and (2) late stage folding, during which increased deformation associated with fold tightening caused the expulsion of fluid from the lower unit into the upper unit.

METHODOLOGY

Fifty-eight rock samples from 33 sub-localities in nine areas of the SMO Salient and two water samples were collected for carbon and oxygen isotopic analyses (Table 6.1). Individual generations of vein and fault cements were microsampled for their carbon and oxygen isotopic composition in order to further interpret the environments in which fracture cementations occurred. To have better control of sampling, oriented samples were cut perpendicular to bedding, fracture, foliation, or fault plane and parallel to slickenfibers, striations or the inferred slip direction of the faults.

Host rocks and rudists, evaporate collapse (solution) breccias, anhydrite nodules and travertine cements, were also sampled to compare with fracture-cement isotopic values. Meteoric water samples were analyzed to constrain travertine precipitation temperatures.

Number	Locality	Sample Name	Composition
1	La Escalera	Esc1-98So (2c)	calcite
2	La Escalera	Esc1-98So (2d)	dolomite
3	La Escalera	Esc1-98So (2m)	dolomite
4	La Escalera	LEsc8H-01 (40)	calcite
5	La Escalera	LEsc9-01 (41)	calcite
6	La Escalera	LEsc13C (42)	calcite
7	La Escalera	LEsc13C-01 (42c)	dolomite
8	La Escalera	LEscT2-01 (43)	calcite
9	Las Palmas	LaPaNeckA (5c)	calcite
10	Las Palmas	LaPaNeckA (5d)	dolomite
11	Las Palmas	LaPa 4-98 So A (7m)	dolomite
12	Las Palmas	LaPa4-98 SoA (7 r)	calcite
13	Las Palmas	LAPA8M	dolomite
14	Las Palmas	LAPA8C	calcite
15	Las Palmas	LAPA8D	dolomite
16	Las Palmas	LAPA8CD	dolomite
17	Las Palmas	LAPA9M	dolomite
18	Las Palmas	LAPA9D	dolomite
19	Las Palmas	LAPA9C	calcite
20	Las Palmas	LAPA9CD1	calcite
21	Las Palmas	LAPA9CD2	dolomite
22	Las Palmas	LaPa8-98 (18 c2)	calcite
23	Las Palmas	LaPa8-98 (18 d1)	dolomite
24	Las Palmas	LaPa8-98 (18 d2)	dolomite
25	Las Palmas	LaPaNeckB (20d)	dolomite
26	Las Palmas	LaPa3-98 (25 m)	calcite
27	Las Palmas	LaPa3-98 (25 r)	calcite
28	Las Palmas	LPal5calc-01(36)	calcite
29	Las Palmas	LPal4-01 (57)	calcite

Table 6.1. List of samples, localities and composition for carbon and oxygen isotopic analyses. Cupido and Tamaulipas Inferior Formations.

Number	Locality	Sample Name	Composition
30	Los Chorros	LCh1-98So (14 m)	calcite
31	Los Chorros	LCh8-98 SoA (16 m)	calcite
32	Los Chorros	LCh8-98 SoA (16 c1)	calcite
33	Los Chorros	LCh8-98 SoA (16 c2)	calcite
34	Los Chorros	LCH1-01 (45)	calcite
35	Los Chorros	LCH1B-01 (46)	travertine
36	Los Chorros	LCH1C (47)	dolomite
37	Los Chorros	LCh1C-01 (47 m)	dolomite
38	Los Chorros	LCh4-01 (48)	calcite
39	Los Chorros	LCh4-01 (48c)	calcite
40	Potrero García	PG1-01 (28)	calcite
41	Potrero García	PG2-01 (29)	calcite
42	Potrero García	PG2-01 (29 m)	dolomite
43	Potrero García	PG4-01 (30 m)	dolomite
44	Potrero García	PG4calc-01 (31)	calcite
45	Potrero García	PG5-01 (32)	travertine
46	Iturbide-Santa Rosa	StR3-98 (9 m)	calcite
47	Iturbide-Santa Rosa	StR9-98 SoA (10 c1)	calcite
48	Iturbide-Santa Rosa	StR9-98 (10 m)	calcite
49	Iturbide-Santa Rosa	StR9 (11 m)	calcite
50	Cerro Prieto	CP1-01 (52)	calcite
51	Cerro Prieto	CP1-01 (52 m)	dolomite
52	Cerro Prieto	CP2-01 (53)	calcite
53	Cerro Prieto	CP2-01 (53m)	dolomite
54	Cerro Prieto	CP2C-01 (54)	calcite
55	Ciénegas	CC5-01 (56)	calcite
56	Las Cortinas	LCort1-01 (44)	calcite
57	Molano	01RM69-01 (51)	calcite
58	Los Chorros	01RM69-01 (50)	travertine
A	Los Chorros	01RM 136 A	water
B	Los Chorros	01RM 136 A	water

Continuation Table 6.1. A and B are modern water samples.

GEOCHEMICAL SAMPLING AND ANALYTICAL METHODOLOGY

Geochemical samples were selected to span the relative-age range of cements and to include samples of both dolomite and calcite in limestones and dolostones. Because recrystallization can easily reset isotopic values, areas where this process occurred were avoided for isotopic sampling. Individual generations of fracture filling cement samples collected in synkinematic and postkinematic cements were analyzed. In addition, cements of host rock, fault breccias, flexural slip faults, evaporate collapse (solution) breccias, anhydrite nodules and travertines were included.

Oriented rock samples with the fracture sets identified (strike and dip) were collected from the field. Thin slab samples were cut perpendicular to bedding, vein, foliation, or fault plane and parallel to slickenfibers, striations or the inferred slip direction of the fault. Sample powders for chemical analysis were obtained from polished thin slabs using a bench-top drill press with a 0.4 mm dental drill bit. A standard microscope was used in this procedure (Fig. 6.2). Although efforts were made to minimize physical mixing, this could have occurred for matrix samples and thin veins. The $\delta^{13}\text{C}$ and $\delta^{18}\text{O}$ values were obtained from ~20 mg powder samples analyzed using both the conventional phosphoric acid method (McCrea, 1950) in some samples and automated Micromass Multiprep device in others. The first procedure resulted in complete reaction with ~2.5 mg of phosphoric acid (H_3PO_4) at 25 °C for calcite and 50 °C for dolomite of the very fine-grained (micro drilled) carbonate powder. In the second procedure the $\delta^{13}\text{C}$ and $\delta^{18}\text{O}$ values were obtained from ~2-mg powder samples analyzed using an automated Micromass Multiprep device reacting the samples at 90 °C. In both cases the CO_2 was purified and analyzed on a VG Prism Series II mass spectrometer. In-house carbonate standards (Yule marble) were simultaneously analyzed with the samples.

The standards used to report the isotopic composition of water and carbonate minerals are SMOW (Standard Mean Ocean Water) and the PDB (Peedee Formation Belemnite). The SMOW standard is commonly used to report the oxygen and deuterium isotopic composition of fluids and of silicate minerals; the PDB standard is used to report the carbon and oxygen isotopic composition of carbonate minerals, and it is used in this study.

Values of oxygen against carbon isotope analyses were crossplotted to investigate the isotopic signature of different cements and the possible relationships with fracture sets.



Fig. 6.2. Clean-room laboratory equipped with standard light parallel microscope and bench-top drill press with a dental drill bit for micro-sampling. Sample preparation for isotopic analysis in this room is done under ultra-clean conditions to avoid contamination. In the top right corner is a close up of polished thin slab. Small bottles are to store samples.

Estimation of Marine Carbonate Composition

The initial composition of Cretaceous marine carbonate as a starting isotopic composition from which the composition diagenetic components evolve is necessary to evaluate the progression of diagenetic events. As this study is focused on fracture cement values of initial composition were taken from literature. “Least altered” Cretaceous marine invertebrates and marine carbonate cements isotopic values derived from values reported by several papers in the literature for the Cretaceous period was compiled by Allan and Wiggins (1993). A range of $\delta^{18}\text{O}$ between -2.3 ‰ and + 0.9 ‰ is the most representative as initial composition of Cretaceous marine materials. Similar range (-2.3 ‰ $\delta^{18}\text{O}$ and + 4.0 ‰ $\delta^{13}\text{C}$) is reported by Moldovanyi and Lohmann (1984) using analyses results of rudists, micrite and equant cements, within reefal facies of the Lower Cretaceous Sligo and Cupido Formations. This range was used to compare both calcite and dolomite cements in this study.

Data Analysis

Isotopic data can help to estimate the conditions and environments of deposition where cementation took place. However, in order to constrain precipitation condition it is necessary to know the original isotopic composition of the fluids which generated the cementation. Values of oxygen and carbon isotopes analyses were plotted. Calcite isotopic values were compared with the initial composition of Cretaceous marine cements and host rock values. Groups with different isotopic signature were recognized and classified.

Dolomite isotopic values were analyzed using two empirical approaches proposed by Allan and Wiggins (1993). Dolomite isotopic values were compared with high temperature/low temperature dolomite fields, established based on 64 examples of dolomites whose origin has been previously established by using different approaches such as fluid inclusion, trace and minor elements, and Sr isotopes. In addition, isotopic values of dolomite were compared with “least altered” (i.e., isotopically heaviest) Cretaceous marine invertebrates and marine carbonate cements.

Paleo-temperature Calculation

As an alternative approach, temperatures of dolomite cement precipitation can be calculated using the Friedman and O’Neil (1997) equation:

$$[3.2 * 10^6 T (\text{°K}) - 2] - 1.5 = \delta^{18}\text{O}_{\text{dol}} - \delta^{18}\text{O}_{\text{water}}$$

using an estimated value of $\delta^{18}\text{O}_{\text{water}} = -29.97 \text{‰}$ (PDB)

This equation has two unknown variables, the oxygen isotopic composition of water ($\delta^{18}\text{O}_{\text{water}}$) and temperature (T), and one known parameter, the oxygen isotopic composition of dolomite ($\delta^{18}\text{O}_{\text{dol}}$) measured from the sample. Also unknown is the fractionation factor from water to dolomite. Because we want to know temperature (T) it is necessary to constrain the value of ($\delta^{18}\text{O}_{\text{water}}$). One approach for estimating $\delta^{18}\text{O}_{\text{water}}$ is to use fluid inclusion homogenization temperatures from a sample on which both fluid inclusion and isotope data have been collected (Allan and Wiggins, 1993). If fluid inclusion data are not available, as in this case, it is necessary to estimate the $\delta^{18}\text{O}_{\text{water}}$ value. However, the error in calculating T can be large if values of $\delta^{18}\text{O}_{\text{water}}$ are uncertain. Therefore, the interpretation of isotope data in this study is based on the two approaches of high temperature/low temperature fields proposed by Allan and Wiggins (1993).

RESULTS OF STABLE ISOTOPE ANALYSES

Twenty dolomite cements and thirty-eight calcite cements for isotopic analyses were selected to span all type of cements identified. In addition, two modern water samples were also analyzed. Results of carbon and oxygen isotopic analyses are described below in three main groups: dolomite cements, calcite cements, and water samples.

DOLOMITE CEMENT ANALYSIS

Petrographic evidence and field observations permitted to identify three main dolomite cements (see Chapter 4): D1 dolomite is characterized by fine-grain ($< 50 \mu$) crystals and millimeter fine laminations. A second pervasive dolomitization (D2) was identified and is the most abundant in these rocks. This D2 cement produced replacement of no iron-rich dolomite that locally modifies partially or completely the rock. Most dolomite crystals that replace both rock matrix and grains are anhedral and fine grain size ($< 50 \mu$). The third cement is baroque or saddle dolomite (D3), occurs as clear to brown or white euhedral to subhedral crystals that fill, bridge or line opening-mode fractures and postdate D1 and D2 dolomites. D3 dolomite is most obvious along fracture walls in dolostone beds, but also partly replaces matrix and in some cases is a selective replacement phase affecting mainly fossils and clasts in evaporite collapse breccias and also in fault breccias. Crystal sizes range from 0.025 mm to more than 2 mm. Twenty samples for isotopic analyses were selected to span all dolomites from host rocks, fracture cements, fault breccias and collapse breccias (Table 6.2).

Analysis of dolomite cement was made using the two different approaches proposed by Allan and Wiggins, 1993. Dolomite isotopic values were plotted on the low

temperature/high temperature plot as a first attempt to separate low from high temperature dolomite. Second, the same values were compared with “least altered” Cretaceous marine invertebrates and marine carbonate cements. If cement samples have similar isotopic compositions to host rocks and Cretaceous marine carbonate material, then most probably these cements were deposited close to or on the surface at low temperatures. Combining the results it is possible to constrain in part the origin and diagenetic environment of precipitation of the different dolomite cements identified.

DOLOMITE				
ORDER BY LOCALITIES				
Number	Sample Name	delta 13 C per mil (PDB)	delta 18 O per mil (PDB)	Features
Las Palmas				
25	LaPaNeckB (20d)	1.883	-1.001	Fracture cement
10	LaPaNeckA (5d)	2.950	-1.600	Fracture cement
17	LAPA9M	3.108	-2.043	Host rocks
24	LaPa8-98 (18 d2)	3.432	-2.313	Fracture cement
23	LaPa8-98 (18 d1)	1.918	-2.631	Fracture cement
13	LAPA8M	3.206	-2.711	Host rocks
16	LAPA8CD	3.029	-2.847	Fracture cement
15	LAPA8D	1.597	-2.929	Fracture cement
21	LAPA9CD2	2.695	-3.340	Fracture cement
11	LaPa 4-98 SoA(7m)	3.813	-3.939	Host rocks
18	LAPA9D	2.116	-4.506	Fracture cement
Los Chorros				
3	Esc1-98So (2m)	2.480	-1.900	Host rocks
2	Esc1-98So (2d)	1.890	-3.760	Fracture cement
7	LEsc13C-01 (42c)	1.840	-5.240	fault breccia
Potrero García				
37	LCh1C-01 (47 m)	3.838	-4.055	fault breccia
36	LCH1C (47)	3.480	-3.820	fault breccia
Cañón Prieto				
43	PG4-01 (30 m)	2.427	-5.149	Fracture cement/flexural slip
42	PG2-01 (29 m)	0.988	-6.569	collapse breccia
Cañón Prieto				
53	CP2-01 (53m)	1.999	-1.901	Host rocks
51	CP1-01 (52 m)	0.832	-4.868	collapse breccia

Table 6.2. List of samples by localities, including dolomite isotopic composition and sample origin, used in this study from Cupido and Tamaulipas Inferior Formations, SMO. Sample numbers from Table 6.1.

Host Rocks

Five samples of dolostone and dolomitized limestone matrix (host rock) were isotopically analyzed from Cañón Prieto, La Escalera, and Las Palmas localities (Table 6.3). Only one D1 dolomite sample from Cañón Prieto was analyzed. D1 dolostone host rock sample has $\delta^{13}\text{C}$ value of 1.999 ‰ and $\delta^{18}\text{O}$ values of -1.901 ‰. These host rock isotope values provide a basis with which to compare other dolomite isotope data of this study. Dolostone host rock samples are mainly composed of D2 dolomite replacement phase, but a mixture of both types of dolomite (D2-D3) also was commonly found. D2 dolomite from dolostone host rock have $\delta^{13}\text{C}$ values that range from 2.480 to 3.206 ‰ and $\delta^{18}\text{O}$ values between -1.900 to -2.711 ‰. D3 dolostone host rock samples have $\delta^{13}\text{C}$ values that range from 3.206 to 3.813‰ and $\delta^{18}\text{O}$ values that range from -2.711 to -3.939 ‰ (Table 6.3).

Dolomite Cements				
Host rocks				
Locality	Sample Name	Composition	$\delta^{13}\text{C}$ per mil (PDB)	$\delta^{18}\text{O}$ per mil (PDB)
Cañón Prieto	CP2-01 (53m)	D1	1.999	-1.901
La Escalera	Esc1-98So (2m)	D2	2.480	-1.900
Las Palmas	LAPA-9m	D2	3.108	-2.043
Las Palmas	LAPA-8m	D2-D3	3.206	-2.711
Las Palmas	LaPa 4-98 So A (7m)	*D3	3.813	-3.939

Table 6.3. Carbon and oxygen isotopic composition of host rocks from dolostones and dolomitized limestones of Cupido Formation, SMO. Location and chemical composition of samples is included. D1, synsedimentary dolomite; D2, replacement microcrystalline dolomite; D3, baroque dolomite; *sample from dolomitized limestone; T, temperature.

Fracture Dolomite Cements

Ten fracture dolomite cements were analyzed (Table, 6.4). Samples for isotopic analyses were selected to span all dolomite identified, however dolomite cement contemporaneous to D1 was nowhere found to be fracture cement. Two dolomite cements from low aspect ratio (length vs. aperture) veins in boudin “necks” at Las Palmas locality were analyzed. These samples are probably contemporaneous with D1 dolomite (named d1), and have $\delta^{13}\text{C}$ values vary from 1.883 to 2.95 ‰. $\delta^{18}\text{O}$ value ranges from -1.001 to -1.60 ‰. D2 dolomite was found as replacements phase in host rock matrix. Two samples of D2 synkinematic dolomites in veins from dolostones at La Palmas were analyzed and compared with host rock isotopic values. $\delta^{13}\text{C}$ values for these dolomite cements vary from 3.432 to 3.029 ‰ and from -2.313 to -2.84 ‰ of $\delta^{18}\text{O}$ (Table 6.4). These values are in between D2 and D3 isotopic values from host rock samples (Table 6.3), indicating possible mixture of these two dolomites types. Distinguishing these two cements is almost impossible with the technique used in this study. Finally, six samples of synkinematic D3 baroque dolomite from Las Palmas and La Escalera, and one flexural slip plane dolomite sample from Potrero García, were also analyzed. $\delta^{13}\text{C}$ values for D3 dolomite cement composition ranges from 1.597 ‰ to 2.695 ‰. $\delta^{18}\text{O}$ values range from -2.631 ‰ to -5.149 ‰ (Table 6.4).

Dolomite Cements					
Fracture Cements					
Locality	Sample Name	Composition	Fracture event	$\delta^{13}\text{C}$ per mil (PDB)	$\delta^{18}\text{O}$ per mil (PDB)
Las Palmas	LaPaNeckB (20d)	*d1	F1	1.883	-1.001
Las Palmas	LaPaNeckA (5d)	*d1	F1	2.950	-1.600
Las Palmas	LaPa8-98 (18 d2)	D2	F3	3.432	-2.313
Las Palmas	LAPA-8CD	D2-D3	F3	3.029	-2.847
Las Palmas	LAPA-8D	D3	F4	1.597	-2.929
Las Palmas	LAPA-9CD2	D3	F4	2.695	-3.340
Las Palmas	LaPa8-98 (18 d1)	D3	F4	1.918	-2.631
La Escalera	Esc1-98So (2d)	D3	F4	1.890	-3.760
Las Palmas	LAPA-9D	D3	F4	2.116	-4.506
Potrero García	PG4-01 (30 m)	ψ D3	F6	2.427	-5.149

Table 6.4. Carbon and oxygen isotopic composition of fracture cements from dolostones and dolomitized limestones of Cupido Formation, SMO. Location and chemical composition of samples is included. D2, replacement microcrystalline dolomite; D3, baroque dolomite; d1, dolomite cement probably contemporaneous with D1 dolomite; *, postkinematic cement; ψ , flexural slip plane sample.

Fault Breccias

Faults commonly affect the whole column of Cupido Formation, creating breccias cemented by both calcite and dolomite. Three samples of D3 baroque dolomite found in these breccias from Los Chorros and La Escalera localities were analyzed. Dolomite cements of these breccias have $\delta^{13}\text{C}$ values from 1.84 to 3.838 ‰ and $\delta^{18}\text{O}$ values that range from -3.82 to -5.24 ‰ (Table 6.5).

Dolomite Cements					
Fault Breccias					
Locality	Sample Name	Composition	Fracture Event	$\delta^{13}\text{C}$ per mil (PDB)	$\delta^{18}\text{O}$ per mil (PDB)
Los Chorros	LCh1C-01 (47)	D3	F4	3.48	-3.82
Los Chorros	LCh1C-01 (47 m)	D3	F4	3.838	-4.055
La Escalera	LEsc13C-01 (42c)	D3	F4	1.840	-5.240

Table 6.5. Carbon and oxygen isotopic composition of baroque dolomite from fault breccias of Cupido Formation, SMO. Location and chemical composition of samples is included. D3, baroque dolomite.

Collapse (Solution) Breccias

Collapse breccias were found interbedded with limestones and dolostones in the sedimentary columns at the Monterrey Salient (see Chapter 3). Collapse breccias are cemented by both calcite and dolomite. Two dolomite cements from both types of collapse breccias (monomict and polimict) were sampled for isotopic analyses. Dolomite

cements of these collapse breccias have $\delta^{13}\text{C}$ values from 0.832 to 0.988 ‰ and $\delta^{18}\text{O}$ values that ranges from -4.868 to -6.569 ‰ (Table 6.6).

Dolomite Cements				
Evaporite Collapse Breccias				
Locality	Sample Name	Composition	$\delta^{13}\text{C}$ per mil (PDB)	$\delta^{18}\text{O}$ per mil (PDB)
Cañón Prieto	CP1-01 (52 m)	γ D3 dolomite	0.832	-4.868
Potrero García	PG2-01 (29 m)	τ D3 dolomite	0.988	-6.569

Table 6.6, Carbon and oxygen isotopic composition of baroque dolomite cement from collapse breccias of Cupido Formation, SMO. Location and chemical composition of samples is included. γ , dolomite cement in dolostone clasts; τ dolomite cement from matrix of polymict collapse breccias.

DOLOMITE ISOTOPIC CHARACTERIZATION

Figure 6.3 shows the cross-plot of oxygen and carbon isotopic composition of all dolomite cements analyzed from the Cupido Formation, and the dolomite temperature fields according to Allan and Wiggins (1993). “Most low temperature dolomite” field ranges from 0 to 2.5 $\delta^{18}\text{O}\text{‰}$ PDB, the overlap between low temperature and high temperature dolomite field ranges from 2.5 to 6.5 $\delta^{18}\text{O}\text{‰}$, and the “most high temperature” dolomite field is defined for values of 6.5 $\delta^{18}\text{O}\text{‰}$ to higher.

All D1 and D2 dolomite host rock samples fall in the “most low temperature” field. Fracture dolomite cements from F1, identified as contemporaneous with D1, fall also in the “most low temperature” field. A D2 synkinematic dolomite from F3 fractures falls also in this field. All D3 synkinematic baroque dolomite cements from fractures in dolostones, fault breccias, collapse breccias, flexural slip plane, and host rocks, fall in the “overlap between low temperature and high temperature” field. Only one dolomite sample from a collapse-breccia at Potrero García locality, with value of -6.59 $\delta^{18}\text{O}\text{‰}$, barely falls in the most high temperature field, indicating precipitation of baroque dolomite occurred at elevated temperatures (Fig. 6.3). The cross-plot of oxygen and carbon isotopic composition of dolomite cements shows a progressive trend toward lower $\delta^{18}\text{O}$ values from the earliest cements (D1) on the right, to the latest (D3) on the left. A similar dolomite trend from F1 to F6 passes through matrix cement (outlined with big dashed arrow in Figure 6.3), indicating probable evolution of fluids from original marine composition and increasing temperatures of dolomite precipitation during progressive burial. However, most D3 dolomites fall in the “overlap between low temperature and high temperature dolomite” field including a sample from F3 fractures, all F4 and F6 fracture cements, D3 host rock dolomites, dolomite cements from fault breccias, and

collapse breccias. Therefore most of D3 cements could have formed either in the shallow burial or during deep burial. To distinguish between these two possibilities, the same isotopic values were plotted and compared with Cretaceous marine carbonate material (Fig. 6.4).

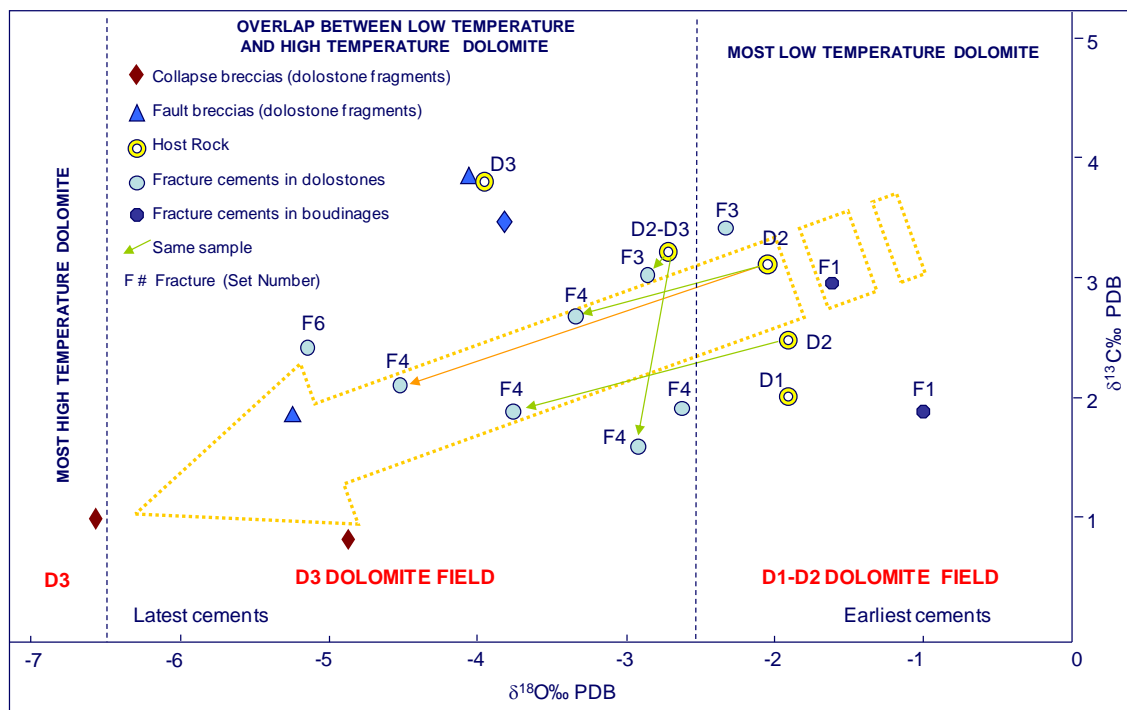


Fig. 6.3 Oxygen and carbon isotope plot for dolomite from the Cupido Formation. The plot shows consecutive cements from the earliest on the right to the latest on the left displaying a progressive trend toward lower $\delta^{18}\text{O}$ values. Two dolomite fields are defined: “D1-D2 dolomite field” (most low temperature dolomite) encompasses D1 and most D2 host rock dolomite, fracture cements from F1 and a sample from F3 fractures. The “D3 dolomite field” (overlap between low temperature and high temperature dolomite) encompasses most D3 dolomite: a sample of F3 fracture cement, all F4 and F6 fracture cements, D2-D3 host rock dolomites, dolomite cements from fault breccias, and all collapse breccias. Dolomite cements show a general progressive trend toward lower $\delta^{18}\text{O}$ values from the earliest cements (D1) on the right, to the latest (D3) on the left. A similar dolomite trend from F1 to F6 passing through matrix cement is outlined with big dashed arrow, indicating probable evolution of fluids from original marine composition and increasing temperatures of dolomite precipitation during progressive burial. D1; syndimentary dolomite, D2, replacement dolomite phase; D3, baroque dolomite. Fractures identified are numbered according to their relative timing: F6 fractures are the youngest. Small arrows are connecting fracture cements values with their correspondent host rocks. Temperature dolomite fields from Allan and Wiggins (1993).

Dolomite isotopic values were compared with “least altered” Cretaceous marine carbonate material (Allan and Wiggins, 1993) (Fig. 6.4). All D1 and D2 dolomites isotopic values from host rocks fall within the range established for Cretaceous marine carbonate material, indicating low temperature origin for these dolomite cements, which is consistent with the first interpretation using the low/high temperature fields (Fig. 6.3). All values of D3 baroque dolomite and one sample of D2-D3 dolomite cement from a host rock are depleted in $\delta^{18}\text{O}$, and fall left to the Cretaceous marine carbonate field, indicating precipitation at elevated temperature and suggesting a late burial origin for D3 dolomite. Different isotopic composition between baroque and replacement dolomite suggests they probably formed from the same fluid but precipitated at different temperatures.

D1 and D2 dolomite isotopic values are typical of unaltered marine dolostones for the Cretaceous period, and support in part the origin of both D1 (syndimentary) and D2 dolomites (reflux replacement phase). Isotopic values from D3 support its origin as baroque dolomite in burial conditions.

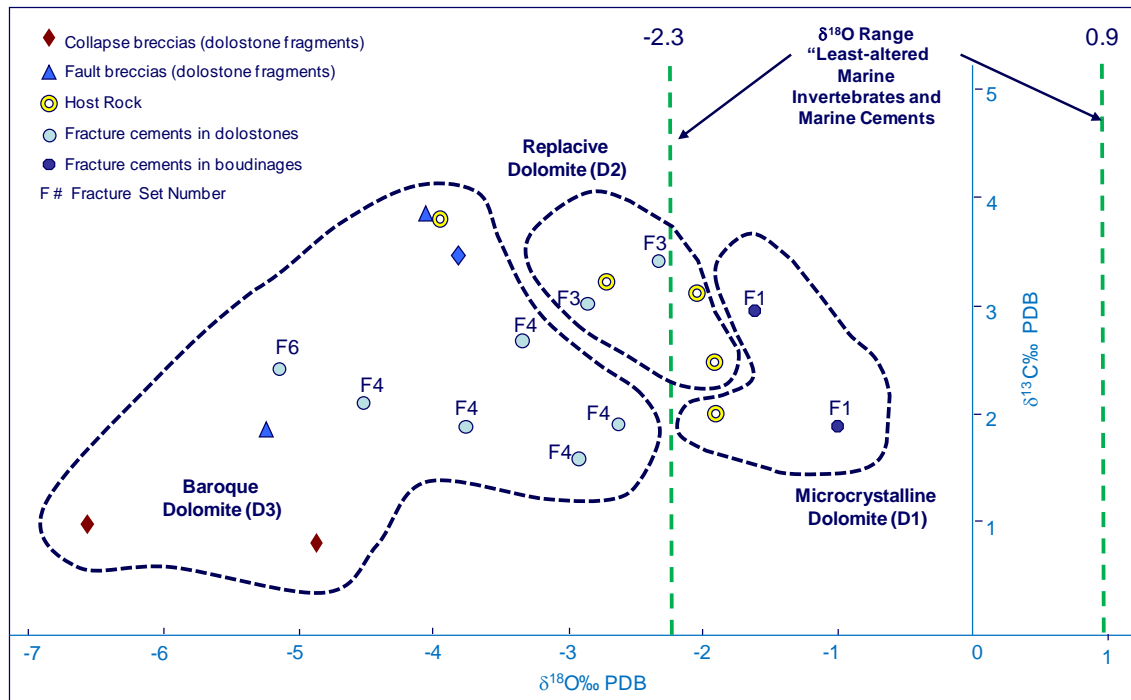


Fig. 6.4 Same oxygen and carbon isotope data shown in Fig. 6.3 for dolomite from the Cupido Formation is plotted here and compared to the $\delta^{18}\text{O}$ range of "least altered" (i.e., isotopically heaviest) Cretaceous marine invertebrates and marine carbonate cements from Allan and Wiggins (1993). Three main fields are outlined: D1 dolomite field is mainly dolomite from synkinematic dolomite of F1 fractures and from host rocks. D2 dolomite field is formed by replacement D2 dolomite from host rocks and synkinematic cement of F3 fractures. D3 dolomite field encompasses a sample of host rock, all collapse breccias and fault breccias, and all synkinematic baroque dolomite cements of F4 fractures. One sample of D3 baroque dolomite from F6 fractures (flexural slip) from Potrero García locality falls also in this group. Notice that all values of microcrystalline dolomite (probably D1), and most D2 dolomite, fall within the range established for Cretaceous marine carbonate material, indicating low temperature origin for these dolomites. All values of D3 baroque dolomite, and one D2-D3 matrix dolomite are depleted in $\delta^{18}\text{O}$ and fall to the left of Cretaceous marine carbonate field, indicating precipitation at elevated temperature.

CALCITE CEMENT ANALYSES

Petrographic evidence and field observations permitted identification of four calcite cements (see Chapter 4): thin isopachous fringe of fibrous calcite precipitated around allochems (i.e., ooids, peloids, and bioclasts) is C1; equant and clear anhedral calcite cement that fills cavities and pore-space between grains that postdates C1 is named C2. C2 includes also non-isopachous equant calcite spar cement around clasts in solution breccias. C1 and C2 cements were interpreted as marine in origin, deposited early in the diagenetic history, during and just after deposition of the sediments. C2 calcite also includes F2 fractures and calcite around clasts in evaporite solution breccias probably precipitated due to fresh water percolation or meteoric water influence.

C3 calcite for practical purposes includes all calcite cement that postdates D2 replacement dolomite (except C3t and C4). C3 calcite is blocky cement that partially replaces D2 and D3 dolomite, and sometimes also quartz, in fractures and fills remnant porosity (Chapter 4). C3 also fills microfractures in some fault breccias. The timing of C3 differs from C1 and C2 because it postdates D2 dolomite, deposited during deep burial. C3 is separate from C3t that includes twinned calcite cement present mainly in flexural slip fault planes, interpreted as a result of flexural slip during Laramide-age folding of the Cupido Fm.

The last cement, C4 calcite is blocky and clear cement that fills porosity in fractures and was interpreted as a precipitation due to the exposure and dissolution of the carbonate sequence in the SMO. C4 calcite is petrographically indistinguishable from C3 calcite, but can be separated by using isotopic analysis and timing relationships.

Thirty-eight samples for isotopic analyses were selected to span all calcite cements identified (Table 6.7). However, distinguishing C1 calcite from C2 is impossible

using the methodology of this study. I include a few samples of modern travertine for isotopic analysis to correlate isotopic values with water sample values.

ORDER BY LOCALITIES				
Number	Sample Name	delta 13 C per mil (PDB)	delta 18 O per mil (PDB)	Features
Las Palmas				
19	LAPA9C	2.349	-2.214	Fracture cement
22	LaPa8-98 (18 c2)	2.893	-2.35	Fracture cement
20	LAPA9CD1	2.393	-2.356	Fracture cement
9	LaPaNeckA (5c)	2.272	-2.547	Fracture cement
14	LAPA8C	1.433	-2.681	Fracture cement
27	LaPa3-98 (25 r)	3.953	-3.25	Rudist
26	LaPa3-98 (25 m)	3.602	-3.453	Host rock
12	LaPa4-98 SoA (7 r)	3.896	-3.498	Rudists
28	LPa15calc-01(36)	2.240	-4.710	Flexural-slip fault plane
29	LPa14-01 (57)	-0.300	-15.450	Fracture cement
La Escalera				
4	LEsc8H-01 (40)	2.200	-3.120	Anhydrite nodules
5	LEsc9-01 (41)	0.306	-3.316	Fracture cement
1	Esc1-98So (2c)	1.404	-3.749	Fracture cement
8	LEscT2-01 (43)	2.380	-6.270	Fracture cement
6	LEsc13C (42)	-0.810	-13.660	Fault breccia
Los Chorros				
58	O1RM69-01 (50)	-6.37	-9.43	travertine
31	LCh8-98 SoA (16 m)	4.469	-2.467	Host rocks
30	LCh1-98So (14 m)	3.246	-3.771	Host rock
39	LCh4-01 (48c)	3.669	-3.948	Fracture cement

Table 6.7 List of samples by localities, including calcite isotopic composition, and sample origin used in this study from Cupido and Tamaulipas Inferior Formations, SMO. Sample numbers from Table 6.1.

CALCITE				
ORDER BY LOCALITIES				
Number	Sample Name	delta 13 C per mil (PDB)	delta 18 O per mil	Features
Los Chorros				
32	LCh8-98 SoA (16 c1)	2.145	-4.13	Fracture cement
34	LCH1-01 (45)	1.890	-6.510	Fault breccia
35	LCH1B-01 (46)	-4.940	-8.230	travertine
33	LCh8-98 SoA (16 c2)	0.81	-13.306	Fracture cement
38	LCh4-01 (48)	-7.184	-8.445	travertine
Iturbide-Santa Rosa				
46	StR3-98 (9 m)	1.462	-4.625	Host rock
48	StR9-98 (10 m)	2.532	-4.699	Host rock
49	StR9 (11 m)	2.579	-4.734	Host rock
47	StR9-98 SoA (10 c1)	2.789	-5.904	Fracture cement
Potrero García				
41	PG2-01 (29)	1.410	-3.850	Collapse breccia
44	PG4calc-01 (31)	2.560	-4.680	Flexural-slip fault plane
40	PG1-01 (28)	-7.030	-6.460	Anhydrite nodules
45	PG5-01 (32)	-10.750	-7.400	travertine
Cañón Prieto				
54	CP2C-01 (54)	-9.19	-4.965	Anhydrite nodules
52	CP2-01 (53)	-1.850	-5.440	Collapse breccia
50	CP1-01 (52)	-0.950	-5.440	Collapse breccia
Cuatro Ciénegas				
55	CC5-01 (56)	2.519	-19.622	Flexural-slip fault plane
Las Cortinas				
56	LCort1-01 (44)	3.980	-5.920	Flexural-slip fault plane
Molano				
57	01RM69-01 (51)	-0.110	-11.110	Fault breccia

Continuation Table 6.7.

Calcite cement isotope analyses are divided in seven major groups: host rock cement, calcite veins in dolostones and limestones, calcite veins in collapse breccias, calcite from fault gouge breccias, calcite from flexural slip fault planes, calcite replacing anhydrite nodules, and travertines.

Host Rock Cement

Limestone host rock.- Six samples from limestone host rock cements were analyzed from Los Chorros, Las Palmas, and Santa Rosa localities. Limestone host rock samples are composed mainly by C2 calcite or a mixture of C1 and C2 cements from matrix rocks. Host rock shows $\delta^{18}\text{O}$ values that range from -4.734 to -2.467 ‰ and $\delta^{13}\text{C}$ values that range from 1.462 to 4.469 ‰ (Table 6.8). Isotopic values are typical of unaltered marine limestones for the Cretaceous period reported by various authors. Host rock isotope values provide a basis with which to compare other calcite isotope data of this study.

Calcite Cement				
Host rocks				
Locality	Sample Name	Cement Composition	$\delta^{13}\text{C}$ per mil (PDB)	$\delta^{18}\text{O}$ per mil (PDB)
Los Chorros	LCh8-98 SoA (16m)	C1-C2	4.469	-2.467
Las Palmas	LaPa3-98 (25 m)	C1-C2	3.602	-3.453
Los Chorros	LCh1-98So (14 m)	C1-C2	3.246	-3.771
Santa Rosa	StR3-98 (9 m)	C1-C2	1.462	-4.625
Santa Rosa	StR9-98 (10 m)	C1-C2	2.532	-4.699
Santa Rosa	StR9 (11 m)	C1-C2	2.579	-4.734

Table 6.8 Carbon and oxygen isotopic composition of host rocks (matrix cements) from limestones of Cupido Formation, SMO. Location and chemical composition of samples is included. C1, isopachous fringe of fibrous calcite; C2 blocky calcite.

Rudists

As a complement to the host rock samples, two samples of rudists from Las Palmas locality were analyzed. The $\delta^{18}\text{O}$ values range from -3.498 to -3.25 ‰ and $\delta^{13}\text{C}$ values that range from 3.896 to 3.953 ‰ (Table 6.9). Values are typical of unaltered marine limestones for the Cretaceous period and similar to the host rock limestone values.

Calcite Cement				
Rudists				
Locality	Sample Name	Cement Composition	$\delta^{13}\text{C}$ per mil (PDB)	$\delta^{18}\text{O}$ per mil (PDB)
Las Palmas	LaPa3-98 (25 r)	C1-C2	3.953	-3.25
Las Palmas	LaPa4-98SoA(7 r)	C1-C2	3.896	-3.498

Table 6.9 Carbon and oxygen isotopic composition of host rocks from rudists in limestones of Cupido Formation, SMO. Location and chemical composition of samples is included. C1, isopachous fringe of fibrous calcite; C2, blocky calcite.

Fracture Calcite Cements

Twelve calcite fracture cements from Las Palmas, La Escalera, Santa Rosa, Los Chorros, Potrero García and Cañón Prieto localities were sampled (Table 6.10). Two samples were identified as synkinematic C1-C2 calcite cement from F1-F2 fractures, two synkinematic C3 from F5 fractures, one C3t calcite from a F6 fracture. Seven C4 postkinematic calcite samples are from F3, F4 and F5 fractures.

F1-F2 fractures have C1-C2 calcite isotopic composition values ranging from +2.272 ‰ to +3.669 ‰ $\delta^{13}\text{C}$ and from -3.948 ‰ to -2.547 ‰ $\delta^{18}\text{O}$ (Table 6.10). Those values are similar to carbonated host rocks (Table 6.8), and similar to unaltered Cretaceous marine carbonate material, indicating precipitation at low temperatures.

C3 calcite isotopic composition values, from F5 fractures, range from +2.38 ‰ to +2.78 ‰ $\delta^{13}\text{C}$ and from -5.904 ‰ to -6.27 ‰ $\delta^{18}\text{O}$ (Table 6.10). The $\delta^{18}\text{O}$ values are depleted (lower) with respect to Cretaceous marine carbonate material suggesting precipitation at higher temperature than surface. The $\delta^{18}\text{O}$ values are also lower than the host rock isotopic values. These temperatures are inconsistent due probably to contamination of postkinematic C4 calcite.

In contrast, a C3t calcite sample from Los Chorros has an isotopic composition of +0.81 ‰ $\delta^{13}\text{C}$ and -13.3 ‰ $\delta^{18}\text{O}$ (Table 6.10). The $\delta^{18}\text{O}$ value is lower than the host rock isotopic values and depleted with respect to Cretaceous marine carbonate material suggesting precipitation at higher temperature than surface.

C4 calcite cement, from F3, F4 and F5 fractures, ranges from +0.30 ‰ to +2.89 ‰ and from -2.21 ‰ to -4.13 ‰ $\delta^{18}\text{O}$ (Table 6.10). Both the $\delta^{13}\text{C}$ and the $\delta^{18}\text{O}$ values are in general similar to carbonate host rocks. All $\delta^{18}\text{O}$ values are similar to unaltered marine limestones for the Cretaceous period, indicating precipitation at low temperature.

Calcite Cement					
Fracture cements in dolostones and limestones					
Locality	Sample Name Lithology	Cement Composition	Fracture event	$\delta^{13}\text{C}$ per mil (PDB)	$\delta^{18}\text{O}$ per mil (PDB)
Las Palmas	LaPaNeckA (5c) dolostone- boudinage	C1-C2	F1	2.272	-2.547
Los Chorros	LCh4-01 (48c) dolomitized limestone	C2	F2	3.669	-3.948
Santa Rosa	StR9-98 SoA (10 c1) limestone	C3?	F5	2.789	-5.904
La Escalera	LEscT2-01 (43) dolostone	C3	F5	2.38	-6.27
Los Chorros	LCh8-98 SoA (16 c2) dolomitized limestone	C3t	F6	0.81	-13.3
Las Palmas	LAPA-9C dolostone	*C4	F5	2.349	-2.214
Las Palmas	LaPa8-98 (18c2) dolostone	*C4	F3	2.893	-2.35
Las Palmas	LAPA- 9CD1dolostone	*C4	F4	2.393	-2.356
Las Palmas	LAPA-8C dolostone	*C4	F4	1.433	-2.681
La Escalera	LEsc9-01 (41) dolostone	*C4	F4	0.306	-3.316
La Escalera	Esc1-98So (2c) dolostone ^ψ	*C4	F4	1.404	-3.749
Los Chorros	LCh8-98 SoA (16 c1) dolomitized limestone	*C4	F5	2.145	-4.130

Table 6.10. Carbon and oxygen isotopic composition of fracture cements from dolostones and limestones of Cupido Formation, SMO. Location, chemical composition and fracture event of samples is included. *, postkinematic cement; Ψ sinsedimentary breccia.

Flexural Slip Faults

Four calcite flexural slip cements from Potrero García, Las Palmas, Las Cortinas, and Cienegas localities were sampled. All calcite cements found in flexural slip planes (F6 fractures) are considered as “tectonic” calcite. $\delta^{13}\text{C}$ values for tectonic calcite cement composition range from 2.240 ‰ to +3.98 ‰; $\delta^{18}\text{O}$ values range from -4.68 ‰ to -19.62 ‰ (Table 6.11). $\delta^{13}\text{C}$ values in general are similar to the carbonate host rocks. All $\delta^{18}\text{O}$ values are in general lower than the carbonate host rocks and lower than the unaltered marine limestones for the Cretaceous period, indicating precipitation at high temperature.

Calcite Cement					
Fracture slip faults					
Locality	Sample Name Lithology	Cement Composition	Fracture event	$\delta^{13}\text{C}$ per mil (PDB)	$\delta^{18}\text{O}$ per mil (PDB)
Potrero Garcia	PG4 calc-01 (31)	C3t	F6	2.560	-4.680
Las Palmas	LPal5calc-01 (36)	C3t	F6	2.240	-4.710
Las Cortinas	LCort1-01 (44)	C3t	F6	3.980	-5.920
Cienegas	CC5-01 (56)	C3t	F6	2.519	-19.62

Table 6.11. Carbon and oxygen isotopic composition of calcite cements from four samples of flexural-slip fault planes (F6 fractures). Location, chemical composition and fracture event of samples is included. Samples 31 and 36 might have been contaminated with dolomite cement during sampling, because both minerals are present in the flexural-slip fault planes.

Fault Breccias

Three calcite fault breccia cements from La Escalera, Los Chorros, and Molano localities were sampled. All calcite cements were taken from fault breccia planes and they are considered as Ct calcite cement. $\delta^{13}\text{C}$ values for calcite cement composition range from -0.81 ‰ to +1.89 ‰; $\delta^{18}\text{O}$ values range from -6.51 ‰ to -13.66 ‰ (Table 6.12). All $\delta^{18}\text{O}$ values are lower than the unaltered marine limestones for the Cretaceous period, indicating precipitation at high temperatures.

Calcite Cement				
Fault breccias (gouge)				
Locality	Sample Name	Cement Composition	$\delta^{13}\text{C}$ per mil (PDB)	$\delta^{18}\text{O}$ per mil (PDB)
Los Chorros	LCH1-01 (45)	C3t	1.890	-6.510
Molano	01RM69-01 (51)	C3t	-0.11	-11.11
La Escalera	LEsc13C (42)	C3t	-0.810	-13.660

Table 6.12. Carbon and oxygen isotopic composition of calcite cements from fault breccia planes of Cupido Formation, SMO. Location and chemical composition of samples is included.

Calcite in Evaporite Collapse Breccias

Four calcite samples of evaporite collapse breccias from Potrero García, Cañón Prieto, and Las Palmas localities were sampled.

Based on petrographic evidence calcite sampled from collapse breccias at Potrero García and Cañón Prieto can be either C2 or C4 (see Chapter 4). $\delta^{13}\text{C}$ values range from -1.85 ‰ to 1.41 ‰, $\delta^{18}\text{O}$ values range from -5.44 to -3.85 ‰ (Table 6.13). All $\delta^{13}\text{C}$ values are lower than the carbonate host rocks. $\delta^{18}\text{O}$ values are similar to the carbonate host rocks but lower than the unaltered marine limestones for the Cretaceous period.

In contrast, calcite sample of a collapse breccia from Las Palmas locality (close to the Cupido and Cupidito boundary, see Chapter 3) is probably C3t type cement, and this cement fills remnant porosity in that breccia (see Chapter 4). Calcite cement composition has -0.30 ‰ $\delta^{13}\text{C}$ and -15.45 ‰ $\delta^{18}\text{O}$ values (Table 6.13). Both $\delta^{13}\text{C}$ and $\delta^{18}\text{O}$ values are lower than the carbonate host rocks and lower than the unaltered marine limestones for the Cretaceous period, indicating precipitation at high temperature.

Calcite Cement				
Collapse breccias				
Locality	Sample Name	Cement Composition	$\delta^{13}\text{C}$ per mil (PDB)	$\delta^{18}\text{O}$ per mil (PDB)
Potrero García	PG2-01 (29)	Calcite	1.41	-3.85
Cañón Prieto	CP1-01 (52)	Calcite	-0.95	-5.44
Cañón Prieto	CP2-01 (53)	Calcite	-1.85	-5.44
Las Palmas	LPal4-01 (57)	C3t	-0.30	-15.45

Table 6.13. Carbon and oxygen isotopic composition of calcite cements of collapse breccias from Cupido Formation, SMO. Location and chemical composition of samples is included.

Anhydrite Nodules

Three anhydrite nodules replaced by calcite from Potrero García, La Escalera, and Cañón Prieto localities were sampled. Two types of nodules were recognized in the field. Type one are the most abundant and represent anhydrite nodules replaced by white calcite, and usually they form pseudo-layer. Type two nodules are less abundant but they can be recognized because they are light-yellow in color and do not form pseudo-layers. Petrographic analysis suggested that both types nodule cements are a calcite replacement phase. $\delta^{13}\text{C}$ values for calcite cement range from +2.20 to -9.19 ‰; $\delta^{18}\text{O}$ values range from -3.12 to -6.46 ‰ (Table 6.14). $\delta^{13}\text{C}$ values are lower than the carbonate host rocks. All $\delta^{18}\text{O}$ values are lower than the carbonate host rocks and lower than the “least altered” Cretaceous marine carbonate material, indicating precipitation at high temperature.

Calcite Cement				
Anhydrite nodules				
Locality	Sample Name	Cement Composition	$\delta^{13}\text{C}$ per mil (PDB)	$\delta^{18}\text{O}$ per mil (PDB)
La Escalera	LEsc8H-01 (40) ^φ	Calcite	2.200	-3.120
Cañón Prieto	CP2C-01 (54) ^ψ	Calcite	-9.19	-4.965
Potrero García	PG1-01 (28) ^ψ	Calcite	-7.030	-6.460

Table 6.14. Carbon and oxygen isotopic composition of calcite cements from anhydrite nodule samples. Location and chemical composition of samples is included. ^ψ type one, white anhydrite nodule; ^φ type two, light-yellow nodule.

Travertine

Four travertine samples from Los Chorros and Potrero García localities were analyzed. $\delta^{13}\text{C}$ values range from -10.750 to -4.940 ‰. Values of $\delta^{18}\text{O}$ from -7.40 to -9.43 ‰ are lower than the carbonate host rocks (Table 6.15). The relatively low $\delta^{18}\text{O}$ values are consistent with travertine formation from fluids of meteoric origin. Temperature calculations from meteoric water values vary from 27 °C to 37 °C. These temperatures and the lower $\delta^{18}\text{O}$ values of the travertine deposits are consistent with meteoric fluids having lower $\delta^{18}\text{O}$ values at higher elevations.

Calcite Cement					
Travertine					
Locality	Sample Name	Cement Composition	$\delta^{13}\text{C}$ per mil (PDB)	$\delta^{18}\text{O}$ per mil (PDB)	T of formation (°C)
Los Chorros	01RM137A-01(50)	Travertine	-6.37	-9.43	27.07
Los Chorros	LCh4-01 (48)	Travertine	-7.184	-8.445	31.91
Los Chorros	LCH1B-01 (46)	Travertine	-4.94	-8.23	33.00
Potrero García	PG5-01 (32)	Travertine	-10.75	-7.40	37.33

Table 6.15. Carbon and oxygen isotopic composition of calcite cements of travertine samples from Los Chorros and Potrero García localities.

CALCITE ISOTOPIC CHARACTERIZATION

Figure 6.5 shows a cross-plot of oxygen and carbon isotopic composition of the thirty-eight calcite cements analyzed from the Cupido Formation. Based on their isotopic composition six groups were identified.

Group C1-C2 includes calcite from all host rocks and rudist samples. One calcitized nodule (type one) also is part of this subgroup. This group has in general the lightest $\delta^{18}\text{O}$ values in these rocks, varying from -2 to -4.5 ‰ PDB. C1 and C2 calcites are the dominant cements of this group.

Group C3 includes two samples from calcite fracture cements, one from a flexural-slip plane, and one from a fault breccia. C3 calcite is the main cement in this group, clearly separate from other cements.

Group C4 includes mainly calcite from fracture cements. This group has also in general the lightest $\delta^{18}\text{O}$ values in these rocks, varying from -2 to -4 ‰ PDB. C4 calcites are the dominant cements of this group.

Group C2-C4 corresponds to collapse breccias material and these samples have moderate $\delta^{18}\text{O}$ values (-4 to -6‰). Calcite from these collapse breccias can be either C2 or C4. However, due to the small quantity of samples this group probably is not representative of all collapse breccias identified in the study area. Values of $\delta^{13}\text{C}$ ‰ vary from -2 to 1.5 ‰.

Group C3t subgroup includes two fault breccia cements, one sample from fracture cement, one from a collapse breccia, and one from flexural slip plane. All calcite is considered as tectonic cement (C3t), and correspond with the heaviest isotopic composition. The fracture cement sample corresponds to a postkinematic cement filling remnant porosity and comes from a dolomitized limestone of Los Chorros locality

(LCh8-98; 16c2), and it is the heaviest isotopic composition of fracture cements in this study. The collapse breccia sample has heavier isotopic composition than group C2-C4, with a $\delta^{18}\text{O}$ value of 15.5 ‰. This breccia from Cañón de Las Palmas probably is partially recrystallized. Calcite crystals alone were taken for isotopic analysis from this breccia in order to avoid destruction of the outcrop. This breccia is one of the best examples of collapse breccias in these outcrops. The flexural slip plane calcite (C3t) sample has the heaviest composition of all analyzed samples in this study. This sample comes from the Cienegas locality.

Finally, a group of modern travertines is separated from other groups and includes two calcitized nodules (type one). Because type one nodules share a similar isotopic signature with modern travertine, they are interpreted as former type one anhydrite nodules that were replaced by calcite cement. However, type two nodules are different: one sample from La Escalera locality falls in the region of most fracture cement (group C1-C2) (Fig. 6.5).

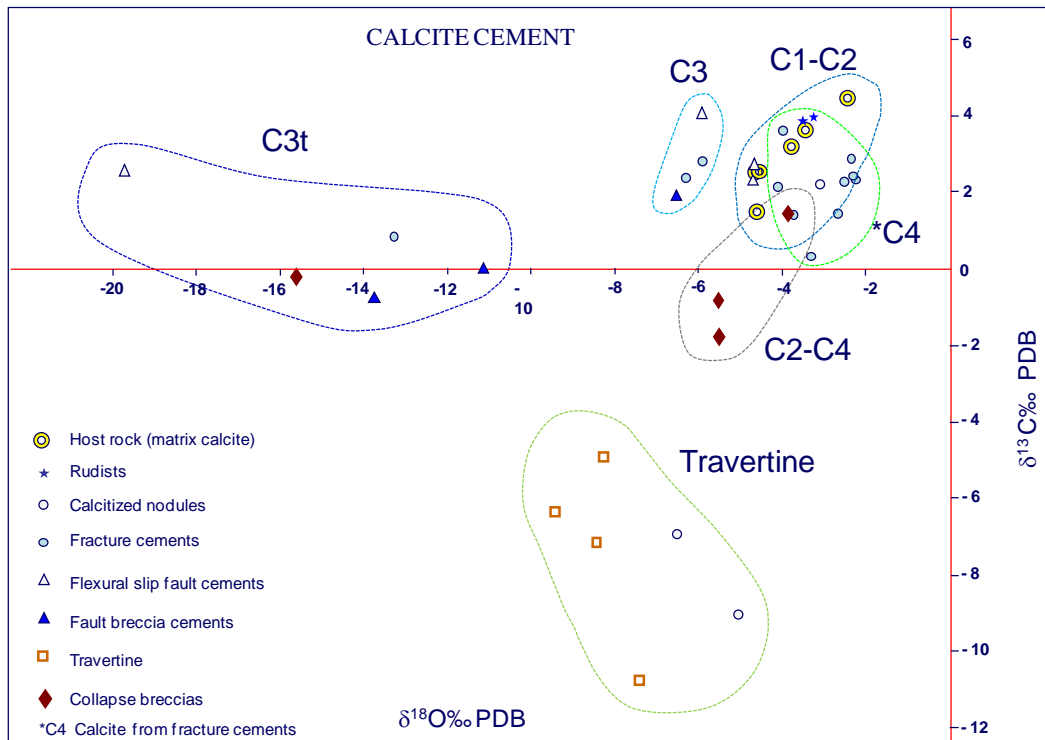


Fig. 6.5. Cross-plot of oxygen and carbon isotopic composition of calcite cements from the Cupido and Tamaulipas Inferior Formations. Six different groups of calcite cements can be differentiated: Group C1-C2 calcite includes rudists, host rocks, calcitized nodules (type one). *C4 calcite group are fracture cements; Group C3 includes two samples from fracture calcite cements, one from a flexural-slip plane, and one fault breccia. Group C2-C4 includes mainly collapse breccia cements; Group C3t includes calcite cement from fault breccia cements, two samples of flexural slip plane and one fracture cement; Group of modern travertine includes also calcitized nodules (type two). The collapse breccia sample from Palmas, with $\delta^{18}\text{O}$ value of -15.5 falls out of its group (C2-C4) probably due to partial recrystallization. Notice all $\delta^{18}\text{O}$ values of groups C2-C4, C3, and C3t are lower than -2.3 ‰ (unaltered marine limestones for the Cretaceous period). Isotopic values are in million (‰) PDB (Peedee Formation Belemnite standard).

Meteoric Water Analyses

Two measurements of meteoric water samples from the Los Chorros locality were analyzed. $\delta^{18}\text{O}$ values range from -38.64 ‰ to -38.66 ‰ (Table 6.16). Those values were used to constrain travertine precipitation temperature.

Meteoric Water				
Locality	Sample Name	Composition	$\delta^{13}\text{C}$ per mil (PDB)	$\delta^{18}\text{O}$ per mil (PDB)
Los Chorros	01RM 136 A	Water	-	-38.641
Los Chorros	01RM 136 A	Water	-	-38.661

Table 6.16. Oxygen isotopic composition of meteoric water from spring at the Los Chorros locality, SMO.

STABLE ISOTOPE ANALYSIS AND FRACTURE DEVELOPMENT

Field observations and petrographic studies of crosscutting relations and fracture-fill mineralogy demonstrate six main fracture events in the Cupido Formation in the Monterrey Salient (see Chapters 4 and 5). Carbon and oxygen isotopes were measured in fracture dolomite cement samples for each fracture event identified from different localities in the study areas. Synkinematic and postkinematic cements were distinguished and analyzed separately. Dolomite is synkinematic with respect to F3 and F4 fractures and therefore its origin is related to fracture development. Postkinematic calcite cements were also sampled in order to evaluate the role of postkinematic cementation in fracture development and preservation of fracture porosity. Calcite currently present in the study area is likely postkinematic with respect to F3 through F6 fractures, within which this cement is found.

F1-F2 fractures are characterized by veins with C2 synkinematic calcite. These fractures were found associated with evaporate solution collapse breccias and differential compaction boudinage structures as well. A few samples from F1-F2 fractures were analyzed: a calcite sample from Los Chorros (LCh4-01, 48c) and two dolomite samples from Las Palmas (LaPaNeckB, 20d; LaPaNeckA, 5d). The calcite isotopic composition has a $\delta^{13}\text{C}$ value of +3.669 ‰ (PDB) and $\delta^{18}\text{O}$ of -3.948 ‰. If we consider that synkinematic calcite was precipitated at the same time as fracture development, then the isotopic results confirm that F1-F2 fractures developed at temperatures from near-surface meteoric to shallow burial, early in the history of the Cupido Fm.

Minor dolomite contemporaneous with D1 cement is also associated with the F1 fractures in boudinage structures. $\delta^{13}\text{C}$ values for this D1 dolomite range from +1.883 to +2.950‰ (PDB) and the $\delta^{18}\text{O}$ values range from -1.001 ‰ to -1.600 ‰ at Las Palmas

locality. These values fall in the “most low temperature dolomite” field (Fig. 6.3) established by Allan and Wiggins (1993), indicating dolomite precipitation at low temperature. $\delta^{18}\text{O}$ values for D1 dolomite fall in the “Least-altered Marine Invertebrates and Marine Cements” field (Fig. 6.4), also indicating precipitation at low temperature. The isotopic signatures indicate D1 dolomite could have formed either at the surface or during shallow burial time, and before D2 regional dolomitization took place, which is consistent with petrographic observations (Chapter 4). Therefore F1-F2 fractures are interpreted as related to near-surface processes (exposure surfaces, karst, and shallow burial).

The F3 fractures are characterized by fractures with irregular or jagged paths with synkinematic D2 dolomite and postkinematic calcite cement. F3 fractures are the most abundant at both Las Palmas and La Escalera localities, and they are developed preferentially in dolostone layers. Bridges of fibrous dolomite in these fractures has similar petrographic characteristics to D2 regional dolomite (Chapter 4). Two samples from Las Palmas locality (LaPa8-98; 18 d2 and LAPA-8CD) were taken for isotopic analysis. D2 dolomite composition $\delta^{18}\text{C}$ ranges from +3.432 to + 3.029 ‰ (PDB) and the $\delta^{18}\text{O}$ values range from -2.847 to -2.313 ‰, at Las Palmas locality, and fall in the most low temperature dolomite field (Fig. 6.3) established by Allan and Wiggins (1993), indicating dolomite precipitation at low temperature. $\delta^{18}\text{O}$ D2 dolomite value falls in the Cretaceous marine carbonate field (Fig. 6.4), indicating also precipitation at low temperature. The isotopic signature indicates dolomite precipitation at moderate to low temperatures in shallow burial conditions, supporting the idea that F3 fractures were developed synchronously with the D2 regional dolomitization.

F4 fractures are characterized by low aspect ratio (length/width), straight paths, and synkinematic and large fibrous baroque dolomite crystals (D3). Calcite and a minor percent of quartz are present mainly as postkinematic cements. D3 synkinematic baroque dolomite from F4 fractures were sampled at Las Palmas and La Escalera localities. F4 fractures cross-cut D2 dolomite, indicating that F4 fractures postdate D2 regional dolomite. $\delta^{13}\text{C}$ values for fracture D3 dolomite range from to +1.597 to +2.695 ‰ (PDB), and the $\delta^{18}\text{O}$ values range from -2.631 ‰ to -4.506 ‰. These values fall in the “overlap between low and high temperature dolomite” field (Fig. 6.3) established by Allan and Wiggins (1993). However, values of D3 baroque dolomite are depleted in $\delta^{18}\text{O}$, and fall to the left of the Cretaceous marine carbonate field (Fig. 6.4), indicating precipitation at elevated temperature. The isotopic values support the idea that D3 baroque dolomite precipitated in moderate to deep burial conditions, after D2 regional dolomitization.

F5 fractures include fractures characterized by synkinematic C3 calcite cement. These fractures were found in limestone and partially dolomitized rocks at Santa Rosa, Los Chorros, Las Palmas, and La Escalera localities. F5 fracture morphology generally is long and very narrow. Incomplete and irregular baroque dolomite crystal borders overlapped by calcite, corroded dolomite crystals, and broken dolomite crystals are evidence that F5 postdates D3 baroque dolomite and therefore postdates also F4 fractures (see Chapters 4 and 5). C3 calcite is synkinematic with respect to F5 fractures and was sampled in Santa Rosa and La Escalera localities. $\delta^{13}\text{C}$ values for C3 calcite cement composition range from +2.38 ‰ to +2.79 ‰; $\delta^{18}\text{O}$ values range from -6.27 ‰ to -5.90 ‰ $\delta^{13}\text{C}$. All $\delta^{18}\text{O}$ values are in general lower than the carbonate host rocks and lower than the “least altered” Cretaceous marine carbonate material, indicating precipitation at high

temperature. Isotopic values indicate C3 calcite precipitated in moderate burial conditions, after D3 dolomitization.

F6 fractures are mainly flexural slip fault planes developed along stratigraphic horizons or at the boundaries of mechanical layers (Chapter 4 and 5). F6 fractures are characterized mainly by thick fibrous and twinned C3t calcite cement. Flexural slip cements were sampled at Las Palmas, Las Cortinas, Potrero García and Cienegas localities. $\delta^{13}\text{C}$ values for C3t calcite cement range from 2.240 ‰ to +3.98 ‰; $\delta^{18}\text{O}$ values range from -4.68 ‰ to -19.62 ‰. All $\delta^{18}\text{O}$ values are in general lower than the carbonate host rocks and lower than “least altered” Cretaceous marine carbonate material, indicating precipitation at high temperature.

Camerlo (1998) analyzed calcite twins in samples collected in the San Blas (Cañón Boquilla Corral de Palmas) and San Juan Bautista anticlines in the SMO, interpreted as formed at temperatures lower than 200°C. The temperature range suggests precipitation during shallow to deep burial conditions. This interpretation is consistent with burial and thermal histories, and timing of tectonic folding inferred for the SMO from fluid inclusions and thermochronology (Pottorf et al., 1997, Gray, 2001, Gray, 2011), which suggests that rocks of the Sierra el Abra, part of the SMO, reached maximum temperature of 170 °C during burial of approximately 5 km.

A few samples (e.g. Potrero Garcia) of baroque D3 dolomite were found as cement in F6 fractures, indicating precipitation of D3 at least during early tectonic time. D3 dolomite cement from a flexural slip plane at Potrero García has $\delta^{13}\text{C}$ value of +2.240 ‰ and a $\delta^{18}\text{O}$ value of -5.149 ‰. $\delta^{18}\text{O}$ value is lower than the carbonate host rocks, and lower than the “least altered” Cretaceous marine carbonate material, indicating precipitation at high temperature and deep burial conditions for F6 faults development.

PARAGENETIC SEQUENCE AND FRACTURE TIMING INTERPRETATION

Table 6.17 shows the regional paragenetic sequence established, for the Cupido Formation in the Monterrey Salient, in Chapter 5 (Fig. 5.4). This table summarizes diagenetic assemblages and processes, the approximate timing of occurrence of each diagenetic event, and the different inferred diagenetic stages. Ranges of temperatures of precipitation for dolomite and calcite cements are speculative; they are inferred based on published data (e.g. Moldovanyi and Lohmann, 1984; Aulstead, et al., 1987; Hardie, 1987; Minero, 1988; Warren, 2000; Lefticariu, L., 2004; Guzzy-Arredondo, et al., 2007). Baroque dolomite precipitates at wide range of temperatures, however dolomite that tend to be sparry and nonplanar with saddle morphologies forms at temperatures > 50 °C (Warren, 2000). Temperatures of precipitation for quartz cement are also based on published data (e.g. Primmer, et al., 1997; Newel and Goldstein, 1999; Leigh, 2011). Estimation of maximum burial temperature indicates quartz cements precipitate over a wide range of burial temperatures, although fluid inclusions studies suggest that minimum temperatures of 75 °C are usually required for precipitation (Primmer, et al., 1997). Relative fracture timing relationships were established based on crosscutting relationships between fracture sets and with other diagenetic processes, type of cements and general characteristics like morphology.

The interpretation of paragenetic sequence (Table 6.17) indicates that fractures from F1 and F2 originated at shallow burial depths, early in the diagenetic history, contemporaneous with evaporites dissolution and breccia development.

Thermal and thermochronological data from the SMO indicate that a foreland basin formed on the leading edge of the fold belt during and after the late stages of the Laramide orogeny (Pottorf et al., 1997). This basin appears to have been at least 4 km

thick by 50 Ma and to have reached maximum temperatures of 165 to 170 °C under 5 to 7 km of burial (Pottorf et al., 1997). Consequently, the thermal gradient in the SMO can be estimated in approximately 23 °C/km, assuming 30 °C as the surface temperature.

F3 fractures (fracture set W) developed contemporaneously with regional D2 dolomitization, in moderate burial conditions. Fluid inclusions in similar dolomites indicate precipitation between 50 to 60 °C (e.g. Warren, 2000). Considering the estimated thermal gradient, F3 fractures developed at 0.8 to 1.4 km depth. Therefore, F3 fractures (fracture set W) developed at moderate burial conditions.

F4 fractures (fracture set X) contain synkinematic baroque D3dolomite cement, this type of dolomite precipitate at temperature range between 60 to 150 °C (e.g. Warren, 2000). F4 probably originated when the Cupido Formation was from 1.4 to 4.8 km depth, under deep burial conditions.

F5 fractures (fracture set Y) also originated under deep burial conditions but before quartz cementation (which is found associated with tectonic stylolites). Assuming the same geothermal gradient for the study areas, the quartz identified as postkinematic cement in F5 fractures precipitated at about 75-200 °C, implying that F5 fractures probably originated in a range of 2.0 to more than 6 km deep. A maximum depth of 5.2 km was calculated by Moldovanyi and Lohmann (1984), based on petrographic and stable isotopic analyses of cements of the Cupido and Sligo Formations in northeastern Mexico and in South Texas, respectively.

Finally, F6 fractures, with C3t calcite precipitated at temperature of about 150 °C, originated during folding of the SMO probably at depth of about 4.8 km.

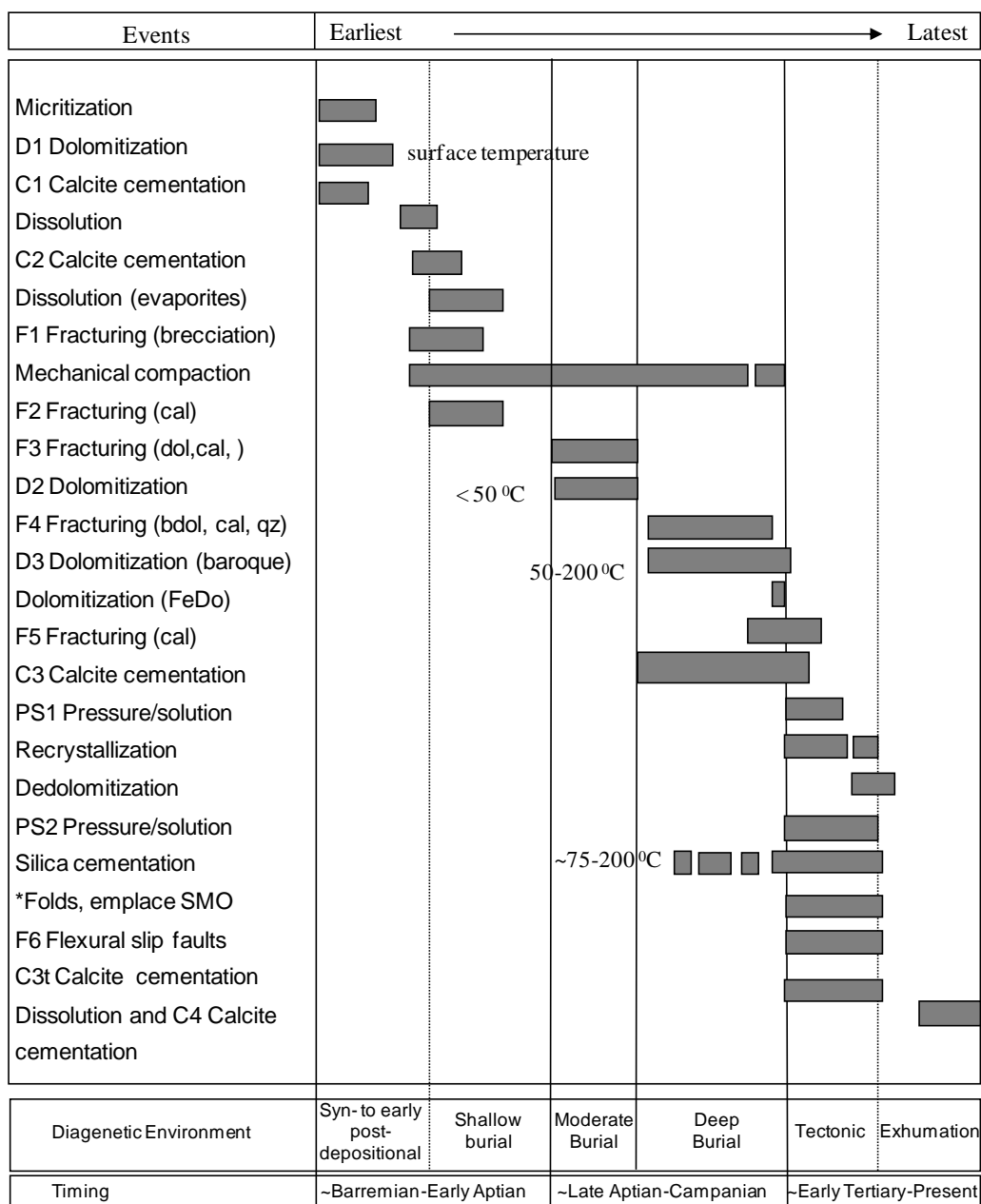


Table 6.17. Generalized paragenetic sequence, relative duration of diagenetic events and inferred diagenetic stages. Bars represent diagenetic processes, including fracture events and main cement stages. Relative timing is from cement and fracture overlapping and crosscutting relations. Absolute start-stop times are conjectural. Temperatures of precipitation for calcite, dolomite and quartz cements are inferred from published data of the precipitation conditions of these cements.

FRACTURE ORIGINS BASED ON ISOTOPIC RESULTS

Fracture timing was interpreted based on cross-cutting relationships among fractures sets, and with other diagenetic processes. Isotopic results agree with prediction from the paragenetic sequence and timing of fracture sets, and give us important information about the origin of the fracture cements and therefore of fracture development in the carbonate sequence of Cupido Formation.

F1 through F6 fractures are filled with dolomite and calcite cements. Dolomite is the main synkinematic cement in the most abundant fractures (F3 and F4 fractures). Consequently, dolomite isotopic values are important to interpret fracture origins and development in these rocks. Calcite is postkinematic cement in F3 and F4 fractures, and its isotopic values are also important if it assume simple progressive burial for pre-Laramide history.

D2 and D3 dolomites are the main synkinematic cements in F3 and F4 fractures, respectively. Dolomite within F3 fractures has similar petrographic characteristics to D2 dolomite that replaces matrix in host rocks (dolostones), and for these reasons it is difficult to distinguish these fractures at outcrop scales. D2 replacement phase dolomite is the most abundant cement in the area, and the isotopic values from host rocks support the interpretation of a reflux model for D2 dolomite origin. Its general distribution in the Monterey Salient (Chapter 4) corroborates that this dolomitization took place at a regional scale. I interpret F3 fractures, with synkinematic D2 dolomite, to have developed while this dolomitization took place in the Cupido Formation rocks, during shallow burial conditions.

Synkinematic D3 dolomite within F4 fractures has euhedral to subhedral equant to saddle-shaped crystals, locally having undulatory extinction. These attributes are

qualitative indications of elevated precipitation temperatures (Gregg and Sibley, 1984). According to that analysis, below some critical temperature (~50 °C), called the critical roughening temperature, dolomite crystal growth produces dominantly euhedral crystals, whereas above that temperature subhedral and distorted saddle-shaped crystals are formed. Such crystal morphologies are found in water-filled horizons in the depth range of oil-window diagenesis (~100 to 140 °C). Elevated temperatures during burial favor dolomite precipitation, both by removing kinetic barriers and by raising the Ca/Mg ratio at which dolomite can precipitate (Allan and Wiggins, 1993). Based on the petrographic characteristics and corroborated with the isotopic values, the origin of synkinematic baroque dolomite, and therefore the F4 fractures, likely reflects such conditions. Thus, D2 and D3 are probable related to progressive burial of the strata of the Cupido Formation, and increasingly high temperatures, but nevertheless likely predated Laramide-age tectonics and fold-related shortening.

In fact, the general dolomite isotopic pattern shown in Fig. 6.3 is consistent with increasing temperatures of dolomite precipitation during progressive burial and a marine or basinal-brine-dominated burial diagenetic model. A trend to lighter values of dolomite cement is visible from F1 to F6 fracture-filling dolomite, passing through isotopic values from matrix cement. A similar trend is also visible from D1 to D3 dolomite isotopic values (Fig. 6.3). Values for these fracture-filling dolomites varying in this fashion suggest evolution of fluids from original marine composition and increasing temperature of dolomite precipitation during progressive burial.

In addition, C3 and C4 postkinematic calcite cement volume is also important in interpreting F3-F6 fractures. Consequently, preexisting F1- F2 fractures probably formed at comparable temperatures and depths, or at even shallower conditions. C3t calcite

contains twins and it was identified mainly in flexural slip planes (F6 fractures). Isotopic values indicate C3t calcite precipitation at higher temperatures, given the position of these cements in the relative sequence of events these conditions probably occurred during Laramide-age deformation of the SMO.

C4 calcite is the most abundant cement in F3-F6 fractures. The isotopic compositions of C4 calcite suggest precipitation from cool waters. Crosscutting and overlapping relations identified in thin section and in the field, demonstrates that most of the C4 calcite cement postdates dolomite cements (D1, D2 and D3). C4 calcite cement occluded remnant pore space in most fractures, especially in the formerly porous F3 and F4 fractures. The high relative abundance of this late calcite cement with respect to dolomite in fractures from events F3 and F4 indicates remnant fracture porosity prior to calcite cementation was very high (by measurement, in some cases more than 50%). Petrographic evidence such as calcite filling spaces between dolomite crystals and replacing dolomite shows that calcite is postkinematic, and so must have precipitated in fractures after the time of fracture formation. C4 calcite isotopic values, and other features suggestive of post-depositional deformation, suggest that much calcite cement in F3 through F6 fractures records fluids and temperature conditions that existed after the fractures formed, possibly during exhumation and breaching of the SMO folds when cool fluids may have had access through the open fracture networks.

Table 6.18 summarizes fracture events identified in the Cupido Formation and their main cementation phases, indicating the fracture sets and isotopic composition of samples, probable origin conditions and timing of fractures, and the estimated abundance or proportion in the area. Regional fracture sets (defined in Chapter 5) are included for correlation. Notice that most of the fractures, around 80%, developed during shallow to

progressively deeper burial conditions before folding of the SMO. In the sense that fold-related fractures are ‘tectonic’ (Nelson, 1985) most of the fractures in this area are pre-tectonic.

Local Events Identified	Regional Sets Ψ	Synkinematic ∇ Cements	Postkinematic ∇ Cements	Diagenetic Environment (Stage)	Isotopic Data (Samples)	Loading Conditions	Proportion of total fracture Population
F1	Not measured	C1	C2/ D1	Syn-Post-depositional	C1-C2, D1	Burial & surface exposure	~10%
F2	Not measured	C2	D2	Deep Burial \uparrow Shallow Burial	C2	Basin-ward extension and vertical loading	~80%
F3	W	D2	C3, D3, C4		D2-D3		
F4	X	D3	C3, Qz, C4		D3, C4		
F5	Y	C3	C4, qz		C3, C4		
F6	Z	C3t	C4	Burial Tectonic	C3t	Folding	~10%

Table 6.18. Fracture events identified in the Monterrey Salient, SMO and their main characteristics. Location and isotopic composition of samples is shown. Regional fracture sets are included for correlation. Sets and cements were distinguished by fracture crosscutting relations. Fracture set orientation varies from one locality to another. D1, syn-sedimentary dolomite; D2, dolomite replacement phase; D3, baroque dolomite; C1-C2 early calcite; C3 burial calcite cement; C4 calcite cement; Ψ From Ortega and Marrett (2001) and Ortega (2002); ∇ in fractures and host rocks.

DISCUSSION

Burial diagenesis of platform carbonates can be a complex process spanning tens of millions of years, occurring in a range of tectonic settings, and involving waters of diverse origins and compositions (Moore, 1989; Choquette and James, 1990). In this isotopic study I assumed values for seawater and original marine carbonate composition for Lower Cretaceous time based on published accounts for the SMO and other Cretaceous and Tertiary fold-thrust belts in North America, and other places (Moldovanyi and Lohmann, 1984; Budai and Wiltschko, 1987; Allan and Wiggins, 1993). Although fluid flow and fluid compositions in the SMO are undoubtedly more complex, my simple assumptions are suitable for the comparative purposes of this study. D3, C3 and C3t synkinematic cements, and C4 late postkinematic calcite with respect to F3 to F6 fractures are the most abundant host rock and fracture-filling cements in the Monterrey Salient area. Synkinematic D3 baroque dolomite $\delta^{13}\text{C}$ values range from 0.832 ‰ to 2.695 ‰ and $\delta^{18}\text{O}$ values range from -2.631 ‰ to -6.59 ‰ (Table 6.4). Allan and Wiggins (1993) found a range of temperature of 80 to 90°C from fluid inclusions in similar baroque dolomites. Thus, it is consistent with the mainly equant shapes of dolomite crystals observed lining fracture walls. However, stability fields of ordered dolomite, calcite and magnesite as a function of temperature and Ca/Mg molar ratio shows that above about 60-70 °C, most sedimentary formation waters are capable of dolomitizing limestones, whereas at surface temperatures, lower Ca/Mg ratios may be required (Hardie, 1987). In addition, isotopic composition of D3 dolomite is depleted in $\delta^{18}\text{O}$ with respect to Cretaceous marine carbonate material, indicating precipitation at high temperatures.

In general, D3 dolomite isotopic values of the Cupido Formation are most similar to the fourth stage cement of Moldovanyi and Lohmann (1984). The fourth stage cement is the latest event recorded in subsurface rocks of the Sligo Formation, and it was formed at high temperature under conditions of deep burial where Laramide-age tectonic folding did not occur. Although D3 temperatures are lower than the highest experienced by the Cupido Formation in my study (which likely reached temperature levels of gas-window diagenesis, 140 to 200 °C or more, based on unpublished industry reports and Pottorf et al., 1997; Laubach and Ward, 2006), subsequent Laramide-age deformation probably can account for the difference between Sligo and Cupido Formations.

Pottorf et al., (1997), based on fluid inclusions, suggest that rocks of the Sierra el Abra, part of the SMO, reached a maximum temperature of 170 °C, a value that implies a temperature (geothermal) gradient of 23 °C/km. This maximum temperature post-dates folding (Gray et al., 2001). Assuming this geothermal gradient, D3 dolomite precipitated between depths of ~1.4 to ~4.8 km, shallower than the maximum burial depth of more than 5 km that has been inferred for this part of the SMO based on structural restoration, vitrinite reflectance and other data (unpublished industry reports; Marrett, 2001).

In addition, $\delta^{13}\text{C}$ values for synkinematic calcite cement (C3) range from +2.38 ‰ to +2.79 ‰ (PDB); $\delta^{18}\text{O}$ values range from -6.27 ‰ to -5.90 ‰, and this is the main cement in subgroup C3 (Fig. 6.5), clearly separate from other cements. Isotopic composition of the C3 calcite is clearly different than other calcite cements in these rocks. Furthermore, $\delta^{13}\text{C}$ values from postkinematic C4 calcite (relative to F3, F4 and F5 fractures), ranges from +0.30 ‰ to +2.89 ‰ and from -2.21 ‰ to -4.13 ‰ of $\delta^{18}\text{O}$ (Table 6.9), indicating precipitation at low temperatures from the surface to the first hundred meters of depth.

In addition, crosscutting and overlapping relations, identified in thin section and in the field, demonstrate that C3 and C4 calcite cements postdates D3 dolomite cement. Petrographic evidence and paragenetic sequence analysis also suggests C3 and C4 calcite cements are late diagenetic events in the history of these rocks. One interpretation is that most of C3 and C4 calcite cement precipitated before or perhaps after folding, probably during the uplift of the SMO.

Finally, all C3t calcite from flexural slip planes in the SMO could coincide with the end of the third stage of cementation reported by Minero (1988). This author associated the third stage of cementation with Laramide-age deformation and development of karst during the Cenozoic.

The overall history of the SMO is one of progressively deeper burial and subsequent unroofing and exposure. The isotopic composition behavior found from the earliest (D1) to the latest (D3) dolomite cements display a progressive trend toward lower $\delta^{18}\text{O}$ values and also from F1 to F6 passing through matrix cement, supporting the idea of evolution of fluids from original marine composition and increasing temperatures of dolomite precipitation during progressive burial. The interpretation of the origin of these synkinematic dolomites is that they formed during shallow to deep burial conditions as a progressive event, implying that fractures were in place prior to deepest burial of the SMO, that is, before folding commenced. Thus, the hypothesis of Marrett and Laubach (2001) is supported by the isotopic data presented here.

CONCLUSIONS

Field, petrographic, and stable isotope studies link authigenic dolomite and calcite to fracture history. Dolomite precipitation is associated with formation of the large majority of fractures in the Cupido Formation. It mostly occurs as a fracture-occluding phase in the smallest fractures (<0.5 mm kinematic aperture), but bridges larger fractures. Over the history of the SMO, dolomite therefore will tend to preserve fracture porosity by propping fractures open during progressive burial or deformation. D1 and D2 dolomite isotopic values are typical of unaltered marine dolostones for the Cretaceous period, and support in part the origin of both D1 (syndimentary) and D2 dolomites (reflux replacement phase). Isotopic values from D3 support its origin as baroque dolomite in burial conditions. All isotopic values of D3 dolomites are depleted in $\delta^{18}\text{O}$, indicating precipitation at elevated temperature and suggesting a late burial origin for D3 dolomite. Different isotopic composition between baroque and replacement dolomite suggests they probably formed from the same fluid but precipitated at different temperatures.

Calcite, in contrast to dolomite, mostly fills fractures as a late, postkinematic phase. Except for the youngest, fold-related fracture set, conditions of calcite precipitation are not necessarily indicative of conditions of fracture formation. Stable isotope results for calcite might indicate precipitation from relatively cool waters. Calcite is principally responsible for destroying both fracture and host-rock porosity in the Cupido Formation.

The latest calcite cements C3 and C4 occluded remnant pore space in most fractures, especially in the formerly porous last-formed fractures. Based on relative abundance of late, syn- or post-folding postkinematic calcite cement, it is inferred that fracture porosity was very high until late calcite cementation took place. For fractures,

petrographic evidence such as calcite filling spaces between dolomite crystals and replacing dolomite shows that calcite is postkinematic, and so could have precipitated in fractures after the time of fracture formation. With the exception of C3t calcite found in flexural slip planes associated with deformation of the SMO, much calcite cement in F3 through F6 fractures records fluids and temperature conditions that existed after the fractures formed, possibly during exhumation and breaching of the SMO folds.

Late calcite playing similar destructive roles in dolomite reservoirs is known from unpublished results from domestic U.S. reservoirs and elsewhere (Gale et al., 2004; Gale and Gomez, 2007). To the extent that the well-exposed fractures and associated diagenesis of the SMO can illuminate controls on late calcite distribution, this area could be a guide to patterns of reservoir quality in petroleum-bearing basins. The results suggest that pervasive occlusion of fracture pore space could cause major damage to fractured reservoir quality.

This study demonstrates results consistent with early, relatively shallow (but possibly progressively deepening) formation of some dolomite, prior to folding, whereas much of the calcite cement currently found in fractures formed late, possibly after folding. Interpretations and results of this study are consistent with burial and thermal histories and timing of tectonic folding inferred for the SMO from fluid inclusion and thermochronology results (Pottorf et al., 1997; Gray et al., 2001). This study shows that isotopic analyses need to account for the timing of cement deposit accumulation; synkinematic and postkinematic cements can form at very different times within the fracture system, and only if the relative timing of the cements is known can isotopic results be reliably applied to understanding the evolution of the system. These relationships are important to characterize a fractured carbonate reservoir using

subsurface data (cores and well logs). We can apply this methodology to characterize fracture cements, to interpret fracture genesis, and to find relationships between fracture and diagenesis, in order to predict conductive fracture sets in oil and gas reservoirs.

Appendices

Paper copy of this Dissertation is kept at the Geology Library, Jackson School of Geosciences, The University of Texas at Austin.

Outcrop samples are kept by my Supervisor Dr. Randall Marrett in the Jackson School of Geosciences, The University of Texas at Austin.

APPENDIX 2.1- TYPE SECTIONS OF THE CUPIDO AND TAMAULIPAS INFERIOR FORMATIONS AT FOUR LOCALITIES INCLUDED IN THIS STUDY FROM THE MONTERREY SALIENT, SIERRA MADRE ORIENTAL, MEXICO.

More than 900 m of stratigraphic column were measured in the field as part of this study to provide a stratigraphic context for layers studied in detail. Stratigraphic columns were measured, using a tape and compass, in the following localities: Cañón de los Chorros, Cañón la Escalera, and Cañón Santa Rosa. Additionally, a stratigraphic column of Cañón Boquilla Corral de Palmas from Ortega (2002) is used in this study as context for the diagenetic and structural data collected. Bed thicknesses, lithology, sedimentary facies, and structural features were described in the field. Sampled beds numbers for this study are indicated in the stratigraphic columns. Plates I to IV included in Chapter 2 are type sections of the Cupido, and Tamaulipas Inferior Formation at the study localities.

APPENDIX 3.1 – LIST OF SEDIMENTOLOGIC AND STRUCTURAL CHARACTERISTICS OF CARBONATE BEDS INCLUDED IN THIS STUDY

The following are field description for each carbonate bed included in this study by localities. Note that orientation of each bed is included. Location of each bed is indicated in the stratigraphic columns (Appendix 2.1).

Appendix 3.1 Bed information. Field-based descriptions

Locality	*Bed Number	Thickness (cm)	Lithology	Original Texture (Dunham, 1962)	Sedimentary Environment	Orientation (strike, dip) (degrees)
Los Chorros	1	81.3	Limestone	Grainstone	Shoals	66, 65
Los Chorros	2	66.0	Limestone	Packstone	Shoals	66, 75
Los Chorros	3	12.7	Limestone	Grainstone	Shoals	72, 69
Los Chorros	4	17.8	Limestone	Wackestone/ Packstone	Lagoonal	65, 68
Los Chorros	5	88.9	Limestone	Boundstone	Reef	75, 64
Los Chorros	6	71.1	Dolostone	Boundstone	Reef	68, 75
Los Chorros	7	25.4	Limestone	Grainstone	Shoals	68, 63
Los Chorros	8	38.1	Dolostone	Grainstone/ Packstone	Shoals	72, 74
La Escalera	1	76.2	Dolomitized Breccia	Breccia	Fore-reef	288, 85
La Escalera	2	25.0	Dolostone	Mudstone/ Wackestone	Lagoonal	295, 83
La Escalera	3	8.2	Dolostone	Mudstone	Lagoonal	290, 83
La Escalera	4	83.8	Dolostone	Mudstone/ Wackestone	Lagoonal	280, 80
La Escalera	5C	99.1	Limestone	Mudstone/ Wackestone	Lagoonal	285, 80
La Escalera	5B	99.1	Limestone	Wackestone	Lagoonal	285, 80
La Escalera	5A	99.1	Limestone	Packstone	Lagoonal	285, 80
La Escalera	6C	45.7	Dolostone	Packstone	Shoals	285, 86
La Escalera	6B	45.7	Dolostone	Packstone/ Grainstone	Shoals	285, 86
La Escalera	6A	48.3	Limestone	Packstone	Shoals	286, 86
La Escalera	7	91.4	Dolostone	Packstone	Lagoonal	288, 78
La Escalera	8	76.2	Dolostone	Mudstone/ Wackestone	Lagoonal	294, 77
La Escalera	9	177.8	Dolostone	Mudstone	Lagoonal	290, 87
La Escalera	10	27.9	Limestone	Grainstone	Shoals	289, 84
La Escalera	11	68.6	Limestone	Grainstone	Shoals	289, 87
La Escalera	12	17.2(av)	Limestone	Packstone	Lagoonal	287, 86

Continuation Appendix 3.1

Locality	*Bed Number	Thickness (cm)	Lithology	Original Texture (Dunham, 1962)	Sedimentary Environment	Orientation (strike, dip) (degrees)
Corral de Palmas	1	175.3	Limestone	Boundstone	Shelf biostrome	310, 50
Corral de Palmas	2	20.3	Limestone	Boundstone	Shelf biostrome	292, 45
Corral de Palmas	3	142.2	Limestone	Boundstone	Shelf biostrome	286, 50
Corral de Palmas	4	124.5	Limestone	Boundstone	Shelf biostrome	292, 45
Corral de Palmas	5	7.6	Limestone	Grainstone	Shoals	287, 47
Corral de Palmas	6	55.9	Limestone	Grainstone	Shoals	288, 44
Corral de Palmas	7	25.4	Limestone	Grainstone	Shoals	298, 51
Corral de Palmas	8	50.8	Dolostone	Mudstone	Lagoonal	293, 43
Corral de Palmas	9	10.2	Dolostone	Wakestone	Lagoonal	283, 50
Corral de Palmas	10	14.0	Dolostone	Mudstone	Lagoonal	293, 54
Santa Rosa-Iturbide	1	24.1	Limestone	Mudstone	Open marine	150, 54
Santa Rosa-Iturbide	2	29.2	Limestone	Mudstone	Open marine	149, 52
Santa Rosa-Iturbide	3	106.7	Limestone and chert	Mudstone	Open marine	144, 56
Santa Rosa-Iturbide	4	121.9	Limestone	Mudstone	Open marine	145, 49
Santa Rosa-Iturbide	5	6.7(av)	Limestone	Mudstone	Open marine	145, 50
Santa Rosa-Iturbide	6	12.1(av)	Limestone	Mudstone	Open marine	153, 66
Santa Rosa-Iturbide	7	59.7	Limestone	Mudstone	Open marine	154, 51
Santa Rosa-Iturbide	8	11.4(av)	Chert	Chert	Open marine	145, 53
Santa Rosa-Iturbide	9	25.4	Limestone	Mudstone	Open marine	147, 51
Santa Rosa-Iturbide	10	76.2	Limestone	Mudstone	Open marine	147, 55

* Bed numbers are indicated in the stratigraphic columns (Appendix 2.1); av, average.

APPENDIX 3.2 – LIST OF THIN SECTIONS PREPARED AND USED IN THIS STUDY BY LOCALITY

The following list shows the thin sections included in this study from Cañón de los Chorros, Cañón de la Escalera, Cañón Boquilla Corral de Palmas, and Cañón Santa Rosa localities.

Appendix 3.2 List of thin sections prepared and used in this study by locality

Locality	Sample #	No. of thin sections	Subtotal
Cañón de los Chorros	CulCh1-98-So	1	
Cañón de los Chorros	CulCh2-98	2	
Cañón de los Chorros	CulCh3-98	2	
Cañón de los Chorros	CulCh4-98-SoB	2	
Cañón de los Chorros	CulCh5-98-SoB	2	
Cañón de los Chorros	CulCh6-98	2	
Cañón de los Chorros	CulCh7-98	3	
Cañón de los Chorros	CulCh8-98- SoA	2	16
Cañón la Escalera	CuEsc1-98	1	
Cañón la Escalera	CuEsc2-98	2	
Cañón la Escalera	CuEsc3-98	2	
Cañón la Escalera	CuEsc4-98	2	
Cañón la Escalera	CuEsc5A-98	2	
Cañón la Escalera	CuEsc5C-98	2	
Cañón la Escalera	CuEsc6A-98	2	
Cañón la Escalera	CuEsc6B-98	3	
Cañón la Escalera	CuEsc6C-98	2	
Cañón la Escalera	CuEsc7-98	2	
Cañón la Escalera	CuEsc8-98	2	
Cañón la Escalera	CuEsc9-98	4	
Cañón la Escalera	CuEsc10-98	2	
Cañón la Escalera	CuEsc11-98	3	
Cañón la Escalera	CuEsc12-98	2	
Cañón la Escalera	CuEsc-Yeso	2	35
Cañón Boquilla Corral de Palmas	CulPa1-98	2	
Cañón Boquilla Corral de Palmas	CulPa2-98-So	1	
Cañón Boquilla Corral de Palmas	CulPa3-98	3	
Cañón Boquilla Corral de Palmas	CulPa4-98- SoA	2	
Cañón Boquilla Corral de Palmas	CulPa5-98-SoA	3	
Cañón Boquilla Corral de Palmas	CulPa6-98	2	
Cañón Boquilla Corral de Palmas	CulPa7-98	1	
Cañón Boquilla Corral de Palmas	CulPa8-98-So	4	
Cañón Boquilla Corral de Palmas	CulPa9-98	3	
Cañón Boquilla Corral de Palmas	CulPa10-98	3	
Cañón Boquilla Corral de Palmas	CulPa1-00-So	2	
Cañón Boquilla Corral de Palmas	CulPa2-00-Trav.	2	
Cañón Boquilla Corral de Palmas	TsLPa1-00-So	1	
Cañón Boquilla Corral de Palmas	TsLPa4-00-So	1	
Cañón Boquilla Corral de Palmas	CulPa1-01	1	31

Continuation Appendix 3.2

Locality	Sample #	No. of thin sections	Subtotal
Cañón Santa Rosa-Iturbide	CuStR1-98	4	
Cañón Santa Rosa-Iturbide	CuStR2-98	2	
Cañón Santa Rosa-Iturbide	CuStR3-98	2	
Cañón Santa Rosa-Iturbide	CuStR4-98	2	
Cañón Santa Rosa-Iturbide	CuStR5-98	2	
Cañón Santa Rosa-Iturbide	CuStR6-98	2	
Cañón Santa Rosa-Iturbide	CuStR7-98	2	
Cañón Santa Rosa-Iturbide	CuStR8-98	0	
Cañón Santa Rosa-Iturbide	CuStR9-98	2	
Cañón Santa Rosa-Iturbide	CuStR9-rock-sample	0	
Cañón Santa Rosa-Iturbide	CuStR10-98	2	
Cañón Santa Rosa-Iturbide	CuStR11-98	0	20
Cañón Cerro Prieto	CP1-01	1	
Cañón Cerro Prieto	CP2-01	1	2
Potrero García	PG1-01	1	
Potrero García	PG2-01	1	2
	TOTAL	106	

APPENDIX 4.1 – PETROGRAPHIC SUMMARY SHEETS

The following section includes 36 petrographic summary sheets based on 106 thin section descriptions for the four localities includes in this study.

Petrographic Summary Sheet

Hand sample description: Dolomitized rudist bank with matrix of wackestones of bioclasts.

Thin Section:

Number	Formation	Facies	Age	Polish Quality	Location
CulPa-1-98, CulPa-1-98SoA	Cupido	Rudist Bank	Lower Cretaceous	Ok	Las Palmas, SMO Mexico

Outcrop quality	Rock Type	Petrographic description by
Good	Limestone	Fms

Oriented?	Notch?	North?	Macrofractures?	Location?
Yes	Yes (3)	Yes	Yes	CulPa1-98SoA

Description:

Rudstone. Rudist bank with matrix of wackestone of ooids and bioclasts (10%). Inside of fossils: packstone of ooids and intraclasts, partially dolomitized (5-10%). The rock is recrystallized (85-90%) and shows in some places selective dolomitization in the matrix. Dolomite is present as individual crystals in the matrix.

Diagenetic Processes:

	Processes	%	Description (size, etc)
D	Dolomitization	5-10	Individual crystals in matrix
Rx	Recrystallization	85-90	Affecting the rock
Dd	Dedolomitization	5	Probably due to recrystallization
Qz	Quartz cementation	1	Selective cementation inside of some rudists.

Paragenesis: F1 (calcite)-F2 (calcite)-D-Rx-Dd-Qz

Fracture Description: 2 sets of fractures both with blocky calcite cement, “en echelon” pattern. A third set was identified with brown calcite cement in thin section SoA.

Petrographic Summary Sheet

Hand sample description:

Dolomitized rudist bank with matrix of packstone of bioclasts

Thin Section:

Number	Formation	Facies	Age	Polish Quality	Location
CulPa-2-98So	Cupido	Rudist Bank	Lower Cretaceous	Ok	Las Palmas, SMO Mexico

Outcrop quality	Rock Type	Petrographic description by
Good	Limestone	Fms

Oriented?	Notch?	North?	Macrofractures?	Location?
Yes	Yes (3)	Yes	Yes	CulPa2-98So

Description: Rudstone. Rudist bank with matrix of packstone of bioclasts (miliolids, fragments of rudists, and ooids). The whole rock can be classified as packstone of intraclasts, where intraclasts are formed by similar composition of the matrix. Stylolites are present with quartz cement associated.

Diagenetic Processes:

	Processes	%	Description (size, etc)
D	Dolomitization	< 5	Individual crystals in matrix and associated with stylolites (5 to 20 div, 10x). Crystals are sub-euhedral and irregular borders. Calcite zones inside of dolomite
Rx	Recrystallization	95-100	Affecting the rock
Dd	Dedolomitization	30	Dedolomitization affecting dolomite crystals
PS	Pressure-solution	1	Stylolites with both quartz and dolomite cement

Paragenesis: F1 (calcite)-PS-D-Rx-

Fracture Description: Fractures with calcite cement in “en echelon” pattern.
 Note: Probably, some “intraclasts” correspond to bioturbation features.

Petrographic Summary Sheet

Hand sample description: CulPa-3-98So. Rudist bank with matrix of packstone of bioclasts. The sample presents two fracture sets at the bottom. One set is perpendicular to bedding and another with different strike direction but perpendicular to bedding also. F2 (apertures varies from 0.33 to 1.15 mm) cuts F1 (apertures vary from 0.05 to 0.75 mm). Both sets of fractures form an angle of 45 degrees between each other.

Thin Section:

Number	Formation	Facies	Age	Polish Quality	Location
CulPa-3-98So CulPa-3-98p CulPa-3-98	Cupido	Rudist Bank-lagoon facies	Lower Cretaceous	Ok	Las Palmas, SMO Mexico

Outcrop quality	Rock Type	Petrographic description by
Good	Limestone	Fms

Oriented?	Notch?	North?	Macrofractures?	Location?
Yes	Yes (3)	Yes	Yes	CulPa3-98 at the bottom of sample

Description:

Rudstone. Rudist bank with matrix of wackestones-packstone of intraclasts, bioclasts (miliolids, fragments of rudists, and ooids), and pellets. The whole rock is recrystallized (1 div; 10x) and partially dolomitized (a few crystals of dolomite, 4 div; 10x) as well. In tin section there is one microfracture filled with calcite cement (aperture, 2 div; 10x). There are intraclasts with miliolids, indicative of lagoon facies, pellets and algae fragments also are identified.

Diagenetic Processes:

	Processes	%	Description (size, etc)
D	Dolomitization	15	Individual crystals in matrix (4-5 to 10 x).
Rx	Recrystallization	80-85	Affecting the whole rock

Paragenesis: Bioturbation, F1 (calcite)-D-Rx-Dd (dedolomitization)-quartz

Fracture Description: In thin section Culpa3-98p, one set of microfractures (3-4 div; 10x) with two calcite cements, one is clearly synkinematic and the second one is post-kinematic. In thin section Culpa3-98So, two fracture sets can be differenced. Both with calcite cement. F2 (aperture 3 div; 10x) cuts F1 (apertures 70 div; 10x). F2 with remnant porosity is present. In thin section Culpa3-98, fractures (apertures ranging between 0.21 to 0.75 mm) present fibrous calcite cement. Note: Bioturbation features are very fine grain size.

Petrographic Summary Sheet

Hand sample description:

CulPa-4-98SoA. Rudist bank with a matrix of packstone of bioclasts. The sample present one fractures filled with calcite cement.

Thin Section:

Number	Formation	Facies	Age	Polish Quality	Location
CulPa-4-98SoA CulPa-4-98 SoB	Cupido	Rudist Bank-lagoon facies	Lower Cretaceous	Ok	Las Palmas, SMO Mexico

Outcrop quality	Rock Type	Petrographic description by
Good	Limestone	Fms

Oriented?	Notch?	North?	Macrofractures?	Location?
Yes	Yes (3)	Yes	Yes	Left side of thin section CulPa4-98SoB

Description:

Rudstone. Rudist bank with matrix of packstone of ooids and intraclasts, bioclasts (miliolids, algae fragments). Dolomite is affecting mainly the matrix but also some fossils. In some parts of the thin section, dolomite content can be greater than 40%. The whole rock is recrystallized.

Diagenetic Processes:

	Processes	%	Description (size, etc)
D	Dolomitization	30	Sub-euhedral crystals in matrix (5-10 div; 20 x).
Rx	Recrystallization	95-100	Affecting the whole rock, matrix and fracture cements.

Paragenesis: F1 (calcite)-Calcite cementation-D-Rx

Fracture Description:

In thin section Culpa4-98SoB: F1 fractures with synkinematic blocky calcite cement and dolomite as postkinematic cement. F1 present in some places "en echelon" pattern.

Petrographic Summary Sheet

Hand sample description:

CulPa-5-98. Packestone-grainstone of ooids.

Thin Section:

Number	Formation	Facies	Age	Polish Quality	Location
CulPa-5-98SoB CulPa-5-98SoA	Cupido	Lagoon	Lower Cretaceous	Ok	Las Palmas, SMO Mexico

Outcrop quality	Rock Type	Petrographic description by
Good	Limestone	Fms

Oriented?	Notch?	North?	Macrofractures?	Location?
Yes	Yes (3)	Yes	Yes	Middle of thin section

Description:

Recrystallized grainstone of ooids, pellets, bioclasts, intraclasts with algae fragments, and miliolids (foraminifera). There are a few dolomite crystals in the matrix. Ooids with two generation of calcite cement. One cementation C1 is thin isopachous fringe of fibrous calcite around ooids and exist a second C2 equant spar filling the intragranular porosity.

Diagenetic Processes:

	Processes	%	Description (size, etc)
D	Dolomitization	< 5	Sub-euhedral crystals in the matrix (5 div. 20x)
Rx	Recrystallization	90	Affecting the whole rock, matrix and fracture cements.

Paragenesis: Micritization-compaction-cementation (calcite marine cement)-dissolution-calcite cementation (blocky cement)-F1 (calcite)-D-C3?-Rx

Fracture Description:

In thin section Culpa4-98SoB, there are induced fractures and a F1 fracture set with synkinematic blocky calcite cement. Note: In SoA section there are some lineations of deformed grains, probably due to a deformation event?.

Petrographic Summary Sheet

Hand sample description:

CulPa-6-98. Packestone-grainstone of ooids.

Thin Section:

Number	Formation	Facies	Age	Polish Quality	Location
CulPa-6-98SoB CulPa-6-98SoA	Cupido	Ooids back/grainstone	Lower Cretaceous	Ok	Las Palmas, SMO Mexico

Outcrop quality	Rock Type	Petrographic description by
Good	Limestone	Fms

Oriented?	Notch?	North?	Macrofractures?	Location?
Yes	Yes (3)	Yes	Yes	Single fracture at the bottom of CulPa6-98SoA

Description:

Grainstone of ooids (oolites), intraclasts, bioclasts (miliolids and algae fragments), recrystallized, and dolomitized (anhedral dolomite crystals affecting some ooids but also the matrix).

Diagenetic Processes:

	Processes	%	Description (size, etc)
D	Dolomitization	5-10	Isolate anhedral very fine grain (1-8div. 20x) average 2 div.
Rx	Recrystallization	95-100	Affecting the whole rock, matrix and fracture cements.

Paragenesis: Micritization-cementation-F1 (calcite)-D-Rx

Fracture Description: In thin section Culpa6-98SoA, there is a single fracture cemented with calcite.

Petrographic Summary Sheet

Hand sample description:

CulPa-7-98. Packestone-grainstone of ooids.

Thin Section:

Number	Formation	Facies	Age	Polish Quality	Location
CulPa-7-98	Cupido	Ooids back/grainstone	Lower Cretaceous	Ok	Las Palmas, SMO Mexico

Outcrop quality	Rock Type	Petrographic description by
Good	Limestone	Fms

Oriented?	Notch?	North?	Macrofractures?	Location?
Yes	Yes (3)	Yes	No	

Description:

Recrystallized packstone-grainstone of ooids, bioclasts and intraclasts. The matrix presents some isolate anhedral crystals of dolomite.

Diagenetic Processes:

	Processes	%	Description (size, etc)
D	Dolomitization	< 5	Isolate anhedral very fine size crystals (3-20 div. 20x) average 5-10 div.
Rx	Recrystallization	80	Affecting the whole rock, but mainly allochems.

Paragenesis: Micritization-D-Rx

Fracture Description:

No fractures in this section.

Petrographic Summary Sheet

Hand sample description:

Microdolostone.

Number	Formation	Facies	Age	Polish Quality	Location
CulPa-8-98p CulPa-8-98So	Cupido	peritidal	Lower Cretaceous	Ok	Las Palmas, SMO Mexico

Outcrop quality	Rock Type	Petrographic description by
Good	Dolostone	Fms

Oriented?	Notch?	North?	Macrofractures?	Location?
Yes	Yes (3)	Yes	Yes	Everywhere in thin section

Description:

Dolostone formed by matrix with very fine grain micro-dolomite crystals. Probably the primary texture was mudstone-wackestone.

Diagenetic Processes:

	Processes	%	Description (size, etc)
D	Dolomitization	95-100	Very fine euhedral crystals (2-3 div. 20x).
Dd	Dedolomitization		

Paragenesis: D (very fine size)- F1 (fibrous crystals of dolomite (95%), calcite (5%)) - F2 (blocky dolomite (10%), calcite (90%)) - F3 (dolomite (60%), calcite (40%)) - F4 (dol (60%), calcite (40%))—F5 (dol (90%), calcite (10%))—F6 (dol (80%), calcite (20%))- Dedolomitization –Stylolites.

Probably some fractures identified as different sets belong to the same set. Main stylolite presents in this section cuts all fractures and present quartz grains with overgrowths. Quartz cement and dolomite macro-crystals are also present in stylolite. Dolomite crystal size inside of stylolite is different of dolomite crystals microcrystalline.

Fracture Description:

The thin section Culpa-898-So presents at least 5 fracture sets. Most fractures present macro-dolomite crystals as synkinematic cement. Some dolomite crystals probably are present as postkinematic cement. Note: One notch means north; two notches mean south. The sample is parallel to stratification surface.

Structural-diagenetic Petrographic Summary Sheet

Hand sample description: CulPa-9-98.

Dolostone. There are at least three main fracture sets. All fractures are perpendicular to the stratification plane. Fractures present both fibrous and blocky cement. At the bottom of the sample CulPa9-98 there are two sets of fractures. One presents fibrous dolomite cement and calcite. The second one cuts the first and is composed by blocky calcite cement and dolomite.

Thin Section:

Number	Formation	Facies	Age	Polish Quality	Location
CulPa-9-98p CulPa-9-98So	Cupido	peritidal	Lower Cretaceous	Ok	Las Palmas, SMO Mexico

Outcrop quality	Rock Type	Petrographic description by
Good	Dolostone	Fms

Oriented?	Notch?	North?	Macrofractures?	Location?
Yes	Yes (3)	Yes	Yes	Everywhere in thin section

Description: Dolostone formed by matrix with very fine grain micro-dolomite crystals. Probably the original texture was a mudstone. Culpa 9-98So: Most of the rock and fractures are affected by dolomitization.

Diagenetic Processes:

	Processes	%	Description (size, etc)
D	dolomitization	95-100	Very fine euhedral crystals (0.015-0.20 mm). Replacement phase.
Ps	pressure-solution		Stylolites

Paragenesis: D (very fine crystals) – F1 (calcite cement) – F2 (calcite and dolomite cement) – PS (stylolites) – F3 (calcite and dolomite)

Fracture Description: Culpa-9-98So sample presents two fractures sets. The first one is a microfracture set with calcite cement. The second set cuts the first one and is composed by fibrous euhedral meso-crystals of dolomite and blocky calcite cement. Stylolites cut F1 and F2, but not F3. Because in some cases stylolites cut F1 and F2 fractures and vice versa probably both events were developed at the same time. Note: SEM studies for this sample. P, sample perpendicular to stratification; So, sample parallel to stratification.

Petrographic Summary Sheet

Hand sample description:

CulPa-10-98. Microdolostone. Probably dolomitized mudstone.

Thin Section:

Number	Formation	Facies	Age	Polish Quality	Location
CulPa-10-98SoB CulPa-10-98SoA	Cupido	peritidal	Lower Cretaceous	Ok	Las Palmas, SMO Mexico

Outcrop quality	Rock Type	Petrographic description by
Good	Dolostone	Fms

Oriented?	Notch?	North?	Macrofractures?	Location?
Yes	Yes (3)	Yes	Yes	Everywhere in thin section

Description:

Wackestone-mudstone bioturbated and dolomitized. Dolomite is affecting both matrix and fractures. Bioturbation is very high and it is present as burrows filled with wackestone of intraclasts and ooids.

Diagenetic Processes:

	Processes	%	Description (size, etc)
D	Dolomitization	90-95	Fine sub-euhedral crystals (3-5 div. 20x). Most dolomite crystals present calcite "zones" inside. Some crystals present irregular borders also, indicating possible dedolomitization.
Dd	Dedolomitization		

Paragenesis: D (very fine grain)- F1 –Dedolomitization – Stylolites.

Fracture Description:

Culpa-10-98SoB presents two fractures sets, forming an angle of 45 degrees. Fractures are filled with calcite cement.

Petrographic Summary Sheet

Hand sample description:

CulPa-1-00-So. Wackestone of bioclasts.

Thin Section:

Number	Formation	Facies	Age	Polish Quality	Location
CulPa-1-00-So	Cupido	lagoon	Lower Cretaceous	Ok	Las Palmas, SMO Mexico

Outcrop quality	Rock Type	Petrographic description by
Good	Wackestone	Fms

Oriented?	Notch?	North?	Macrofractures?	Location?
Yes	Yes (3)	Yes		

Description:

Wackestone-Packstone of ooids and bioclasts (foraminifera sp., and ostracods), recrystallized with a few (5%) crystals of dolomite (patches of dolomite crystals).

Diagenetic Processes:

	Processes	%	Description (size, etc)
D	Dolomitization	5	Fine size concentrated crystals as patches
Rx	Recrystallization	100	

Paragenesis:

F1 (calcite) - D- F2 (dolomite and calcite)

Fracture Description:

Fractures with dolomite bridges (synkinematic) and calcite postkinematic. Calcite filled porosity and replacement dolomite.

Petrographic Summary Sheet

Hand sample description:

CulPa-TsLpa-1-00-So. Mudstone-wackestone.

Thin Section:

Number	Formation	Facies	Age	Polish Quality	Location
CulPa-TsLpa-1-00-So	Cupido	peritidal	Lower Cretaceous	Ok	Las Palmas, SMO Mexico

Outcrop quality	Rock Type	Petrographic description by
Good	Mudstone	Fms

Oriented?	Notch?	North?	Macrofractures?	Location?
Yes	Yes (3)	Yes	Yes	At the top of thin section

Description:

Recrystallized wackestone of bioclasts (foraminifera sp., and ostracods). Mudstone constituted by very fine size calcite crystals (1-5 div. 40x: 10 div = 0.025 mm).

Diagenetic Processes:

	Processes	%	Description (size, etc)
D	Dolomitization	2	Isolate very fine size crystals
Rx	Recrystallization	100	

Paragenesis: dolomitization-recrystallization

Fracture Description:

There is one macrofracture at the top of thin section with calcite synkinematic and blocky calcite postkinematic cements. There is a lineation of fluid inclusions between cements.

Petrographic Summary Sheet

Hand sample description:

Chert nodule

Thin Section:

Number	Formation	Facies	Age	Polish Quality	Location
TsLPa 4 Nodule	Cupido	Nodule	Lower Cretaceous	Ok	Las Palmas, SMO Mexico

Outcrop quality	Rock Type	Petrographic description by
Good	Limestone	Fms

Oriented?	Notch?	North?	Macrofractures?	Location?
Yes	Yes (3)	Yes	Yes	Left side of thin section

Description:

Chert nodule with big crystals of gypsum replaced by calcite.

Diagenetic Processes:

	Processes	%	Description (size, etc)
D	Dolomite	?	crystals
C	Calcitization	100	2 events affecting nodules
Rx	Recrystallization	100	Affecting the whole rock

Paragenesis: Gypsum precipitation- Calcite replacement- F1 (calcite)- D- F2 (quartz (synkinematic, and calcite postkinematic) calcitization?- Rx- Stylolites

Fracture Description:

F2 fractures with synkinematic quartz cement (90%) and postkinematic calcite cement (10%). F2 is affecting both gypsum and dolomite.

Petrographic Summary Sheet

Hand sample description:

Grainstone of ooids, bioclasts and peloids.

Thin Section:

Number	Formation	Facies	Age	Polish Quality	Location
CulCh1-98So	Cupido	Lagoon	Lower Cretaceous	Ok	Los Chorros, SMO Mexico

Outcrop quality	Rock Type	Petrographic description by
Good	Limestone	Fms

Oriented?	Notch?	North?	Macrofractures?	Location?
Yes	Yes (3)	Yes	Yes	Culch1-98

Description:

Grainstone of bioclasts (20%), ooids (20%), grapestones and algae (35%), peloids (15%), and intraclasts (5%). There are at least two fracture sets.

Diagenetic Processes:

	Processes	%	Description (size, etc)
C	cementation		calcite

Paragenesis: Compaction- Cementation (CaCO₃, marine cement)-C (blocky calcite cement)-F1 (calcite)-F2 (calcite)-Sty.

Fracture Description:

Maybe there are two blocky calcite cements. The primary porosity was very high but all porous were cemented with calcite, probably in two events (generation). The morphology of the F1 is different of F2. F1 seem to be more irregular, mainly follow the borders of allochems. F2 fracture walls are more linear. Both cements probably are synkinematic.

Notes: Stylolite cuts fractures.

Petrographic Summary Sheet

Hand sample description:

Packstone of bioclasts, ooids and intraclasts. There are two main fracture sets perpendicular to bedding (So). Both sets form a very low angle, and show remnant porosity. Stylolites have dissolution zones.

Thin Section:

Number	Formation	Facies	Age	Polish Quality	Location
CulCh2-98So	Cupido	Lagoon	Lower Cretaceous	Ok	Los Chorros, SMO Mexico

Outcrop quality	Rock Type	Petrographic description by
Good	Limestone	Fms

Oriented?	Notch?	North?	Macrofractures?	Location?
Yes	Yes (3)	Yes	Yes	Culch2-98So

Description: Packstone of intraclasts (70%), (algae (10%), pellets (5%), foras (10%), ooids (5%).

Diagenetic Processes:

	Processes	%	Description (size, etc)
M	Micritization	90	Micritization affected mainly bioclasts
C	Cementation		calcite
Di	Dissolution	3	Dissolution affected a few allochems.

Paragenesis:

Micritization-Compaction- Cementation (CaCO₃, 2 generation)-F1 (calcite)-F2 (calcite)-F3 (calcite)-Ps (stylolites).

Fracture Description: Very thin fractures (0.004 to 0.02 mm wide).

Notes: The third fracture event is sub-horizontal. The relationship between microfractures and stylolites are very clear in T.S. 2-98 p. Stylolites cut microfractures. Conjugate fractures with similar remnant porosity. In the thin section CulCh2-98 there are fractures with calcite synkinematic cement.

Marine cement and second generation of calcite cement very clear.

Petrographic Summary Sheet

Hand sample description:

Grainstone of ooids, intraclasts and bioclasts.

Thin Section:

Number	Formation	Facies	Age	Polish Quality	Location
CulCh3-98	Cupido	Lagoon	Lower Cretaceous	Ok	Los Chorros, SMO Mexico

Outcrop quality	Rock Type	Petrographic description by
Good	Limestone	Fms

Oriented?	Notch?	North?	Macrofractures?	Location?
Yes	Yes (3)	Yes	No	

Description:

Packstone-grainstone of oolites, (10%), other ooids, (18%), pellets (15%) and algae fragments (15 %), miliolids (9%), and grapestones (33%).

Diagenetic Processes:

	Processes	%	Description (size, etc)
C	Cementation		Two events (marine cement and late blocky cement)

Paragenesis:

Micritization-Compaction- C1 (CaCO₃, marine)-C2 (blocky calcite).

Fracture Description:

No fractures.

Petrographic Summary Sheet

Hand sample description:

Packstone of bioclasts.

Thin Section:

Number	Formation	Facies	Age	Polish Quality	Location
CulCh4-98-SoB	Cupido	Lagoon/oolitic bank	Lower Cretaceous	Ok	Los Chorros, SMO Mexico

Outcrop quality	Rock Type	Petrographic description by
Good	dolostone	Fms

Oriented?	Notch?	North?	Macrofractures?	Location?
Yes	Yes (3)	Yes	Yes	Culch4-98SoB

Description:

Dolomitized packstone-grainstone of pellets (42%), with Favreina, sp. (30%) and packstone-grainstone of ooids and pellets (13%).

Diagenetic Processes:

	Processes	%	Description (size, etc)
D	dolomitization	85-90	Average size: (5 div., 20x)

Paragenesis:

Micritization-Compaction- C1 (CaCO₃, marine)-C2 (blocky calcite)--F1 (calcite)-D (dolomitization)-F2 (calcite)

Fracture Description:

F2 fractures with calcite cement postdate dolomitization.

Petrographic Summary Sheet

Hand sample description:

Packstone of intraclasts.

Thin Section:

Number	Formation	Facies	Age	Polish Quality	Location
CulCh5-98-SoB	Cupido	Lagoon	Lower Cretaceous	Ok	Los Chorros, SMO Mexico

Outcrop quality	Rock Type	Petrographic description by
Good	Limestone-dolomitized	Fms

Oriented?	Notch?	North?	Macrofractures?	Location?
Yes	Yes (3)	Yes	No	

Description:

Dolomitized packstone-wackestone of intraclasts (17%) and pellets (13%).

Diagenetic Processes:

	Processes	%	Description (size, etc)
D	dolomitization	45-50	Average size: (5-7 div., 20x)

Paragenesis:

Micritization-Compaction- C1 (CaCO₃, marine)-C2 (blocky calcite)-D (dolomitization)

Fracture Description:

No fractures.

Petrographic Summary Sheet

Hand sample description:

Packstone of intraclasts.

Thin Section:

Number	Formation	Facies	Age	Polish Quality	Location
CulCh5-98-SoB	Cupido	Lagoon	Lower Cretaceous	Ok	Los Chorros, SMO Mexico

Outcrop quality	Rock Type	Petrographic description by
Good	Limestone-dolomitized	Fms

Oriented?	Notch?	North?	Macrofractures?	Location?
Yes	Yes (3)	Yes	No	

Description:

Dolomitized packstone-wackestone of intraclasts (17%) and pellets (13%).

Diagenetic Processes:

	Processes	%	Description (size, etc)
D	dolomitization	45-50	Average size: (5-7 div., 20x)

Paragenesis:

Micritization-Compaction- C1 (CaCO₃, marine)-C2 (blocky calcite)-D (dolomitization)

Fracture Description:

No fractures.

Petrographic Summary Sheet

Hand sample description:

Packstone of rudists, bioclasts and ooids, with at least 3 macrofractures sets.

Thin Section:

Number	Formation	Facies	Age	Polish Quality	Location
CulCh6-98p CulCh6-98So	Cupido	Rudist bank	Lower Cretaceous	Ok	Los Chorros, SMO Mexico

Outcrop quality	Rock Type	Petrographic description by
Good	Limestone-dolomitized	Fms

Oriented?	Notch?	North?	Macrofractures?	Location?
Yes	Yes (3)	Yes	Yes	Culch6-98So, p

Description: Partially dolomitized rudist bank, matrix of packstone of bioclasts (25%), ooids (20), and intraclasts. There is a fracture partially filled with dolomite. CulCh6-98s: Dolomitized packstone of intraclasts (of peloids, pellets, and ooids).

Diagenetic Processes:

	Processes	%	Description (size, etc)
D	dolomitization	70	Very fine crystal size (1-5 div; 2.5x, average = 3 div., 2-10 div., 20x)
Rx	recrystallization	?	Poorly developed
C	cementation		calcite

Paragenesis: Micritization of ooids and peloids.

Micritization-Cementation (CaCO₃)-F1(calcite cement) -D (dolomitization)-F(dolomite)-F2 (calcite cement)-Sty (stylolite)-Rx.

Fracture Description:

Fractures partially filled with dolomite (crystal size of 30 div. (10x)).

Microfractures filled with calcite, aperture very narrow (3 div. 10x).

Stylolite dissolved dolomite crystals. In T.S. 6-98 So, matrix dolomite brooked by calcite fill vein, imply dolomite predates calcite veins. Dolomite crystals crosscut fractures cemented with calcite, from one side to the other.

Notes: Thin section CulCh6-98So was glued to the top, no to the base.

Petrographic Summary Sheet

Hand sample description:

Packstone of intraclasts.

Thin Section:

Number	Formation	Facies	Age	Polish Quality	Location
CulCh7-98-SoB	Cupido	Lagoon	Lower Cretaceous	Ok	Los Chorros, SMO Mexico

Outcrop quality	Rock Type	Petrographic description by
Good	Limestone	Fms

Oriented?	Notch?	North?	Macrofractures?	Location?
Yes	Yes (3)	Yes	No	

Description:

Poorly dolomitized packstone of pellets (25%), intraclasts (20%), bioclasts (20%), miliolids, (7%), and peloids (25%).

Diagenetic Processes:

	Processes	%	Description (size, etc)
D	dolomitization	5	Average size: (5-7 div., 20x)

Paragenesis:

Micritization-Compaction- C1 (CaCO₃, marine)-C2 (blocky calcite)-D (dolomitization)

Fracture Description:

No fractures.

Petrographic Summary Sheet

Hand sample description:

Packstone of ooids.

Thin Section:

Number	Formation	Facies	Age	Polish Quality	Location
CulCh8-98-SoB	Cupido	Lagoon	Lower Cretaceous	Ok	Los Chorros, SMO Mexico

Outcrop quality	Rock Type	Petrographic description by
Good	Dolostone	Fms

Oriented?	Notch?	North?	Macrofractures?	Location?
Yes	Yes (3)	Yes	Yes	Culch8-98SoB

Description:

Dolomitized packstone-grainstone of pellets (50%), intraclasts (25%), and ooids (5%).

Diagenetic Processes:

	Processes	%	Description (size, etc)
D	dolomitization	90	Average crystal size: (5-7 div., 20x)

Paragenesis:

Dolomitization- F (dolomite-calcite).

Fracture Description:

Fractures with dolomite bridges synkinematic cement, and postkinematic calcite.

Petrographic Summary Sheet

Hand sample description:

Synsedimentary breccia

Thin Section:

Number	Formation	Facies	Age	Polish Quality	Location
CuEsc-1-98So	Cupido	Lagoon?	Lower Cretaceous	Ok	La Escalera, SMO Mexico

Outcrop quality	Rock Type	Petrographic description by
Good	dolostone	Fms

Oriented?	Notch?	North?	Macrofractures?	Location?
Yes	Yes (3)	Yes	Yes	CuEsc-1-98 So

Description:

Synsedimentary breccia composed by matrix of mudstone and clasts of wackestone-packstone of ooids and intraclasts. The whole rock is dolomitized.

Diagenetic Processes:

	Processes	%	Description (size, etc)
D	Dolomitization	100	Matrix: very fine crystal size (2-5 div 40x), anhedral crystals, baroque dolomite with undulatory extinction.
Qz	Quartz cementation	5	Affecting only fractures (veins). Quartz present undulatory extinction.

Paragenesis: D- F (dolomite) - F2 (calcite) – Qz

Fracture Description: Big vein with dolomite synkinematic cement, and calcite postkinematic cement.

Note: Quartz probably partially replaced dolomite. Calcite partially replaced dolomite in the big vein.

Petrographic Summary Sheet

Hand sample description: Fractured dolostone

Thin Section:

Number	Formation	Facies	Age	Polish Quality	Location
CuEsc-2-98SoA CuEsc-2-98SoB	Cupido	Mudstone?	Lower Cretaceous	Ok	La Escalera, SMO Mexico

Outcrop quality	Rock Type	Petrographic description by
Good	dolostone	Fms

Oriented?	Notch?	North?	Macrofractures?	Location?
Yes	Yes (3)	Yes	Yes	Everywhere in both thin sections

Description: Dolostone with probably original texture of wackestone.

Diagenetic Processes:

	Processes	%	Description (size, etc)
D	Dolomitization	75-80	Fine size (7-10 div 40x) crystals, poorly defined due to partially calcite replacement.

Paragenesis: F (calcite) – F2 (calcite) – D – F3 (dolomite, calcite, anhydrite) - Qz

Fracture Description:

Big vein at the top of thin section with synkinematic dolomite and postkinematic calcite, and quartz cementation. Dolomite in fractures presents undulatory extinction (baroque dolomite). Some fractures with dolomite (synkinematic) and calcite (postkinematic) where deformed. In thin section CuEsc-2-98SoB dolomite in fractures presents curved crystals. Probably anhydrite is present in fractures. Calcite partially replaced both dolomite and anhydrite.

Petrographic Summary Sheet

Hand sample description:

Fractured dolostone

Thin Section:

Number	Formation	Facies	Age	Polish Quality	Location
CuEsc-4-98SoB	Cupido		Lower Cretaceous	Ok	La Escalera, SMO Mexico

Outcrop quality	Rock Type	Petrographic description by
Good	dolostone	Fms

Oriented?	Notch?	North?	Macrofractures?	Location?
Yes	Yes (3)	Yes	Yes	Everywhere in thin section

Description: Dolostone formed by micro-crystals of dolomite. Probably some ooids where partially dissolved. Matrix is composed by dolomite and anhydrite; dissolution affected ooids and fractures. In thin section CuEsc-4-98SoB chert nodules are present.

Main diagenetic Processes:

	Processes	%	Description (size, etc)
D	Dolomitization	95-100	Fine size (1-5 div 20x) crystals very well defined.
Qz	Silicification	5	

Paragenesis: Gypsum precipitation – dissolution? – D – F (dolomite, calcite) – dissolution (affecting fractures and ooids) – Calcite cementation (replacement) – Qz – dissolution (microkarst) – Stylolites.

- 1.- Dissolution: affected ooids, fossils, anhydrite nodules and crystals.
- 2.- Dolomitization: replaced matrix, filled some porous spaces.
- 3.- Fracturing: dolomite and calcite cements
- 4.- Fracturing: calcite cement.
- 5.- Calcite cementation: filled some porous spaces, partially replaced dolomite in both matrix and fractures.

Fracture Description: Veins with dolomite and calcite cement.

Notes: Fractures with dolomite cement probably developed at the same time of dolomitization. Karst features are present (microkarst).

Petrographic Summary Sheet

Hand sample description:

Packstone of ooids.

Thin Section:

Number	Formation	Facies	Age	Polish Quality	Location
CuEsc-5A-98SoB	Cupido	lagoon	Lower Cretaceous	Ok	La Escalera, SMO Mexico

Outcrop quality	Rock Type	Petrographic description by
Poor	dolostone	Fms

Oriented?	Notch?	North?	Macrofractures?	Location?
Yes	Yes (3)	Yes	No	

Description:

Packstone of ooids, bioclasts (algae fragments), peloids, and intraclasts.

Main diagenetic Processes:

	Processes	%	Description (size, etc)

Paragenesis: No processes identified.

Fracture Description:

Notes: Thin section is dark and has poor quality for petrographic description.

Petrographic Summary Sheet

Hand sample description:

Bioturbated mudstone-wackestone.

Thin Section:

Number	Formation	Facies	Age	Polish Quality	Location
CuEsc-5C-98SoA CuEsc-5C-98SoB	Cupido	Lagoon	Lower Cretaceous	Ok	La Escalera, SMO Mexico

Outcrop quality	Rock Type	Petrographic description by
Good	limestone	Fms

Oriented?	Notch?	North?	Macrofractures?	Location?
Yes	Yes (3)	Yes	Yes	Left side of thin section

Description: Bioturbated mudstone-wackestone. Bioturbation generated burrows, which are filled with coarse-grained size sediment (bioclasts, pellets, etc.). Incipient dolomitization is present in the matrix. Burrows are also partially dolomitized.

Main diagenetic Processes:

	Processes	%	Description (size, etc)
B	Bioturbation	50	Bioturbation generated burrows
Rx	Recrystallization	85-90	Affecting the whole rock. "big" calcite crystals around dolomite crystal. Rx affected dolomite crystals also.
D	Dolomitization	10-15	Isolate crystals present in the matrix. Crystal size varies from 2 to 5 div (20x). Few large crystals reach ~ 10 div. Dolomitization into burrows can reach 40%.

Paragenesis: Bioturbation – F1 (calcite) – F2 (calcite) – dolomitization –recrystallization.

Fracture Description: There are at least two main fracture sets. Both sets are filled with calcite cement. Similar fractures are present in thin section CuEsc-5C-98SoB.

Notes: Most of the dolomite crystals have been affected by recrystallization. The thin section presents some induced fractures generated during preparation.

Petrographic Summary Sheet

Hand sample description: Packstone of bioclasts, pellets, and intraclasts.

Thin Section:

Number	Formation	Facies	Age	Polish Quality	Location
CuEsc-6A-98SoA CuEsc-6A-98SoB	Cupido	Lagoon	Lower Cretaceous	Ok	La Escalera, SMO Mexico

Outcrop quality	Rock Type	Petrographic description by
Good	limestone	Fms

Oriented?	Notch?	North?	Macrofractures?	Location?
Yes	Yes (3)	Yes	Yes	Left side of thin section

Description: Dolomitized and recrystallized packstone of pellets, intraclasts and bioclasts (mainly algae fragments). Dolomite is replacing both matrix and allochems, but affected mainly the pellets, which served as a nucleus. Note: Favreina sp. is the most abundant (20%) pellets in the sample.

Main diagenetic Processes:

	Processes	%	Description (size, etc)
Rx	Recrystallization	55-60	Rx affected the whole rock, including dolomite crystals.
D	Dolomitization	45-60	Subhedral crystals present in the matrix vary in size from 0.005 to 0.05 mm.

Paragenesis:

F1 (calcite)–Dolomitization–F2(calcite)–PS(pressure-solution)–Recrystallization (sample CuEsc-6A-98SoB). Compaction–F1 (calcite)–F2 (calcite)–Dolomitization– Recrystallization (sample CuEsc-6A-98SoA). F1 and F2 fracture sets are conjugated.

Fracture Description: There are at least two main fracture sets. Both sets are filled with calcite cement. Similar fractures are present in both this sections.

Notes: Most of the dolomite crystals have been affected by recrystallization.

Petrographic Summary Sheet

Hand sample description:

Packstone-grainstone of ooids and bioclasts.

Thin Section:

Number	Formation	Facies	Age	Polish Quality	Location
CuEsc-6B-98SoA CuEsc-6B-98SoB	Cupido	Lagoon	Lower Cretaceous	Ok	La Escalera, SMO Mexico

Outcrop quality	Rock Type	Petrographic description by
Good	limestone	Fms

Oriented?	Notch?	North?	Macrofractures?	Location?
Yes	Yes (3)	Yes	Yes	Left side of thin section

Description:

Dolomitized and fractured grainstone of ooids (probably oolites) and bioclasts (foraminifera sp.). Dolomite crystals are subhedral, poorly defined and they are replacing both matrix and allochems. Dolomite is replacing phase that affected the matrix and fractures.

Main diagenetic Processes:

	Processes	%	Description (size, etc)
D	Dolomitization	90-95	Subhedral crystals present in the matrix vary in size from 7-8 div (20x).

Paragenesis: F1 (calcite, dolomite) – Dolomitization – Sty (stylolites, pressure-solution)

Fracture Description: There is a possibility that dolomite in fractures is similar to dolomite in the matrix. Probably calcite cementation occurred after dolomitization in fractures or dolomite is replacing calcite.

Petrographic Summary Sheet

Hand sample description:

Mudstone.

Thin Section:

Number	Formation	Facies	Age	Polish Quality	Location
CuSTR-1-98SoA	Lower Tamaulipas	Basinal	Lower Cretaceous	Ok	Iturbide Santa Rosa, SMO Mexico

Outcrop quality	Rock Type	Petrographic description by
Good	Limestone	Fms

Oriented?	Notch?	North?	Macrofractures?	Location?
Yes	Yes (3)	Yes	Yes	

Description:

Mudstone with 5% of microorganisms, partially dolomitized (~10%) and recrystallized (85%). Some parts of the rock present silicification (~1%).

Main diagenetic Processes:

	Processes	%	Description (size, etc)
D	dolomitization	85	Rhomboheda individual crystals. Ferroan dolomite
X	recrystallization	85	

Paragenesis: F1 (calcite, calcite) –F2 (calcite) – dolomitization-Sty (stylolites, pressure-solution)-recrystallization

Fracture Description: both fracture set with synkinematic and postkinematic calcite cement. Most fracture walls are rectilinear; however there are a few with irregular walls. In general all fracture walls are well defined. F2 fractures are “en echelon pattern” and they form two conjugated sets.

Petrographic Summary Sheet

Hand sample description:

Mudstone.

Thin Section:

Number	Formation	Facies	Age	Polish Quality	Location
CuSTR-2-98SoB	Lower Tamaulipas	Basinal	Lower Cretaceous	Ok	Iturbide Santa Rosa, SMO Mexico

Outcrop quality	Rock Type	Petrographic description by
Good	Limestone	Fms

Oriented?	Notch?	North?	Macrofractures?	Location?
Yes	Yes (3)	Yes	Yes	

Description:

Mudstone with a few bioclasts and partially dolomitized. This rock presents some oxides.

Main diagenetic Processes:

	Processes	%	Description (size, etc)
D	dolomitization	3-4	Rhombohedra individual crystals.
O	oxides	3	

Paragenesis: F1 (calcite, calcite) –F2 (calcite) – dolomitization

Fracture Description: both fracture set with synkinematic and postkinematic calcite cement. Most fracture walls are rectilinear; however there are a few with irregular walls. In general all fracture walls are well defined. F1 fractures are “en echelon pattern”.

Petrographic Summary Sheet

Hand sample description:

Mudstone.

Thin Section:

Number	Formation	Facies	Age	Polish Quality	Location
CuSTR-3-98SoB	Lower Tamaulipas	Basinal	Lower Cretaceous	Ok	Iturbide Santa Rosa, SMO Mexico

Outcrop quality	Rock Type	Petrographic description by
Good	Limestone	Fms

Oriented?	Notch?	North?	Macrofractures?	Location?
Yes	Yes (3)	Yes	Yes	

Description:

Mudstone with low percentage of organic matter.

Main diagenetic Processes:

	Processes	%	Description (size, etc)

Paragenesis: F1 (calcite, calcite) –F2 (calcite) – Sty (stylolites, pressure-solution)

Fracture Description: both fracture set with synkinematic and postkinematic calcite cement. Most fracture walls are rectilinear; however there are a few with irregular walls. In general all fracture walls are well defined.

Petrographic Summary Sheet

Hand sample description:

Mudstone

Thin Section:

Number	Formation	Facies	Age	Polish Quality	Location
CuSTR-4-98So	Lower Tamaulipas	Basinal	Lower Cretaceous	Ok	Iturbide Santa Rosa, SMO Mexico

Outcrop quality	Rock Type	Petrographic description by
Good	Limestone	Fms

Oriented?	Notch?	North?	Macrofractures?	Location?
Yes	Yes (3)	Yes	Yes	everywhere

Description:

Mudstone with low percentage of organic matter and replacement dolomite. This rock presents bioturbation, stylolites that crosscut fractures, and low percentage of quartz. Some places of the thin section probably are recrystallized.

Main diagenetic Processes:

	Processes	%	Description (size, etc)
B	bioturbation		Most of the rock presents bioturbation.
D2	dolomitization	5	Anhedral isolate crystals.
Rx	recrystallization	3	Most of the fossils are recrystallized

Paragenesis: B-F1 (calcite, calcite) –F2 (calcite, calcite)-D2- PS (stylolites)-Rx

Fracture Description: Fracture set with synkinematic and postkinematic calcite cement. Fractures were affected by dolomitization. F2 present twined calcite

Petrographic Summary Sheet

Hand sample description:

Mudstone with microfractures (<0.05mm) cemented by calcite. There is one fracture set almost perpendicular to the stratification plane (So).

Thin Section:

Number	Formation	Facies	Age	Polish Quality	Location
CuSTR-5-98p	Lower Tamaulipas	Basinal	Lower Cretaceous	Ok	Iturbide Santa Rosa, SMO Mexico

Outcrop quality	Rock Type	Petrographic description by
Good	Limestone	Fms

Oriented?	Notch?	North?	Macrofractures?	Location?
Yes	Yes (3)	Yes	Yes	everywhere

Description:

Partially dolomitized mudstone, with low percentage (1%) of detrital quartz grains.

Main diagenetic Processes:

	Processes	%	Description (size, etc)
Si	silicification	1	Silica cemented some dissolution parts in microfossils
Qzt	quartz	5	Detrital quartz grains
Do	dolomitization	10-15	
FeDo	Ferroan-dolomite	2	Isolated dolomite crystals characterized by iron zoning

Paragenesis: Pressure-solution (Stylolites)-Do-F1 (calcite, calcite) –F2 (calcite, calcite)-Si

Fracture Description: Fracture set with synkinematic and postkinematic calcite cement. F2 fractures presents calcite bridges, F2 present blocky calcite cement. In thin section CuSTR-5-98So there is another fracture set “en echelon2 pattern with synkinematic and postkinematic cement.

Petrographic Summary Sheet

Hand sample description:

Mudstone with macro-fractures and stylolites.

Thin Section:

Number	Formation	Facies	Age	Polish Quality	Location
CuSTR-7-98SoA	Lower Tamaulipas	Basinal	Lower Cretaceous	Ok	Iturbide Santa Rosa, SMO Mexico

Outcrop quality	Rock Type	Petrographic description by
Good	Limestone	Fms

Oriented?	Notch?	North?	Macrofractures?	Location?
Yes	Yes (3)	Yes	Yes	

Description:

Mudstone with low percentage of organic matter. It presents stylolites that cut calcite veins (macrofractures).

Main diagenetic Processes:

	Processes	%	Description (size, etc)
D2	dolomitization	5	Small dolomite crystals
F	fracturing		
Sty	stylolites		

Paragenesis: F1 (calcite, calcite) –F2 (calcite, calcite)-stylolites.

Fracture Description: Fracture sets with synkinematic and postkinematic calcite cement. Fracture walls in general are irregular and well defined; most fractures present crack seal structures. Stylolites crosscut all fracture sets.

Petrographic Summary Sheet

Hand sample description:

Mudstone with organic matter and macro-fractures.

Thin Section:

Number	Formation	Facies	Age	Polish Quality	Location
CuSTR-9-98SoA	Lower Tamaulipas	Basinal	Lower Cretaceous	Ok	Iturbide Santa Rosa, SMO Mexico

Outcrop quality	Rock Type	Petrographic description by
Good	Limestone	Fms

Oriented?	Notch?	North?	Macrofractures?	Location?
Yes	Yes (3)	Yes	Yes	

Description:

Fractured mudstone with a few microfossils. The sample presents some oxides associated with stylolites. This rock has low percentage of organic matter. It presents four fracture sets with calcite cement and stylolites, and a few detrital quartz grains.

Main diagenetic Processes:

	Processes	%	Description (size, etc)
D	Dolomitization	5-8	Very fine size anhedral crystals
Si	Silicification	1	Silica affected preferentially fossils

Paragenesis: F1 (calcite, calcite) –F2 (calcite, calcite)- F3 (calcite, calcite)- F4 (calcite, calcite)-stylolites-Si.

F2 fractures are two conjugated sets.

Fracture Description: Two fracture sets (microfractures and macrofractures) with synkinematic and postkinematic calcite cement. Macrofractures crosscut microfractures. Stylolites crosscut all fracture sets, preferentially along fracture walls.

Petrographic Summary Sheet

Hand sample description:

Mudstone with organic matter and macro-fractures.

Thin Section:

Number	Formation	Facies	Age	Polish Quality	Location
CuSTR-9-98SoB	Lower Tamaulipas	Basinal	Lower Cretaceous	Ok	Iturbide Santa Rosa, SMO Mexico

Outcrop quality	Rock Type	Petrographic description by
Good	Limestone	Fms

Oriented?	Notch?	North?	Macrofractures?	Location?
Yes	Yes (3)	Yes	Yes	

Description:

Mudstone with low percentage of organic matter and oxides. It presents two fracture sets with calcite cement and stylolites.

Main diagenetic Processes:

	Processes	%	Description (size, etc)
F	Fracturing		
Sty	Stylolites		

Paragenesis: F1 (macrofracture, calcite, calcite) –F2 (microfractures, calcite, calcite)-stylolites.

Fracture Description: Two fracture sets (macrofractures and microfractures) with irregular fracture walls and synkinematic and postkinematic calcite cement. Microfractures crosscut macrofractures. Stylolites crosscut all fracture sets, preferentially along fracture walls. Microfractures present pyrite.

Petrographic Summary Sheet

Hand sample description:

Mudstone with organic matter and macro-fractures.

Thin Section:

Number	Formation	Facies	Age	Polish Quality	Location
CuSTR-9-98SoB	Lower Tamaulipas	Basinal	Lower Cretaceous	Ok	Iturbide Santa Rosa, SMO Mexico

Outcrop quality	Rock Type	Petrographic description by
Good	Limestone	Fms

Oriented?	Notch?	North?	Macrofractures?	Location?
Yes	Yes (3)	Yes	Yes	

Description:

Mudstone with low percentage of organic matter and oxides. It presents two fracture sets with calcite cement and stylolites.

Main diagenetic Processes:

	Processes	%	Description (size, etc)
Sty	Stylolites		

Paragenesis: F1 (macrofracture, calcite, calcite) –F2 (microfractures, calcite, calcite)-stylolites.

Fracture Description: Two fracture sets (macrofractures and microfractures) with irregular fracture walls and synkinematic and postkinematic calcite cement. Microfractures crosscut macrofractures. Stylolites crosscut all fracture sets, preferentially along fracture walls. Microfractures present pyrite.

APPENDIX 4.2 – PERCENTAGE OF DOLOMITE.

The following table contains the original texture (Dunham, 1962), and visual and point counting percent estimated of D2 dolomite in rock samples included in this study.

Appendix 4.2 Visual estimation and point counting D2 dolomite percentage in rock samples included in this study.

Locality	Bed #	Lithology	Original Texture Dunham (1962)	Visual Dolomite Estimation (%)	Dolomite (%) Point counting
Chorro	1	Limestone	Grainstone	0	0
Chorro	2	Limestone	Packstone	0	0
Chorro	3	Limestone	Grainstone	0	0
Chorro	4	Limestone	Wackestone/ Packstone	85-90	82
Chorro	5	Limestone	Boundstone	45-50	47
Chorro	6	Dolostone	Boundstone	70	75
Chorro	7	Limestone	Grainstone	5	7
Chorro	8	Dolostone	Grainstone/ Packstone	90	80
Escalera	1	Dolomitized Breccia		100	95
Escalera	2	Dolostone	Mudstone/ Wackestone	90	95
Escalera	3	Dolostone	Mudstone	80	80
Escalera	4	Dolostone	Mudstone/ Wackestone	90	95
Escalera	5	Limestone	Packstone	20	25
Escalera	6B	Dolostone	Packstone/ Grainstone	90	80
Escalera	6A	Limestone	Grainstone	25	25
Escalera	7	Dolostone	Packstone	100	98
Escalera	8	Dolostone	Mudstone/ Wackestone	100	95
Escalera	9	Dolostone	Mudstone	100	99
Escalera	10	Limestone	Grainstone	0	0
Escalera	11	Limestone	Grainstone	20	25
Escalera	12	Limestone	Packstone	20	25
Palmas	1	Limestone	Boundstone	5-10	7
Palmas	2	Limestone	Boundstone	< 5	3
Palmas	3	Limestone	Boundstone	15-20	21
Palmas	4	Limestone	Boundstone	30	28
Palmas	5	Limestone	Grainstone	< 5	3
Palmas	6	Limestone	Grainstone	5-10	11
Palmas	7	Limestone	Grainstone	< 5	3
Palmas	8	Dolostone	Mudstone	95-100	98
Palmas	9	Dolostone	Wackestone	95-101	98
Palmas	10	Dolostone	Mudstone	90-95	93
Palmas	1-00	Dolostone	Mudstone	5	7
Palmas	4-00	Nodule	Chert, nodule	5	7
Iturbide	1	Limestone	Mudstone	10	6
Iturbide	2	Limestone	Mudstone	3-4	2
Iturbide	3	Limestone and chert	Mudstone	5	5
Iturbide	4	Limestone	Mudstone	5	5
Iturbide	5	Limestone	Mudstone	10-15	3
Iturbide	6	Limestone	Mudstone	10	12
Iturbide	7	Limestone	Mudstone	10	12
Iturbide	8	Chert	Chert		
Iturbide	9	Limestone	Mudstone	5-8	4
Iturbide	10	Limestone	Mudstone	3	3

APPENDIX 4.3 – DOLOMITE CRYSTALS SIZE MEASUREMENTS

The following table contains the ranges of D2 dolomite crystal size measurements for each sample included in this study.

Appendix 4.3 Replaced phase D2 dolomite crystal sizes from dolostones and dolomitized limestones included in this study.

Sample	Microscope (x objective)	Minimum crystal size (div)	Maximum crystal size (div)	Minimum Dolomite Size (mm)	Maximum Dolomite Size (mm)	Lithology
La Escalera						
Esc1-98So	40	2	5	0.0050	0.0125	sed. breccia
Esc2-98So	20	7	10	0.0350	0.0500	dolostone
Esc3-98So	20	1	5	0.0050	0.0250	mudstone
Esc3-98So	20	2	12	0.0100	0.0600	grainstone
Esc4-98So	20	1	1	0.0050	0.0050	packstone
Esc4-98SoB	20	1	5	0.0050	0.0250	dolostone
Esc5A-98SoB		-	-	-	-	packstone (no dolomite)
Esc5C-98So	20	2	5	0.0100	0.0250	mudstone-wacke
Esc6A-98So	20	3	5	0.0150	0.0250	packstone
Esc6A-98SoA	20	1	10	0.0050	0.0500	packstone
Esc6B-98SoB	20	2	15	0.0100	0.0750	grainstone
Esc6C-98SoB	20	2	8	0.0100	0.0400	packstone
Las Palmas						
LaPal1-98So	20	5	20	0.0250	0.1000	wackestone
LaPal2-98So	20	5	15	0.0250	0.0750	rudist bank(packstone)
LaPal3-98So	20	4	15	0.0200	0.0750	rudist bank(wackest/packstone)
LaPal4-98So	20	5	10	0.0250	0.0500	rudist bank(packstone)
LaPal5-98So	20	1	5	0.0050	0.0250	grainstone
LaPal6-98So	20	1	8	0.0050	0.0400	grainstone
LaPal7-98So	20	5	10	0.025	0.05	packstone/grainstone
LaPal8-98So	20	2	5	0.0100	0.0250	dolostone
LaPal9-98So	20	3	4	0.0150	0.0200	dolostone
LaPal10-98So	20	3	5	0.0150	0.0250	wackestone/mudstone
TSLaPal1-00So	40	1	5	0.0025	0.0125	mudstone
TSLaPal4-00So	4	1	50	0.0250	1.2500	nodule

Continuation Appendix 4.3

Sample	Microscope (x objective)	Minimum crystal size (div)	Maximum crystal size (div)	Minimum Dolomite Size (mm)	Maximum Dolomite Size (mm)	Lithology
Los Chorros						
LCh1-98So	20	-	0	-	-	grainstone (no dolomite)
LCh2-98So	20	-	0	-	-	packstone (no dolomite)
LCh3-98So	20	-	0	-	-	packstone/grainstone (no dolomite)
LCh4-98So	20	1	5	0.0050	0.0250	packstone
LCh5-98So	20	1	1	0.0050	0.0050	
LCh6-98So	20	1	5	0.0050	0.0250	rudist bank (packstone)
LCh7-98So	20	5	10	0.025	0.05	packstone
LCh8-98So	20	2	5	0.0100	0.0250	grainstone
Santa Rosa						
StR1-98So	40	1	5	0.0025	0.0125	mudstone
StR2-98So	20	1	15	0.0050	0.0750	mudstone
StR3-98So	20	1	1	0.0050	0.0050	mudstone
StR4-98So	20	2	8	0.0100	0.0400	mudstone
StR5-98So	20	1	1	0.0050	0.0050	mudstone
StR6-98So	20	1	1	0.0050	0.0050	mudstone
StR7-98So	20	1	1	0.005	0.005	mudstone
StR8-98So	20	1	1	0.0050	0.0050	chert
StR9-98So	20	1	5	0.0050	0.0250	mudstone
StR10-98So	20	1	1	0.0050	0.0050	mudstone

APPENDIX 5.1 – FIELD FRACTURE DATA

The following table contains the scanlines length of fracture data collected from outcrops in the four localities included in this study. Scanline analysis was out of the scope of this study; however I used fracture data (orientation, etc.) collected along these scanlines.

Appendix 5.1 Scanlines length of fracture data collected from outcrops

Stratigraphic Bed Sampled	Scanline Length (in)			Total (in)	Lithofacies
	First set	Second set	Third		
La Escalera					
Esc-1	27.75	59.5	51	138.25	Breccia
Esc-2	40.3	28.75		69.05	Packstone-Grainstone
Esc-3	66.5	37.75		104.25	Mudstone
Esc-4	60.5			60.5	Dolostone
Esc-5	328			328	Mud-Wack-Packs
Esc-6	56	91		147	Grainstone
Esc-6A	105	79		184	Grainstone
Esc-7	54	75.5		129.5	Dolostone
Esc-8	33.5	36.5		70	Dolostone
Esc-9	65.5	62.5		128	Mudstone
Esc-10	519			519	Grainstone
Esc-11	487			487	Grainstone
Esc-12	34.5	36.25		70.75	Rx. Packstone
Santa Rosa					
StR-1	146.5	245		391.5	Mudstone
StR-2	94.5	203.5		298	Mudstone
StR-3	304.5	168		472.5	Mudstone with chert
StR-4	208	258.56		466.56	Mudstone
StR-5	89			89	Mudstone
StR-6	115			115	Mudstone
StR-7	150	95.5		245.5	Mudstone
StR-8	94.25	66.5		160.75	Chert
StR-9	205	179.5		384.5	Mudstone
StR-10	222	314.5	145	681.5	Mudstone with slumps
Las Palmas					
Lpa-1	101.5			101.5	Rudist bank
Lpa-2	222			222	Rudist bank
Lpa-3	156.5			156.5	Rudist bank
Lpa-4	340			340	Rudist bank
Lpa-5	204.5			204.5	Grainstone
Lpa-6	80			80	Grainstone
Lpa-7	357			357	Grainstone
Lpa-8	67	115	79.5	261.5	Dolostone (mudstone)
Lpa-9	68	46.5		114.5	Dolostone
Lpa-10	67.5	121		188.5	Dolostone (mudstone)
Los Chorros					
LCh-1	179	197		376	Grainstone
LCh-2	48	99		147	Grainstone
LCh-3	127.5	130.5		258	Grainstone
LCh-4	60	31		91	Rx. Wack-Pack
LCh-5	107	103	103	313	Rx. Rudist bank
LCh-6	216.5	246	310.5	773	Rx. Rudist bank
LCh-7	59.5	130		189.5	Grainstone
LCh-8	199.5			199.5	Rx. Pack-Grainstone

Rx, recrystallized

**APPENDIX 5.2 – LIST OF ORIENTED SAMPLES AND FRACTURE SETS ORIENTATION.
CUPIDO FORMATION**

The following table is a list of oriented samples and fracture data collected from outcrops in the four localities included in this study. Note that fracture sets nomenclature is the original used in the field. Fracture sets are not in paragenetic order.

Appendix 5.2 List of oriented samples and fracture sets orientation. Cupido Fm.

Locality	Sample #	Facies	Bed Orientation	First Set	Second Set	Third Set
La Escalera	Esc-1	Breccia	N72W 85NE	N35E 40NW	N10E 63NW	N20-60E 25NW
La Escalera	Esc-2	Packstone-Grainstone	N65W 85NE	N53E 40NW	N24E 42NW	
La Escalera	Esc-3	Mudstone	N70W 83NE	N50E 38NW	N15E 36NW	
La Escalera	Esc-4	Dolostone	N80W 80NE	N15E 35NW		
La Escalera	Esc-5	Mud-Wack-Packs	N75W 80NE	N25E 90		
La Escalera	Esc-6	Grainstone	N75W 86NE	N58E 45NW	N23E 41NW	
La Escalera	Esc-6A	Grainstone	N75W 86NE	N25E 80SE	N58E 45NW	
La Escalera	Esc-7	Dolostone	N72W 78NE	N25E 52NW	N55E 30NW	
La Escalera	Esc-8	Dolostone	N66W 77NE	N26E 23NW	N55E 44NW	
La Escalera	Esc-9	Mudstone	N70W 87NE	N40E 35NW	N08E 40NW	
La Escalera	Esc-10	Grainstone	N71W 84NE	N10E 30NW		
La Escalera	Esc-11	Grainstone	N71W 87NE	N25E 35NW		
La Escalera	Esc-12	Rex. Packstone	N73W 86NE	N49E 42NW	N15E 43NW	
Santa Rosa-Iturbide	StR-1	Mudstone	N30W 54SW	N10W 38NE	N64E 61NW	
Santa Rosa-Iturbide	StR-2	Mudstone	N31W 52SW	N22W 58NE	N88E 65NW	
Santa Rosa-Iturbide	StR-3	Mudstone with chert	N36W 56SW	N54E 65NW	N50W 65NE	
Santa Rosa-Iturbide	StR-4	Mudstone	N35W 49SW	N38E 63NW	N55W 83SE	
Santa Rosa-Iturbide	StR-5	Mudstone	N26W 51SW	N40W 58NE		
Santa Rosa-Iturbide	StR-6	Mudstone	N35W 50SW	N45W 61NE		
Santa Rosa-Iturbide	StR-7	Mudstone	N27W 66SW	N55W 56NE	N75W 63NE	
Santa Rosa-Iturbide	StR-8	Chert	N35W 53SW	N70E 90	N50E 70NW	
Santa Rosa-Iturbide	StR-9	Mudstone	N33W 51SW	N58E 70NW	N62W 55NE	
Santa Rosa-Iturbide	StR-10	Mudstone with slumps	N23W 55SW	N73E 80NW	N80W 58NE	N20W 40NE
Las Palmas	Lpa-1	Rudist bank	N70W 50NE	N28E 85NW		
Las Palmas	Lpa-2	Rudist bank	N68W 45NE	N25E 86NW		
Las Palmas	Lpa-3	Rudist bank	N74W 50NE	N22W 64SW	N69S SE	N25E 82SE
Las Palmas	Lpa-4	Rudist bank	N65W 43NE	N32E 77SE		
Las Palmas	Lpa-5	Grainstone				
Las Palmas	Lpa-6	Grainstone	N72W 44NE	N23E 85SE		
Las Palmas	Lpa-7	Grainstone				
Las Palmas	Lpa-8	Dolostone (mudstone)	N67W 43NE	N32E 57SE	N22W 54SW	N4W 80SW
Las Palmas	Lpa-9	Dolostone				
Las Palmas	Lpa-10	Dolostone (mudstone)	N67W 54NE	N25E 70SE	N35W 57SW	
Las Palmas	CulPa1-00- So					
Las Palmas	TsLPa1-00- So					
Las Palmas	CulPa1-01					
Las Palmas	TsLPa4-00- So	Dolostone (mudstone)	N67W 54NE	N25E 70SE	N35W 57SW	
Los Chorros	LCh-1	Grainstone				
Los Chorros	LCh-2	Grainstone	N65E 75SE	N20W 85NE	N70E 70SE	
Los Chorros	LCh-3	Grainstone				
Los Chorros	LCh-4	Rex-Wack-Pack	N65E 68SE	N18W 54SW	N15E 60NWSE	
Los Chorros	LCh-5	Rex Rudist bank				
Los Chorros	LCh-6	Rex Rudist bank	N68E 75SE	N5W 63SW	N25E 45NW	N12E 20NW
Los Chorros	LCh-7	Grainstone				
Los Chorros	LCh-8	Rex.Pack-Grainstone	N72E 74SE	N10W 65SW	N20E 32NW	
Cañón Cerro Prieto	CP1-01	Limestone				
Cañón Cerro Prieto	CP2-01	Limestone				
Potrero García	PG1-01	Limestone				
Potrero García	PG2-01	Limestone				

References

- Adams, J. E. and M. L. Rhodes 1960. Dolomitization by seepage refluxion. Am. Assoc. Petroleum Geologists Bull., v. 44, p. 1912-1920.
- Alan, J.R., and Wiggins, W.D., 1993. Dolomite Reservoirs. Geochemical techniques for evaluating origin and distribution: American Association of Petroleum Geologists, Continuing education course note series 36, 129 p.
- Aranda-García, M., 1991. El segmento San Felipe del cinturón cabalgado, Sierra Madre Oriental, estado de Durango: Boletín de la Asociación Mexicana de Geólogos Petroleros, v. 41, p. 18-36.
- Aulstead, L. K., Spencer J. R., Krouse, R.H., 1988. Fluid inclusions and isotopic evidence on dolomitization. Devonian of Western Canada. Geochim. Cosmochim. Acta Vol. 52, p. 1027-1035.
- Bai, T., Maerten, L., Gross, M. R., and Aydin, A., 2002. Orthogonal Cross Joints: Do They Imply a Regional Stress Rotation. Journal of Structural Geology, v. 24, p. 77-88.
- Barton, Ch.C., Kevin, S.J., and William R.P., 1988. Fractal scaling of fracture networks, trace lengths and apertures: Geological Society of America. Abstracts Program, 20, A 299.
- Bathurst, R. G. C., 1971. Carbonate Sediments and their Diagenesis: Elsevier, New York, p. 321-543.
- Becker, S.P., Eichhubl, P., Laubach, S.E., Reed, R.M., Lander, R.H., and Bodnar, R.J., 2010. A 48 m.y. history of fracture opening, temperature, and fluid pressure: Cretaceous Travis Peak Formation, East Texas basin. Geological Society of America Bulletin, v. 122, no. 7/8, p. 1081-1093.

- Bjorlykke, K., 1999. Principal Aspects of Compaction and Fluid Flow in Mudstones. In: Aplin, A.C., A.J. Fleet and J.H.S. Macquaker (Eds.), *Muds and Mudstones: Physical and Fluid-Flow Properties*. Geological Society of London, 153, p. 73-78.
- Bose E., 1923. Vestiges of an ancient continent in northeast Mexico: *Am. Jour. Sci.*, 5th ser. Vol. 6.
- Budai, J.M., and D.V. Wiltschko, 1987. Structural controls on syntectonic diagenesis within the Haystack Peak region of the Absaroka thrust sheet, Idaho-Wyoming-Utah thrust belt in W. R. Miller, (ed.) *The Thrust Belt Revised: Wyoming Geological Association Guidebook*, v.38, p. 55-68.
- Burkhard, M., 1993. Calcite twins, their geometry, appearance and significance as stress-strain markers and indicators of tectonic regime: a review, *Journal of Structural Geology*, 15, p. 351-386.
- Campbell, V.Ch., 1967. Lamina, Laminaset, bed and bedset: *Sedimentology*, 8, p. 7-26.
- Camerlo, R.H., 1998. Geometry and kinematic evolution of detachment folds, Monterrey Salient, Sierra Madre Oriental, Mexico: M.S. thesis, University of Texas at Austin, 399 p.
- Campa, M.F., 1985. The Mexican thrust belt: in *Tectonostratigraphic Terrains of The Circum-Pacific region*, Circum-Pacific Council of Energy and Mineral Resources, Earth Sciences Series 1, p. 299-313.
- Choquette, P. W. and James, N.P., 1990. Limestones - the burial diagenetic environment. In: Mellreath, I.A. and Morrow, D.W.(Eds.), *Diagenesis*. Geological Association of Canada: p. 75-112.
- Conklin, J., and More, C., 1977. Environmental analysis of the Lower cretaceous Cupido Formation, northeastern Mexico, in Bebout D.G., and Loucks R.G., eds., *Cretaceous carbonates of Texas and Mexico. Applications to subsurface exploration: University of Texas at Austin, Bureau of Economic Geology, Report of Investigation*, no. 89, p. 302-323.

- Cosgrove, J. W. & Engelder, T. (eds) 2004. The Initiation, Propagation, and Arrest of Joints and Other Fractures: Geological Society Special Publication no. 231. vi+330 pp. Geological Magazine, November 2005, v. 142, p. 824.
- Cox, S., 1987. Antitaxial crack-seal vein microstructures and their relationship to displacement paths. *Journal of Structural Geology*, Vol. 9, No. 7, p. 779-787.
- Craig H. 1965. The measurement of oxygen isotope paleotemperatures. This volume, Isotopic exchange effects in the evaporation of water: 2. Theory of the exchange process (to be published in JGR).
- Davies, G.R., and L.B. Smith, Jr., 2006. Structurally controlled hydrothermal dolomite reservoir facies: An overview, *AAPG Bulletin*, v. 90, n. 11, p. 1641-1690.
- De Cserna, Z., 1955 (1958). Notes on the tectonics of southern Mexico, in Weeks, L.G., ed., *Habitat of oil: Tulsa, Oklahoma, American Association of Petroleum Geologists*, p. 523-532.
- De Cserna, Z., 1956. Tectónica de la Sierra Madre Oriental de México, entre Torreón y Monterrey: *International Geological Congress, 20th, México City, Proceedings*, 87 p.
- Dutton, S.P., and Land, L. S., 1988. Cementation and burial history of a low-permeability quartzarenite, Lower Cretaceous Travis Peak Formation, East Texas: *Geological Society of America Bulletin*, v. 100, no. 8, p. 1271–1282.
- Eguiluz-de Antuñano, S., 1990. Un hiato Aptiano en el noreste de México, *Revista de la Sociedad mexicana de Paleontología*, v. 2 (2), p. 57-68.
- Eguiluz-de Antuñano, S., 1991. Interpretación geológica y geofísica de la Curvatura de Monterrey, en el noreste de México: *Revista Ingeniería Petrolera*, v. 31, p. 25-39.

- Eguiluz-de Antuñano, Aranda-García, M., and Marrett R., 2000. Tectónica de la Sierra Madre Oriental, México: Boletín de la Sociedad Geológica Mexicana, v. LIII, p. 1-26.
- Engelder, T., 1985. Loading paths to joint propagation during a tectonic cycle: an example from the Appalachian Plateau, *J. of Structural Geology*, 7, p. 459-476.
- English, J.M., 2012 (in press), Thermo-mechanical origin of regional fracture systems. *AAPG Bulletin*, v. 96.
- Epstein S., and Mayeda T., 1953. Variation of ^{18}O content of waters from natural sources. *Geochim. Cosmochim. Acta* 4, 213p.
- Ferill, D.A., 1991. Calcite twin widths and intensities as metamorphic indicators in natural low-temperature deformation of limestone. *Journal of Structural Geology*, 13, p. 667-675.
- Fischer, M. P., and P. B. Jackson, 1999. Stratigraphic controls on deformation patterns in fault-related folds: A detachment fold example from the Sierra Madre Oriental, northeast Mexico: *Journal of Structural Geology*, v.21, p. 613-633.
- Fischer, M. P., Higuera-Diaz, C. I., Evans, M. E., Perry, E. C., and Lefticariu, L., 2009. Fracture-controlled paleohydrology in a map-scale detachment fold: insights from the analysis of fluid inclusions in calcite and quartz veins. *Journal of Structural Geology* 31 (12), p. 1490-1510.
- Fisher, W. L., and Rodda, P.U., 1969. Edwards Formation (Lower Cretaceous), Texas-dolomitization in a carbonate platform system: *American Association of Petroleum Geologists Bulletin*, v 53, p. 55-72.
- Folk, R.L., 1965. Some aspects of recrystallization in ancient limestones, *Society of Economic Paleontologists and Mineralogists*, spec. pub. 13, p. 14-48.

- Friedman I., and O'Neil J. R., 1997. Compilation of Stable Isotope Fractionation Factors of Geochemical Interest: Data of Geochemistry. Geo. Surv. Prof. Paper 440-KK, U.S. Gov. Printing Office.
- Friedman, M., 1969. Structural Analysis of Fractures in Cores from Saticoy Field, Ventura County, California. American Association of Petroleum Geologists, Bulletin, 53 (2), p. 367-389.
- Gale, J. F. W., 2008. Natural fractures in the Barnett Shale in the Delaware Basin, Pecos Co., West Texas: comparison with the Barnett Shale in the Fort Worth Basin (abs.), in West Texas Geological Society Fall 2008 Symposium, WTGS digital publication #08-120, p. 13.
- Gale, J. F. W. and Gomez, L. A., 2007. Late opening-mode fractures in karst-brecciated dolostones of the Lower Ordovician Ellenburger Group, west Texas: Recognition, characterization, and implications for fluid flow. AAPG Bulletin 91: p. 1005-1023.
- Gale, J.F.W., Lander, R.H., Reed, R.M., and Laubach, S.E., 2010. Modeling fracture porosity evolution in dolostone. Journal of Structural Geology (published online 2009) doi:10.1016/j.jsg.2009.04.018.
- Gale, J. F. W., Laubach, S. E., Marrett, R. A., Olson, J. E., Holder, J., and Reed, R. M., 2004. Predicting and characterizing fractures in dolostone reservoirs: using the link between diagenesis and fracturing. In: Braithwaite, C. J. R., Rizzi, G. & Darke, G., eds., The Geometry and Petrogenesis of Dolomite Hydrocarbon Reservoirs. Geological Society, London, Special Publications, 235, p. 177-192.
- Galloway, W. E. and Hobday, D. K. 1983. Terrigenous Clastic Depositional Systems. Applications to Petroleum, Coal, and Uranium Exploration, xv + 423 p. New York, Berlin, Heidelberg, Tokyo: Springer-Verlag.
- Goldhammer, R.K., 1999. Mesozoic sequence stratigraphy and paleogeographic evolution of northeast Mexico, in Bartolini, C., Wilson, J.L., and Lawton, T.F., eds., Mesozoic Sedimentary and Tectonic History of North-Central Mexico: Boulder, Colorado, Geological Society of America, Special Paper 340.

- Goldhammer, R.K., and Lehman, P.J., 1991. The origin of fifth-order cycles in the Lower Cretaceous Cupido Fm and one-dimensional forward stratigraphic modeling, in Goldhammer, R.K., Lehman, P.J., Todd, R.G., Wilson, J.L., Ward, W.C., and Johnson, C.R., 1991, Sequence stratigraphy and cyclostratigraphy of the Mesozoic of the Sierra Madre Oriental, northeast Mexico, a field guide book: Gulf Coast Section, Society of Economic Paleontologists and Mineralogists, 85 p.
- Gomez, L. A., 2007. Characterization of the spatial arrangement of opening-mode fractures. Ph. D. Dissertation, The University of Texas at Austin.
- Gomez, L. A., and Laubach, S. E, 2006. Rapid digital quantification of microfracture populations. *Journal of Structural Geology*, v. 28, p. 408-420.
- Gray, G.G., and Lawton T. F., 2011. New constraints on timing of Hidalgoan (Laramide) deformation in the Parras and La Popa basins, NE Mexico: *Boletín de la Sociedad Geológica Mexicana*, Vol. 63, Num. 2, p. 333-343.
- Gray, G.G., Pottorf, R.J., Yurewicz, D.A., Mahon, K.I., Pevear, D.R., Chuchla, R.J., 2001. Thermal and Chronological Record of syn-to post-Laramide burial and exhumation, Sierra Madre Oriental, Mexico, in Bartolini, C., Buffer R.T., Cantú-Chapa, A., The west Gulf of Mexico Basin: Tectonics, Sedimentary Basins, and Petroleum systems: American Association of Petroleum Geologists, Memoir 75, p. 159-181.
- Guzzy-Arredondo G.S., Murillo-Muñetón G., Morán-Zenteno D. J., Grajales-Nishimura J.M., Martínez-Ibarra R. and Schaaf P., 2007. High-temperature dolomite in the Lower Cretaceous Cupido Formation, Bustamante Canyon, northeast Mexico: petrologic, geochemical and microthermometric constraints. *Revista Mexicana de Ciencias Geológicas*, v. 24, núm. 2, p. 131-149.
- Hancock, P.L., 1985. Brittle microtectonics; Principles and practice: *Journal of Structural Geology*, 7, p. 437-457.
- Hardie, L.A., 1987. Dolomitization; a critical view of some current views, *Journal of Sedimentary Research*, v. 57, no. 1, p. 166-183.

- Hooker, J.N., Gale, J.F.W., Gomez, L.A., Laubach, S.E., Marrett, R., Reed, R.M., 2009. Aperture-size scaling variations in a low-strain opening-mode fracture set, Cozzette Sandstone, Colorado, *Journal of Structural Geology* (2009), v. 31, p. 707-718.
- Humphrey, W.E., 1949. Geology of the Sierra de los Muertos area, Mexico (with descriptions of Aptian Cephalopods from the La Peña Formation): *Geological Society of America, Bulletin*, v. 60, p.89-176.
- Imlay, R. W., 1936. Evolution of the Coahuila Peninsula, Mexico, part IV, Geology of the western part of the Sierra de Parras, *Bulletin of the Geological Society of America*, vol. 47, p. 1091-1152.
- King, R.H., 1947. Sedimentation in Permian Castile sea: *American Association of Petroleum Geologists Bulletin*, v. 31, p. 470-4n.
- Land, L.S., 1980. The isotopic and trace element geochemistry of dolomite: the state of the art. *SEPM Spec. Publ. No. 28*, p. 87-110.
- Land, L.S., 1985. The origin of massive dolomite: *Journal of Geological Education*, v. 33, p. 112-125.
- Land, L.S., 1987. Environments of limestone and dolomite diagenesis: some geochemical considerations, *in* J. E. Warme and K.W. Shanley, Eds., *Carbonate Depositional Environments, Modern and Ancient*. Colorado School of Mines Quarterly, v. 81, no. 4, p. 26-41.
- Land, L.S., 1992. The dolomite problem: Stable and radiogenic isotope clues, *in* *Isotopic signatures and sedimentary records*, N. Clauer and S. Chadhuri, Eds., *Lecture Notes in Earth Sciences 43*, Springer-Verlag, p. 49-68.
- Land, L.S., 1999. Failure to precipitate dolomite at 25 °C from dilute solution despite 1000-fold oversaturation after 32 years. *Aquatic Geochemistry*, v. 4, p. 1-8.

- Land, L.S., and Prezbindowski, D.R., 1981. The origin and evolution of saline formation water, Lower Cretaceous carbonates, south-central Texas. *Jour. of Hydrology*. v. 54, p. 51-74.
- Lander, R.H., Larese, R.E. and Bonnell, L.M., 2008. Toward more accurate quartz cement models—The importance of euhedral vs. non-euhedral growth rates. *AAPG Bulletin*, v 92, no. 11, p. 1537-1564.
- Laubach, S. E., 1988. Subsurface fractures and their relationship to stress history in East Texas Basin sandstone: *Tectonophysics*, v. 156, p. 37-49.
- Laubach, S.E., 1989. Fractures analysis of the Travis Peak formation western flank of the Sabine Arch, East Texas: Report of investigation No. 185. Bureau of Economic Geology. The Univeristy of Texas at Austin.
- Laubach, S.E., 1997. A method to detect natural fracture strike in sandstones: *American Association of Petroleum Geologists Bulletin*, v. 81, p. 604-623.
- Laubach, S. E., 2003. Practical approaches to identifying sealed and open fractures , *AAPG Bulletin*, v. 87, No. 4, (April 2003) 561-579. Reprinted in *Fractured reservoirs: A compendium of influential papers (2008)*, AAPG; and reprinted in *Understanding diagenetic controls on sandstone reservoir quality: A compendium of influential papers (2006)*, AAPG.
- Laubach, S.E., and Milliken K.L., 1996. New fracture characterization methods for siliciclastic rocks, in Aubertin, M., Hassani, F., Mitri, H.S., eds., *Rock mechanics tools and techniques: Proceedings 2nd North American Rock Mechanics Symposium*, v. 2, p. 1209-1213.
- Laubach, S. E., and Ward, M. E., 2006. Diagenesis in porosity evolution of opening-mode fractures, Middle Triassic to Lower Jurassic La Boca Formation, NE Mexico: *Tectonophysics*, v. 419, nos. 1-4, p. 75-97.
- Laubach, S.E., Olson, J. E., and Gross, M. E., 2009. Mechanical and fracture stratigraphy: *AAPG Bulletin*, v. 93, no. 11, p. 1413-1426.

- Laubach, S.E., Eichhubl P., Hilger, C., and Lander, R. H., 2010. Structural diagenesis. *Journal of Structural Geology* 32, p. 1866-1872.
- Laubach, S.E., Hentz, T.F., Johns, M.K., Baek, H., and Clift, S.J., 1995. Using diagenesis information to augment fracture analysis: Topical report, Bureau of Economic Geology. The University of Texas at Austin.
- Laubach, S. E., Reed, R. M., Olson, J. E., Lander, R. H., and Bonnell, L. M., 2004. Coevolution of crack-seal texture and fracture porosity in sedimentary rocks: cathodoluminescence observations of regional fractures: *Journal of Structural Geology*, v. 26, no. 5, p. 967-982.
- Lawn, B. R., and Wilshaw, T. R., 1975. *Fracture of brittle solids*: Cambridge, Cambridge University Press, 204 p.
- Lehmann, C., Osleger, D.A., Montañez, I.P., Sliter, W., Arnaud-Vanneau, A., and Banner, J., 1999. Evolution of Cupido and Coahuila carbonate platforms, Early Cretaceous, northeastern Mexico: *Geological Society of America Bulletin*, v. 111, p. 1010-1029.
- Lefticariu, L., 2004. Geochemical constraints on the evolution of the fluid-rock system in the salt-detached Nuncios Fold Complex, Mexico. Ph. D. Dissertation, Northern Illinois University, DeKalb Il, 385 p.
- Lefticariu, L., Perry, E. C., Fischer, M. P., and Banner, J., 2005. Evolution of fluid compartmentalization in a detachment fold complex. *Geology*, 33(1), p. 69-72.
- Leigh, K.A., 2011. A Fluid Inclusion and Cathodoluminescence Approach to Reconstruct Fracture Growth in the Triassic-Jurassic La Boca Formation, Northeastern Mexico. M.S. thesis, University of Texas at Austin, 202 p.
- Longman, M. W., 1980. Carbonate Diagenetic Textures from Nearsurface Diagenetic Environments: *AAPG Bull.*, V. 64, p. 461-487.

- Lu, E., 2000. Orientation, timing, kinematics, and genesis of veins and stylolites in seven anticlines, Sierra Madre Oriental, Mexico: B.S. thesis, University of Texas at Austin, 115 p.
- Lucia, F.J., 1999. Carbonate Reservoir Characterization: Berlin Springer-Verlag, 226 p.
- Lucia, F.J, and Major, R., 1994. Porosity evolution through hypersaline reflux dolomitization, in Purser, B., Tucker, M., and Zenger, D., eds., Dolomites: A Volume in Honor of Dolomieu: International Association of Sedimentologists, Special Publication 21, p. 325–341.
- McBride, E.F., 1988. Contrasting diagenetic histories of concretions and host rock, Lion Mountain Sandstone (Cambrian), Texas: Geol. Soc. America Bull., v. 100, p. 1803-1810.
- McBride, E.F., 1989. Quartz cement in sandstones: a review: Earth Science Reviews, v. 26, p. 69-112.
- Marrett, R., 1996. Aggregate properties of fracture populations: Journal of Structural Geology, 18, p. 169-178.
- Marrett, R., and Aranda-García, 1999. Structure and kinematic development of the Sierra Madre Oriental fold-thrust belt, Mexico, in Marrett, R., Wilson, J.L., and Ward, W.C., eds., Stratigraphy and structure of the Jurassic and Cretaceous platform and basin systems of the Sierra Madre Oriental, Monterrey and Saltillo areas, northeastern Mexico: San Antonio, Texas, South Texas Geological Society, p. 69-98.
- Marrett, R., and Aranda-García, M., 2001. Regional structure of the Sierra Madre Oriental fold-thrust belt, Mexico: in Marrett, R., ed., Genesis and controls of reservoir-scale carbonate deformation, Monterrey Salient, Mexico: Austin, Texas, Bureau of Economic Geology, Guidebook 28, p. 31-55.
- Marrett, R., and Laubach, S.E., 2001. Fracturing during burial diagenesis: in Marrett, R., ed., Genesis and controls of reservoir-scale carbonate deformation, Monterrey

- Salient, Mexico: Austin, Texas, Bureau of Economic Geology, Guidebook 28, p. 109-123.
- Marrett, R., Laubach, S.E. Olson, J.E., 2007. Anisotropy and beyond: geologic perspectives on geophysical prospecting for natural fractures. *The Leading Edge*, 26/9, 1106-1111. Reprinted in *Fractured reservoirs: A compendium of influential papers* (2008), AAPG.
- Milliken, K. L., 2003. "Diagenesis," in Middleton, G. V., et al., eds., *Encyclopedia of sediments and sedimentary rocks*: Kluwer Academic Publishers, p. 214–219.
- Milliman, J. D., 1974. *Marine Carbonates*: Springer-Verlag, New York, p. 270-313.
- Minero, C.J., 1988. Sedimentation and diagenesis along open and island-sheltered platform margin, El Abra Formation, Cretaceous of Mexico, in James, N.P., and Choquette, P., eds., *Paleokarst*. New York, Springer-Verlag, p. 385-405.
- Moldovanyi, E.P., and Lohmann, K.C., 1984. Isotopic and petrographic record of phreatic diagenesis: Lower Cretaceous Sligo and Cupido formations: *Journal of Sedimentary Petrology*, v. 54, p. 972-1985.
- Monroy-Santiago, F., S. E. Laubach, and R. Marrett, 2001. Preliminary Diagenetic and Stable Isotope Analyses of Fractures in the Cupido Formation, Sierra Madre Oriental. In: *Genesis and Controls of Reservoir-Scale Carbonate Deformation, Monterrey Salient, Mexico*. Marrett, R.(ed.). *Field Trip Guidebook 28*, Bureau of Economic Geology, The University of Texas at Austin, p. 83-107.
- Moore, C. H., 1989. *Carbonate Diagenesis and Porosity: Developments in Sedimentary No. 46*, Elsevier, New York, 338 p.
- National Research Council, 1996. *Rock Fractures and Fluid Flow: Contemporary Understanding and Applications*. National Research Council, Washington, DC, 551 p.

- Needham, T., Yielding, G., and Fox, 1996. Fault population description using examples From the offshore U. K.: *Journal of Structural Geology*, 18, p. 155-167.
- Nelson, R.A., 1985. *Geologic Analysis of Naturally fractured Reservoirs, Contributions in Petroleum Geology and Engineering. Volume 1: Gulf Publishing Company, Houston, 30 p.*
- Newell, K. D., and Goldstein, H. R., 1999. A new technique for surface and shallow subsurface paleobarometry using fluid inclusions: an example from the Upper Ordovician Viola Formation, Kansas, USA. *Chemical Geology* 154, p. 97-11.
- Olson, J.,E., Laubach, E. S., and Lander, H. R, 2009. Combining Diagenesis and mechanics to quantify fracture aperture distributions and fracture pattern permeability. In Lonergan, L., Jolly, R. J.H., Rawnsley, K. and Sanderson, D.J. (eds) *Fracture Reservoirs. Geological Society, London, Special publication, 270, p. 101-116.*
- Ortega J. O., 2002. *Fracture-size Scaling and Stratigraphic controls on Fracture Intensity. Ph. D. Dissertation, The University of Texas at Austin.*
- Ortega, O., and Marrett, R., 2001. Stratigraphic controls on fracture intensity in Barremian-Aptian carbonates, northeastern Mexico: in Marrett, R., ed., *Genesis and controls of reservoir-scale carbonate deformation, Monterrey Salient, Mexico: Austin, Texas, Bureau of Economic Geology, Guidebook 28, p. 57-82.*
- Ortega, O. J., Marrett, R., and Laubach, S. E., 2006. A scale-independent approach to fracture intensity and average fracture spacing: *AAPG Bulletin*, v. 90, no. 2 (Feb. 2006), p. 193-208.
- Ortega J. O., Gale, J. F.W., Marrett R., 2010. Quantifying diagenetic and stratigraphic controls on fracture intensity in platform carbonates: An example from the Sierra Madre Oriental, northeast Mexico. *Journal of Structural Geology* 32, p. 1943-1959.

- Padilla y Sánchez, R., 1982. Geologic Evolution of the Sierra Madre Oriental between Linares, Concepción del Oro, Saltillo, and Monterrey, Mexico. Ph. D. Dissertation, The University of Texas at Austin.
- Padilla y Sánchez, R., 1985. Las Estructuras de la curvatura de Monterrey, Estados de Coahuila, Nuevo León, Zacatecas y San Luis Potosí: revista del Instituto de Geología de la Universidad Autónoma de México, v. 6, p. 1-20.
- Philip, Z. G., Jennings, J. W., Jr., Olson, J., Laubach, S. E., and Holder, J., 2005. Modeling coupled fracture-matrix fluid flow in geomechanically simulated fracture networks: Society of Petroleum Engineers, SPE Reservoir Evaluation & Engineering, v. 8, no. 4, p. 300-309.
- Pollard, D.D. and Aydin, A.A., 1988. Progress in understanding jointing over the past century: Geological Society of America Bulletin, v. 100, p. 1181-1204.
- Pottorf, R.; Curry, D., Gray, G., Green, K., Richardson, M., Aden, L., Bierley, R., Chuchla, R., Sykes, M. and Yurewicz, D., 1977. Fluid inclusion technology to unravel histories of hydrocarbon entrapment and preservation—examples from Trinidad and Mexico: Second Joint AAPG/AMGP, Hedberg Research Symposium, Veracruz, Mexico.
- Primmer, J.T., Cade, A.C., Evans, J., Gluyas, G.J., Hopkins, S.M., Oxtoby, H.N., Smalley, C.P., Warren, A.E., and Worden, H.R. Global patterns in sandstone diagenesis: their application to reservoir quality prediction for petroleum exploration. AAPG Memoir 69, p. 61-77.
- Prioul R., and J. Jocker, 2009. Fracture characterization at multiple scales using borehole images, sonic logs, and walkaround vertical seismic profile: AAPG Bulletin, 93, p. 1503-1516.
- Quintero-Legorreta O., and Aranda-García M., 1985. Relaciones estructurales entre el anticlinorio de Parras y el anticlinorio de Arteaga (Sierra Madre Oriental), en la región de Agua Nueva, Coahuila., Univ. Nal. Autón. México, Inst. Geología, Revista, vol. 6, núm. 1, p. 21-36.

- Ramsay, J. G., 1980. The crack-seal mechanism of rock deformation. *Nature* 284, p. 135-139.
- Ramsay, J.G., and Huber, M.I., 1983. The techniques of modern structural geology, volume 1, Academic Press, 307 p.
- Radke, B.M., and Mathis, R.L., 1980. On the formation and occurrence of saddle dolomite. *Journal Sedimentary Petrology*, v. 50, no. 4, p. 1149-1168.
- Rico, L., 1999. Geometric and kinematic evolution of a complete detachment fold in a natural cross-section: M.S. thesis, University of Texas at Austin, 294 p.
- Scholle, P. A., 1978. A Color Illustrated Guide to Carbonate Rock Constituents, Textures, Cements, and Porosities: AAPG Memoir 27, Tulsa, p. 129-168.
- Selvius, D.B., Wilson, J.L., 1985. Lithostratigraphy and algal-foraminiferal biostratigraphy of the Cupido Formation, Lower Cretaceous, northeast Mexico, in Perkins, B.F., Martin, G.B. (eds.), *Habitat of Oil and Gas in the Gulf Coast: Society of Economic Paleontologists and Mineralogists, Gulf Coast Section, Proceedings of the Fourth Annual Research Conference*, p. 285-311.
- Stearns, D.W. 1967. Certain aspects of fractures in naturally deformed rocks. In R. R. Riecker (Ed.), *NSF Advanced Science Seminar in Rock Mechanics*. Bedford, Massachusetts, Air Force Cambridge Research Lab. Spec. Rept., p. 9 -118.
- Stearns, D. W., and M. Friedman, 1972. Reservoirs in Fractured Rock. In: *Stratigraphic Oil and Gas Fields*. American Association of Petroleum Geologists, Memoir 16, p. 82-106.
- Suter, M., 1984. Cordilleran deformation along the eastern edge of the Valles-San Luis Potosí carbonate platform, Sierra Madre Oriental fold-thrust belt, east-central Mexico: *Geological Society of America Bulletin*, v.95, p. 1387-1397.
- Tucker, M., and Wright, P., 1990. Carbonate depositional systems; I, Marine shallow-water and lacustrine carbonates, in Tucker, M.E., Wright, V.P., and Dickson, J.A.D., eds., *Carbonate sedimentology*: Oxford, Blackwell Sci. Publ., p. 101-227.

- Twiss, R., and Moores, E. M., 1997. Structural Geology: W. H. Freeman and Company, p. 103-113.
- Warren, J., 1999. Evaporites. Their evolution and economics. Blackwell Science, 438 p.
- Warren, J., 2000. Dolomite: occurrence, evolution and economically important association. Earth-Sciences Reviews 52, p. 1-81.
- Wilson, J.L., 1981. Lower Cretaceous stratigraphic in the Monterrey-Salttillo area, in Smith, C.I., ed., Lower Cretaceous stratigraphy and structure, northern Mexico: West Texas Geological Society Publication 81-74, p. 78-84.
- Wilson, J.L., 1990. Basement structural controls on Mesozoic carbonate facies in northeastern México a review, in Tucker, M. E., Wilson, J. L., Crevello, P.D., Sarg., J.R., and Read, J.F., eds., Carbonate Platforms, Facies, Sequences and Evolution: International Association of Sedimentologists, Special Publications 9, p. 235-255.
- Wilson, J.L., and Pialli, G., 1977. A Lower Cretaceous shelf margin in northern Mexico, in Bebout, D.G., and Loucks, R.G., eds., Cretaceous Carbonates of Texas and Mexico: The University of Texas, Bureau of Economic geology, Report of Investigations no. 89, p. 302-323.
- Wilson, J.L., Ward, W. C., and Finneran, J., 1984. A Field Guide to Upper Jurassic and Lower Cretaceous Carbonate Platform and Basin Systems, Monterrey-Salttillo Area, Northeast Mexico: SEPM, Gulf Coast Section, 76 p.
- Yielding, G., Needham, T., and Helen, J., 1996. Sampling of fault populations using sub-surface data, a review: Journal of Structural Geology, 18, p. 134-146.
- Zenger, D.H., and Mazzullo, S.J., eds., 1982. Dolomitization: Stroudsburg, Pennsylvania, Hutchinson Ross Publ. Co., 426 p.

Vita

Faustino Monroy Santiago was born on the 15th of February, 1962 in Veracruz, Mexico. The author graduated from high school in 1980, and entered the Universidad Nacional Autónoma de México (UNAM) in 1981. He obtained a degree in Geological Engineering in 1987 and a Master's degree in Petroleum Exploration in 1997, from the UNAM. From 1987 to 1990 he worked as a Technical Assistant in different geology courses at the Department of Geological Sciences, UNAM. Since 1990 the author is working as geologist to Petroleos Mexicanos (Pemex), where he has occupied several positions such as well-site geologist, sedimentologist, and reservoir geologist. The author is currently employed as reservoir geologist with Pemex Exploración y Producción in Villahermosa City, Mexico. He is instructing new geologists in the methodology called SDPS to characterize naturally fractured reservoirs. Currently the author is attending main projects in reservoir characterization of fractured carbonates from Mexico.

Email address: faustino.monroy@pemex.com

This dissertation was typed by the author.